PRODUCTION OPTIMIZATION AND FORECASTING OF SHALE GAS WELLS USING SIMULATION MODELS AND DECLINE CURVE ANALYSIS

By

Peter C. Ikewun

RECOMMENDED:

Dr. Mohabbat Ahmadi

Dr. Catherine Hanks

Dr. Ahmed Kamel

Dr. Catherine Hanks
Chair, Department of Petroleum Engineering

APPROVED:

Dr. Doug Goering
Dean, College of Engineering and Mines

Dr. Lawrence K. Duffy
Dean of the Graduate School

July 31, 2012
Date

PRODUCTION OPTIMIZATION AND FORECASTING OF SHALE GAS WELLS USING SIMULATION MODELS AND DECLINE CURVE ANALYSIS

A

THESIS

Presented to the Faculty

of the University of Alaska Fairbanks

in Partial Fulfillment of the Requirements

for the Degree of

MASTER OF SCIENCE

By

Peter O. Ikewun, B.Eng.

Fairbanks, Alaska

August 2012

Abstract

Production data from the Eagle Ford shale (an analogue to the Shublik shale of Alaska) was compiled from three neighboring counties and analyzed using decline curve analysis (DCA) to correlate production performance with completion method (horizontal leg/stages of fracture) and length of horizontal leg. Generic simulation models were built and run using a realistic range of properties. Simulation results provided a better understanding of interplay between static properties and dynamic behavior.

Results from the DCA of 24 producing wells with production histories of 9-57 months showed, for most cases, an increase in reserves with more fracture stages. However, the DCA generated different forecasts depending on which part of the data were used. This clearly indicated the need for running simulations. Simulation runs can generate more reliable production forecast of which the decline part can be used to evaluate the capability of DCA to reproduce the production profiles.

A combination of simulation models and DCA was used to optimize production and forecasting. Simulation models were used to optimize production for a range of different reservoir and completion parameters. The ability for DCA to reproduce simulated results (built with similar data from the Eagle Ford) for wells with different production periods was also analyzed. This results in better and more reliable production forecasts for the Eagle Ford and other young producing shale reservoirs possessing short production history. Modeling of the complex reservoir geometry and fracture networks of these types of reservoirs would give an extensive understanding of the flow mechanics.

Dedication

To the almighty God for life and divine inspiration

Table of Contents

Page

List of Figures

Page

List of Tables

Page

List of Appendices

Page

Acknowledgements

I want to thank the members of my committee; Dr. Mohabbat Ahmadi, Dr. Ahmed Kamel and Dr. Catherine Hanks for all their support and contributions. I appreciate every advice and constructive criticism offered throughout my work. I am very grateful for their time and attention granted in carefully evaluating every stage of my work. This work would not be successful without their careful guidance during my simulations and analysis.

I give special thanks to Object Reservoir for granting me access to the Resolve simulator and also to Steve Cassel for his recommendations. I also would like to appreciate CMG for providing their simulator. Thanks to staff and students of the Petroleum Engineering department UAF.

I want to express my sincere gratitude to my parents and siblings for believing strongly in me. I owe my accomplishment to my family; I thank them for their financial support, encouragements and unfaltering love throughout my work.

Peter Ikewun

Chapter 1 Introduction

1.1 Shale-gas reservoirs

The increasing global energy demand has called for exploring more unconventional sources of hydrocarbons. Most of the conventional reservoirs have already been harnessed and would not meet the increasing global energy demand in the near future. Shales, which have always been considered as source rocks to conventional reservoirs, have lately been discovered to be a potential reservoir; this has led to an increase in shale gas reserves (Hill and Nelson 2000).

Advancements in technology such as horizontal wells and hydraulic fracturing have resulted in an increase in shale gas reserves in the United States. Improved drilling and completion techniques have also made production from ultra-tight shale reservoir more economical for production. This calls for more exploration of shale and tight sand reservoirs in order to meet the increasing energy demand.

The Shublik Formation of the Alaska North Slope has been considered as a potential source rock to the enormous hydrocarbon reserves at the Prudhoe Bay (Liu et al. 2009). This study evaluates how to optimize production from shale/tight gas reservoirs in general. We looked at the decline curve analysis (DCA) as a forecasting tool and the accuracy of the DCA for shale plays. We also made use of simulation models to analyze optimum completion (which is a key factor to production from shale reservoirs) for shales with a range of different reservoir properties. This information can be used to better predict how the Shublik Formation can be best developed as a shale resource.

The Eagle Ford shale has enormous shale gas and oil reserves (Sondhi 2011) and is currently under production. The Eagle Ford shale is considered an analog to the Shublik shale (Sondhi 2011). Consequently, production data from the Eagle Ford may give an indication as to the projected production from the Shublik shale. Proper analysis of production data from the Eagle Ford is needed not only because production from the shale gas reservoirs are still under observation but also to optimize production and profit. Decline curve analysis (DCA) will be employed in the analysis, as it helps predict production and reserves to abandonment rates which in turn helps for proper field development and also to optimize profit (Arps 1945).

1.2 Purpose and scope of study

Hydraulic fracturing is a key factor in enhancing production from shale reservoirs due to shale's ultra-low permeability. This study addresses the use of simulation models to improve production by optimizing the hydraulic fracturing process. Hydraulic fracture design is beyond the scope of this thesis. This study looks at the reservoir and hydraulic fracture parameters that affect production and shows how they can be used to optimize production from shale gas reservoirs. The reservoir and hydraulic fracture parameters include: medium permeability, presence of natural fracture, gas desorption, fracture closure with depletion, well spacing and hydraulic fracture spacing, half-length and conductivity.

Another objective is to understand how reliable the predictions from decline curve analysis could be for young shale plays with short production histories like that of the Eagle Ford shale. Production data from the Eagle Ford shale from several counties in Texas were evaluated to see how reliably they can forecast future production rates.

Application of results from this study will help to enhance production and forecasting at the Shublik. It will give an indication of the best type of completion (in terms of hydraulic fracture half-length, spacing and conductivity) needed to optimize production at the Shublik. It will also help to optimize production forecasting using DCA at the Shublik, since it presently has little or no production history.

Chapter 2 Literature Review

2.1 Shale Reservoirs

Shale gas reservoirs are a result of deposits of plant and animal remains along with fine grain clastic material deposited over a very long period of time. Shale reservoirs are usually potential source rocks and seals to conventional reservoirs but it has lately been discovered that it could also be a hydrocarbon reservoir (Sondhi 2011). They are considered as unconventional reservoirs due to their extremely low permeability which is normally of the order of micro- to nanodarcies. In shale gas reservoirs, gas is stored as free gas in the natural fractures (if present) and in the micro-pores. Adsorption is another mechanism by which gas is stored in shale gas; it is stored as sorbed gases in the internal surface of the organic matter (Hill and Nelson, 2000).

Shale gas has an estimated reserve of 500-1000 Tcf in the United States according to EIA INTEK shale report (EIA, 2011). This is about 16-37% of the total gas reserves in the United States as of 2008. Table 2.1 shows identified undeveloped shale gas plays in the lower 48 states. Development and production from these increasing shale gas reserves is required to meet the high energy demands in the United States; Figure 2.1 shows major shale plays that are currently being exploited in the United States.

Table 2.1: Undeveloped shale gas plays in the lower 48 states according to EIA INTEK report (2009).

Onshore Lower-48 Gas Supply Region	Shale play	Shale gas resources (trillion cubic feet)
Northeast	Marcellus	410
	Antrim	
	Devonian Low Thermal Maturity	14
	New Albany	11
	Greater Siltstone	8
	Big Sandy	7
	Cincinnati Arch	1
Subtotal		472
Percent of total		0.63
Gulf Coast	Haynesville	75
	Eagle Ford	21
	Floyd-Neal & Conasauga	4
Subtotal		100
Percent of total		0.13
Mid-Continent	Fayetteville	32
	Woodford	22
	Cana Woodford	6
Subtotal		60
Percent of total		0.08
Southwest	Barnett	43
	Barnett-Woodford	32
Subtotal		76
Percent of total		0.1

Table 2.1-Continued.

Rocky Mountain	Mancos	21
	Lewis	12
	Williston-Shallow Niobraran	7
	Hilliard-Baxter-Mancos	4
Subtotal		43
Percent of total		0.06

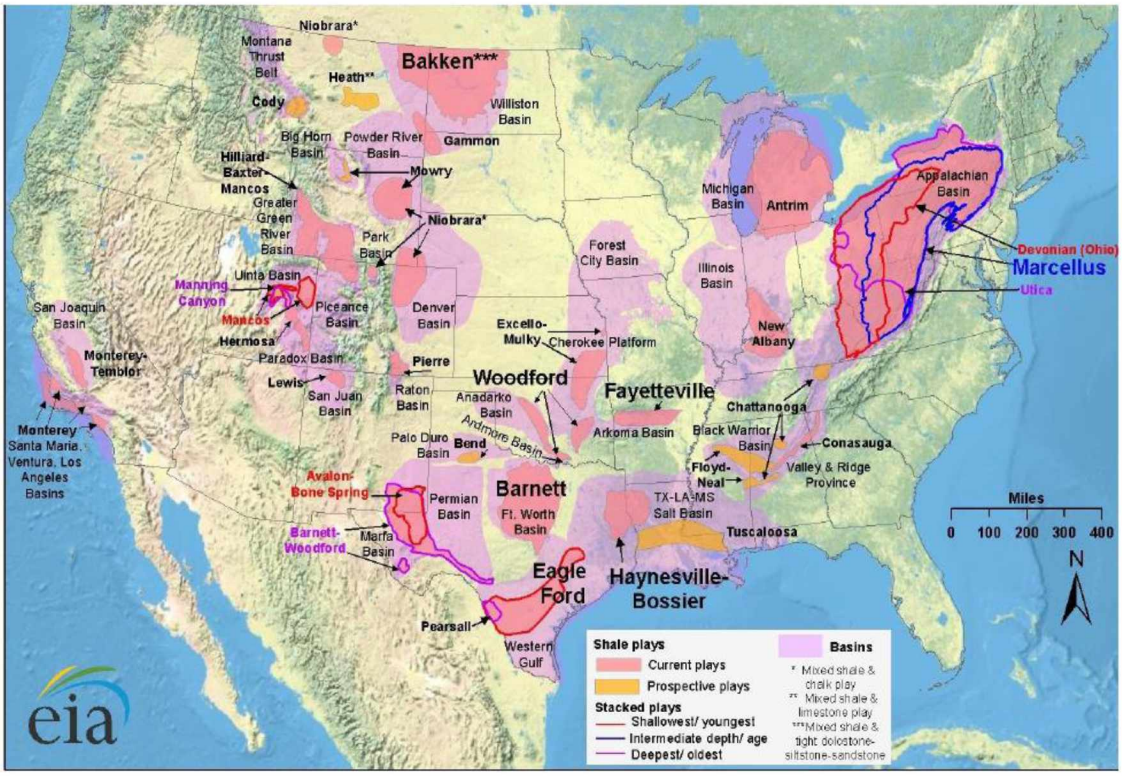

Figure 2.1: Shale gas plays in the lower 48 states (Energy Information Administration, 2011).

2.2 Well completion in shale reservoirs

Advancements in drilling and completions are the key factors that have led to the considerable increase in shale gas reserves and production. The type of completion used for production from shale reservoirs is very important due to the challenges imposed by very low porosity and especially permeability (Moridis et al. 2010). Important advancements in drilling and completion techniques include attainment of long horizontal wells and hydraulic fracturing. Other factors that may affect or increase production from shale reservoirs are the flow property of the reservoir, especially permeability, and presence and favorable properties of natural fractures (Moridis et al. 2010).

Long horizontal wells enhance production from shale gas reservoirs by increasing the surface area of the well directly in contact with the reservoir. This is particularly necessary in shale resource plays, because of shales ultra-low permeability (Bai 2011).

Hydraulic fracturing is another technique essential for economic production from shale gas reservoirs by bringing a large volume of reservoir into contact with the well. Hydraulic fracturing not only creates induced fractures, high conductivity paths, but can potentially open pre-existing natural fractures that has been sealed by minerals (Page and Miskimins 2009). Appropriate design of hydraulic fractures and the response of formation to hydraulic fracture stimulation are beyond the scope of this study and are not addressed here. It is necessary to stress that the choice of horizontal fractures properties used in the simulation studies are for comparison purpose and in reality they are mandated by in-situ stress condition of the formation among other parameters (Page and Miskimins 2009).

2.3 Eagle Ford shale

The Eagle Ford shale, named after the town of Eagle Ford, Texas, is a black calcareous shale formation that out crops in central Texas (Martin et al. 2011). The Eagle Ford Formation is Cretaceous in age and has a high carbon content with average total organic content (TOC) of 2.45 +/- 1.49 wt. % (Sondhi 2011). This high carbon content contributes to its brittle nature and makes the application of hydraulic fracturing very productive. It lies above the Buda Formation and below the Austin Chalk; it has been considered as the source rock to the Austin Chalk but lately it has also been seen as a self-sustaining reservoir. The productive unit varies from 50 to 350 feet in thickness and is 4000 to 14000 feet below sea level; it dips from the outcrop at location A into the subsurface as shown in Figure 2.2. Figure 2.3 shows the Eagle Ford shale play and the various hydrocarbon windows at different depths (Martin et al. 2011).

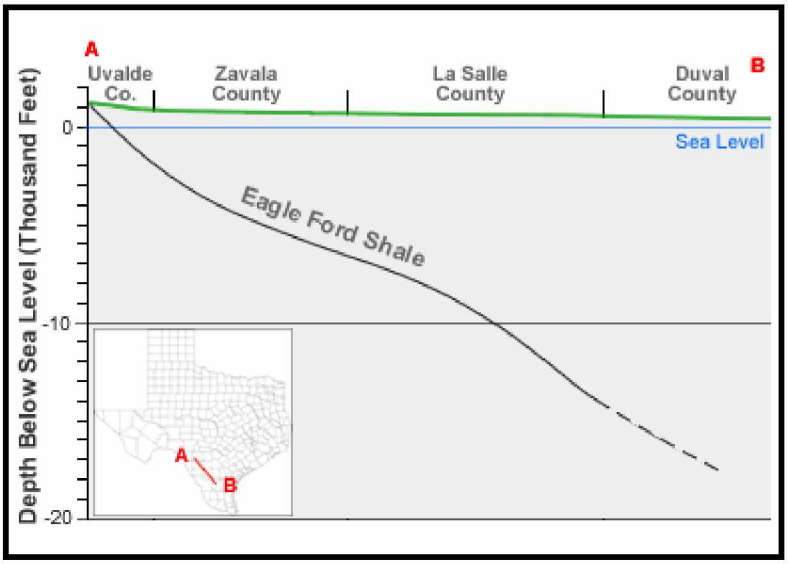

Figure 2.2: Generalized cross-section of the Eagle Ford shale (www.geology.com)

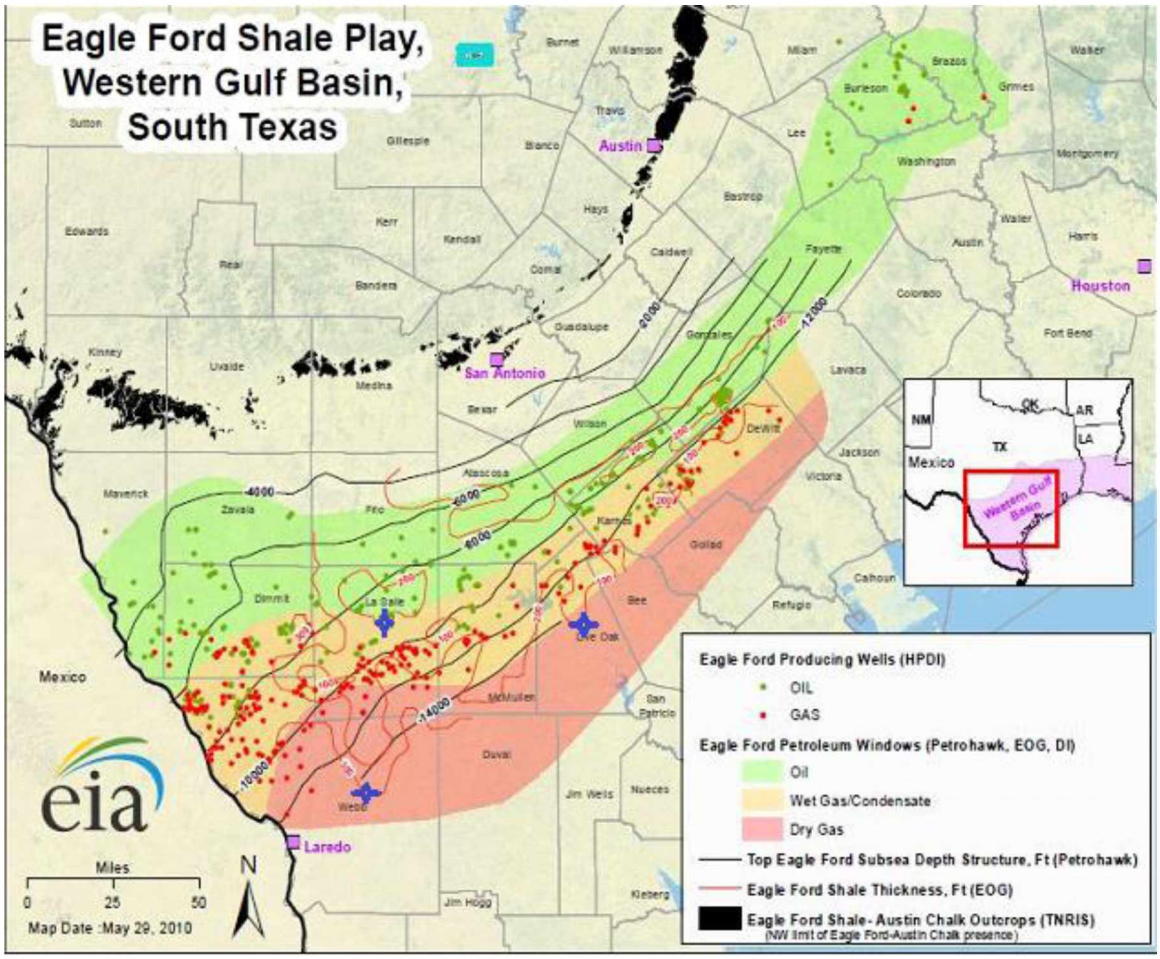

Figure 2.3: Eagle Ford shale play with various hydrocarbon windows at different depths (www.eaglefordshaleblog.com). Blue stars indicate data sources for this study.

The first horizontal well in the Eagle Ford was drilled in 2008 at the La Salle County and it was hydraulically fractured to yield an initial rate of 7.6 MMscf/day (Sondhi 2011). Field production has increased since then with the drilling of more horizontal wells and also the application of hydraulic fracturing (Sondhi 2011).

The productivity characteristics of most of the wells at the Eagle Ford it still uncertain since they are only a few years old. The Eagle Ford shale gas play is still under observation and predictions or forecasts may not be reliable due to its very young production history; this is why it is

necessary to use simulation models for production optimization and in combination with decline curve analysis for better forecasts.

The Eagle Ford and Shublik are both described as shale reservoirs. However these formations are quite complex and include fine grained rocks of varying lithology, composition, bed thickness, TOC, etc. Not all shales are identical or homogeneous, most are actually very heterogeneous.

2.4 Decline curve analysis

Decline curve analysis deals with production decline patterns or behavior and it is used for predicting future production performance. It was first postulated by Arps (1945); he developed three different production decline models: the exponential decline, harmonic decline and hyperbolic decline models. The assumption was that the present decline pattern would be equal to the future decline patterns (Arps 1945).

Results of analyzing production data from over 8,700 horizontal wells in the Barnett shale using decline curve analysis showed that the decline behavior followed a hyperbolic decline trend instead of an exponential decline and the b-factor values were all greater than 1.0 (Fan et al., 2011). This behavior is similar to the findings from Medeiros et al. (2007) which showed that transient flow dominates most of the productive life of the well because of the ultra-low formation permeability in shale.

2.5 Analysis of production from shale and tight gas reservoirs

Hydrocarbon reservoirs are usually modeled for full field development, to optimize production and profits. Modeling shale gas reservoirs has a lot of uncertainties due to its ultra-tight pores, very low permeability, gas desorption, presence of natural fractures etc. (Samandarli et al. 2011). The use of analytical or mathematical models for hydraulically fractured shale wells reduces

uncertainties due to the complex interplay of flow between the matrix and fractures (Brown et al. 2009). Various analytical models (which are mathematical expressions describing the reservoir system in question) that address different challenges have been presented by different authors.

A mathematical model can be used to describe the early and large time pressure response of fractured shale reservoirs, and also the fracture permeability/thickness product from the slope of drawdown plot (Deswaan 1976). It incorporates fluid flow properties (from well-logs and core analysis) and known fracture and matrix parameters.

An analytical solution for pressure response in horizontally fractured wells in layered reservoirs gives a better insight into the performance of fractured wells in layered reservoirs; it provides a general way of applying single layer solutions to multiple layered reservoirs (Bennett et al. 1985). It involves fractured layered reservoirs with different hydraulic fracture conductivities and also approximations with unique solutions at particular times of interest.

The effect of desorption when incorporated into an analytical solution as desorption compressibility only shifts the drawdown curve but does not change its shape for flow testing (Bumb and McKee 1988). The presence of desorption can thus not be detected from well testing because of the consistency in the shape of the curve with or without desorption.

An analytical solution with conventional reservoir properties with pressure squared incorporated to make corrections for real gas properties shows that some shales exhibit a semi-infinite matrix behavior for extended period , suggesting these shales exhibit dual porosity (matrix + fracture) behavior (Carlson and Mercer 1991). Analytical solutions could be used to analyze the production mechanism of shales where the dual porosity concept applies, considering the short and long term effects of storage and flow properties. However, this type of behavior is unlikely for most shale reservoirs

Analytical solutions for commingled gas reservoirs with gas adsorption effects show that the natural fractures have an effect on early time production while gas desorption has considerable effect on late time production (Gao et al. 1994). The analytical model incorporates pseudo-pressure and pseudo-time concepts for each layer to account for changes in gas properties with pressure and sorption effects respectively.

A mathematical model derived and used to analyze the pressure response from multiple fractured horizontal wells showed that perforating between some fracture intervals or spacing greatly affects production while the fracture trajectory has little or no effect on productivity except for situations where formation anisotropy comes to play (Raghavan et al. 1997). This mathematical model looks at variable properties of fractures and assumes impermeable sections between fractures.

Mathematical models with an efficient algorithm for computing well productivity from fractured reservoirs can be used to analyze pressure distributions as a result of both single and multiple fractures in the rectangular reservoir (Chen et al. 1997). These models assume a multiple fractured horizontal well in a rectangular reservoir. The models show that tests such as pressure build-up could be employed to optimize production at early times.

A two step approach (semi-analytical and transient-productivity index) has been used to analyze production data from hydraulically fractured horizontal wells in shale reservoirs (Medeiros et al. 2007). The first aspect of this approach was to use a semi-analytical model which incorporates reservoir heterogeneity and hydraulic fracture features to present production-decline characteristics. The second step was the use of transient-productivity index to analyze the production data because most of the production life of naturally fractured horizontal wells in tight formations is known to be under transient-flow regimes. Natural-fractures in the reservoir can be

detected by a constant transient-productivity index at early times and the drainage volume of the reservoir can be calculated from the boundary-dominated behavior of the transient-productivity index for wells. This semi-analytical approach was very successful, it involves gridding only at interface of the blocks and not within the reservoir blocks which have a computational advantage over full finite-difference simulation. There may also not be adequate data to sufficiently characterize heterogeneous unconventional reservoirs.

The complex interplay of flow from matrix to natural fractures and into the hydraulic fractures poses a big challenge for reservoir simulation. Figure 2.4 shows schematics of a tri-linear model solution for pressure transient analysis of fractured horizontal wells in unconventional reservoirs (Brown et al. 2009). The model was used to analyze pressure transient responses from horizontally fractured wells in unconventional reservoirs. The model included matrix and natural fracture properties in its analysis. It also gives the various flow regimes and the conditions associated with them. Another benefit of the tri-linear model is that it could easily be used to derive analytical approximate solutions to pressure transient flow for horizontally fractured wells in unconventional reservoirs. These approximate solutions are used to make quick appraisals of the pressure transient flow behavior for wells in unconventional shale reservoirs.

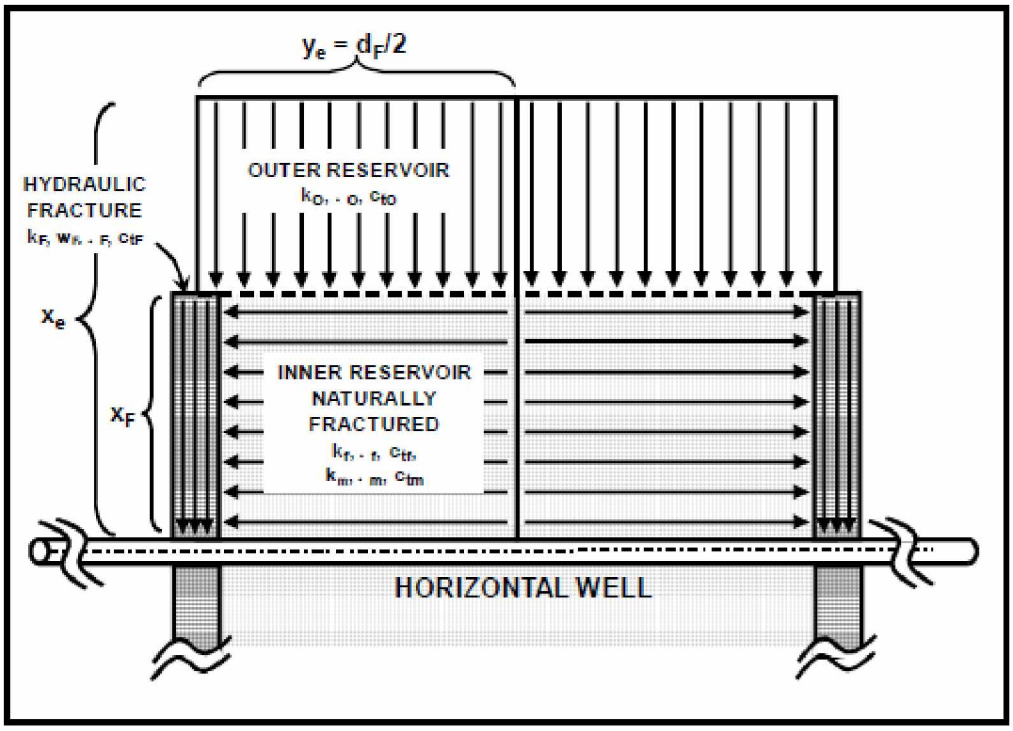

Figure 2.4: Schematic of Tri-linear model showing from the outer and inner naturally fractured reservoir (Brown et al. 2009)

Transient dual porosity models can also be used to analyze hydraulically fractured horizontal wells in shale gas reservoirs (Bello and Wattenbarger 2010). This model is based on transient dual porosity model for a linear reservoir presented by El-Banbi and Wattenbarger (1998). It models a hydraulically fractured horizontal shale gas well as a horizontal well draining a rectangular geometry containing transverse fractures with the horizontal well placed at the middle and separated by matrix blocks in a dual-porosity system. Five flow regions can be identified in the model: transient drainage in the fractures, simultaneous drainage from matrix and fractures, infinite-acting, transient drainage from the matrix which is the only region exhibited by most field production data and boundary dominated flow (Figure 2.5).

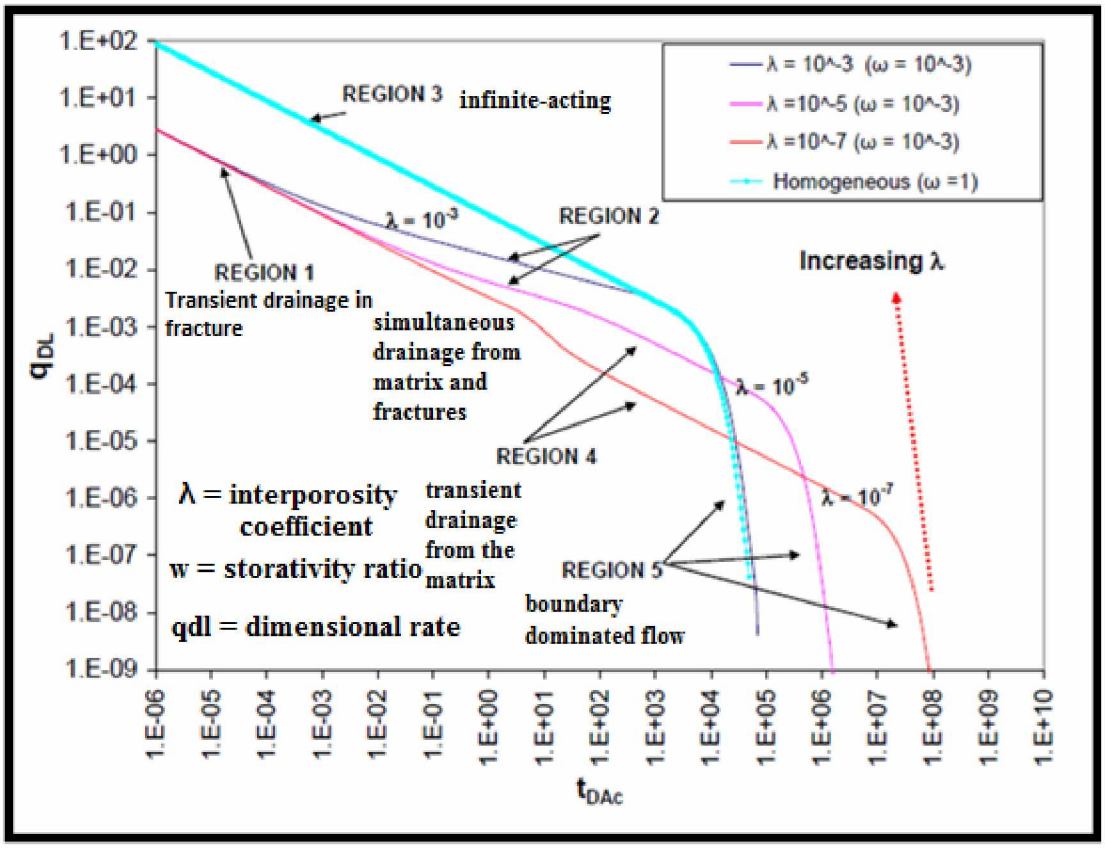

Figure 2.5: Five flow regions for dual porosity slab matrix linear reservoir (Bello and Wattenbarger 2010).

An investigation of the transient effect on long term production for transitions from linear flow to depletion of the stimulated reservoir volume and back to infinite acting shows that the linear flow regimes dominate most fractured shale gas reservoirs especially at early times and may be masked by finite fracture conductivity skin effect (Anderson et al. 2010).

A comparison of the performance of conventional (millidarcy permeability) and unconventional (micro to nanodarcy permeability) reservoirs using the tri-linear analytical model presented by Brown et al. (2009), shows that fractured horizontal wells do not produce beyond the region of the hydraulic fractures for shale reservoirs (Ozkan et al. 2011). Also, applying the tri-linear model

to tight sand and shale gas reservoirs showed that the productivity of the more permeable homogeneous tight sand reservoir is less than that of the shale reservoir with natural fractures.

The semi-analytical method could be used to obtain some reservoir parameters by matching the production history of hydraulically fractured horizontal wells in shale reservoirs (Samandarli et al. 2011). This method uses dual porosity transient equation presented by Bello and Wattenbarger (2010), and considers only the bilinear and linear flow regimes. Results from this approach shows that for permeability values smaller than 5.00E-5 md, the effect of fluid flow from the outer reservoir is not felt.

2.6 Analysis of production from shale and tight gas reservoirs using simulation models

Simulation models, unlike analytical models, make use of numeric and sometimes finite element methods for solutions to reservoir simulations. The challenge to using simulation models are the limitations due to grid dimensions and computational time. The ultra-tight pores of shales and the flow dynamics from matrix to fractures also present a big challenge when simulating production from hydraulically fractured shale wells.

An integrated approach developed to build a shale-specific finite difference reservoir simulation model for the Barnett shale showed that production from the Barnett shale was affected more by matrix porosity, permeability, natural fractures and less affected by desorption (Frantz et al. 2005). Data used in this integrated approach included geological, geophysical, geomechanical, petrophysical, drilling, completion, stimulation, production, pressure transient and microseismic data.

A finite difference numerical simulator that adequately represented typical characteristics of shale/tight gas reservoirs such as tight matrix permeability, horizontal wells with hydraulic

fractures, dual porosity/permeability, desorption etc. shows four major flow regimes (Figure 2.6) in hydraulically fractured shale/tight gas reservoirs (Freeman et al. 2009). The regimes include: the linear flow regime representing flow from fractures at early times and denoted by half slope; the transition flow which results from pressure interference between fractures; compound linear flow regime which indicates flow beyond the tips of hydraulic fractures; and elliptical flow at late times.

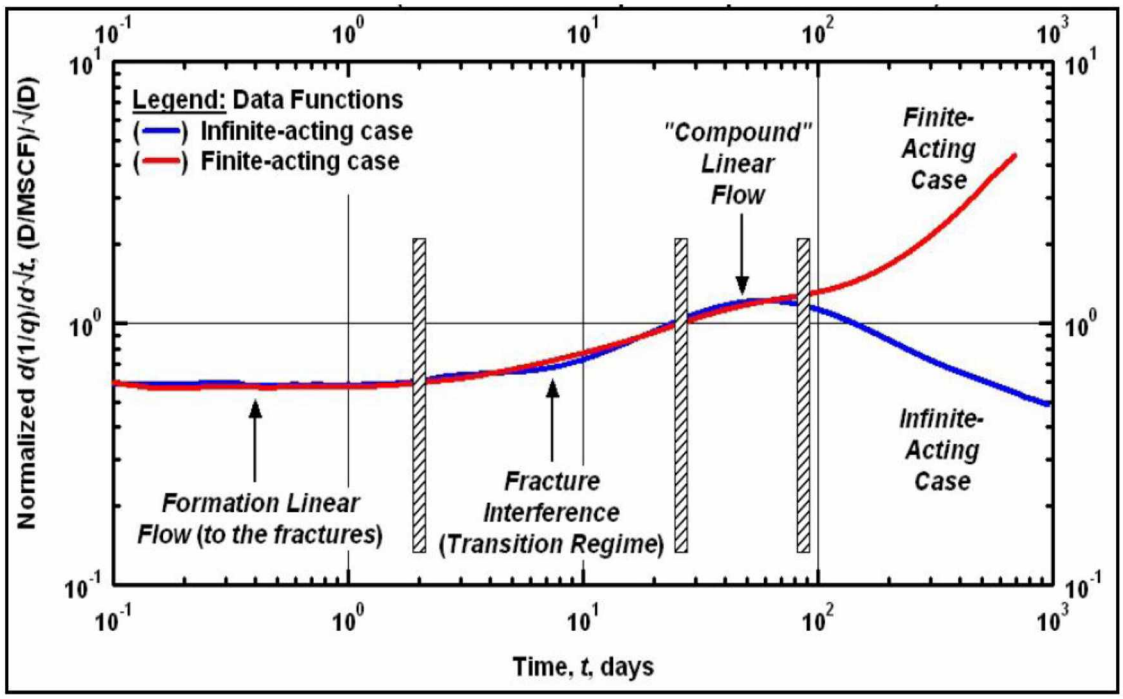

Figure 2.6: Four flow regimes due to effect of boundary and fracture interference (Freeman et al. 2009).

An analysis of the impact of various reservoir and hydraulic fracture parameters on hydraulically fractured shale gas reservoirs using an appropriate reservoir simulation model shows that the stimulated fracture permeability and matrix sigma factor (i.e. storativity ratio) has the most

impact on production performance (Zhang et al. 2009). This analysis was performed with a comprehensive reservoir simulator which comprises of the following: Multiple Interactive Continua concept with matrix sub-gridding and multi porosity system to adequately simulate transient matrix to fracture gas flow; extended Langmuir isotherm to simulate multiple component desorption; and rock compaction tables that make use of pore volume and transmissibility multipliers to account for the effect of propped fracture closure during production; etc.

Analysis of the mechanics of flow in fractured shale and tight gas reservoirs using numerical simulations that account for heat exchange and isothermal flow showed the following results: heat exchange and non-isothermal flow has little or no effect on production; gas desorption plays an important role in the production process and may significantly increase gas production; and fractures should be represented as detailed as possible (Moridis et al. 2010). Four descriptive sub-domains representing fractures were used in this analysis: the native fractures which were natural unaltered fractures, the primary fractures induced by hydraulic stimulation, secondary fractures which were extended protruded fractures from the hydraulic fractures and the radial fractures which were induced by drilling stress around the well-bore (Figure 2.7).

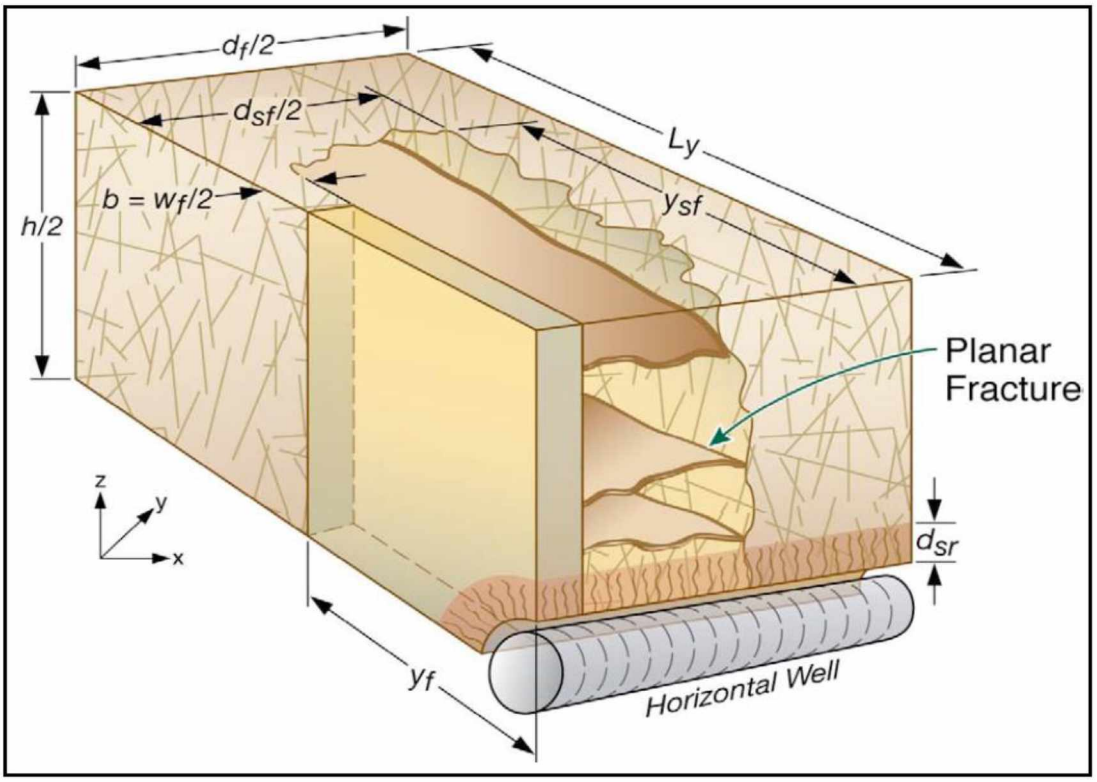

Figure 2.7: Four representative types of fractures (Moridis et al. 2010)

A methodology for modeling induced fracture networks in shale gas reservoirs with dual porosity showed that the fracture conductivity especially close to the well bore has the greatest effect on production performance, while the other parameters only had slight effects (Du et al. 2010). The methodology used in modeling the induced fracture networks includes: calculating the average fracture width using hydraulic fracturing data; estimating the fracture intensity from micro-seismic data; calibrating hydraulic and natural fracture intensity; calculating the dual porosity data; and simulation runs. This is based on the fact that obtaining more data accurately give better simulation results.

Flowback is a process of fluids flowing from the well after a fracturing job and the rate or performance of flowback affects production (Crafton 2010). The presence of natural fractures,

their width and conductivity are some parameters that can affect flowback performance (Crafton 2010). A sensitivity analysis carried out on flowback performance in hydraulically fractured shale reservoirs (with the presence of natural fractures) showed that presence of gas in natural fractures increases flowback performance. The increase in flowback performance was because gas filled natural fractures exhibited high pressures in contrast to the liquid filled fractures (Crafton 2010).

2.7 Hydraulic fracturing

John Gale (1982) looked into the effects of induced stress on both natural and induced fractures and their relationship with permeability. The research involved laboratory experiments on core samples with either induced or natural fractures. The change in flow rates, fluid pressure, deformation and fracture closure were all measured for increasing and decreasing loads on core samples. Results from this research showed that the induced fractures have lower flow rates than the natural fractures under the same condition of loaded stress. This lower flow rates in the induced fracture is evident to the fact that there is greater fracture closure for the induced fracture sample than the natural fracture sample.

Zuber et al. (1987) analyzed how different stimulation methods improved the production performance of the Devonian shale reservoir. The paper examines the contribution of each stimulation method to the increase in production and tries to estimate the optimal stimulation method by taking into account the economics of each stimulation method. Different reservoir qualities such as reservoir permeability anisotropy, fracture conductivity, fracture half-length and orientation were all investigated in order to get the optimal stimulation method. An analytic model solution consistent with that presented by Serra et al. (1983) was used to model hydraulic fracturing (by alternating the permeability anisotropy intensity and the average permeability), and tailored-pulse induced radial fracturing (2 fractures radial from well and perpendicular to each

other). The effect of three stimulation techniques (borehole shooting, hydraulic fracturing and radial fracturing) were evaluated by estimating the incremental production, skin factor, and also the economics or effective profit over a 5-year period. A production data analysis of actual production data from over 500 wells in the Devonian shale was made by first doing a history match with the analytical model and then estimating the effective skin factor for each of the stimulation techniques. A major conclusion from this study is that the fracture orientation affects the production performance for hydraulic fracturing job in formations with permeability anisotropy.

Yost II (1994) reviewed the increase in production performance from shale gas reservoirs as a result of CO_2/Sand fracturing. He analyzed the production performance improvement for four gas wells in the Devonian shale after fracturing with CO_2/Sand. Fifteen different gas wells in the Devonian shale were analyzed; four of these wells where stimulated with CO_2/Sand fracturing, seven were stimulated with Nitrogen fracturing and the last four were stimulated with Nitrogen foam fracturing. The fifteen wells used for the analysis were well spread throughout the Devonian shale in order to make strong or positive deductions from the results of the analysis. The analysis involved two stage treatments for each particular type of fracturing for a nine months period. The CO_2/Sand fracturing treatment made use of up to 120 tons of CO_2 for each stage and about 47,500 of sand with pump rate of about 53 barrels per minute. The Nitrogen gas stimulation involved up to 1.0 MMcf of Nitrogen per stage with a pumping rate of 100 Mscf per minute while the Nitrogen foam stimulation treatment used about 120,000 pounds of sand. Results after a nine-month production period showed that there was an increase in gas production of about 1.9 times more gas for CO_2/Sand treated wells than wells treated with Nitrogen which resulted to an additional gas production of 13.5 MMcf.

Page and Miskimins (2009) presented an analysis of the propagation of propellant and hydraulic fractures in shale gas reservoirs experimentally both in the laboratory and field. The Mancos shale which is a potential source rock and also naturally fractured was investigated by stimulating it with both propellant and slick-water fracturing. The laboratory test involved simulating propellant and hydraulic fracturing both on a big block and core samples of the Mancos shale in the laboratory. Field testing was also carried out on three wells in the Mancos shale formation in order to corroborate laboratory experiment and also to give a good comparison between the propellant and hydraulic fracturing techniques. Some of the major findings in this research includes: results from the laboratory experiment showed that growth of fracture height by propellant stimulation is restrained by thin layering in the Mancos shale. The field testing showed that the height growth for the slick-water fracturing was also restrained and could be attributed to tough layering, shear slippage, etc. Propellant and hydraulic fracturing techniques gave reasonable results when applied appropriately.

The effect of injected water during hydraulic fracturing of horizontal wells in shale reservoirs was analyzed by Cheng (2010). It was shown in this paper that the injected water during hydraulic fracturing has various effects on the production performance of shale gas reservoirs. This is because it has an effect on different reservoir and flow parameters such as capillary pressure, relative permeability, fracture conductivity etc. A generic reservoir simulation model was built in and used to analyze water saturation distribution both in the fractures and matrix. The long and short term effects of this water saturation on the production performance of gas were also investigated. Different cases were considered for the reservoir simulation model to account water injection, water recovery, shut-in, and production. Results from the effect of long term shit-in showed that the gas rate increases up to three time initially but remains the same at the long run, the water rate reduces equally because more water was sucked into the formation by the

imbibition process due to increase capillary pressure. Two capillary pressure curves were used; one for the matrix and the other for the invasion zone (due to alteration or increase in capillary pressure by water invasion). This alteration in capillary pressure leads to changes in relative permeability and resulted in extended higher water and lower gas production but the cumulative gas production did not change.

Bai (2011) gave an insight of stimulation strategies that would optimize hydraulic fracturing in shale gas reservoirs. A sensitivity analysis was carried out in order to analyze the effects of proppant concentration, injection rate, screenout and leak-off percentage on the hydraulic fracturing operation. A study on only leak-off was carried out by considering three leak-off percentages: low leak-off (20%), medium leak-off (76%) and high leak-off (94%). Results from this analysis includes: substantial leak-off results in screenout even with low proppant concentration which is contrary to conventional hypothesis that screenout is just a function of substantial proppant concentration. Decreasing net pressure for low leak-off signifies increasing width, length and height of fracture while increasing net pressure for high leak-off indicates increase of fracture width with restriction on the fracture length and height due to substantial sreenout. Studies on the injection rates were also carried out for three different cases of injection rates; low injection rate (30 bpm), medium injection rate (80 bpm), and high injection rate (130 bpm). Studies on the effects of proppant concentration showed that high proppant concentration gave larger width but smaller area of fracture, the fracture volume and geometry is more affected by proppant volume than the proppant concentration.

The literature on DCA helps to understand the uniqueness of using decline curves for future production performance. This study looks into some of the challenges involved in using the DCA such as the reliability of it giving a good forecast with short production history. The literature on

the use of simulation models for hydraulically fractured shale wells gave an insight of the challenges in modeling both hydraulic and natural fractures. This study uses a simulator with finite element method to effectively model fractured region close to the well. It also compares results from two simulators that handle natural fractures in two different ways.

Chapter 3 Methodology and Data

3.1 Methodology

The first part of this study uses decline curve analysis (DCA) to evaluate production data from gas wells at the Eagle Ford shale. DCA was applied to wells in the Eagle Ford from different counties in order to obtain correlations (if any) between production performance and completion geometry (length of horizontal leg and stages of fracturing). Wells from three neighboring counties (with high, medium and low cumulative productions) were chosen and analyzed using DCA to see if there is any correlation between a spatial variable (e.g., reservoir quality) and well production performance and type of completion.

The second part of the study used simulation models to optimize well completion and forecasting. These simulation results served two purposes: (1) to develop an optimization strategy that will optimize well completion for different matrix permeability and (2) to examine the potential of decline curve analysis to closely predict the simulated profiles. The simulation models used similar reservoir properties to those of the Eagle Ford shale as much as possible. The effects of different parameters are evaluated, including: matrix permeability; presence and properties of natural fractures; hydraulic fracture spacing; hydraulic fracture half-lengths; and conductivities of both the natural and hydraulic fractures. The optimization strategy used two different matrix permeabilities as base cases while other parameters where changed for a range of other cases.

In order to determine if DCA could accurately predict production behavior in shale reservoirs given very limited data, different portions for the decline curve were used for the analysis. Starting from beginning of decline behavior, different portions of generated production profiles from simulation are considered as input to DCA models. The predictions from DCA are then

compared with simulation results. Results obtained from DCA performed on production data from the first part of the study are compared to results for DCA performed on the simulated results to obtain any consistency in production forecast using different portions of the decline curve. This was done to see if the results from production date and simulated results are consistent when using different portions of the curve for the analysis.

3.2 Data

Data mining was a very critical part of this study. A lot of data were needed for both DCA and building simulation models. Most of the data used was obtained from two main sources: Texas Railroad Commission website (http://www.rrc.state.tx.us/data/online) and literature of work previously done on the Eagle Ford. The importance of data obtained was that the use of realistic data would make results from this study more applicable to real life situations at the Eagle Ford and also the Shublik.

Production data (production rates, time and date) from the various wells at the Eagle Ford were needed for DCA. Wells from three different counties at the Eagle Ford were basically evaluated using the DCA. Each county was sub-divided into different units and all the units in this study had only one well. Data used for DCA includes production data (production rates, time and date), horizontal well length and type of completion (number of fracture stages). The data used in the analysis is included in Appendix III.

Results from simulation models depend considerable on input data, which make data very important in simulation model building. A lot of data were needed for building simulation models. These data include: model size, matrix permeability, matrix porosity, bottom hole pressure, desorption parameter (Langmuir pressure and volume), stress sensitive rock mechanics parameter (fracture closure parameter), hydraulic fracture half-length, hydraulic and natural

fracture porosity and permeability. Data used for building simulation models were obtained from literature of work previously done on the Eagle Ford; other simulation data were obtained from the Texas Railroad Commission website.

Desorption parameters used in running simulation models were obtained from previous studied and literation on the Eagle Ford (Freeman et al. 2009, Gao et al. 1994). The desorption parameters includes different Langmuir volumes and pressures. Langmuir volume is the volume of gas stored in a rock sample measured in scf/ton while Langmuir pressure is the pressure below which the adsorbed gas is released from the rock sample.

Fracture closure parameter was also obtained from previous studies summarized in public literature (Orangi et al. 2011). The literature provides fracture permeability multipliers with pressure based on laboratory tests performed on the rock samples from the Eagle Ford.

Chapter 4 Decline Curve Analysis for Selected Eagle Ford Shale Gas Wells

4.1 Introduction

The Eagle Ford shale lies between the Austin Chalk and the Edwards limestone and is considered as a potential source rock with considerable amount of gas reserves (Sondhi 2011). Its thickness varies between 50-350 ft. and have high organic carbon content (average TOC of 2.45 +/- 1.49 wt. %). The first productive well was drilled in 2008 which makes the application of the decline curve method to predict cumulative production very challenging due to its relatively short production history.

Decline curve analysis was performed on 24 wells from three Counties: LaSalle, Live Oak and Webb counties (as indicated in Figure 4.1), with production histories in the range of 9-57 months (Tables 4.1-4.4; Appendix III). These three neighboring counties were chosen for two reasons:

(1) Allows evaluation of spatial variation in well performance, which could be a function of spatial variations in reservoir characteristics; and

(2) The wide variation in cumulative production and completion practices of the wells provides an opportunity to determine if there is any correlation between completion and well performance.

The Arps decline curve model (Arps 1945) was used for this analysis. The initial decline rates (Di) and decline exponent (b) were estimated based on the production history of each of gas well. The reserves and time to reach economic limits of 25, 50 and 75 Mscf/D (Tables 4.5-4.17) were also estimated. The initial rate (qi) is the rate at which a constant decline starts while the decline

exponent (b) is a term that defines the type of decline. The assumption in that the future decline is the same as current decline (Arps 1945).

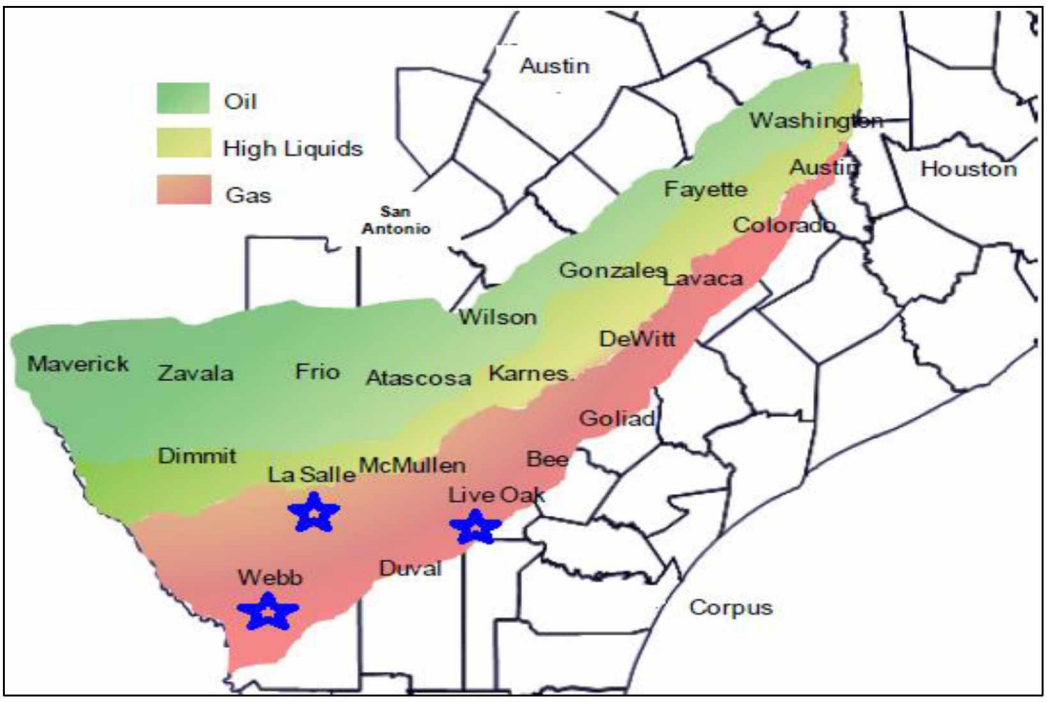

Figure 4.1: Eagle Ford shale counties showing the three neighboring counties appraised (www.rrc.state.tx.us)

Table 4.1: Data summary (LaSalle County)

Unit/wells	Cumulative recovery (MMscf)	Horizontal length	Fracture stages	Cumulative recovery (Mscf)
Evans H	405	3692	12	405397
Hawkville (Eagle Ford)	1351	2990	10	1350745
Brown Trusts	1720	3417	8	1720405
Brown Trusts 2	743	5193	15	742950
South Texas Syndicate	816	3284	12	816351
South Texas Syndicate 2	2020	4802	15	2019580
J.C Martin 1850	1403	4577	18	1402675
STS-Welse 786	644	4295	15	643877
STS	778	4145	15	777820
STS 2	750	4256	15	749797
STS 3	1074	4523	15	1073922
Caroline Pielop	868	3896	12	867786
Golla 7	1189	3682	13	1189324

Table 4.2: Data summary (Live Oak County)

Unit/wells	Cumulative recovery (MMscf)	Horizontal length	Fracture stages	Cumulative recovery (Mscf)
Eskew West Unit	436			436297
Lasca ButlerSearcy Trust	409	4758		409369
Kunde No. 1 Gas Unit	535			535304
Sinor Ranch	662	2553		661829
Kunde	322			321583
Marlene Olson	40			40479

Table 4.3: Data summary (Webb County)

Unit/wells	Cumulative recovery (MMscf)	Horizontal length	Fracture stages	Cumulative recovery (Mscf)
Gates				
Gates 2	67			67438
Gates 3	33			33049
Gates 4	32	4324		32121
Gates 5	43	4053		42796
Gates 6	28			28453

Table 4.4: County maximum and minimum production

County	Maximum production (Mscf)	Minimum production (Mscf)	number of producing wells
LaSalle	184624	7286	13
Live Oak	120529	279	6
Webb	9157	336	5

Table 4.5: Initial rates and forecast to production limit, EvansH unit/well (LaSalle county)

Evans H	Exponential Decline	Harmonic Decline	Harmonic Decline	Harmonic Decline
Minimum rate q_t (Mscf/D)	25	25	50	75
Initial rate, q_i (Mscf/D)	1615	3223	3223	3223
Decline rate, Di (1/days)	0.00345	0.020598	0.020598	0.020598
Time for min. rate, t (days)	1208	6211	3081	2038
Remaining production to limit (MMscf)	461	760	652	589

Table 4.6: Initial rates and forecast to production limit, Hawkville unit/well (LaSalle county)

Hawkville unit/well (Eagle Ford)	Exponential Decline	Harmonic Decline	Harmonic Decline	Harmonic Decline
Minimum rate q_t (Mscf/D)	25	25	50	75
Initial rate, q_i (Mscf/D)	1682	1774	1774	1774
Decline rate, Di (1/days)	0.00106	0.0009	0.0009	0.0009
Time for min. rate, t (days)	3970	77715	38302	25164
Remaining production to limit (MMscf)	1563	8399	7033	6234

Table 4.7: Initial rates and forecast to production limit, Brown Trust unit/well (LaSalle county)

Brown Trusts unit/well	Exponential Decline	Harmonic Decline	Harmonic Decline	Harmonic Decline
Minimum rate q_t (Mscf/D)	25	25	50	75
Initial rate, q_i (Mscf/D)	3879	4434	4434	4434
Decline rate, Di (1/days)	0.00162	0.00071	0.00071	0.00071
Time for min. rate, t (days)	3114	248373	123482	81852
Remaining production to limit (MMscf)	2379	32335	28006	25474

Table 4.8: Initial rates and forecast to production limit, South Texas Syndicate unit/well (LaSalle county)

South Texas Syndicate unit/well	Exponential Decline	Harmonic Decline	Harmonic Decline	Harmonic Decline
Minimum rate q_t (Mscf/D)	25	25	50	75
Initial rate, q_i (Mscf/D)	6441	6860	6860	6860
Decline rate, Di (1/days)	0.00192	0.00045	0.00045	0.00045
Time for min. rate, t (days)	2891	607514	302646	201023
Remaining production to limit (MMscf)	3342	85584	75018	68838

Table 4.9: Initial rates and forecast to production limit, J.C. Martin unit/well (LaSalle county)

J.C Martin 1850 unit/well	Exponential Decline	Harmonic Decline	Harmonic Decline	Harmonic Decline
Minimum rate q_t (Mscf/D)	25	25	50	75
Initial rate, q_i (Mscf/D)	5064	9869	9869	9869
Decline rate, Di (1/days)	0.00321	0.0018	0.0018	0.0018
Time for min. rate, t (days)	1655	218755	109100	72548
Remaining production to limit (MMscf)	1570	32777	28977	26754

Table 4.10: Initial rates and forecast to production limit, STS-Welse unit/well (LaSalle county)

STS-Welse 786 unit/well	Exponential Decline	Harmonic Decline	Harmonic Decline	Harmonic Decline
Minimum rate q_t (Mscf/D)	25	25	50	75
Initial rate, q_i (Mscf/D)	1988	2589	2589	2589
Decline rate, Di (1/days)	0.00273	0.00304	0.00304	0.00304
Time for min. rate, t (days)	1603	33742	16706	11028
Remaining production to limit (MMscf)	719	3952	3362	3017

Table 4.11: Initial rates and forecast to production limit, Caroline Pielop unit/well (LaSalle county)

Caroline Pielop unit/well	Exponential Decline	Harmonic Decline	Harmonic Decline	Harmonic Decline
Minimum rate q_t (Mscf/D)	25	25	50	75
Initial rate, q_i (Mscf/D)	2818	3266	3266	3266
Decline rate, Di (1/days)	0.00278	0.00183	0.00183	0.00183
Time for min. rate, t (days)	1700	70852	35153	23253
Remaining production to limit (MMscf)	1005	8697	7460	6736

Table 4.12: Initial rates and forecast to production limit, Lasca ButlerSearcy unit/well (Live Oak county)

Lasca ButlerSearcy Trust unit/well	Exponential Decline	Harmonic Decline	Harmonic Decline	Harmonic Decline
Minimum rate q_t (Mscf/D)	25	25	50	75
Initial rate, q_i (Mscf/D)	1089	1706	1706	1706
Decline rate, Di (1/days)	0.00211	0.00456	0.00456	0.00456
Time for min. rate, t (days)	1789	14749	7265	4770
Remaining production to limit (MMscf)	504	1580	1321	1169

Table 4.13: Initial rates and forecast to production limit, Sinor Ranch unit/well (Live Oak county)

Sinor Ranch unit/well	Exponential Decline	Harmonic Decline	Harmonic Decline	Harmonic Decline
Minimum rate q_t (Mscf/D)	25	25	50	75
Initial rate, q_i (Mscf/D)	1331	1594	1594	1594
Decline rate, Di (1/days)	0.00263	0.0038	0.0038	0.0038
Time for min. rate, t (days)	1511	16519	8128	5331
Remaining production to limit (MMscf)	497	1743	1453	1282

Table 4.14: Initial rates and forecast to production limit, Gates 4 unit/well (Webb county)

Gates 4 unit/well	Exponential Decline	Harmonic Decline	Harmonic Decline	Harmonic Decline
Minimum rate q_t (Mscf/D)	25	25	50	75
Initial rate, q_i (Mscf/D)	163	166	166	166
Decline rate, Di (1/days)	0.00297	0.02428	0.02428	0.02428
Time for min. rate, t (days)	630	233	96	50
Remaining production to limit (MMscf)	46	13	8	5

Table 4.15: Initial rates and forecast to production limit, Gates 5 unit/well (Webb county)

Gates 5 unit/well	Exponential Decline	Harmonic Decline	Harmonic Decline	Harmonic Decline
Minimum rate q_t (Mscf/D)	25	25	50	75
Initial rate, q_i (Mscf/D)	159	163	163	163
Decline rate, Di (1/days)	0.00251	0.02145	0.02145	0.02145
Time for min. rate, t (days)	737	257	105	55
Remaining production to limit (MMscf)	53	14	9	6

Table 4.16: Initial rates and forecast to production limits first half of curve (EvansH unit/well)

Evans H unit/well	Exponential Decline	Harmonic Decline	Harmonic Decline	Harmonic Decline
Minimum rate q_t (Mscf/D)	25	25	50	75
Initial rate, q_i (Mscf/D)	2083	2733	2733	2733
Decline rate, Di (1/days)	0.005	0.005	0.005	0.005
Time for min. rate, t (days)	885	21662	10731	7087
Remaining production to limit (MMscf)	412	2566	2187	1965

Table 4.17: Initial rates and forecast to production limits second half of curve (EvansH unit/well)

Evans H unit/well	Exponential Decline	Harmonic Decline	Harmonic Decline	Harmonic Decline
Minimum rate q_t (Mscf/D)	25	25	50	75
Initial rate, q_i (Mscf/D)	880	4783	4783	4783
Decline rate, Di (1/days)	0.002	0.008	0.008	0.008
Time for min. rate, t (days)	1781	23790	11833	7847
Remaining production to limit (MMscf)	428	3141	2727	2484

Figure 4.2 gives the actual production and forecasts for three wells, one from each of LaSalle, Live Oak and Webb counties. All three wells analyzed are horizontal and hydraulically fractured; the typical completion for wells in very low permeability shale reservoirs. The lengths of

horizontal leg as well as fracturing stages were considered in order to determine any possible correlation between past production performance and completion. These three wells are representative wells all have the same horizontal length and number of fracturing stages. Figure 4.2 gives an idea of the actual and forecasted cumulative production of the three counties. Table 4.18 shows the production summaries and completion for all the walls in LaSalle, Live Oak and Webb counties.

For some wells the rate vs. time plot was scattered which made the use of DCA untrustworthy. For some wells, the decline behavior changed after an initial production period. For these wells, different outcomes resulted depending on which part of data was used in DCA. It was noted that some of the data was matched equally well with both exponential and harmonic decline. Results from analysis of both models are provided for such wells.

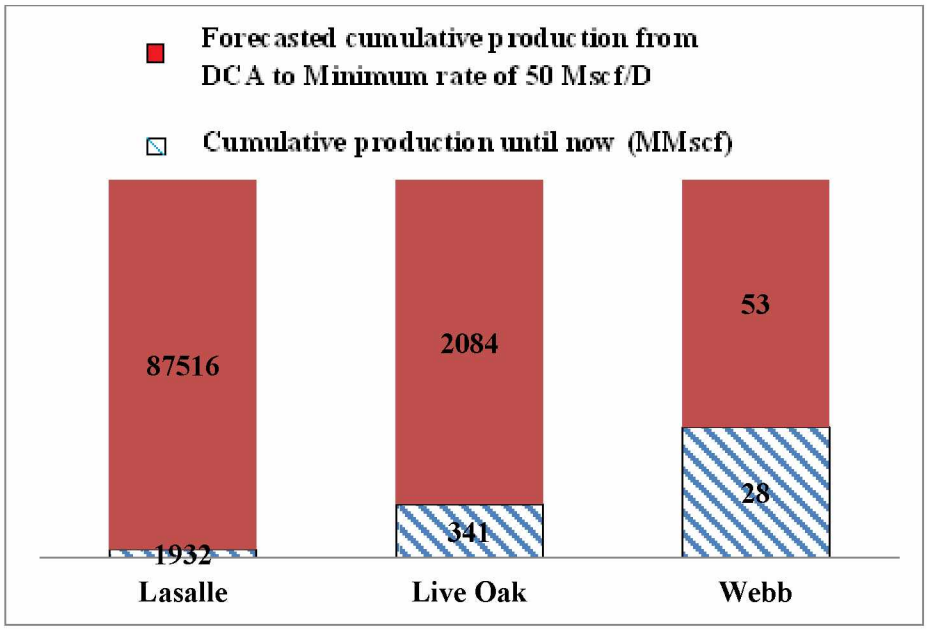

Figure 4.2: Cumulative production of both history and forecasted from DCA for wells from each county.

Table 4.18: Summary of production history and completion for Lasalle, Live Oak and Webb County

County	Unit/well	start date	Cumu. Rate Q, MMscf	Horizontal length (ft)	Num. of Frac. stages	Prod. Time Tp, days	Initial rate qi, Mscf/d	Ratio of cumu. Rate to time Q/t (Mscf/D)
LaSalle	Evans H	9-Aug	405	3692	12	629	2018	0.6
LaSalle	Hawkville	9-Oct	1351	2990	10	579	1934	2.3
LaSalle	Brown Trusts	9-Mar	1720	3417	8	736	2589	2.3
LaSalle	Brown Trusts 2	10-May	743	5193	15	348	3975	2.1
LaSalle	S. T. Syndicate	9-Jul	816	3284	12	646	2318	1.3
LaSalle	S. T. Syndicate 2	9-Oct	2020	4802	15	461	6039	4.4
LaSalle	J.C Martin 1850	9-Jul	1403	4577	18	625	8324	2.2
LaSalle	STS-Welse 786	9-Oct	644	4295	15	524	2952	1.2
LaSalle	STS	9-Oct	778	4145	15	456	1590	1.7
LaSalle	STS 2	9-Dec	750	4256	15	275	1776	2.7
LaSalle	STS 3	10-Jan	1074	4523	15	487	2478	2.2

Table 4.18-Continued.

LaSalle	Caroline Pielop	10-Mar	868	3896	12	427	2694	2
LaSalle	Golla 7	10-Apr	1189	3682	13	396	3035	3
Live Oak	Eskew West Unit	9-Jul	436			660	474	0.7
Live Oak	L. B. Trust	9-May	409	4758		701	2138	0.6
Live Oak	Kunde 1	8-Apr	535			1111	612	0.5
Live Oak	Sinor Ranch	9-Oct	662	2553		562	5091	1.2
Live Oak	Kunde 2	6-Aug	322			1732	518	0.2
Live Oak	Marlene Olson	9-Feb	40			822	95	0.1
Webb	Gates1	11-May	67			300	241	0.2
Webb	Gates2	11-Oct	33			272	159	0.1
Webb	Gates3	11-Oct	32			274	95	0.1
Webb	Gates4	11-Oct	43			274	182	0.2
Webb	Gates5	11-Oct	28			244	143	0.1

4.2 LaSalle County

The LaSalle County lies in the western part of the Eagle Ford shale play trend (Figure 4.1) and is in the gas window. The Eagle Ford wells in this area have the highest cumulative gas production of approximately 62,000,000 Mscf up to February 2011. The total number of wells drilled in this county is 98 (including wild cat, exploratory and appraisal wells). The decline curve method was applied to 12 different units (having one well each) of the LaSalle County: these 12 wells are the only wells with available production history in the Texas Railroad Commission (TRRC) website (http://www.rrc.state.tx.us/data/online).

4.2.1 Observation

The semi-log rate-time and linear rate-cumulative production plot for most of the wells gave straight lines (see Figures 4.3-4.15). These diagnostic plots show that both exponential and harmonic decline can be used.

4.2.2 Discussion and interpretation of plots

The implication of two different decline patterns (exponential and harmonic decline) is that different outcomes were obtained depending on which model was used in forecasting. A typical example is given in Table 4.7 where exponential model gave reserves of 2,379 MMScf while the harmonic model gave 32,335 MMScf for production to minimum rate of 25MScf/day. Tables 4.5 4.17 show results of all the wells analyzed at the Lasalle county. This observation clearly suggests using single well simulation models for better understanding of the well performance in shale reservoirs.

Another uncertainty in the use of the decline curve for young shale gas plays is the choice of data for DCA. The two different decline pattern (exponential and harmonic decline) generated was

mainly due to the very short production history available (Figures 4.3-4.15). The choice of what model should be accepted or used is a source of uncertainty for shale plays with young production history.

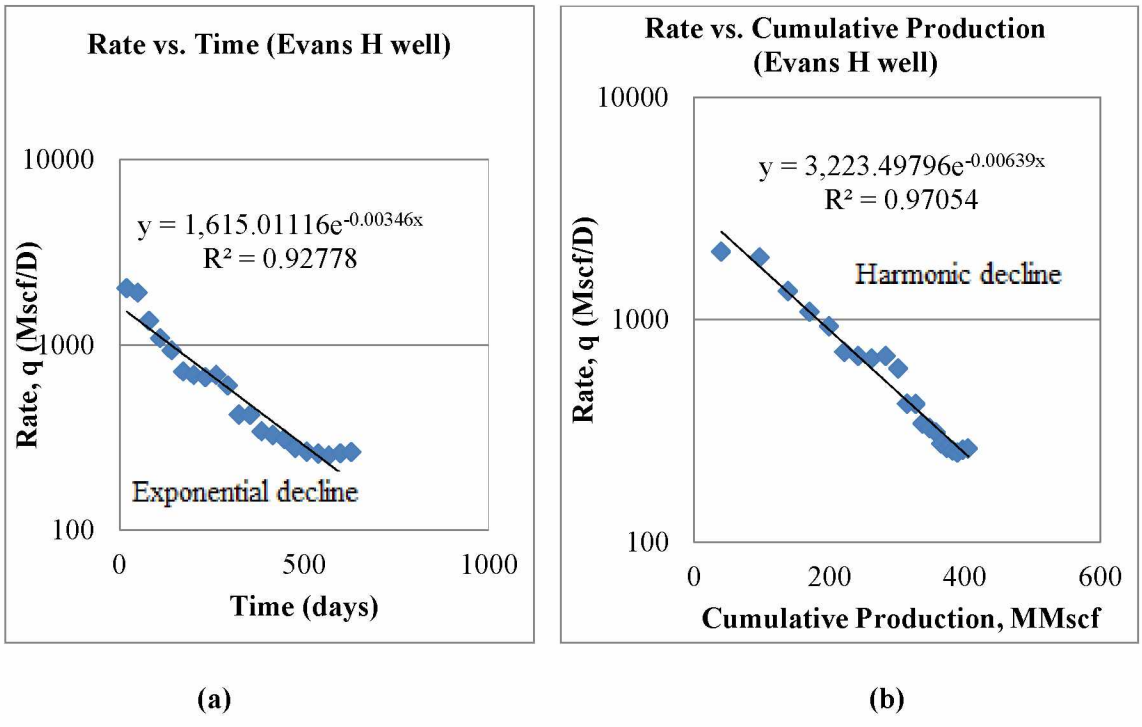

Figure 4.3: Decline curve diagnostic plots for well #1, Evans H unit/well (LaSalle)

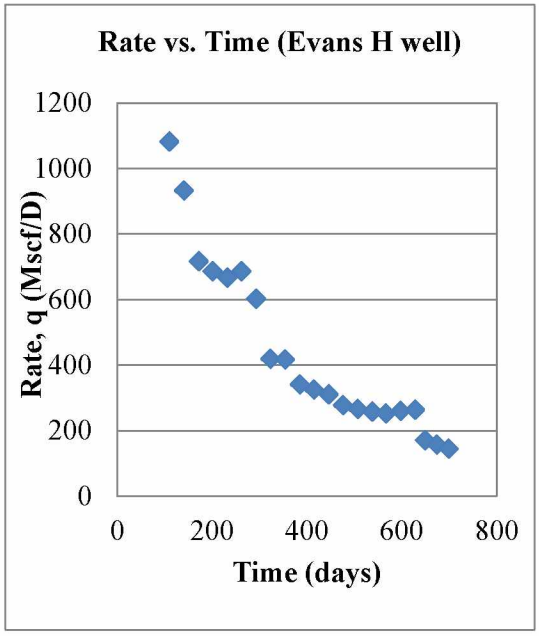

(c)

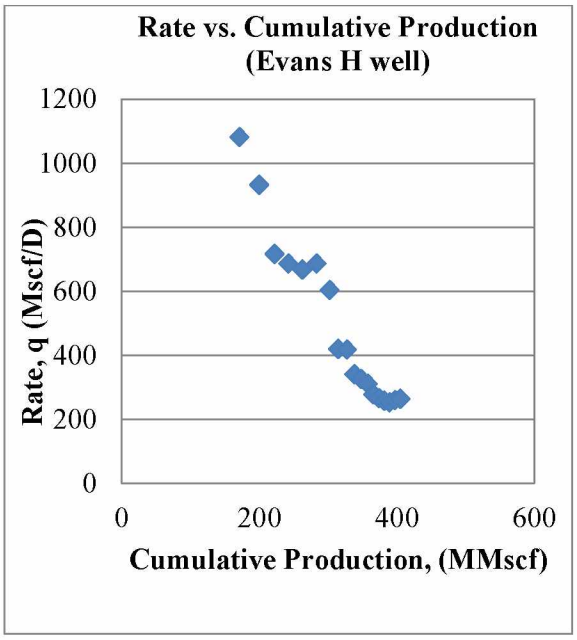

(d)

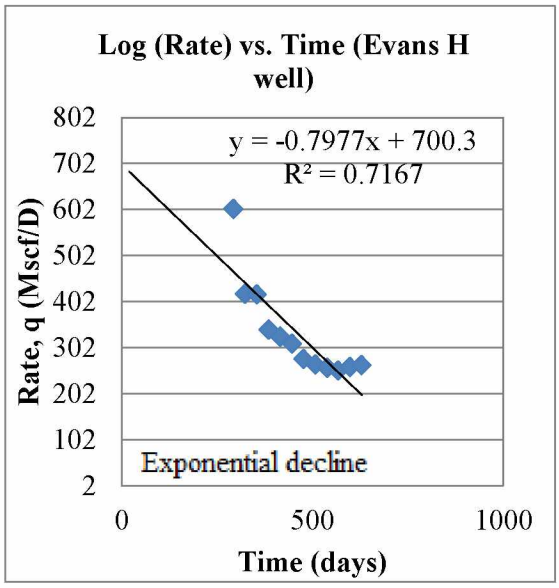

(e)

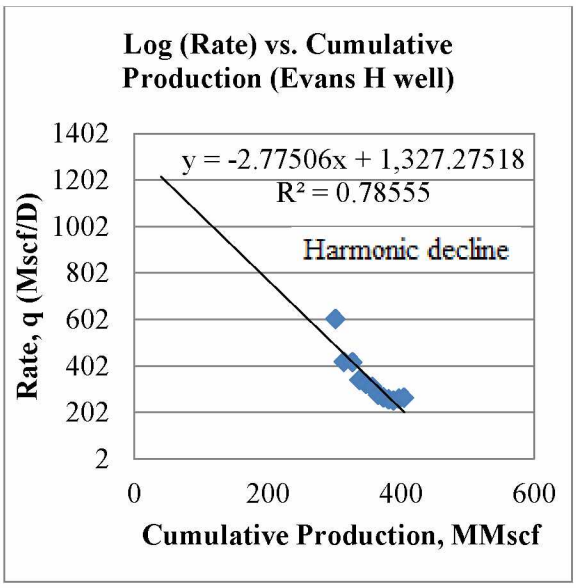

(f)

Figure 4.3-Continued.

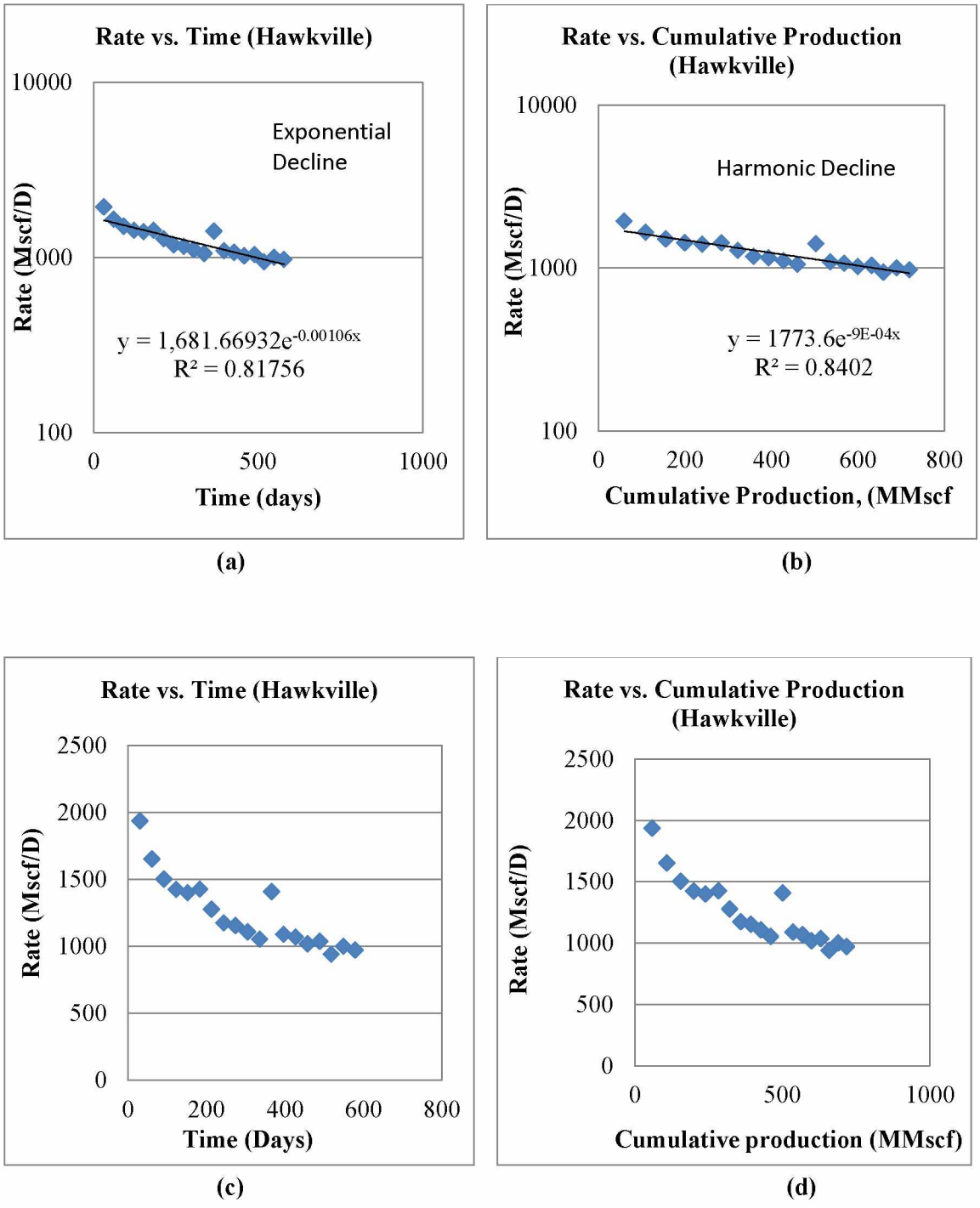

Figure 4.4: Decline curve diagnostic plots for well #1, Hawkville unit (LaSalle)

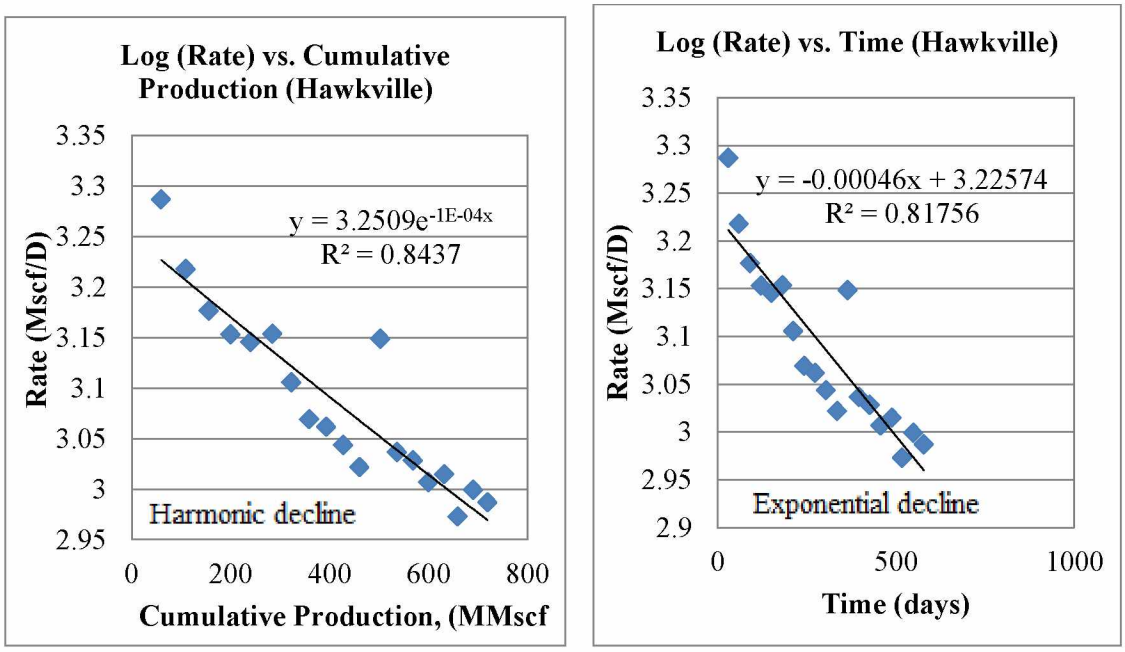

(e) (f)

Figure 4.4-Continued.

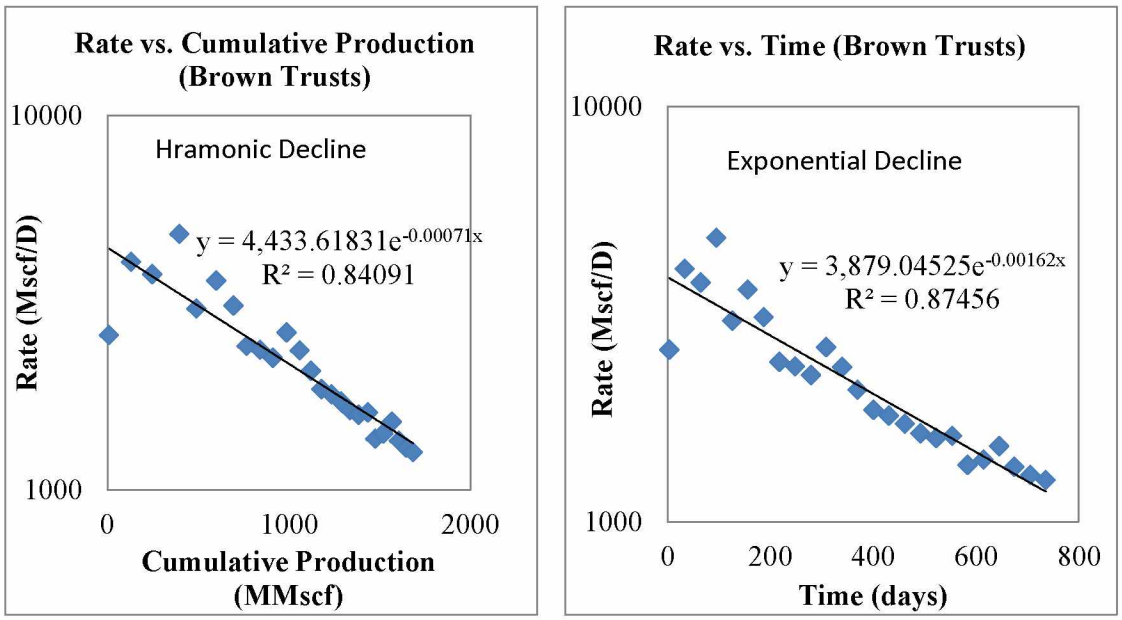

(a) (b)

Figure 4.5: Decline curve diagnostic plots for well #1, Brown Trusts unit/well (LaSalle)

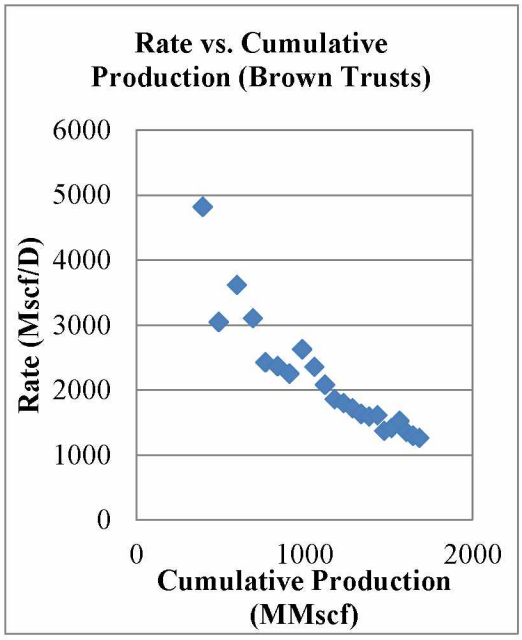

(c)

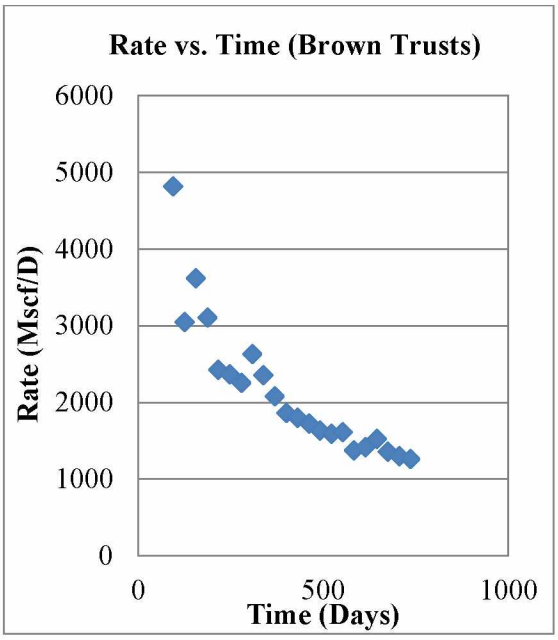

(d)

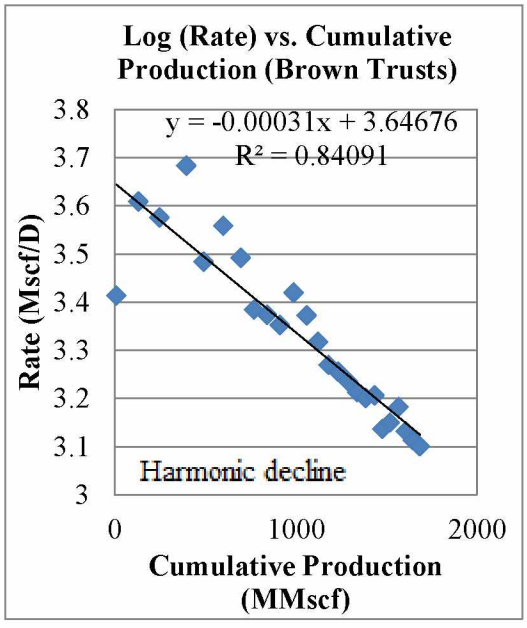

(e)

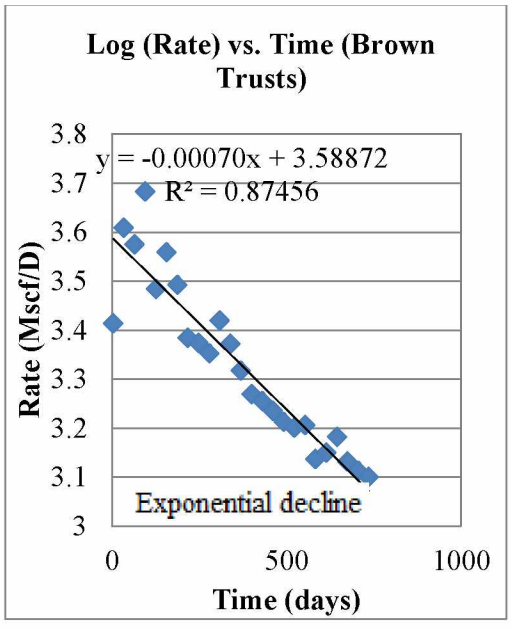

(f)

Figure 4.5-Continued.

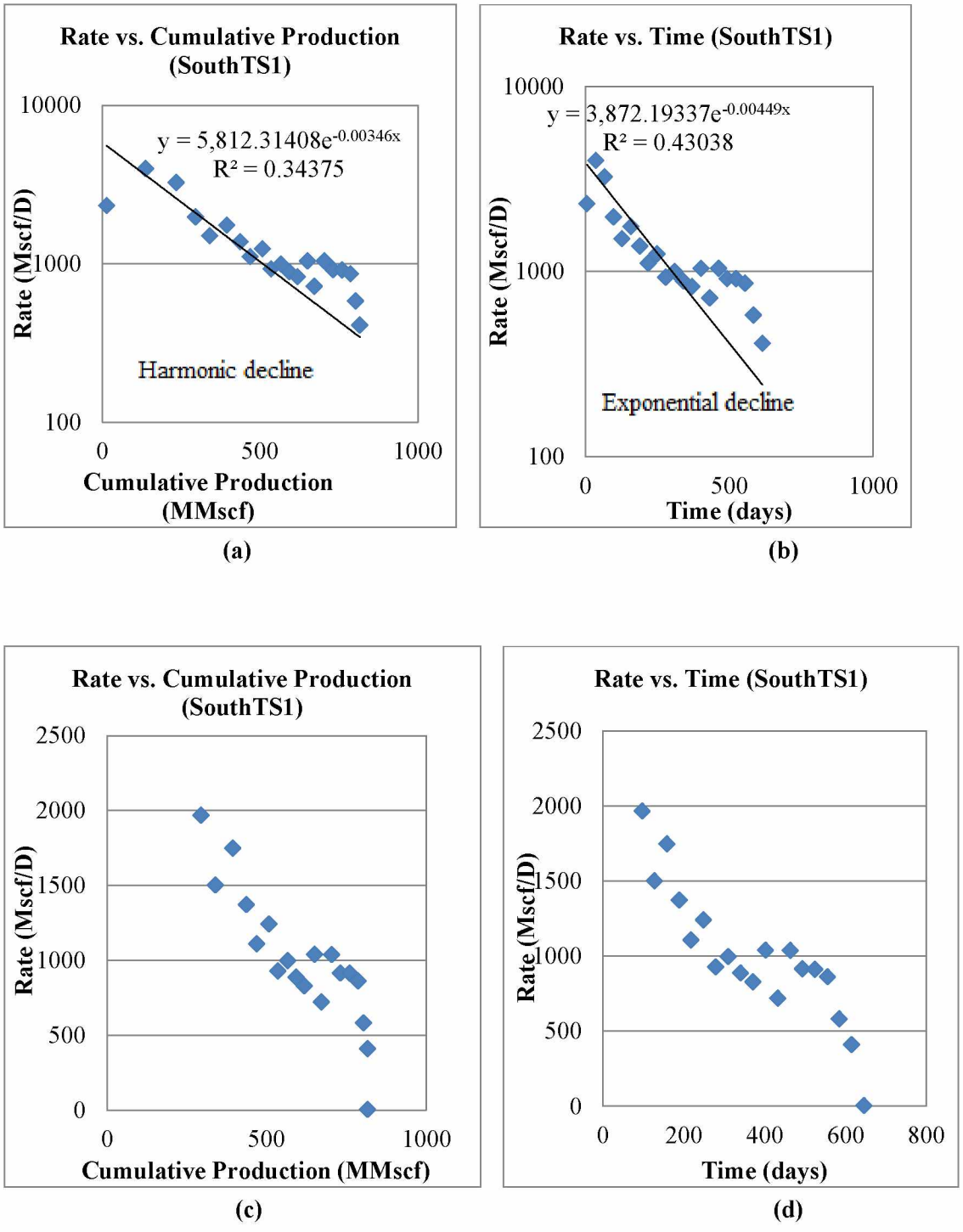

Figure 4.6: Decline curve diagnostic plots for well #1, South T. S unit/well (LaSalle County)

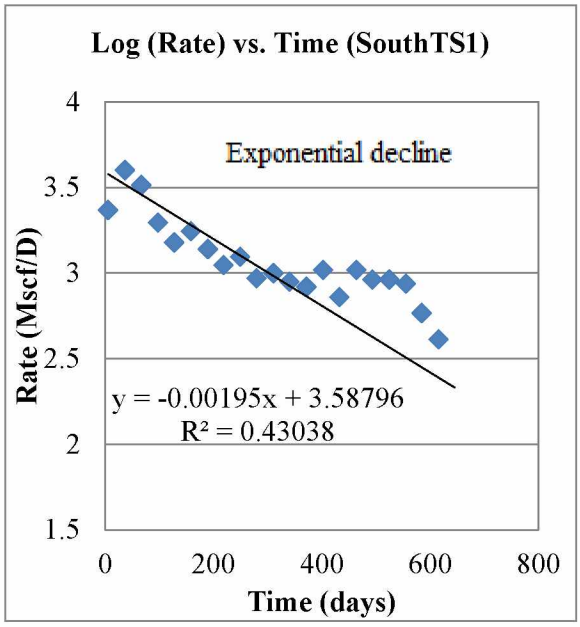

(e)

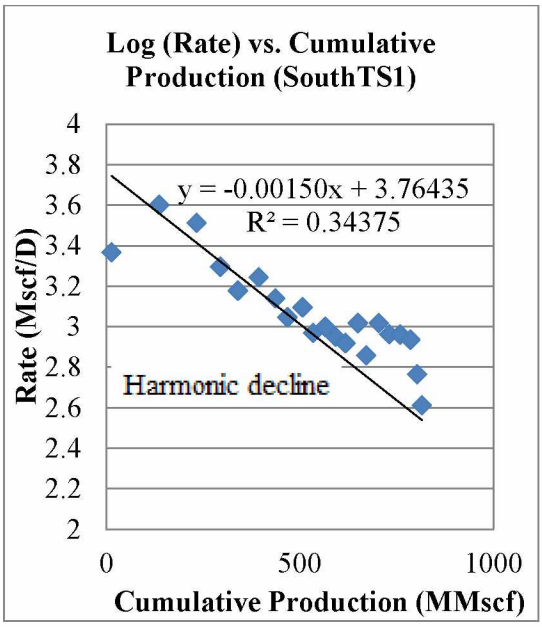

(f)

Figure 4.6-Continued.

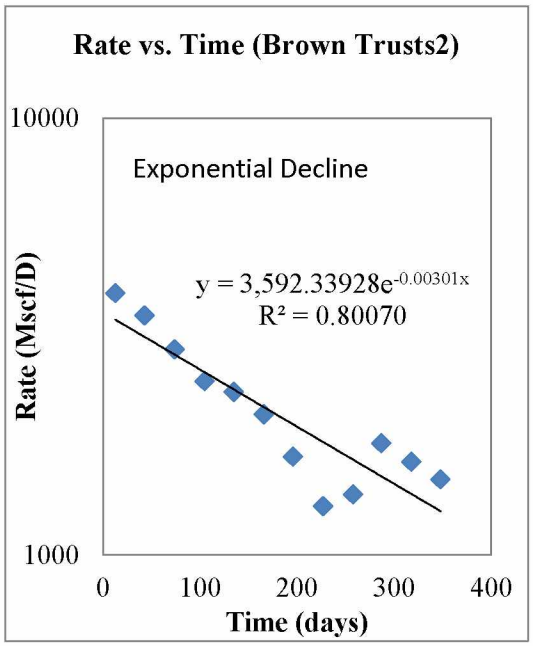

(a)

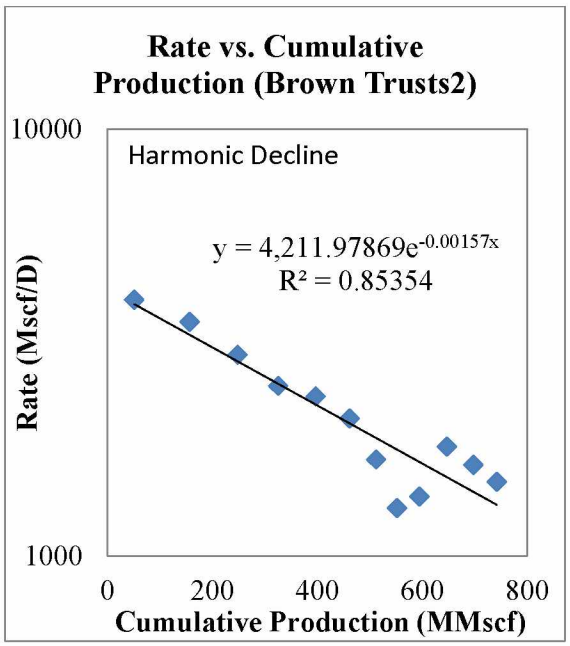

(b)

Figure 4.7: Decline curve diagnostic plots for well #1, Brown Trusts2 unit/well (LaSalle County)

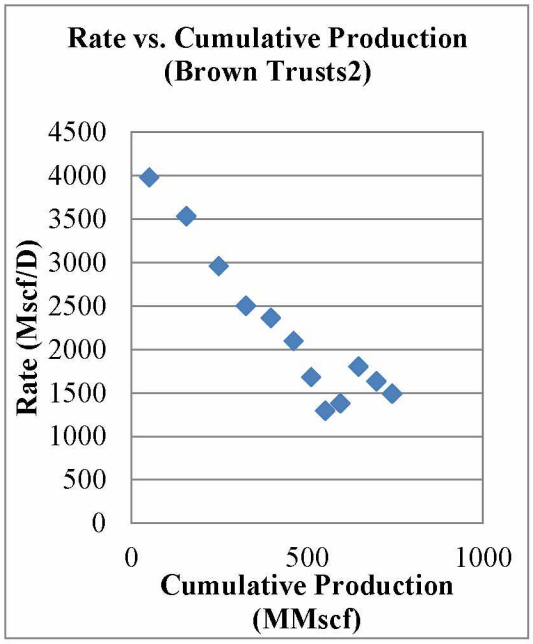

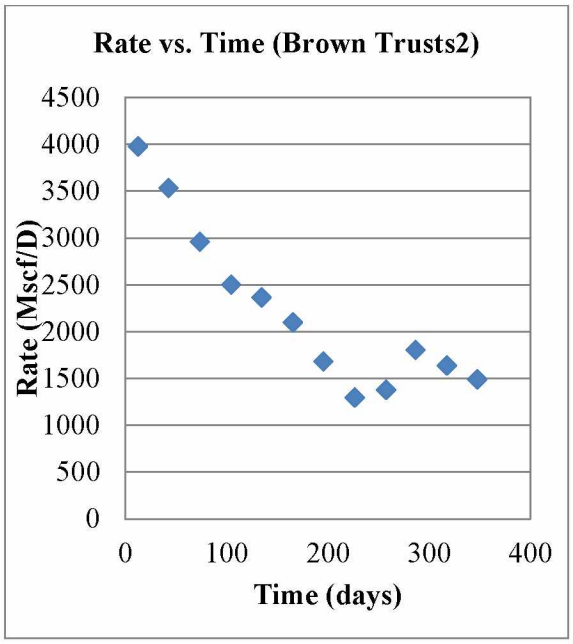

(c) (d)

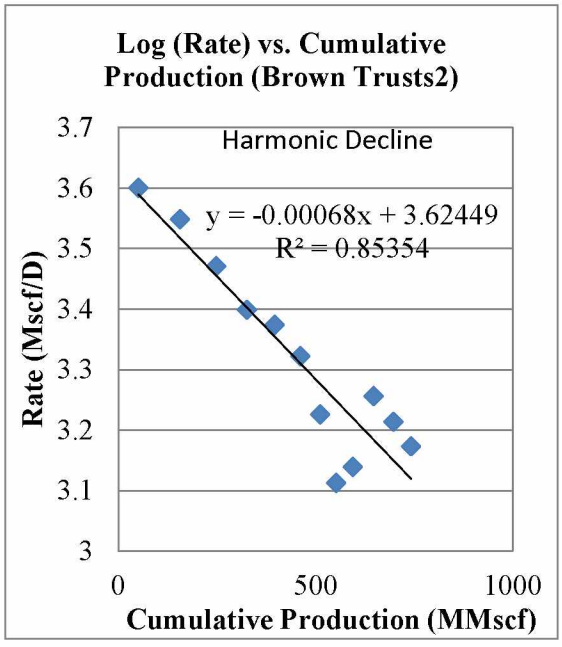

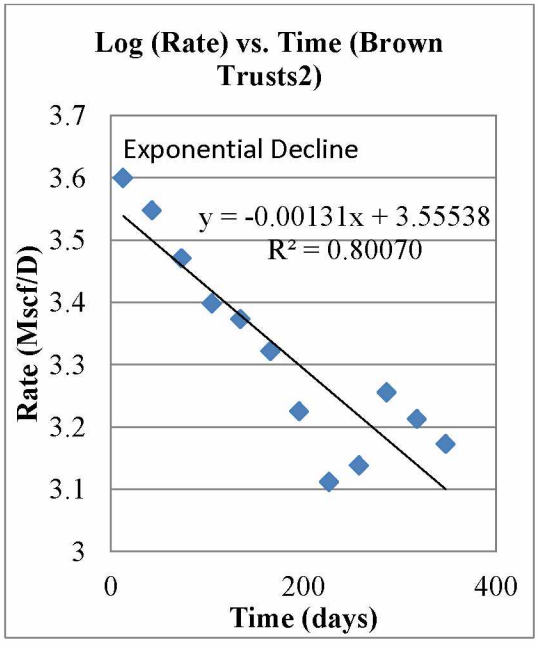

(e) (f)

Figure 4.7-Continued.

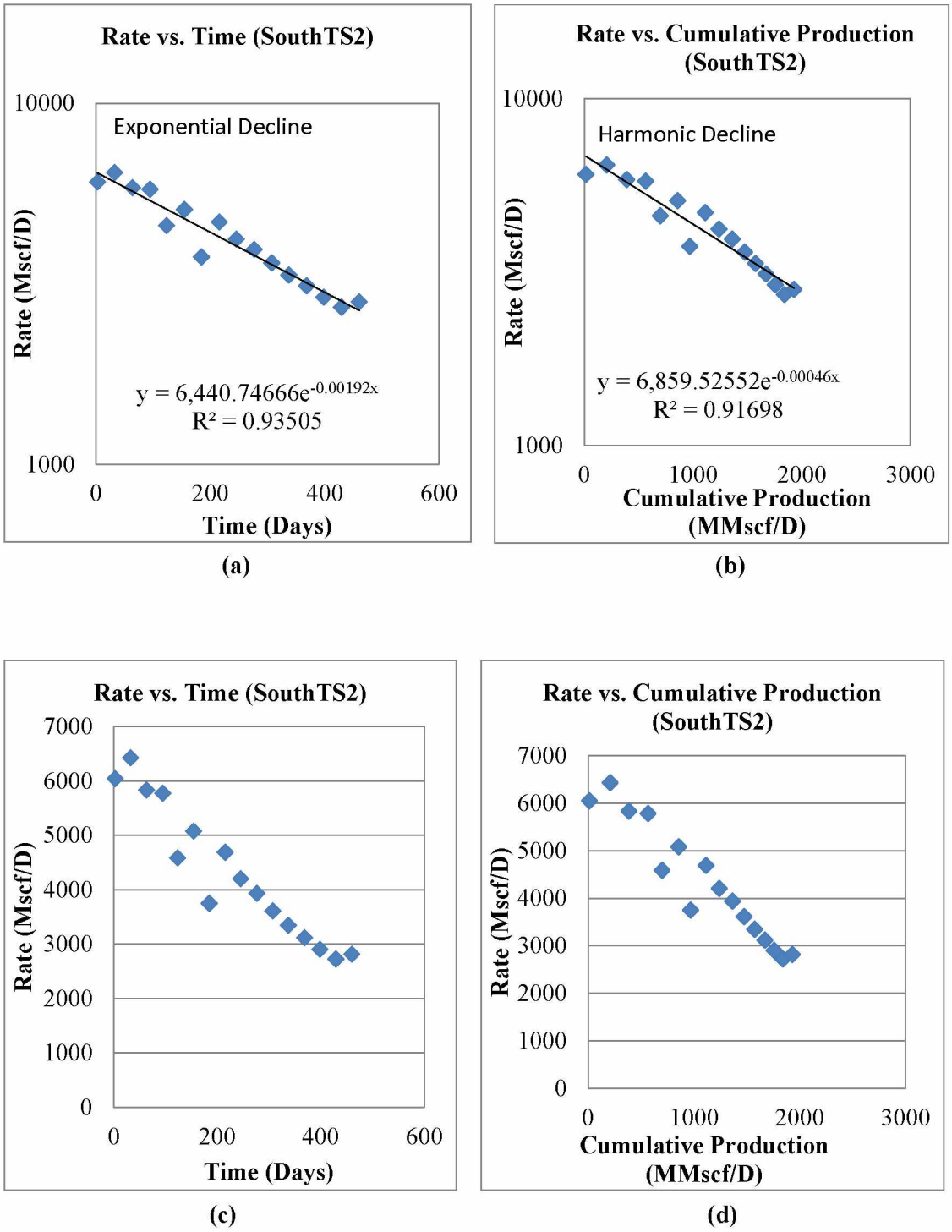

Figure 4.8: Decline curve diagnostic plots for well #1, South TS2 unit/well (LaSalle County)

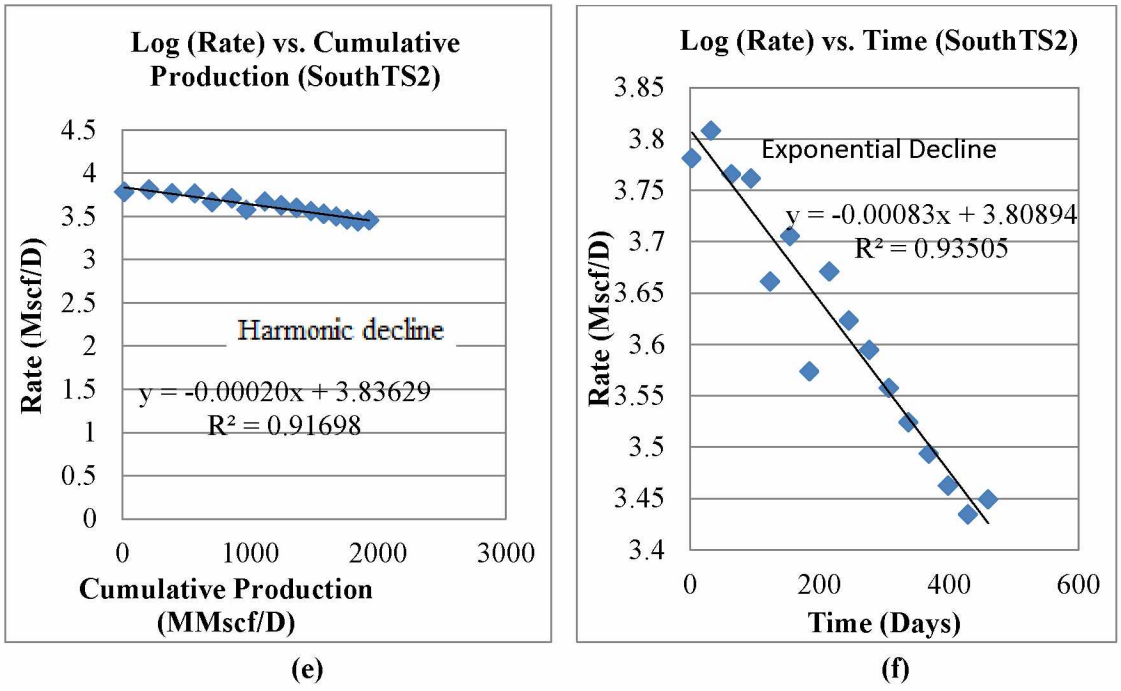

Figure 4.8-Continued.

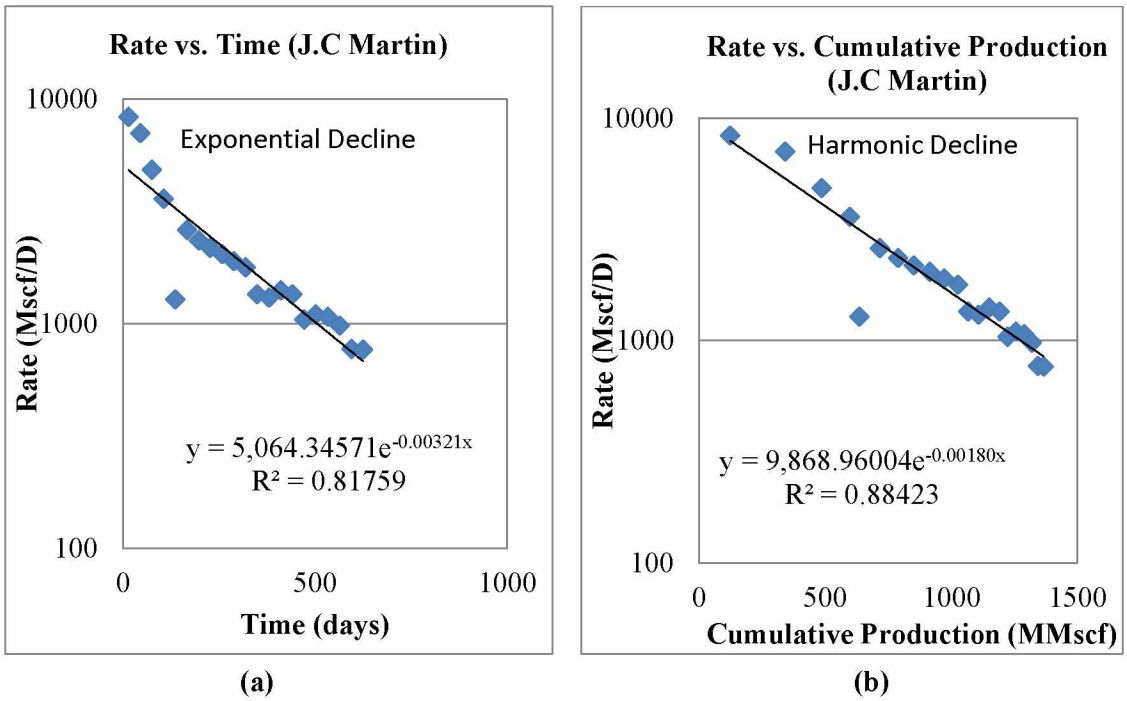

Figure 4.9: Decline curve diagnostic plots for well #1, J.C Martin unit/well (LaSalle County)

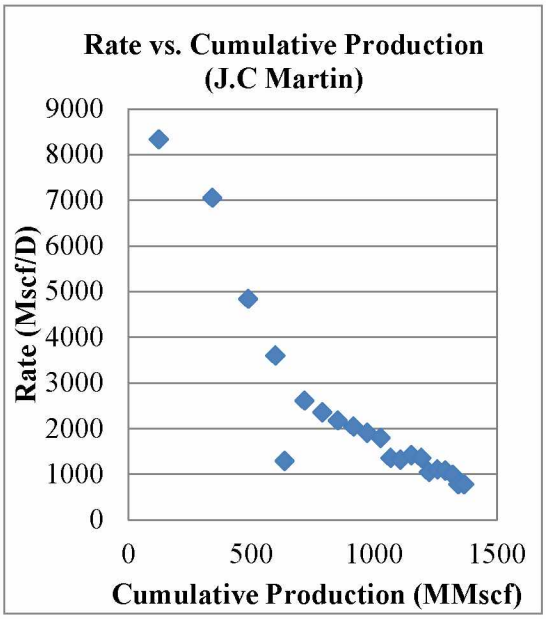

(c)

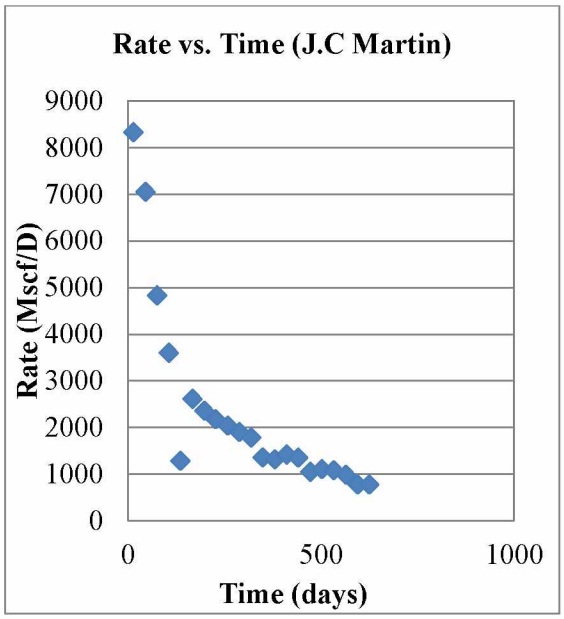

(d)

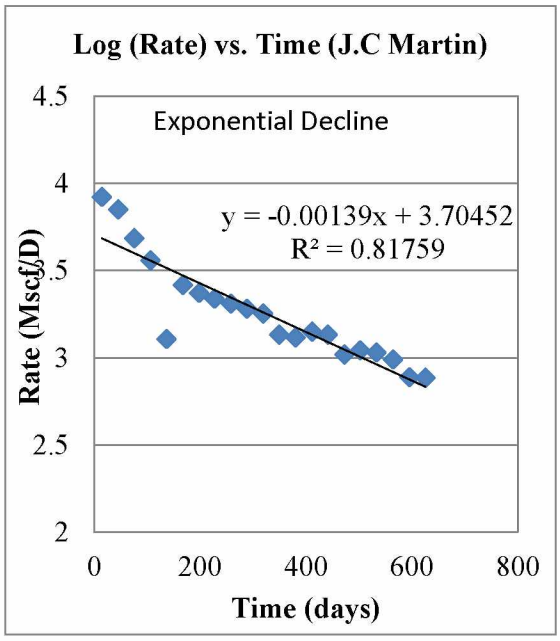

(e)

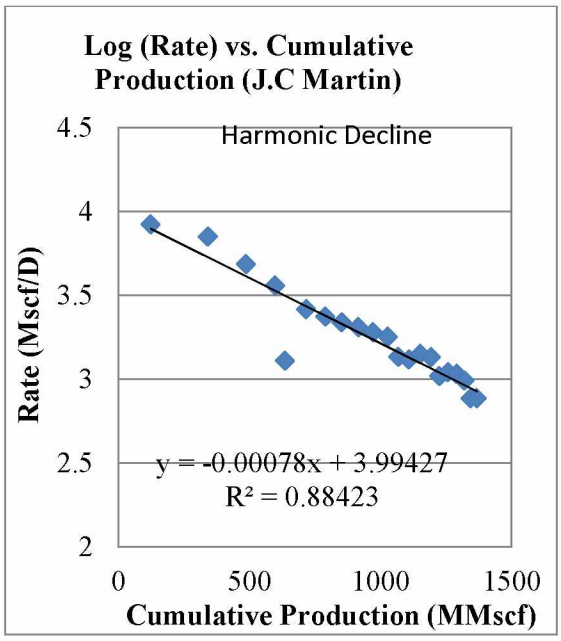

(f)

Figure 4.9-Continued.

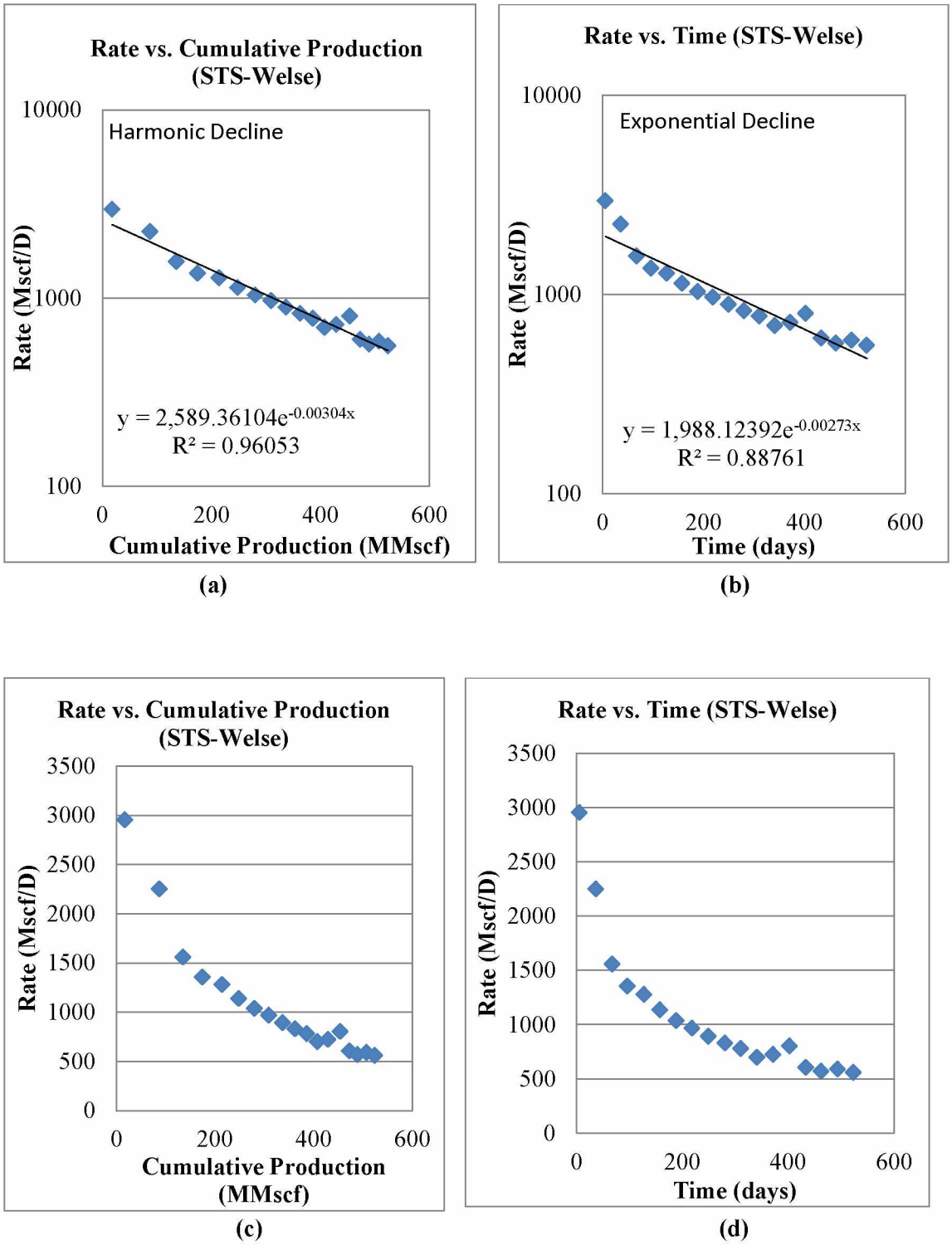

Figure 4.10: Decline curve diagnostic plots for well #1, STS-Welse unit/well (LaSalle County)

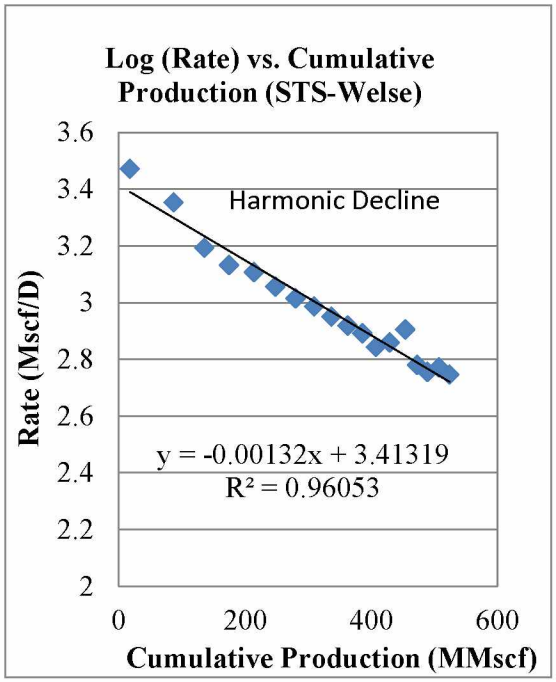

(e)

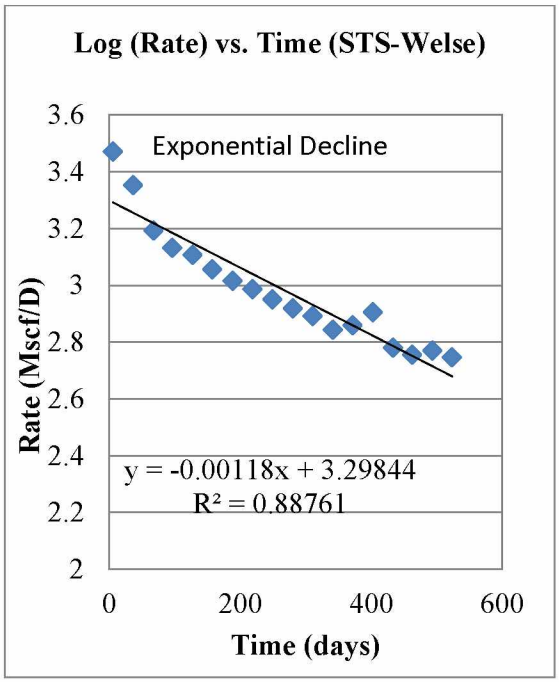

(f)

Figure 4.10-Continued.

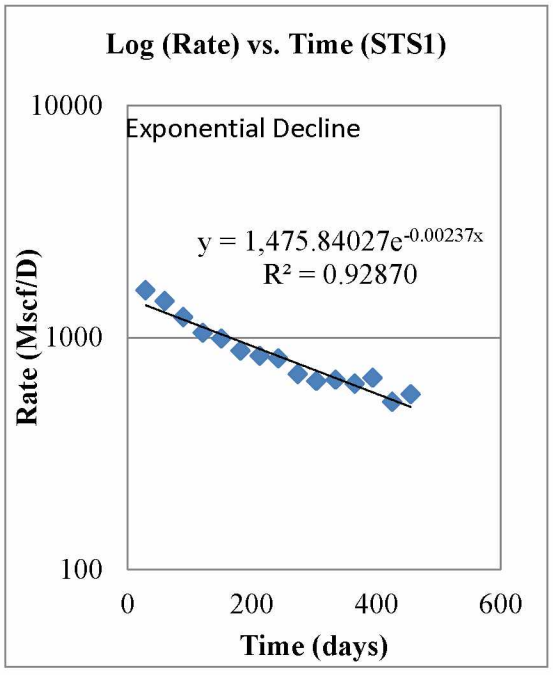

(a)

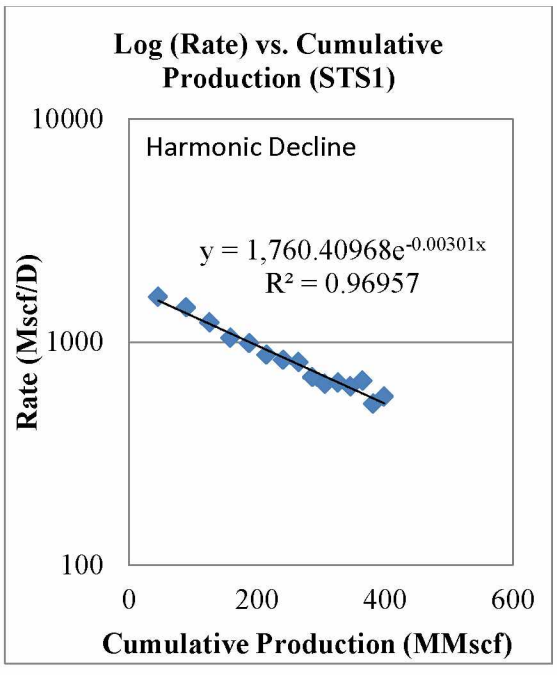

(b)

Figure 4.11: Decline curve diagnostic plots for well #1, STS1 unit/well (LaSalle County)

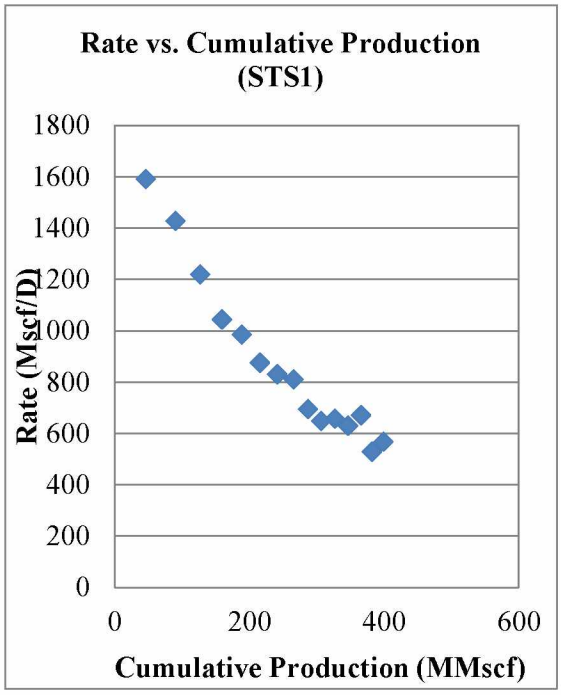

(c)

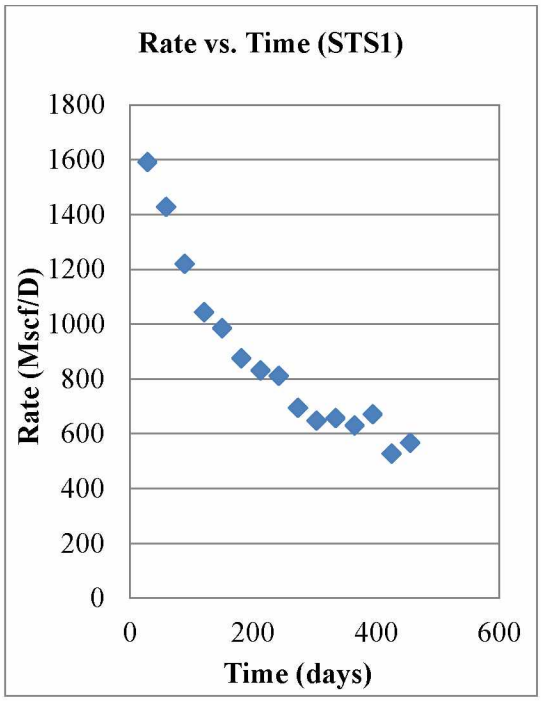

(d)

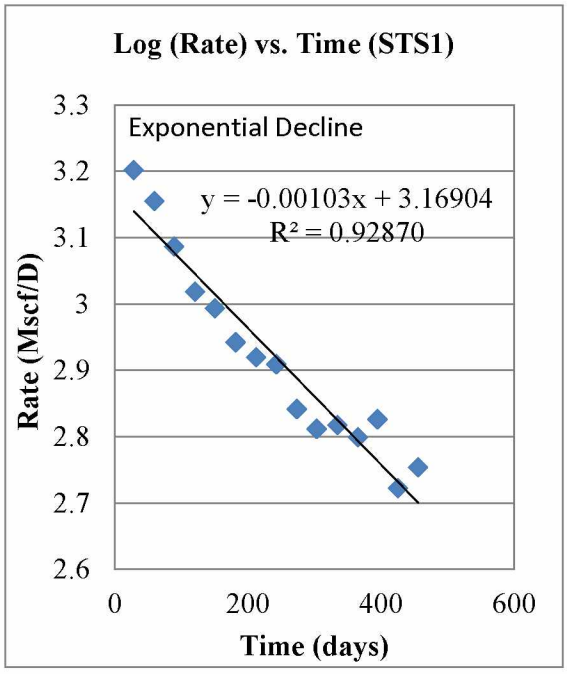

(e)

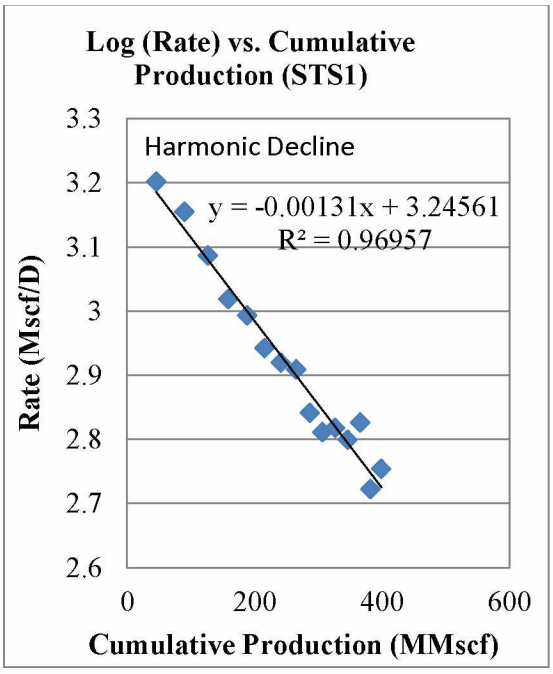

(f)

Figure 4.11-Continued.

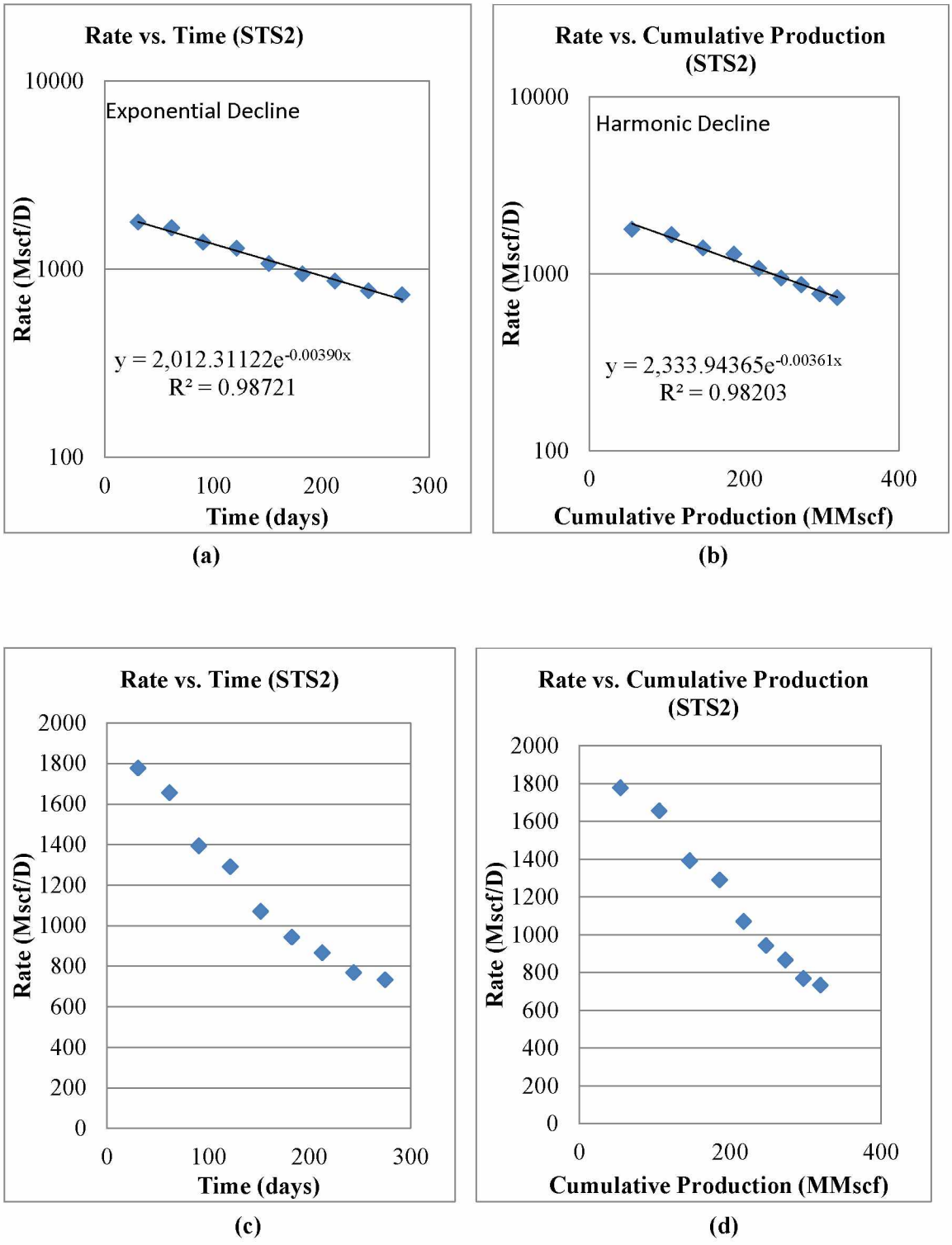

Figure 4.12: Decline curve diagnostic plots for well #1, STS 2 unit/well (LaSalle County)

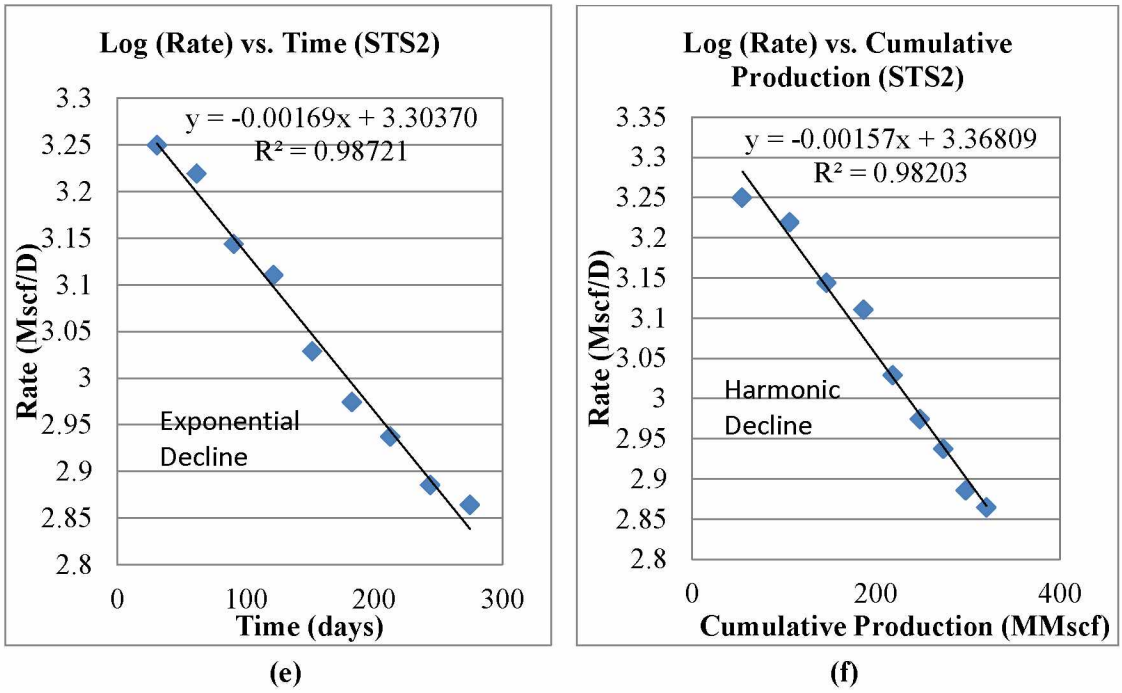

Figure 4.12-Continued.

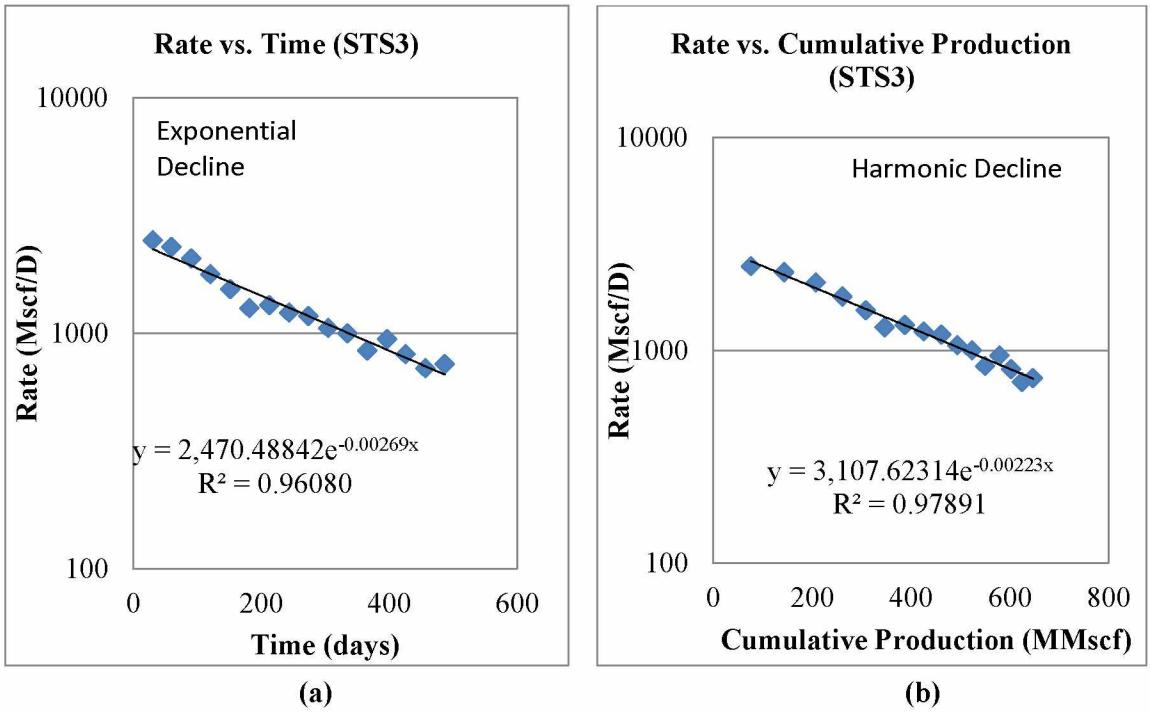

Figure 4.13: Decline curve diagnostic plots for well #1, STS 3 unit/well (LaSalle County)

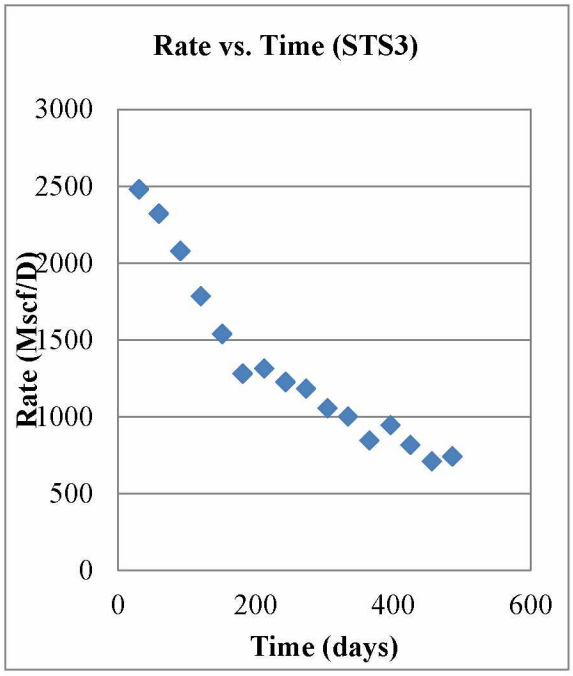

(c)

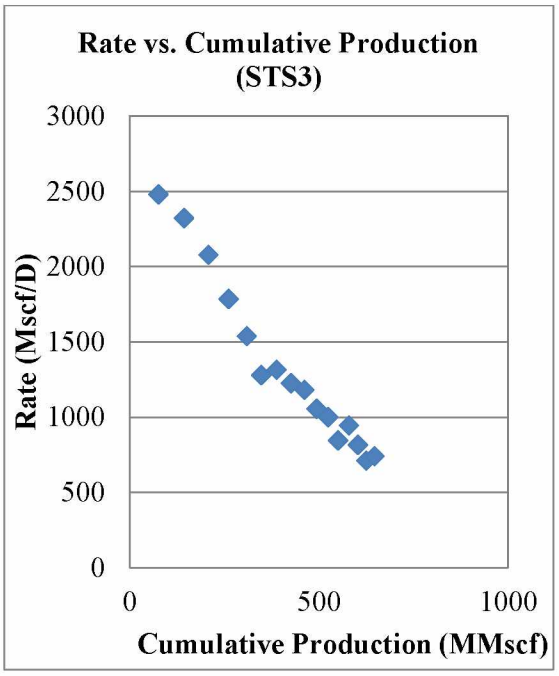

(d)

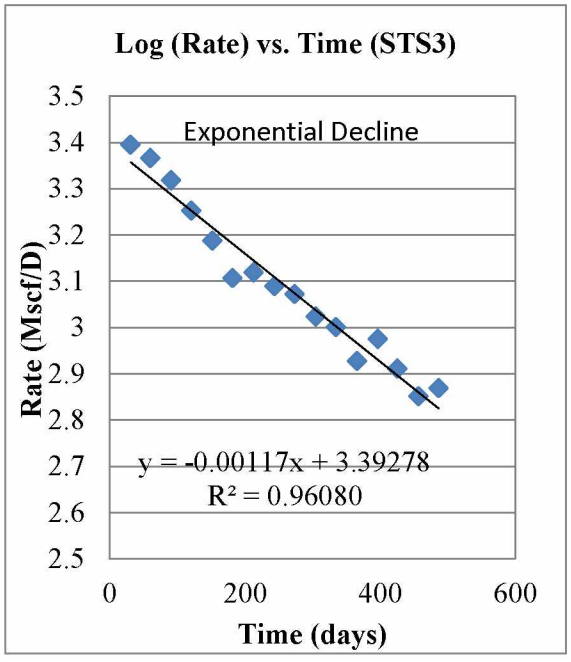

(e)

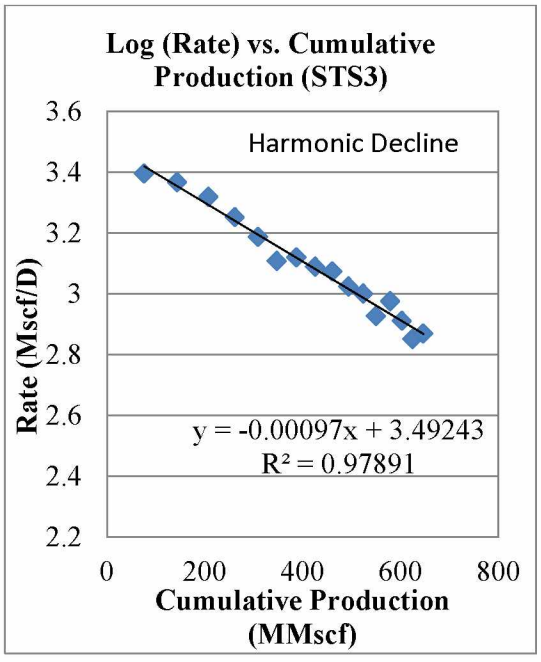

(f)

Figure 4.13-Continued.

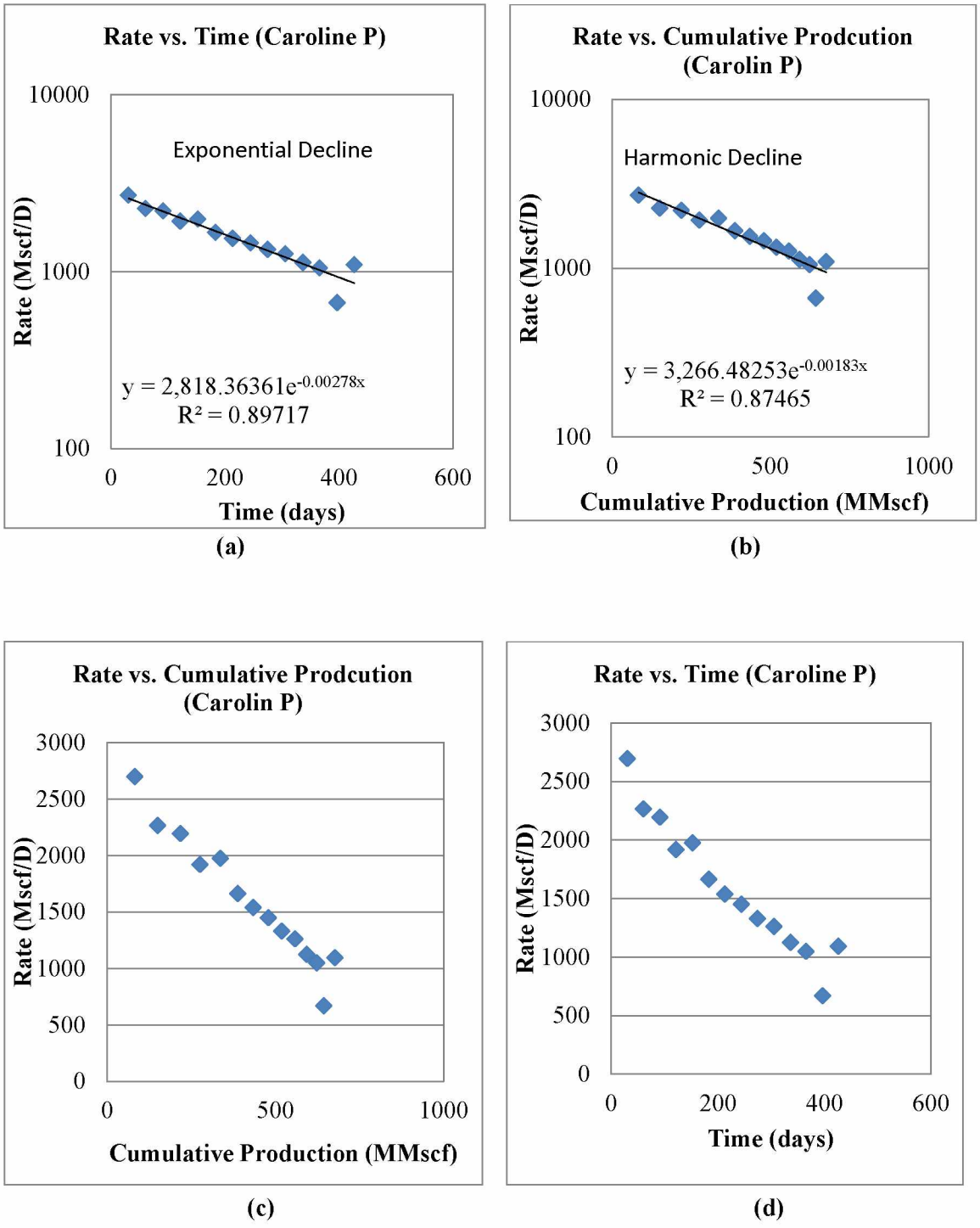

Figure 4.14: Decline curve diagnostic plots for well #1, Caroline P unit/well (LaSalle County)

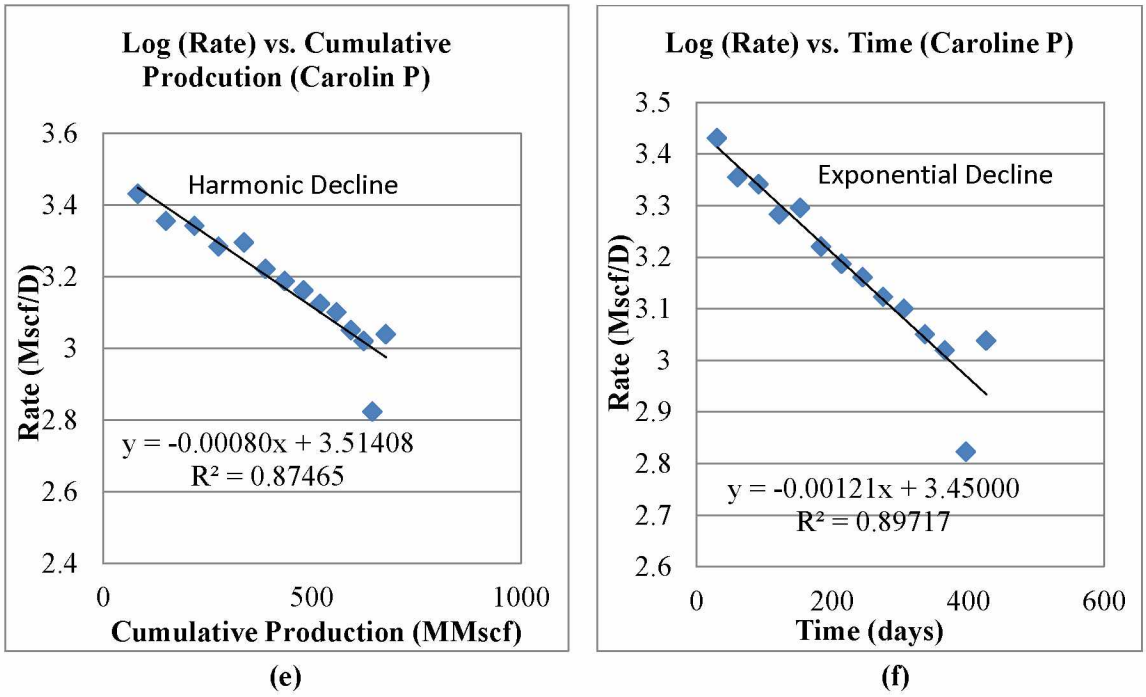

Figure 4.14-Continued.

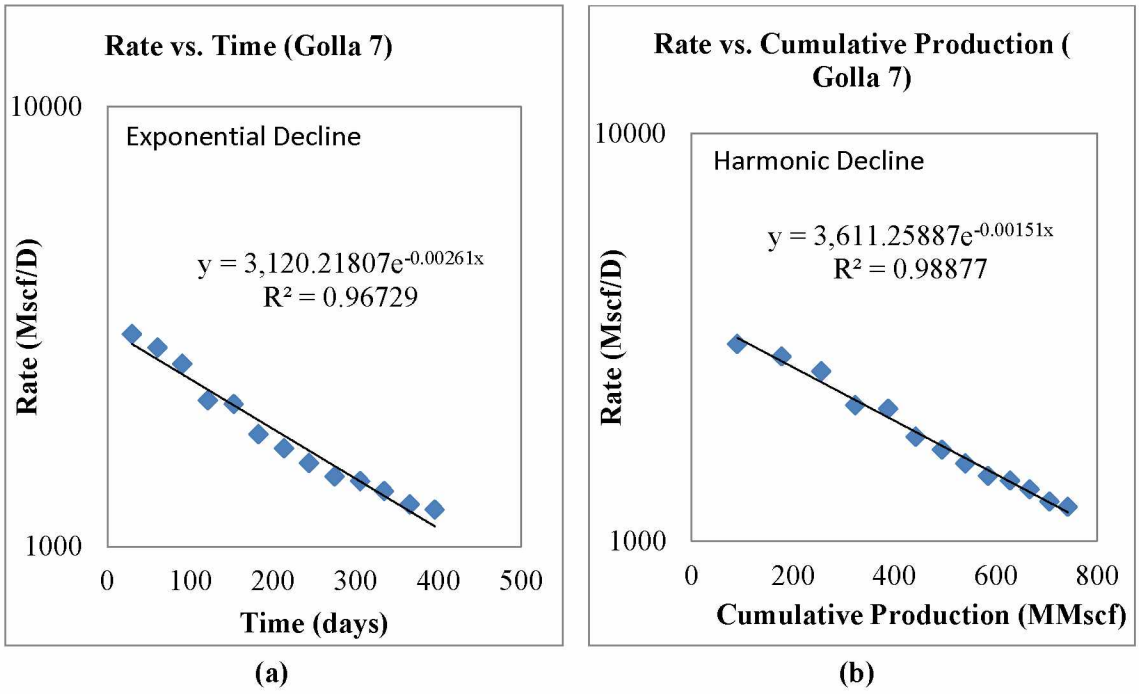

Figure 4.15: Decline curve diagnostic plots for well #1, Golla 7 unit/well (LaSalle County)

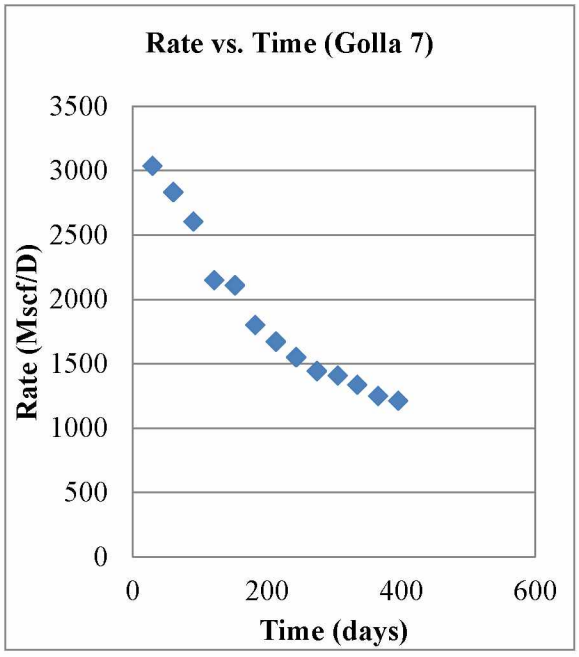

(c)

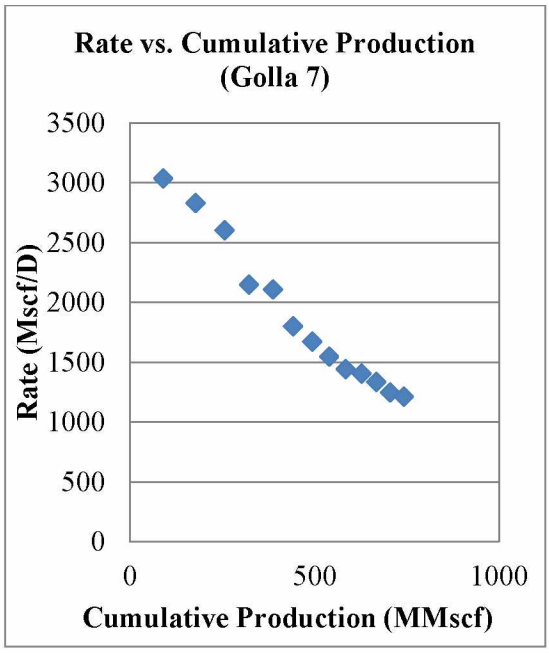

(d)

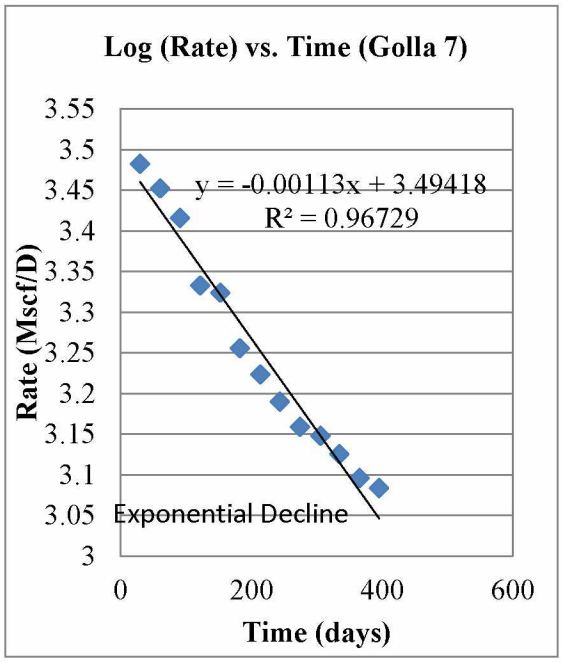

(e)

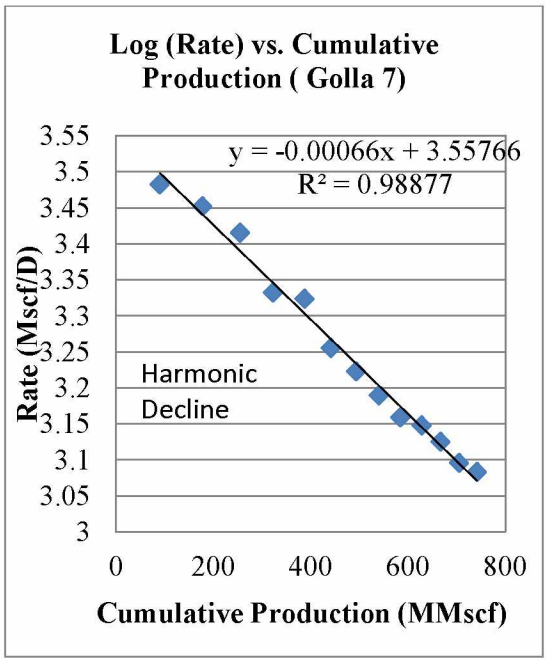

(f)

Figure 4.15-Continued.

The highest and lowest reserves from the harmonic decline analysis was 85,584 MMscf and 13 MMscf while that for exponential decline was 46 MMscf and 3343 MMscf (for production to economic limit of 25 Mscf/day) respectively for all the wells analyzed in the LaSalle County (Tables 4.8 and 4.14). The harmonic model gave a lower minimum reserve and a higher maximum reserve which is inconsistent. This can be attributed to very short production history and adds to the need for the use of simulation models.

There is little or no apparent correlation between cumulative production during the first nine months and completion type or length of horizontal leg and number of fracture stages (Figures 4.16-4.17). This may be due to variations in reservoir quality or very short production data and makes the use of simulation models necessary for further investigation.

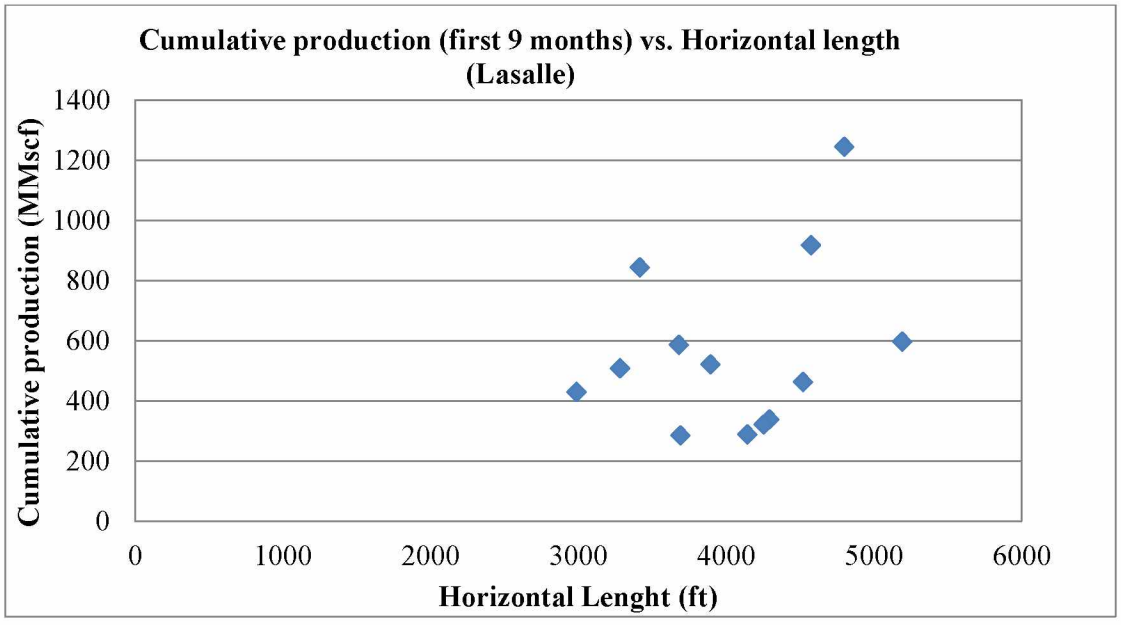

Figure 4.16: Cumulative production (first 9 months) versus Horizontal length (LaSalle)

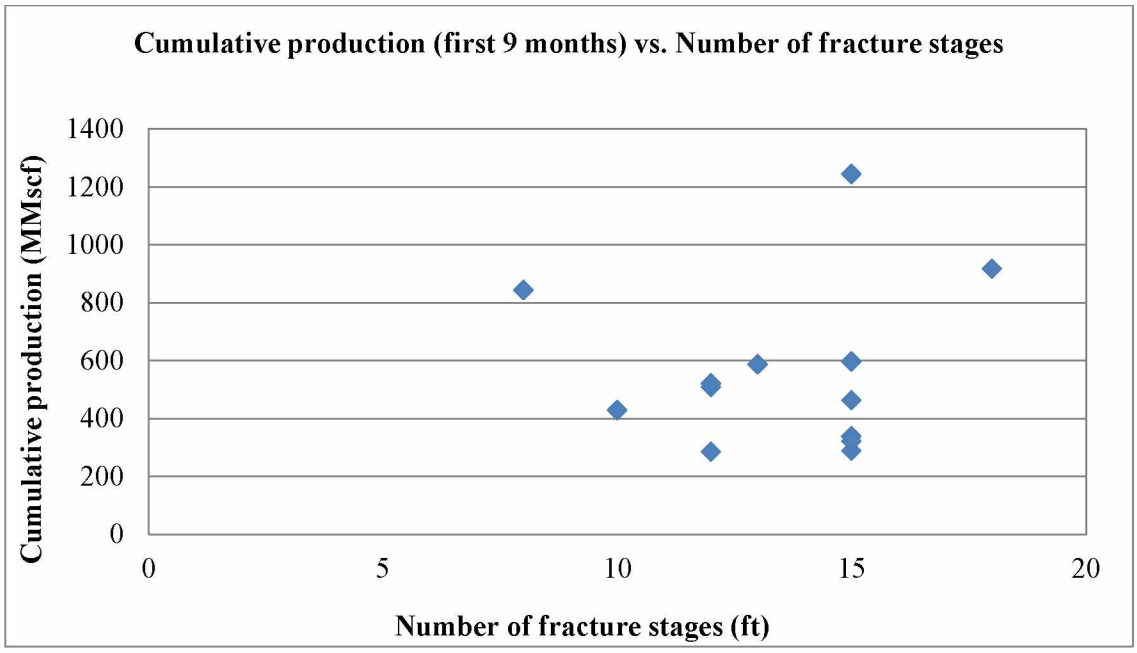

Figure 4.17: Cumulative production versus number of fracture stages for the first 9 months (LaSalle)

4.3 Live Oak County

The Live Oak County is located east of LaSalle county and in the central part of the Eagle Ford play trend (Figure 4.1). Production is currently only from the Sugarcane Field; the field has a medium cumulative gas production of approximately 8,604,000 Mscf as of 03/2012 (this is the reported total production from all the wells at the Live Oat County).

4.3.1 Observations

Decline curve analysis was performed on production data from 6 wells in the Live Oak County. The production histories of some of the wells were quite erratic as shown in Figures 4.18, 4.19 and 4.23. This made the use of DCA almost impractical. Only 3 wells gave straight lines for the semi-log rate vs. time and rate vs. cumulative production plot (Figures 4.20-4.22). Figures 4.20-4.22 showed that the production data matched both the exponential and harmonic models. The

highest and lowest estimated reserves (i.e. reserves till production limit of 25 Mscf/D) from the harmonic decline are 1580 MMscf and 1743 MMscf respectively while that for the exponential decline are 496 MMscf and 504 MMscf.

4.3.2 Discussion and interpretation of plots

The erratic behavior exhibited by the production data shown in Figures 4.18, 4.19 and 4.23 can be attributed to variations in reservoir quality. This emphasizes the need for the use of simulation models to obtain future production forecasts. Figures 4.20-4.22 show that the production data matched both the exponential and harmonic models; this presents a challenge of which model to reliably use for future production forecasts. The use of simulation models will help to generate a longer production and thus give a better production forecast.

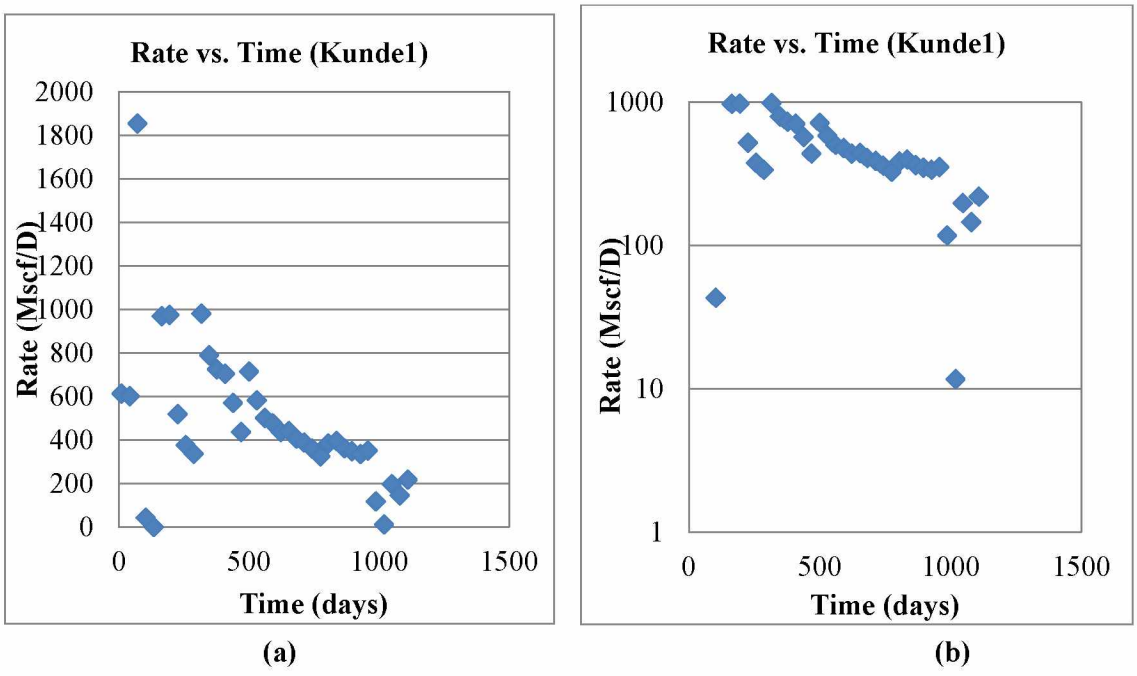

Figure 4.18: Decline curve diagnostic plots for well #1, Kunde 1 unit/well (Live Oak County)

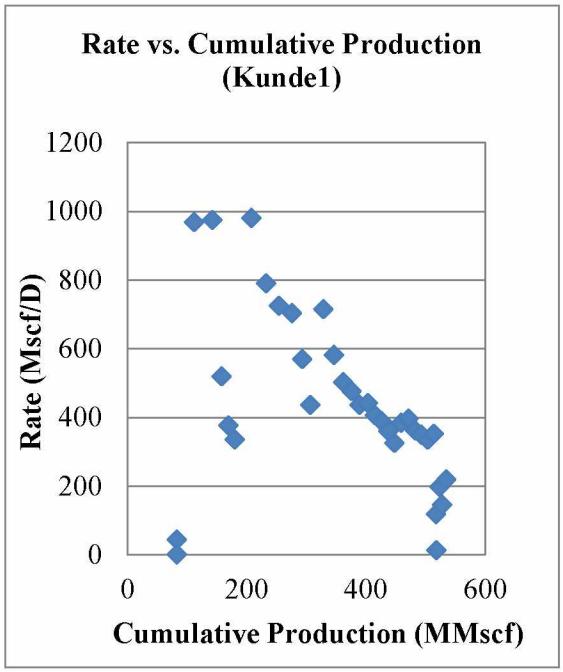

(c)

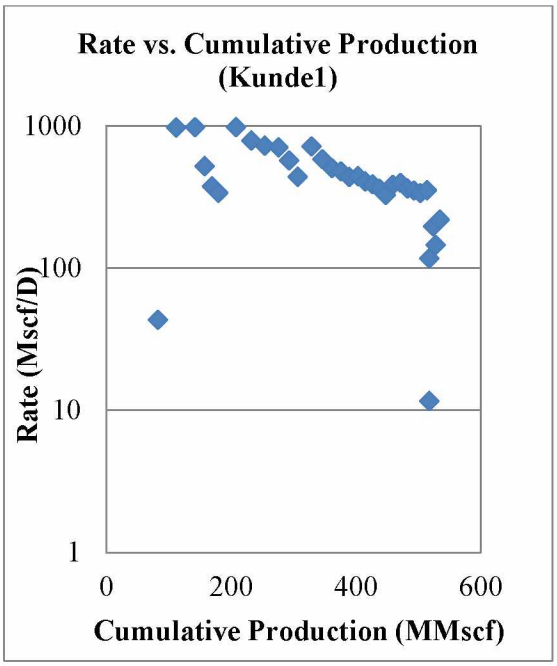

(d)

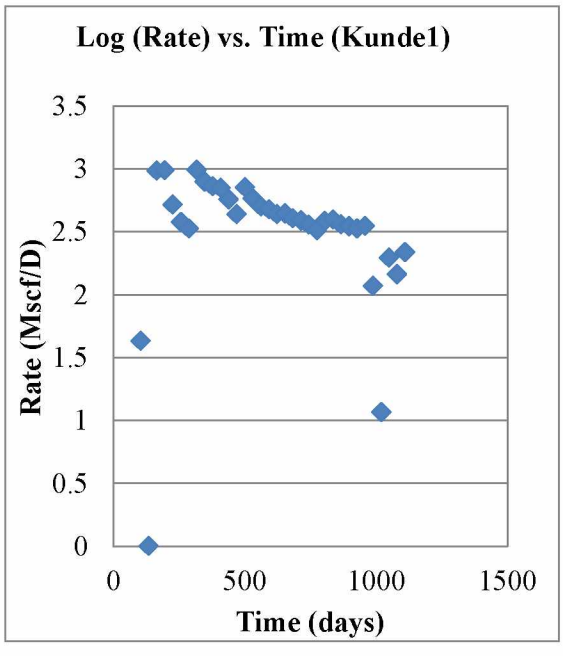

(e)

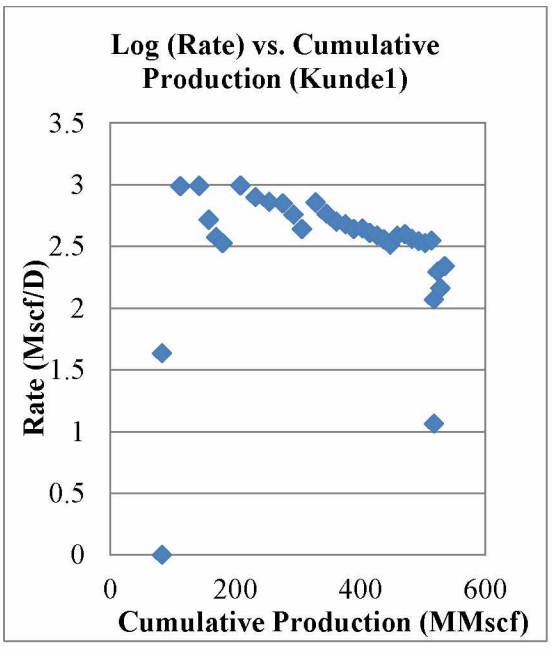

(f)

Figure 4.18-Continued.

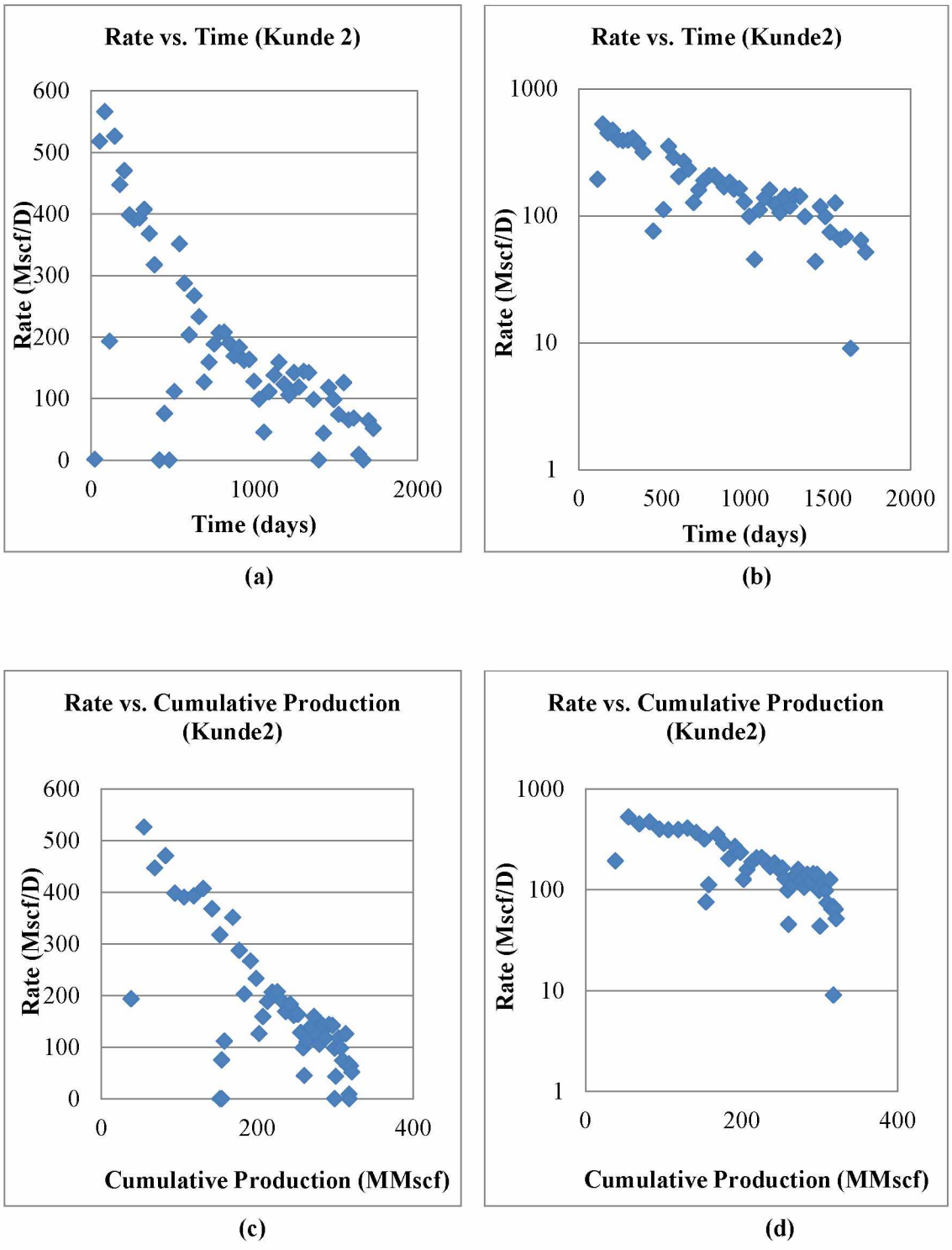

Figure 4.19: Decline curve diagnostic plots for well #1, Kunde 2 unit/well (Live Oak)

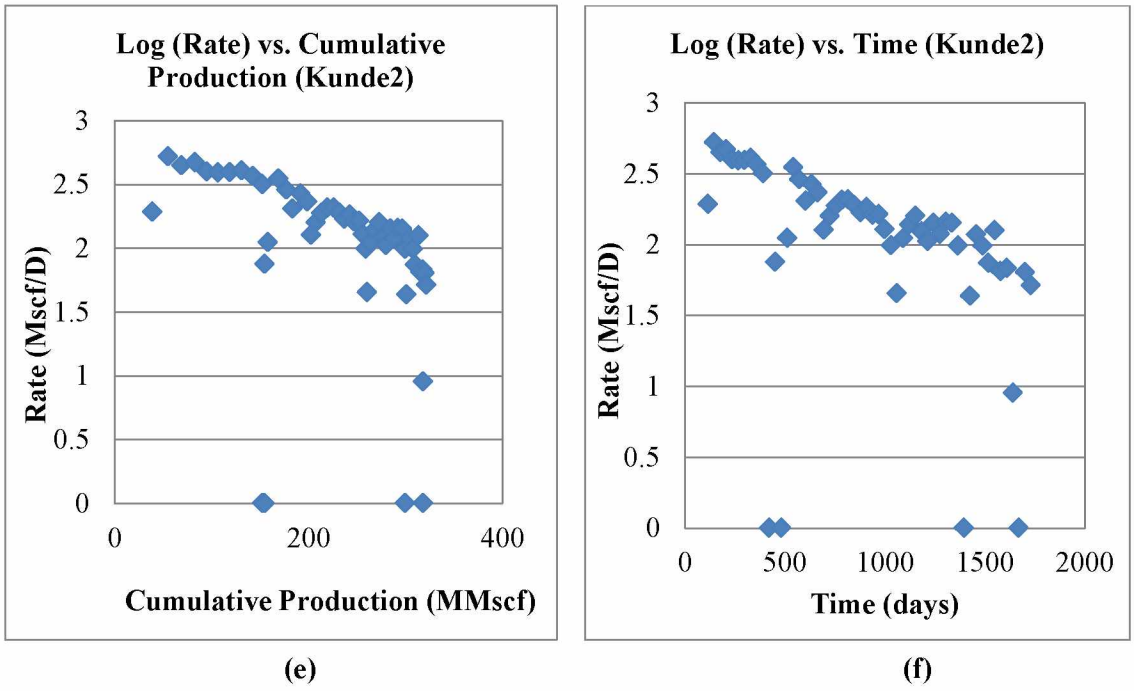

Figure 4.19-Continued.

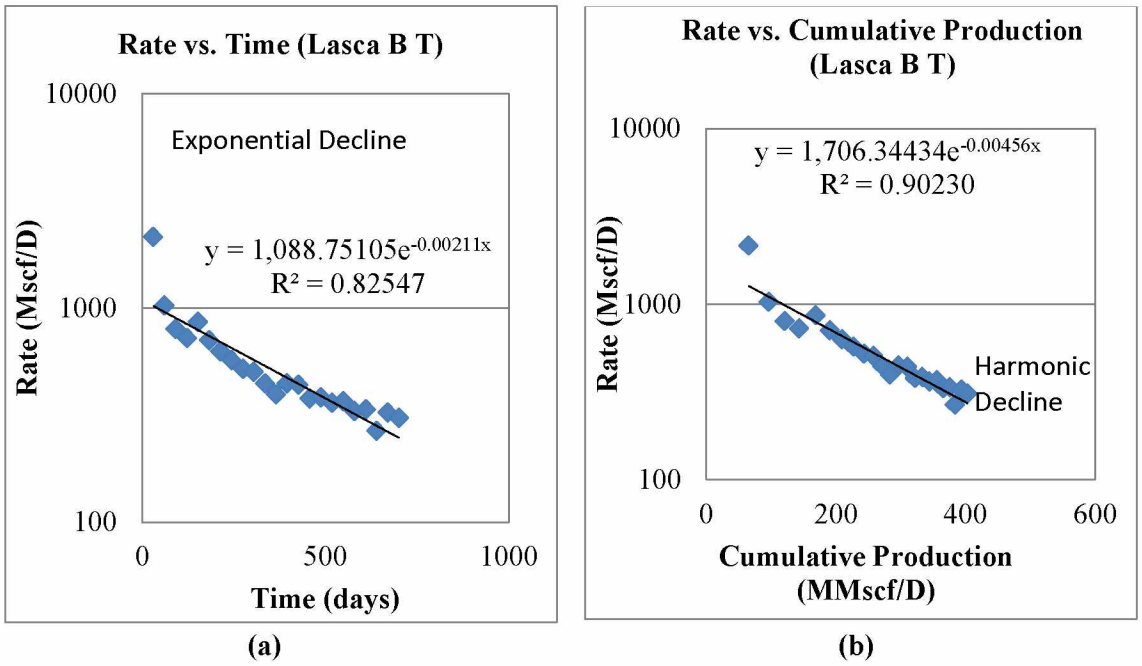

Figure 4.20: Decline curve diagnostic plots for well #1, Lasca B T unit/well (Live Oak)

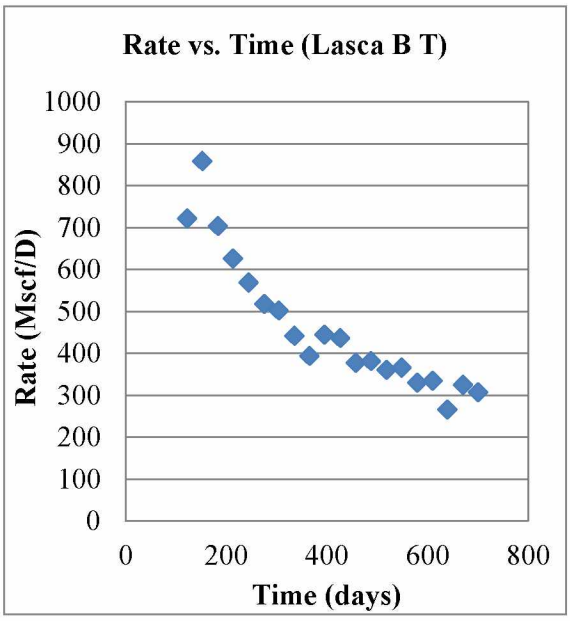

(c)

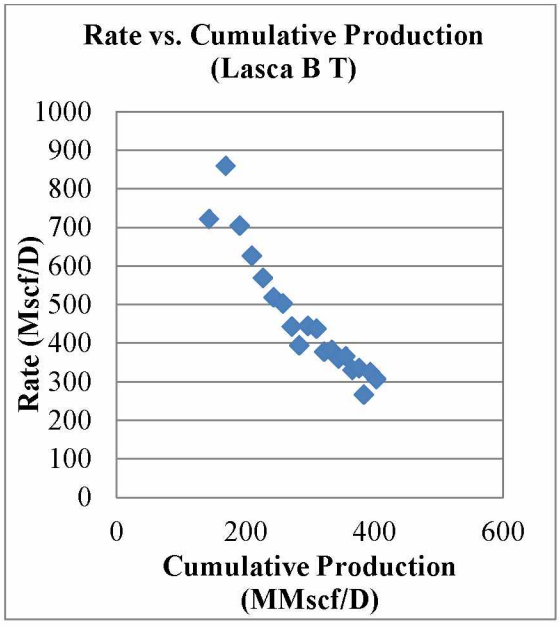

(d)

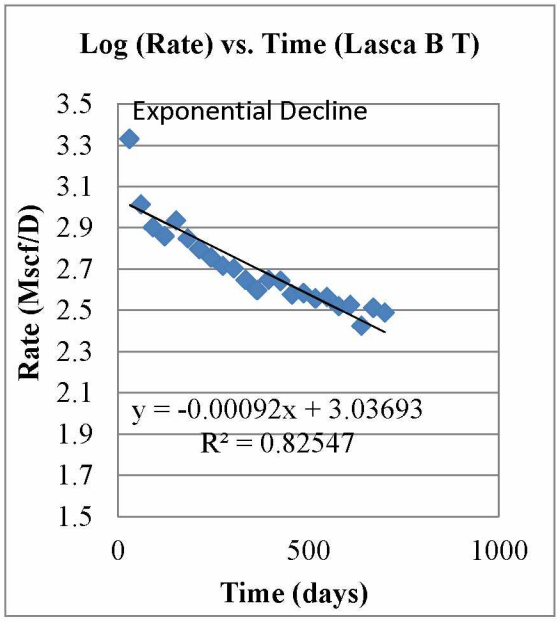

(e)

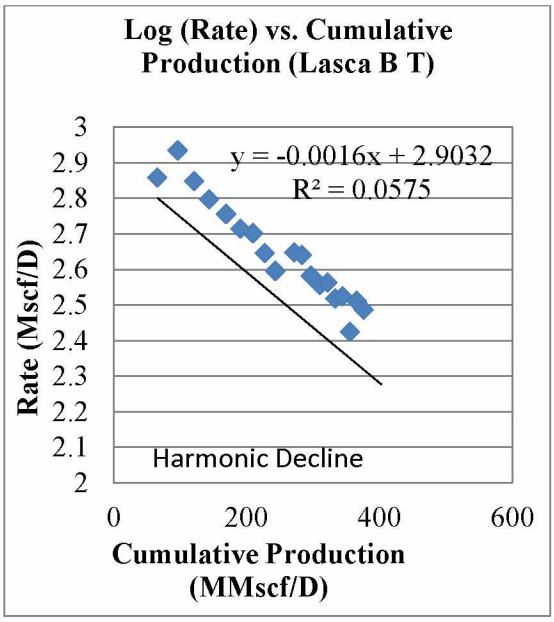

(f)

Figure 4.20-Continued.

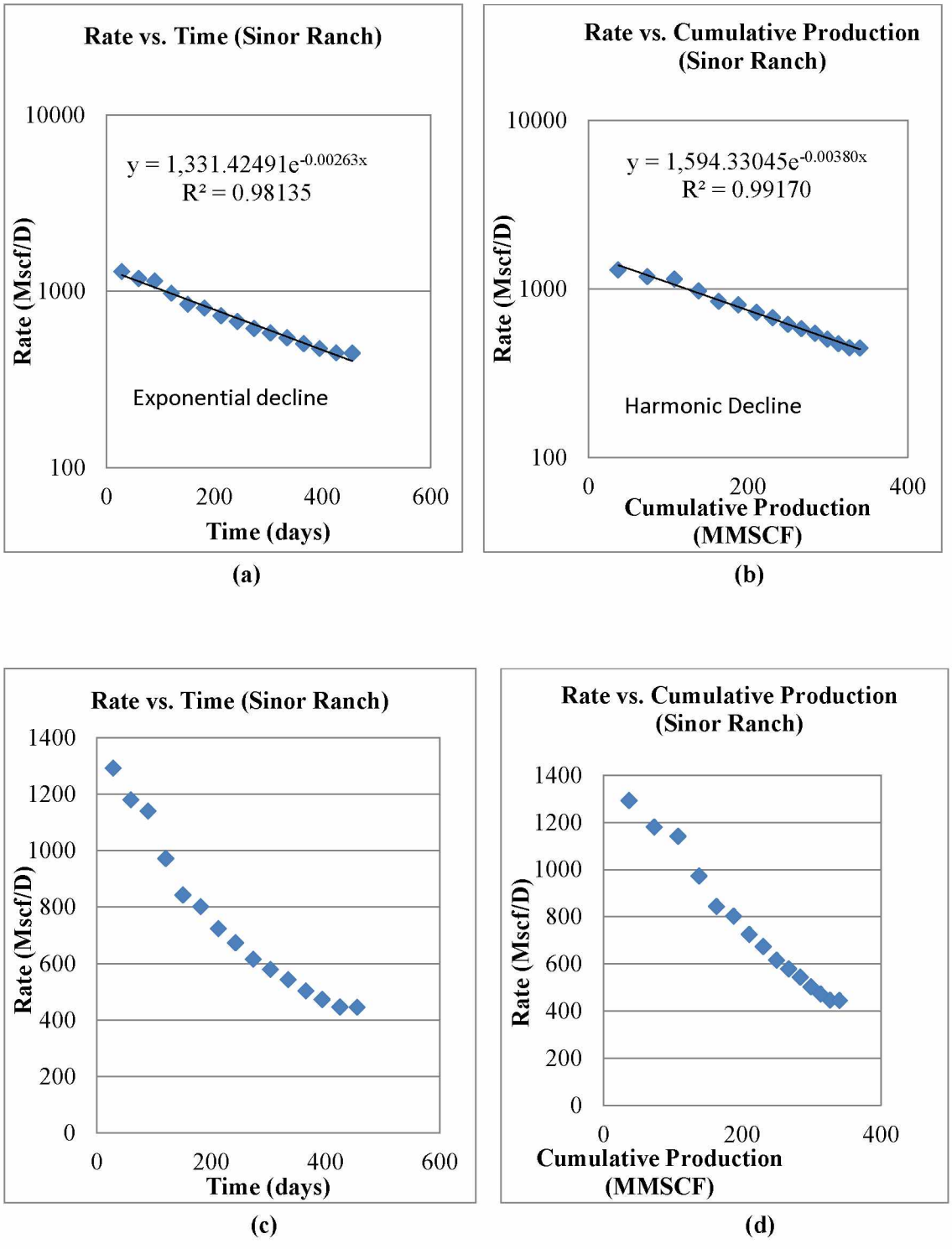

Figure 4.21: Decline curve diagnostic plots for well #1, Sinor Ranch unit/well (Live Oak)

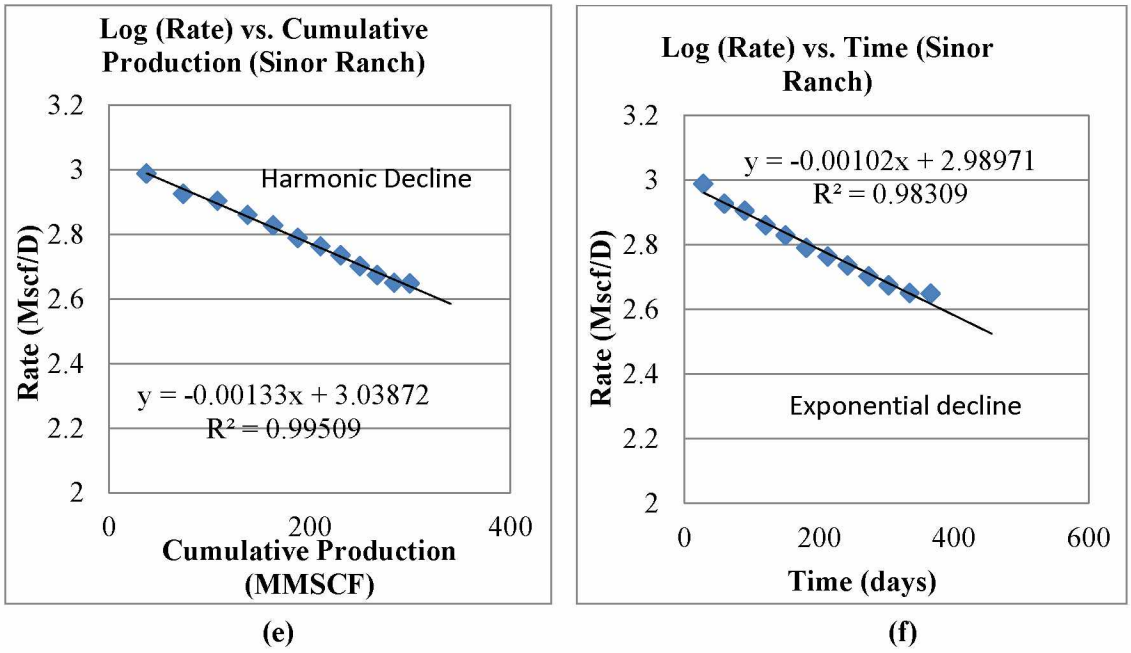

(e) (f)

Figure 4.21-Continued.

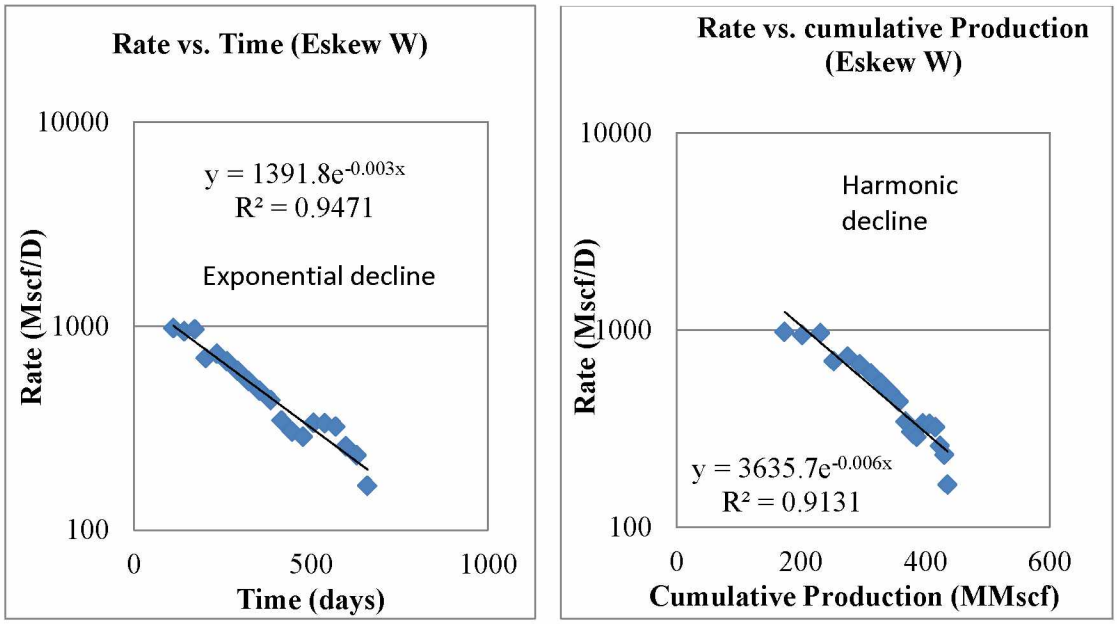

(a) (b)

Figure 4.22: Decline curve diagnostic plots for well #1, Eskew W unit/well (Live Oak County)

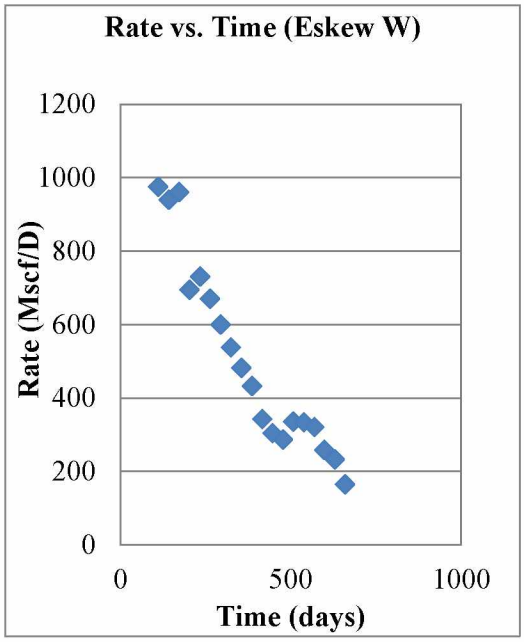

(c)

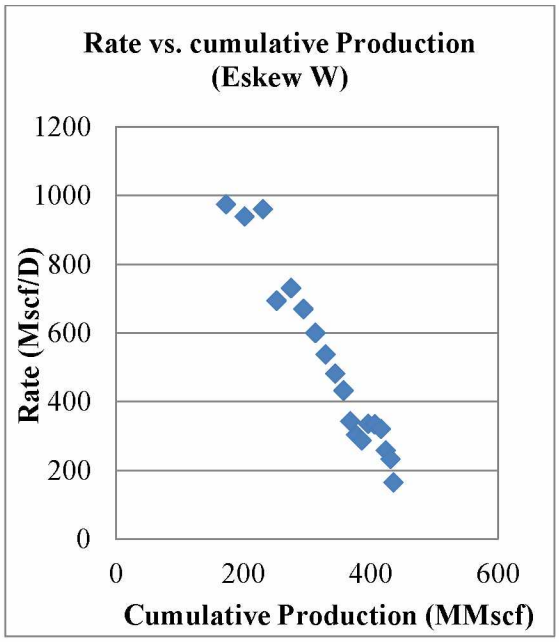

(d)

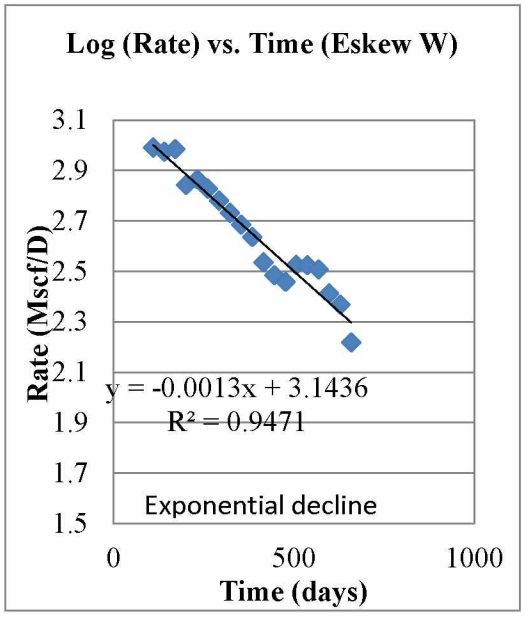

(e)

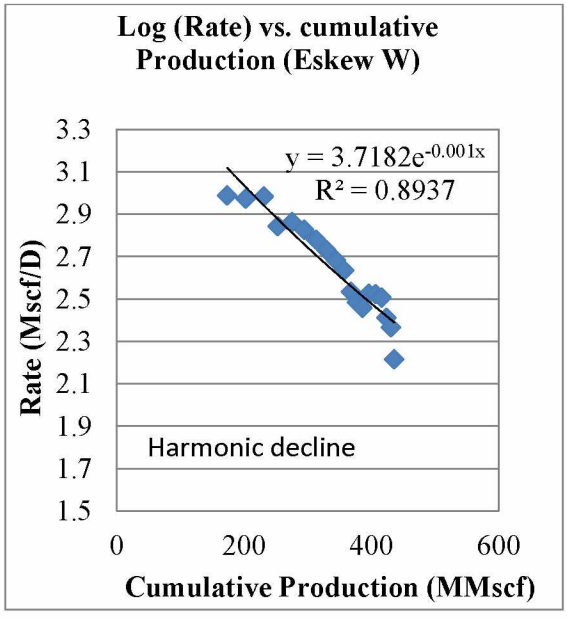

(f)

Figure 4.22-Continued.

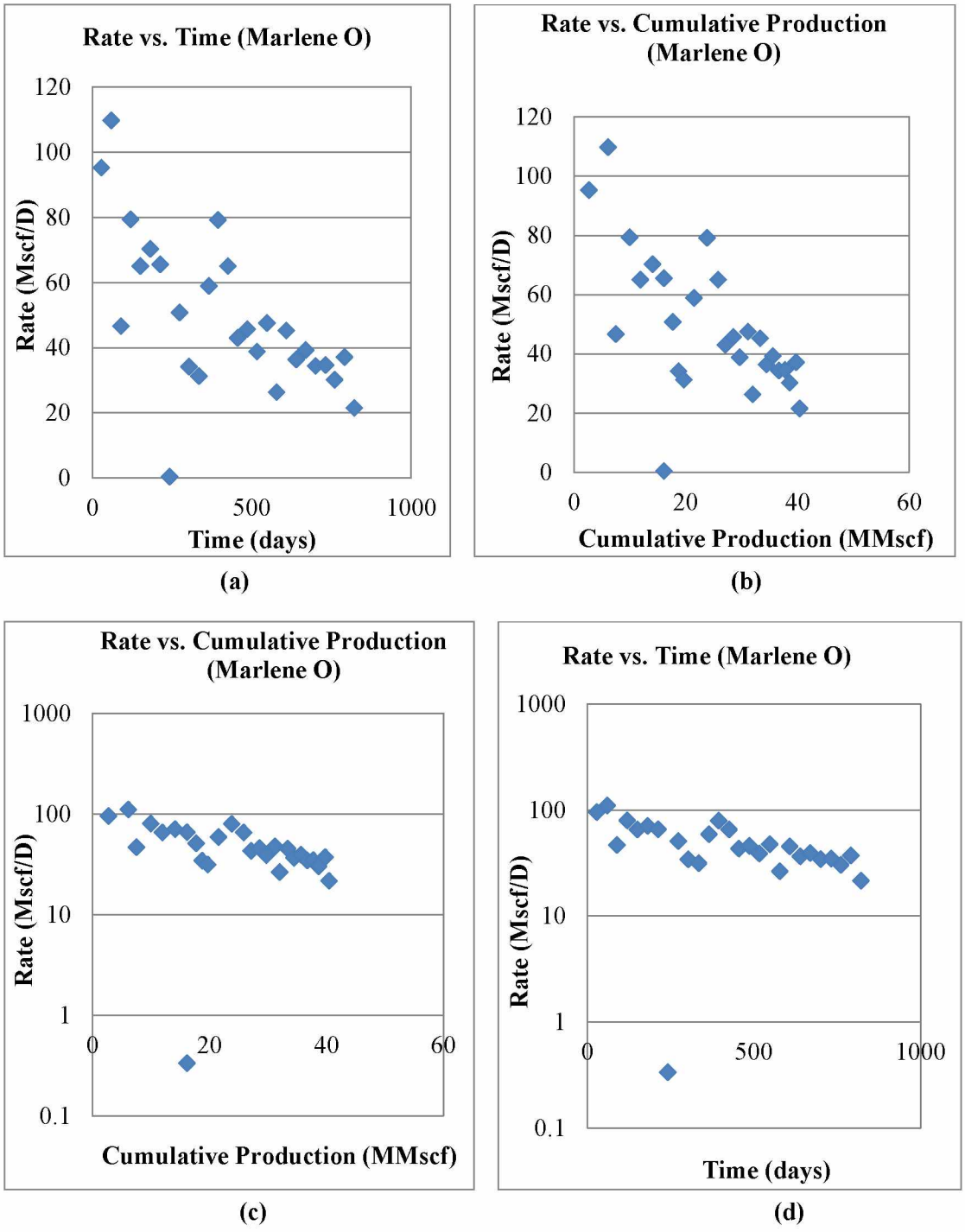

Figure 4.23: Decline curve diagnostic plots for well #1, Marlene O unit/well (Live Oak)

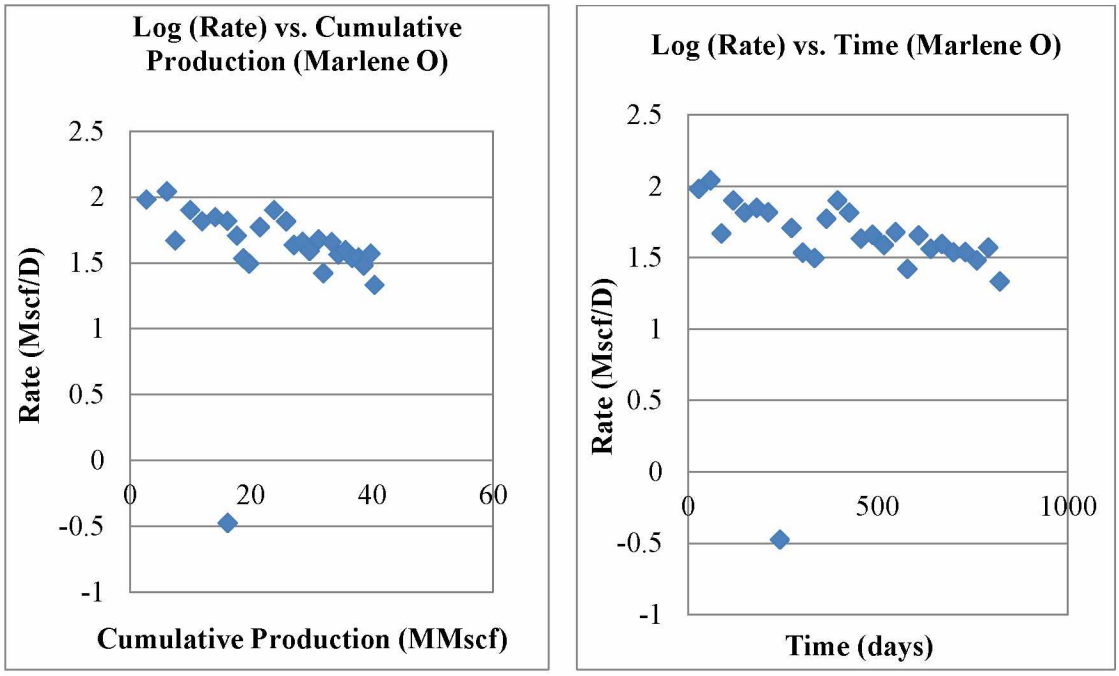

Figure 4.23-Continued.

4.4 Webb County

Webb County is located south west of the other two counties (Figure 4.1) and it has the lowest cumulative production of 2,240,000 Mscf as at 03/2011. All the reported production is from the Gates Ranch Field. The decline curve method was applied to five wells, all of which had only 12 months of production history available (Figures 4.24-4.28).

4.4.1 Observations

DCA was performed on all the wells at the Webb county and only two of the wells gave straight lines for the semi-log rate vs. time and rate vs. cumulative production plots (Figures 4.27-4.28). Figures 4.24-4.26 show erratic production profile which did not fit with any decline model.

Figures 4.27-4.28 matched both the exponential and harmonic decline models (i.e. gave straight lines for the semi-log rate vs. time and rate vs. cumulative production plots).

4.4.2 Discussions and interpretation of plots

Figures 4.24-4.26 show an erratic production behavior which could be attributed to variations in reservoir quality. The use of simulation models will not only help in forecasting but also to obtain any other probable cause of the erratic production profile. Figures 4.27-4.28 matched both the exponential and harmonic decline models; this is probably due to the very short production history. Again, the use of simulation models is needed to generate a longer production profile and for better future forecasts. For the two wells in Figures 4.27-4.28, the exponential decline gave higher estimated reserves than the harmonic decline; the highest cumulative production is 53 MMscf and the lowest cumulative production is 46 MMscf. This emphasizes the need to use simulation models to obtain better and more definite forecasts (instead of the two different forecasts from the short production history). The type of completion for all the wells was not specified and there was no correlation between reserves and length of horizontal leg.

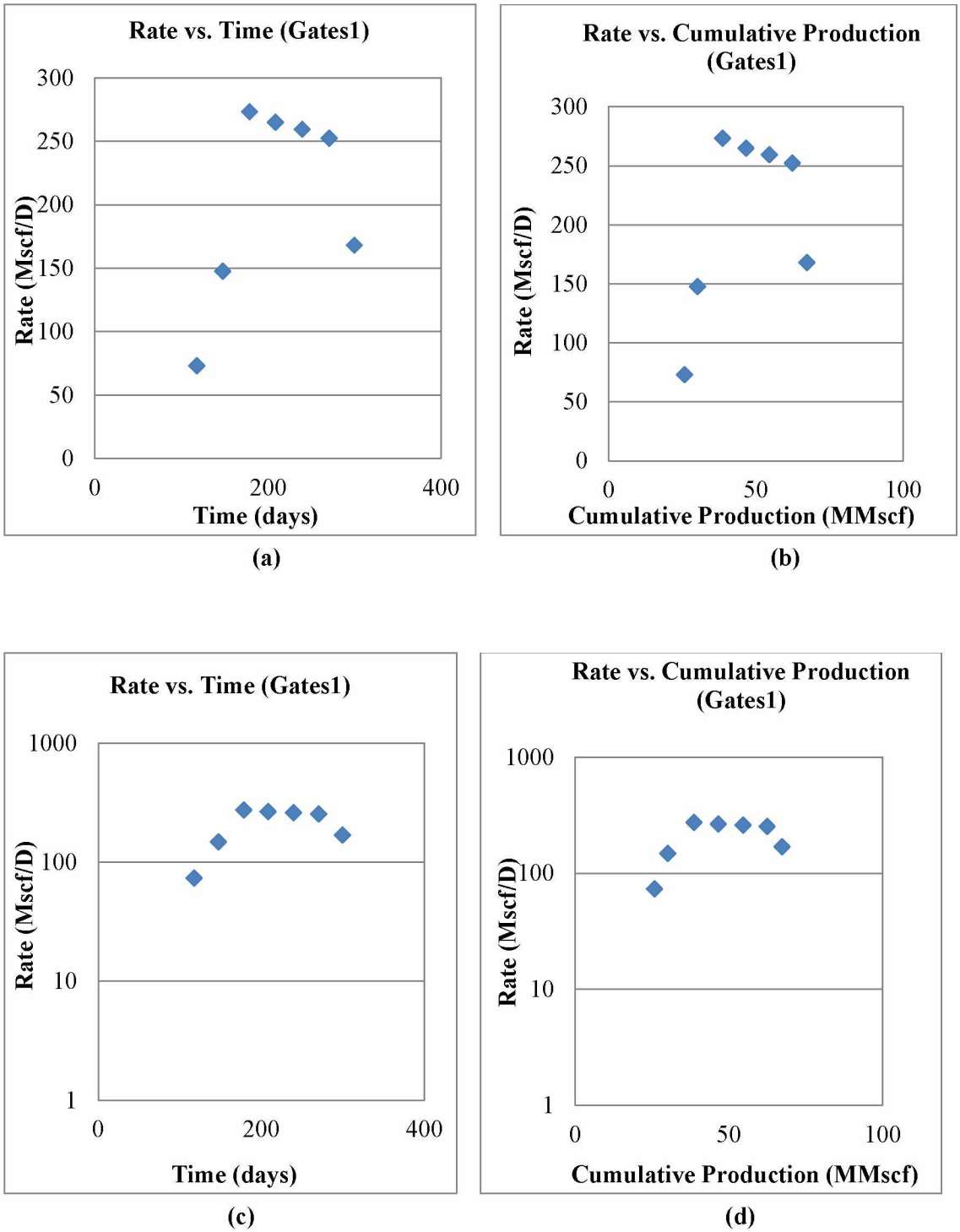

Figure 4.24: Decline curve diagnostic plots for well #1, Gates 1 unit/well (Webb County)

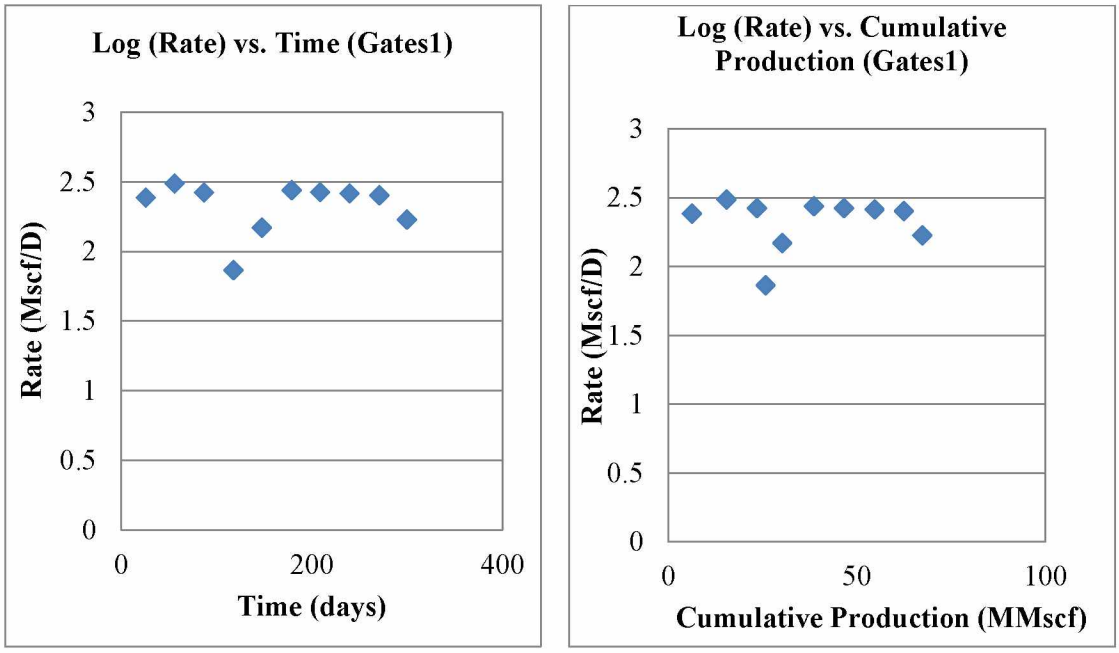

(e) (f)

Figure 4.24-Continued.

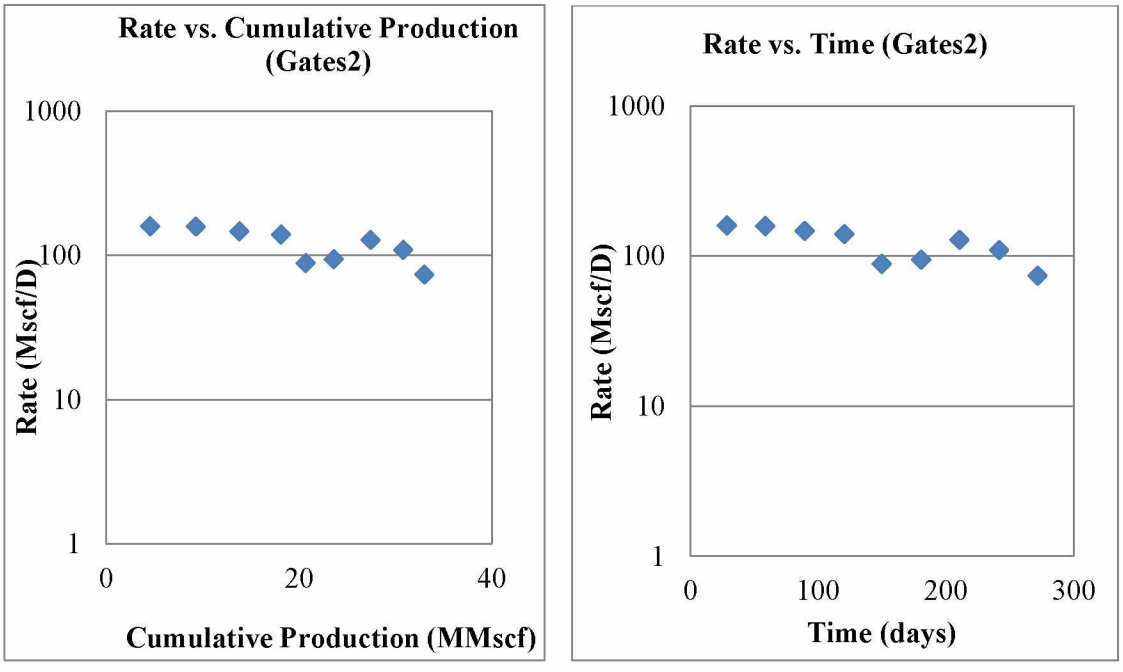

(a) (b)

Figure 4.25: Decline curve diagnostic plots for well #1, Gates 2 unit/well (Webb County)

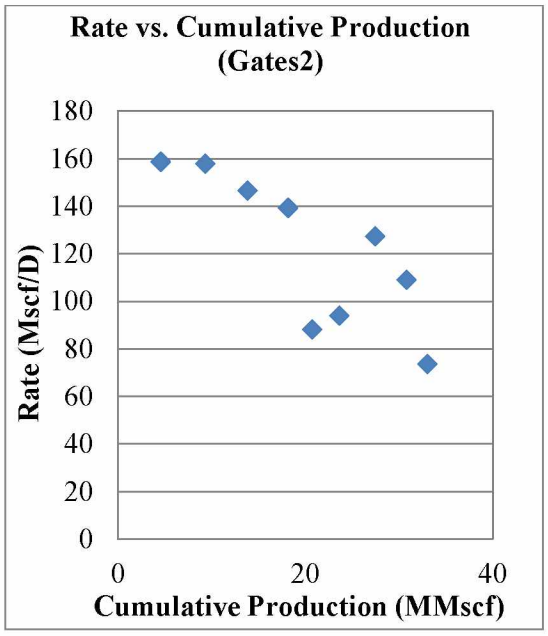

(c)

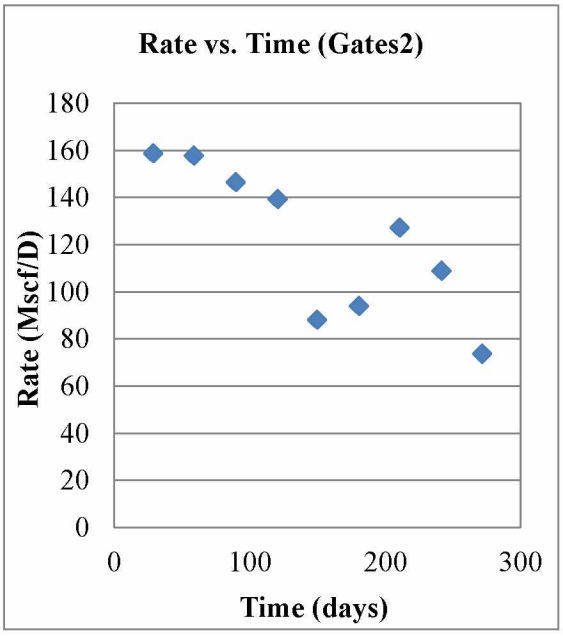

(d)

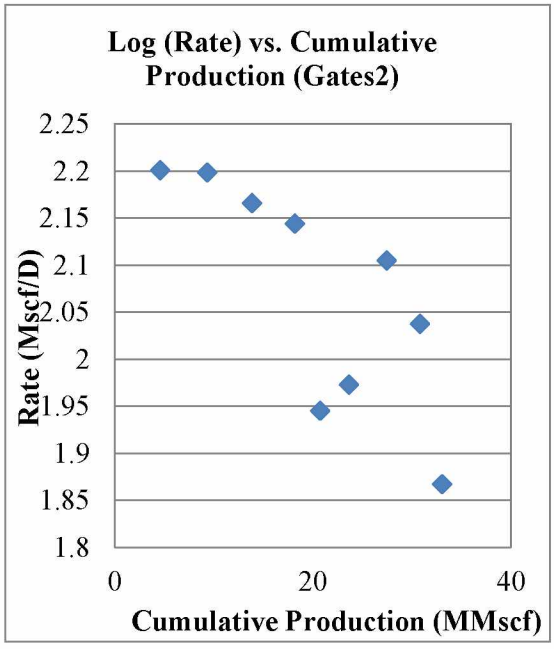

(e)

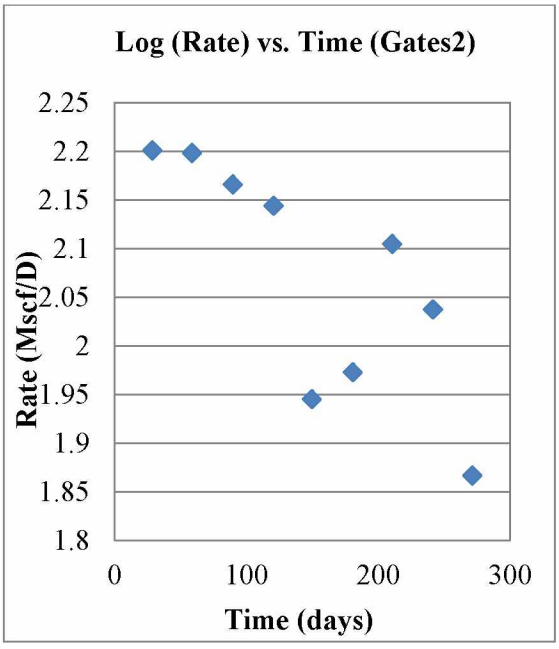

(f)

Figure 4.25-Continued.

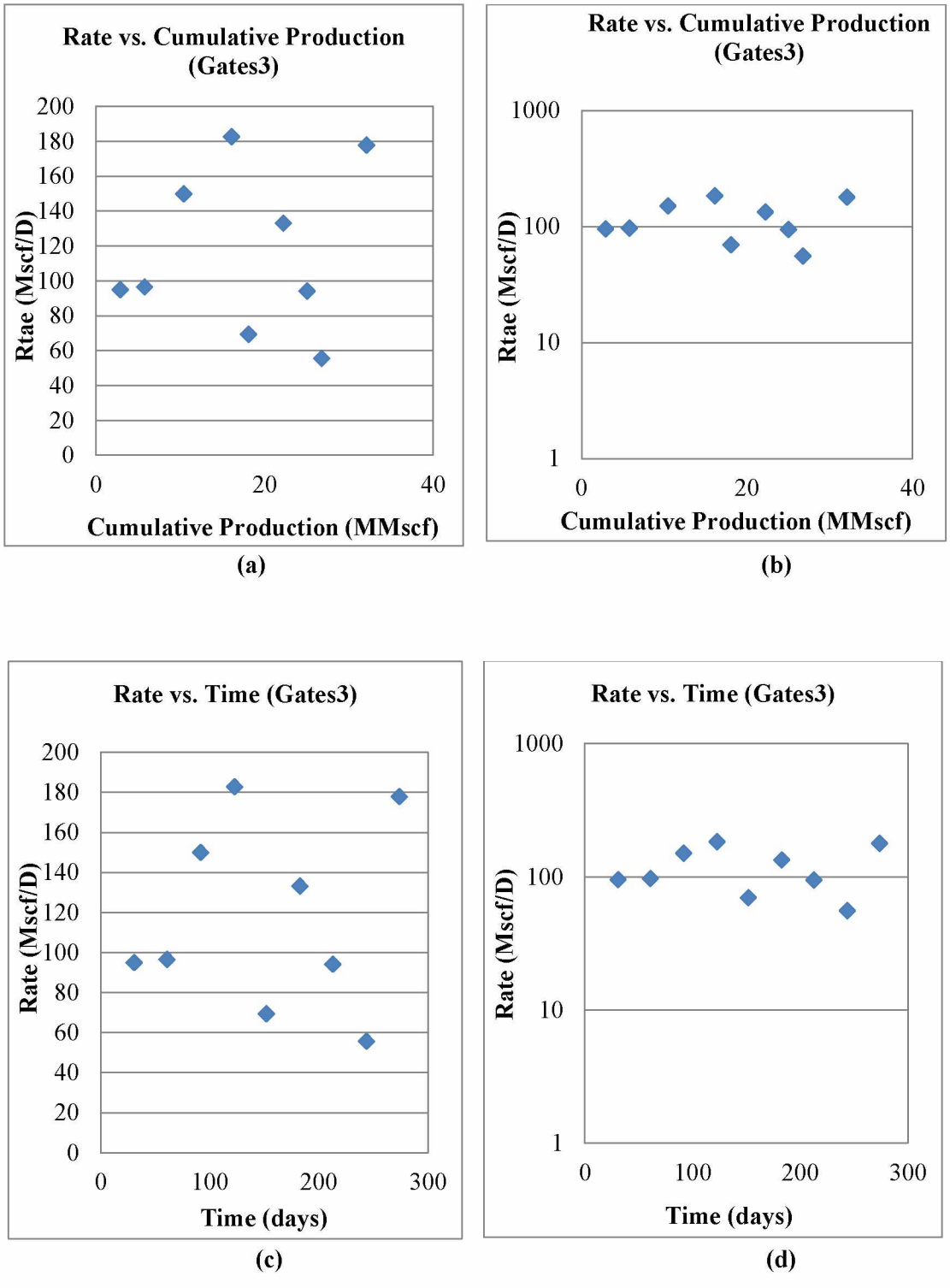

Figure 4.26: Decline curve diagnostic plots for well #1, Gates 3 unit/well (Webb)

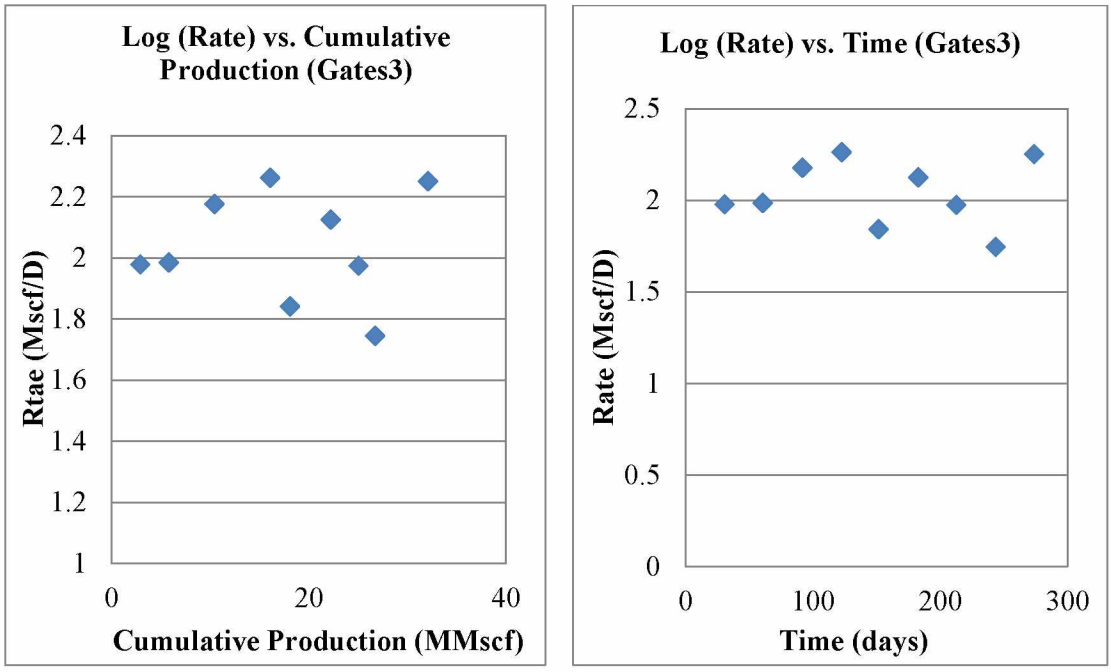

Figure 4.26-Continued.

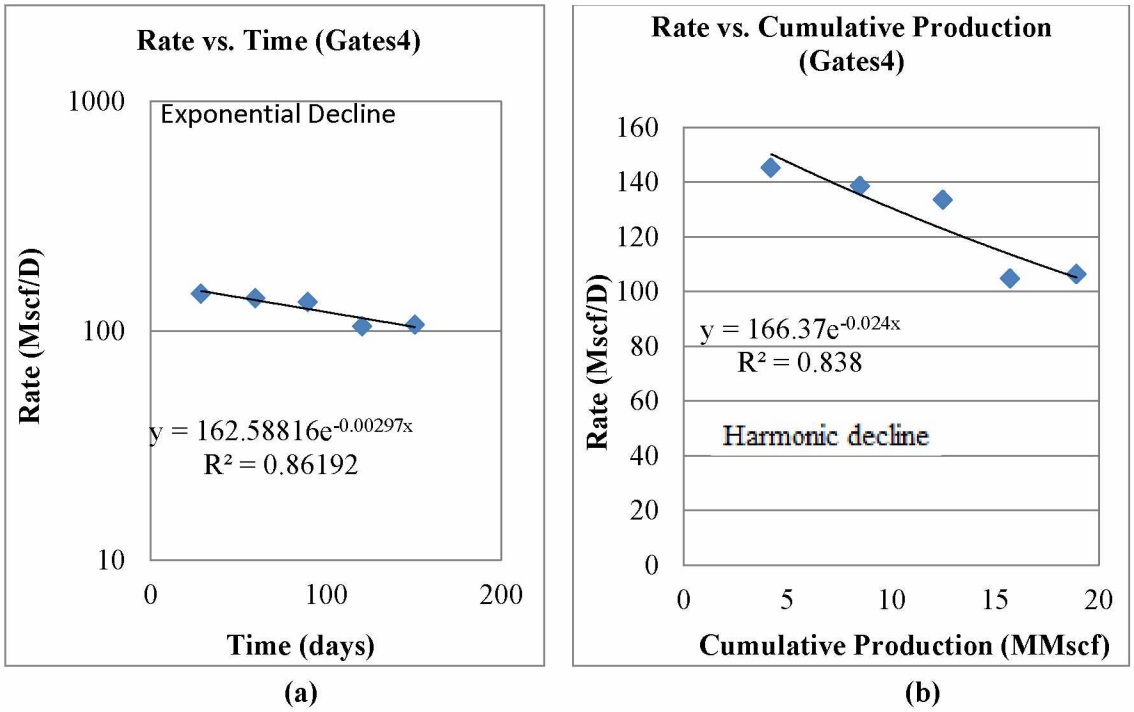

Figure 4.27: Decline curve diagnostic plots for well #1, Gates 4 unit/well (Webb County)

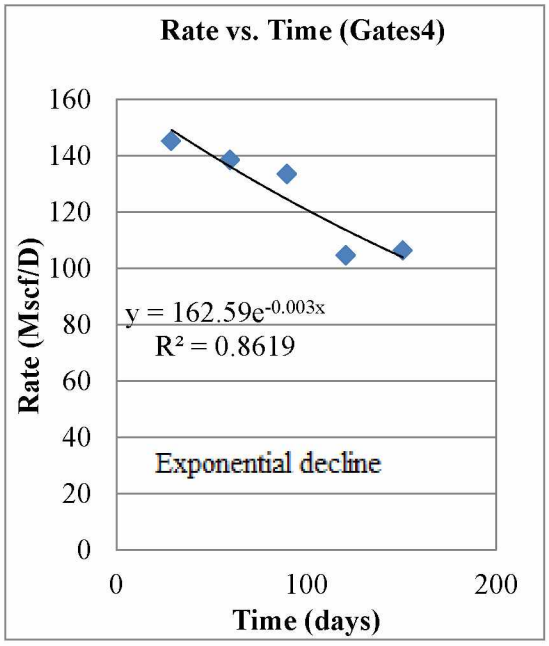

(c)

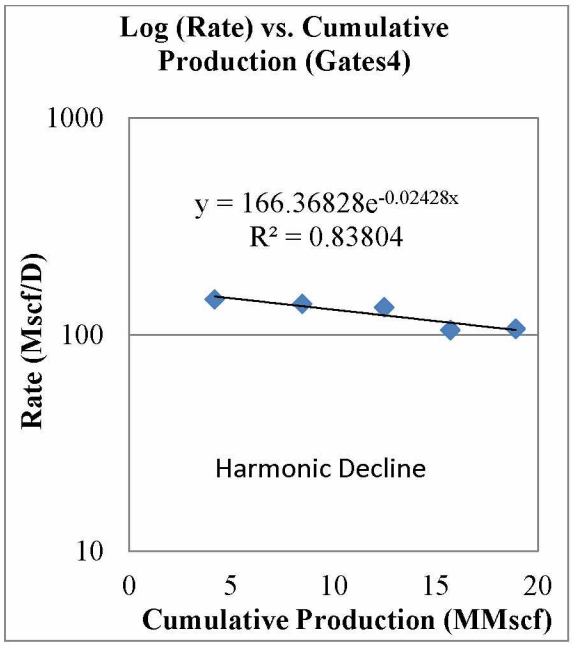

(d)

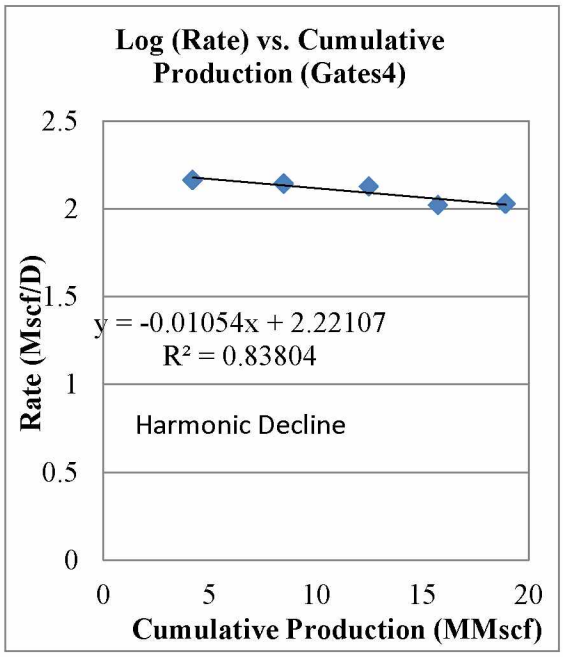

(e)

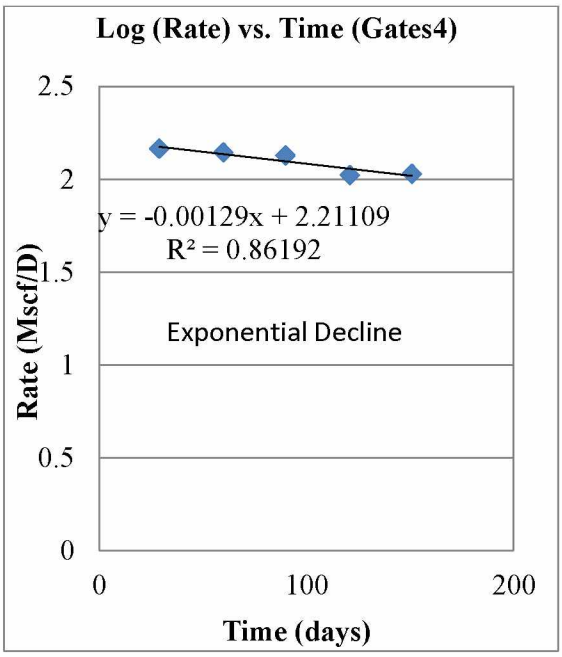

(f)

Figure 4.27-Continued.

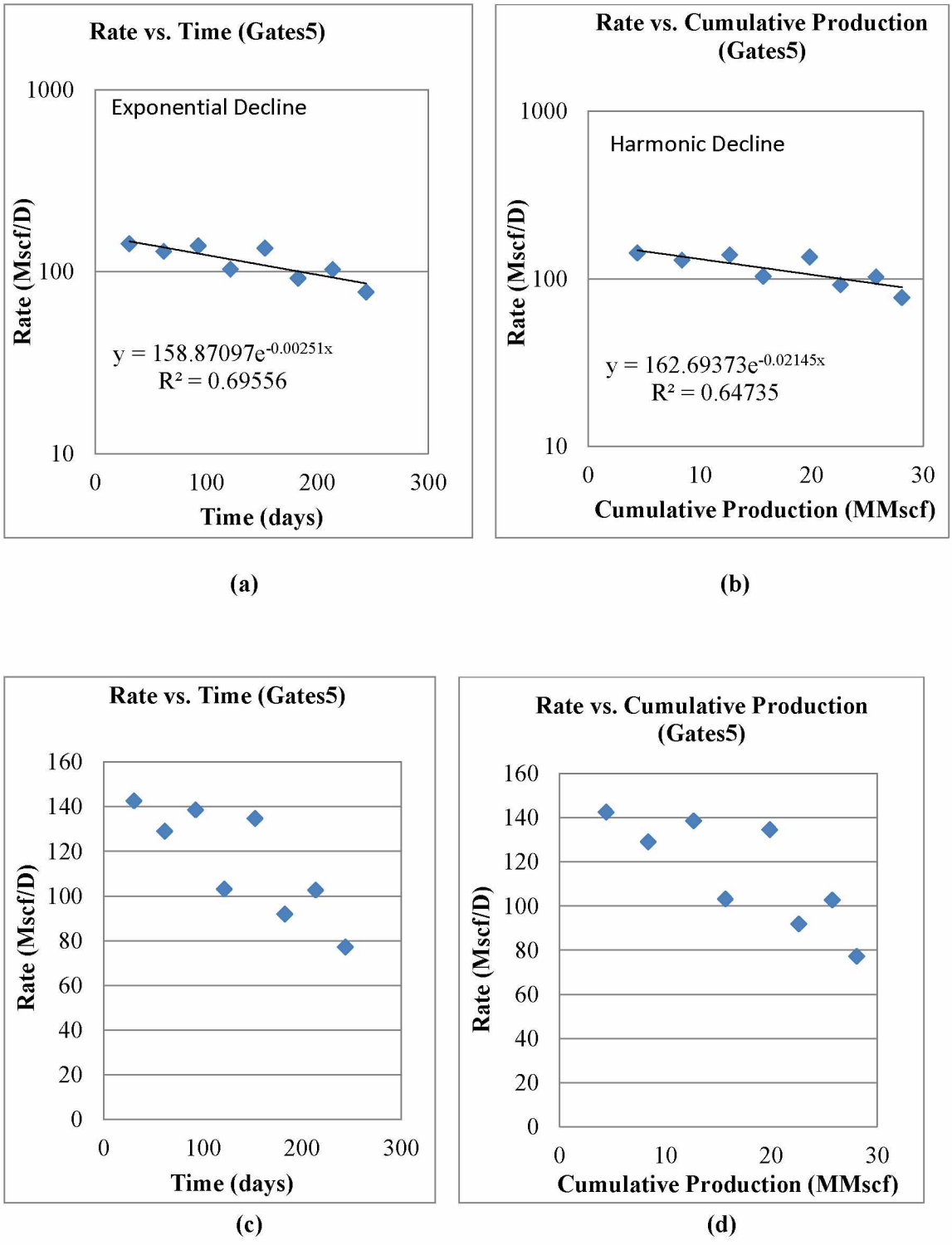

Figure 4.28: Decline curve diagnostic plots for well #1, Gates 5 unit/well (Webb County)

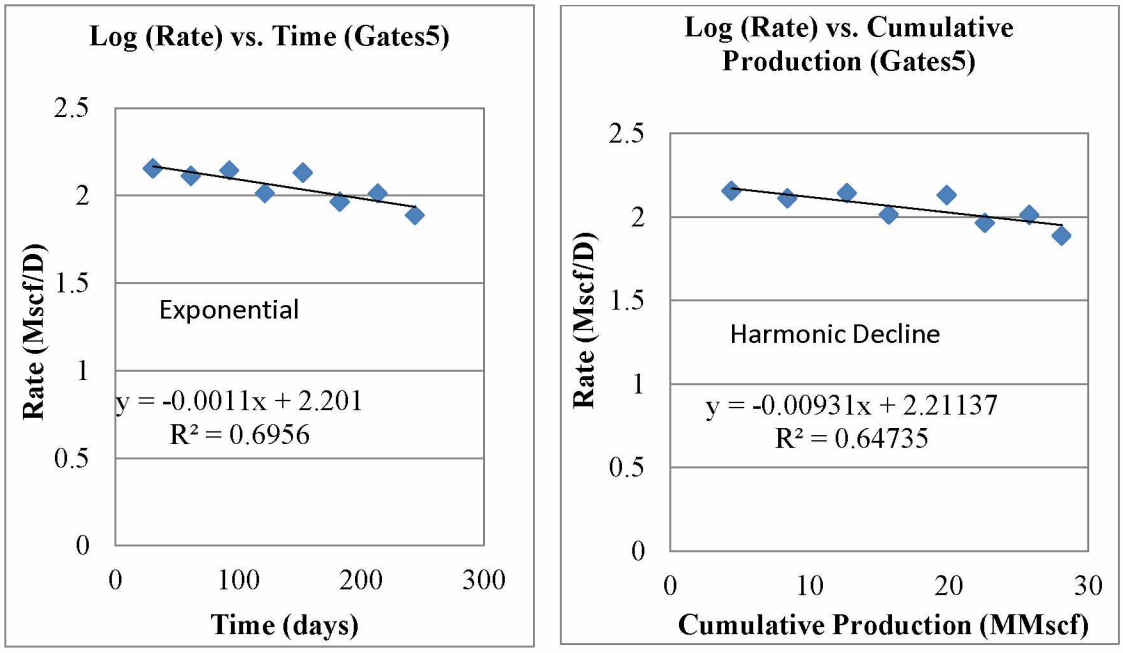

Figure 4.28-Continued.

4.5 Decline curve analysis with different portions of decline curve.

Some wells demonstrated a noticeable change in the decline trend (Figure 4.29) which made it very difficult to choose the right decline path for our production forecast. Different production forecasts were obtained when different portions of the decline curve were used for the analysis (Figures 4.29-4.31). This strongly suggests that the results from the decline curve analysis for wells with short production histories are not totally reliable. Figures 4.32-4.34 show the production profile from a few examples, when the whole and only the second half of the decline curve were used for the decline curve analysis.

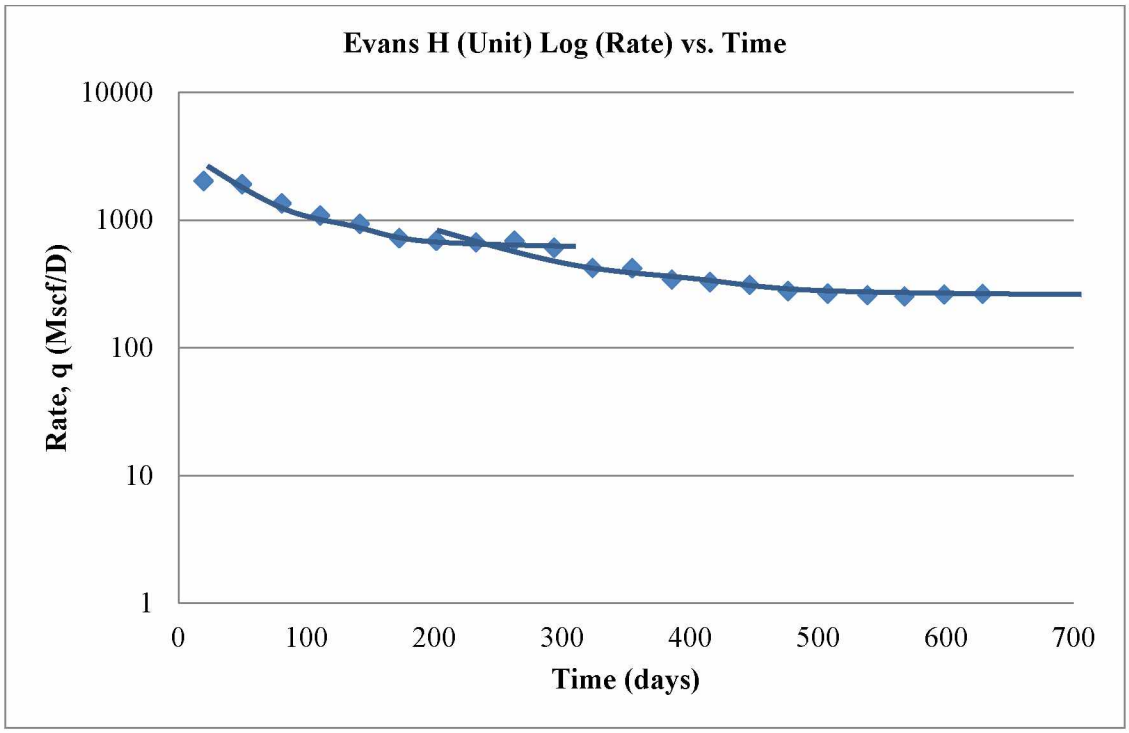

Figure 4.29: Evans H (Unit), Log (Rate) versus Time. Two different decline patterns are observed.

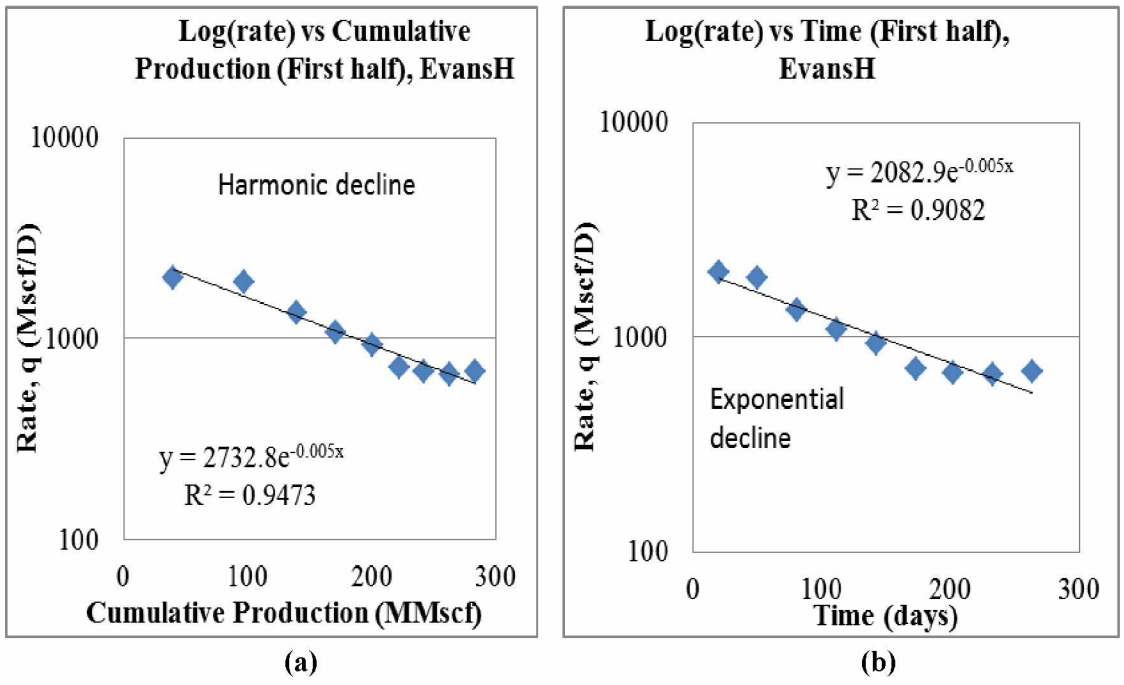

Figure 4.30: Decline curve diagnostic plots for first half of production history, Evans H unit well #1 (Webb County)

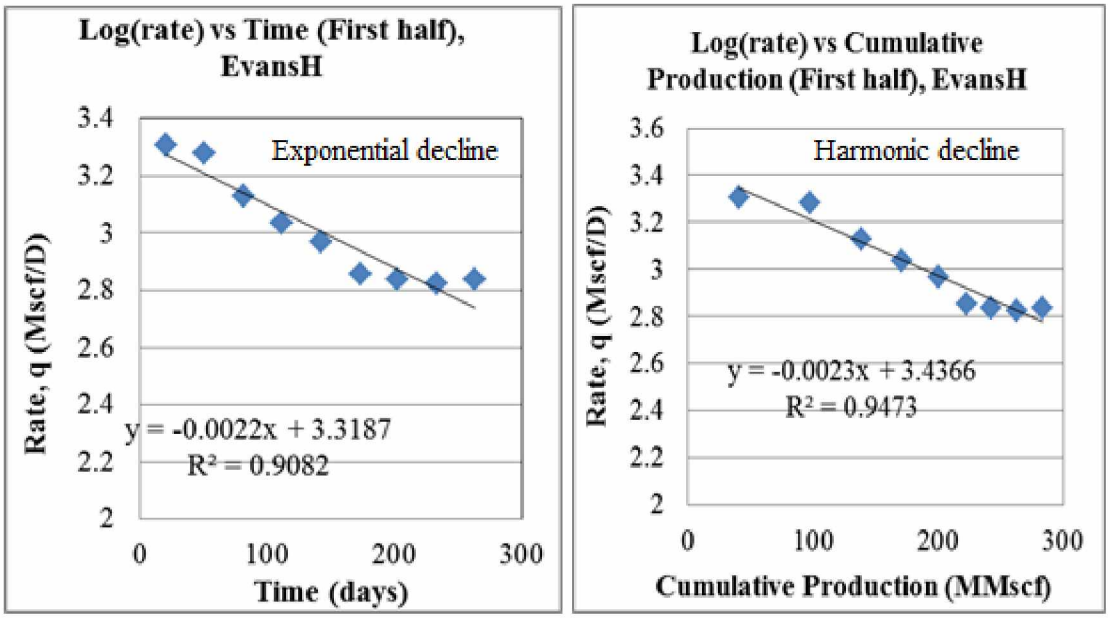

(c) (d)

Figure 4.30-Continued.

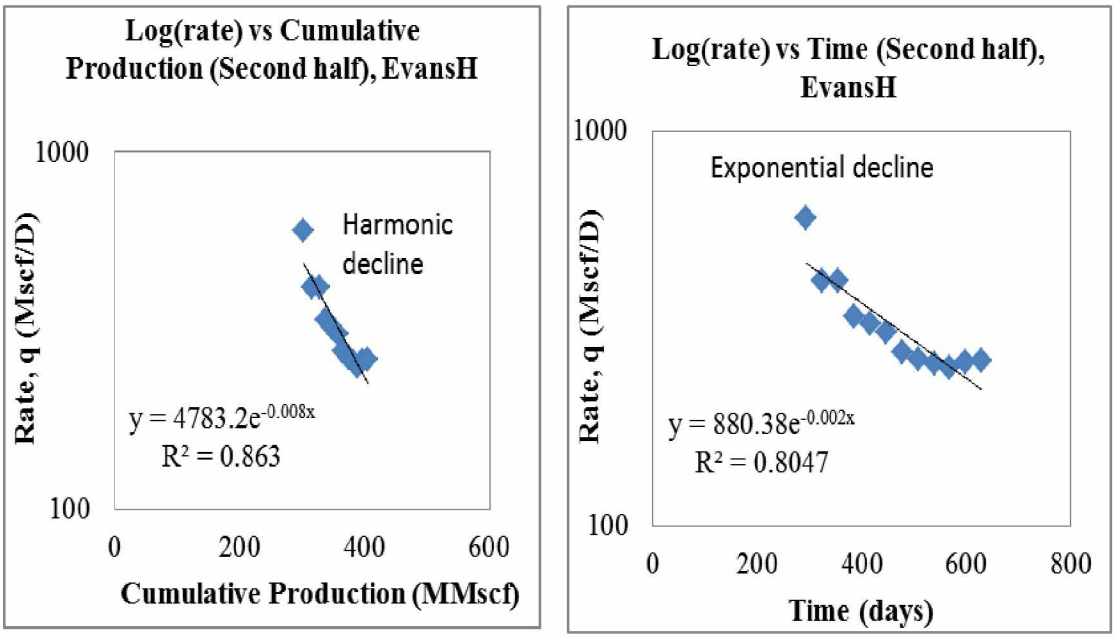

(a) (b)

Figure 4.31: Decline curve diagnostic plots for second half of production history, Evans H unit/well #1 (Webb County)

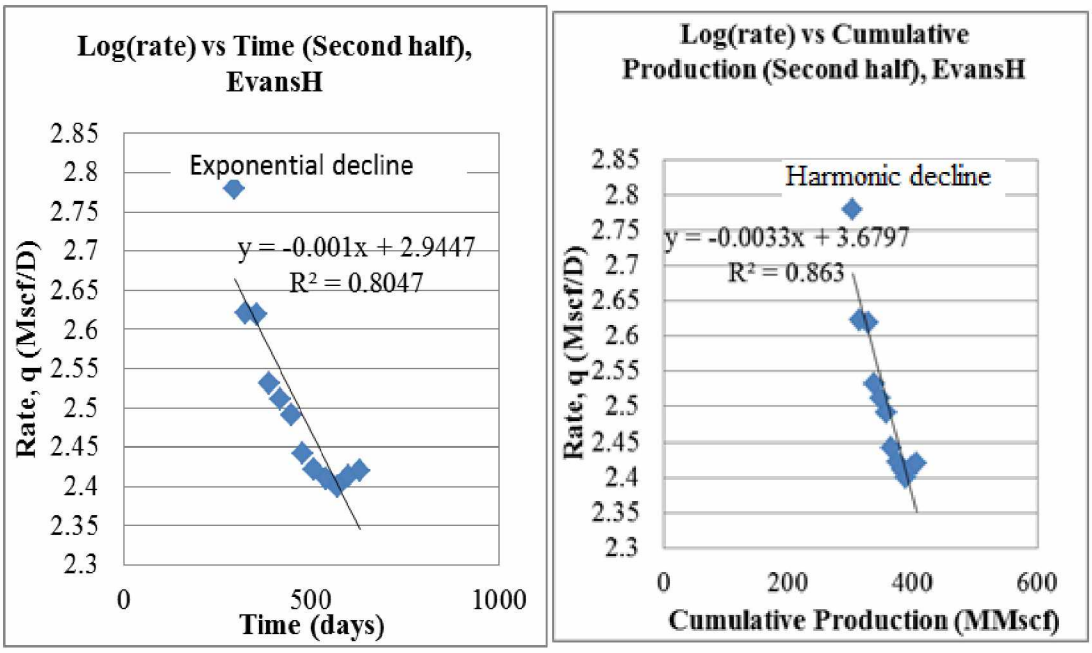

(c) (d)

Figure 4.31-Continued.

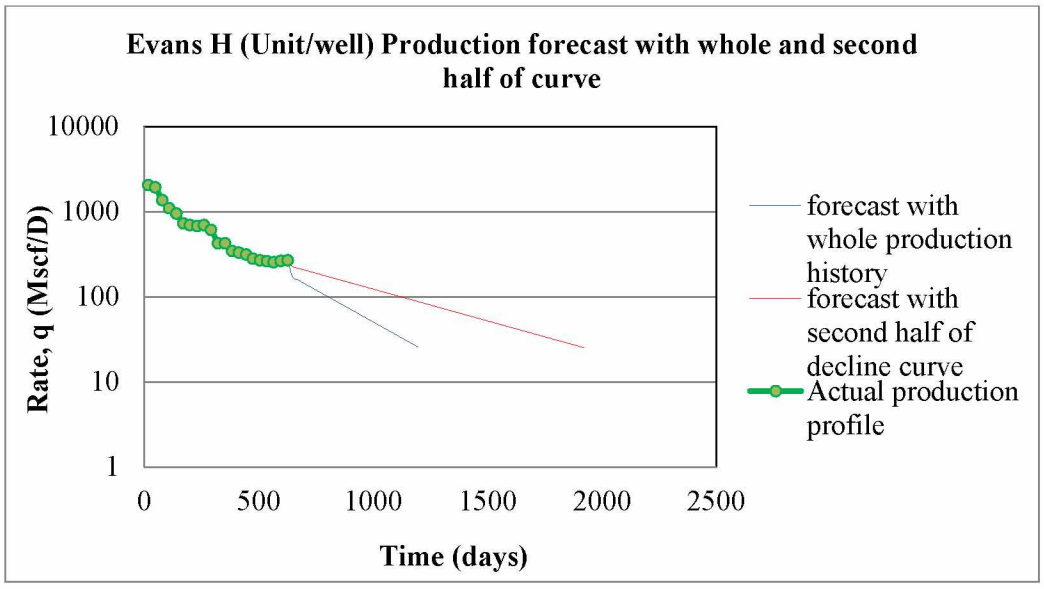

Figure 4.32: Production forecast to limit for whole and second half of decline curve from the DCA (Evans H unit/well).

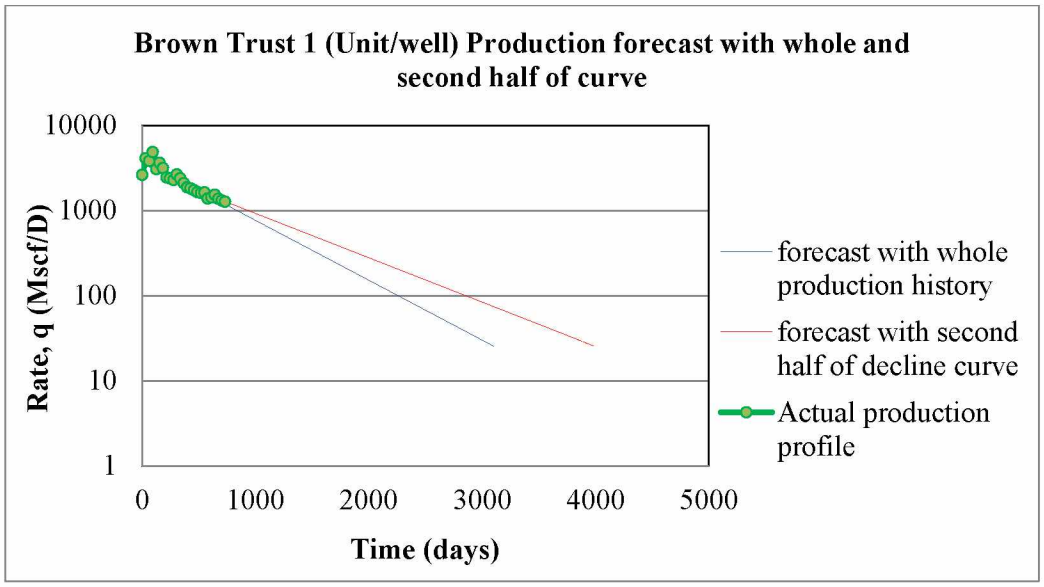

Figure 4.33: Production forecast to limit for whole and second half of decline curve from the DCA (Brown Trust 1 unit/well).

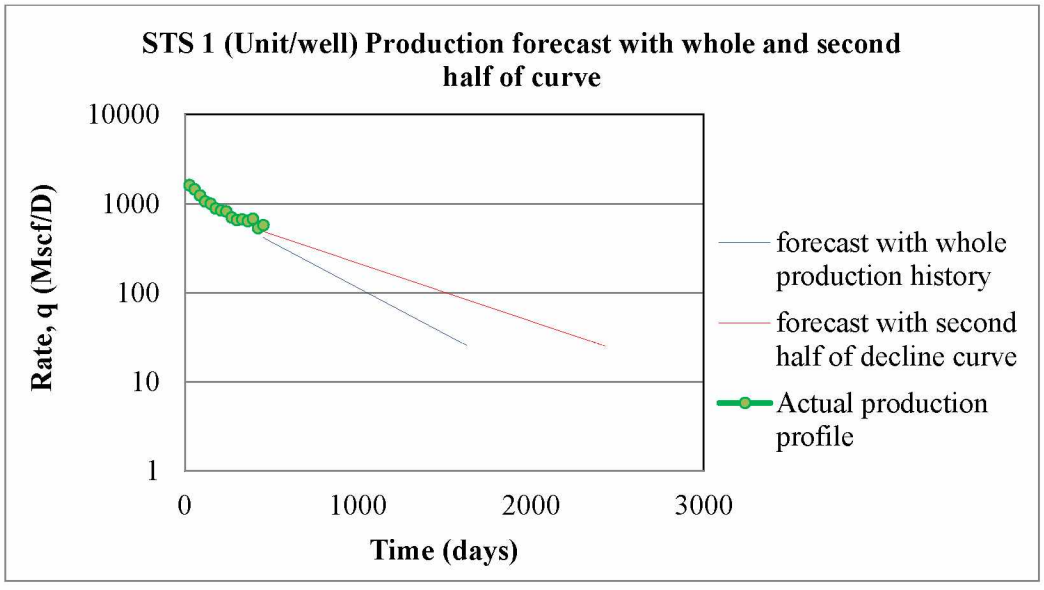

Figure 4.34: Production forecast to limit for whole and second half of decline curve from the DCA (STS 1 unit/well).

4.6 Updated DCA with longer production history

The production history of all the wells analyzed with the DCA and reported so far ended at April 2011. An updated DCA analysis was performed for all the wells with an extended period of production now available at the Texas Railroad Commission website (http://www.rrc.state.tx.us/data/online). The updated production history had an additional 9 months production period i.e. up to January 2012. A comparison of the results of initial and updated DCA is given in a summary table (Table 4.19). The forecasted DCA results to economic limits of the updated production data for all the wells analyzed are given in Table 4.20.

Results from the DCA performed on the updated data shows some variations in forecasted cumulative production (an increase, in some but not all cases, of up to 43% in forecasted reserves) which makes the use of the DCA questionable for wells with short production histories and also points to the need for simulation models for more reliable forecasts.

Table 4.19: Summary of results for DCA with initial and updated production histories

County	well	Initial reserve	Initial reserve	Updated reserve	Updated reserve
Lasalle		(Exp.), MMscf	(Har.), MMscf	(Exp.), MMscf	(Har.), MMscf
Lasalle	Evans H	460	760	459	668
Lasalle	Hawksville	1562	8398	1780	8760
Lasalle	Brown trust 1	2379	32334	2381	30842
Lasalle	Brown trust 2	1185	13754	1541	14308
Lasalle	J. C Martin	1569	32777	1784	31205
Lasalle	STS-Welse	719	3952	903	4040
Lasalle	STS 1	612	2488	877	2736
Lasalle	STS 3	909	6720	1194	6967
Lasalle	Caroline P	1004	8697	1351	9314
Lasalle	Golla 7	1185	11893	1284	11335
Live Oak	Lasca B T	504	1580	504	1557
Live Oak	Sinor Ranch	496	1743	514	1724
Webb	Gates 5	53	14	53	14

Exp.: Exponential

Har.: Harmonic

Table 4.20: Decline analyses results for updated production data with an extended 9 months production period

Evans H (LaSalle)	**Exponential Decline**	**Harmonic Decline**	**Harmonic Decline**	**Harmonic Decline**
Minimum rate q_t (Mscf/D)	25	25	50	75
Initial rate, q_i (Mscf/D)	1615	4298.6	3223.4	3223.4
Di (1/days)	0.00346	0.033099	0.02482	0.02482
Time for min. rate, t (days)	1204.7	5164.5	2557.1	1691.3
Remaining production to limit (MMscf)	459.5	668.4	541	488.4
Hawkville (LaSalle)				
Minimum rate q_t (Mscf/D)	25	25	50	75
Initial rate, q_i (Mscf/D)	1609.7	1735.5	1735.5	1735.5
Di (1/days)	0.00089	0.00084	0.00084	0.00084
Time for min. rate, t (days)	4679.7	81454.7	40132.1	26357.9
Remaining production to limit (MMscf)	1780.6	8760.8	7328.6	6490.9
Brown Trusts 1 (LaSalle)				
Minimum rate q_t (Mscf/D)	25	25	50	75
Initial rate, q_i (Mscf/D)	3883.2	4710	4710	4710
Di (1/days)	0.00162	0.0008	0.0008	0.0008
Time for min. rate, t (days)	3114.5	234250	116500	77250
Remaining production to limit (MMscf)	2381.6	30842	26761.1	24373.9
Brown Trusts 2 (LaSalle)				
Minimum rate q_t (Mscf/D)	25	25	50	75
Initial rate, q_i (Mscf/D)	2876.5	3599	3599	3599
Di (1/days)	0.00185	0.00125	0.00125	0.00125
Time for min. rate, t (days)	2565.1	114368	56784	37589.3
Remaining production to limit (MMscf)	1541.3	14308.2	12312.5	11145.1

Table 4.20-Continued

	Exponential Decline	Harmonic Decline	Harmonic Decline	Harmonic Decline
J.C Martin 1850 (LaSalle)				
Minimum rate q_t (Mscf/D)	25	25	50	75
Initial rate, q_i (Mscf/D)	3896.8	8556.1	8556.1	8556.1
Di (1/days)	0.00217	0.0016	0.0016	0.0016
Time for min. rate, t (days)	2326.7	213277.5	106326.2	70675.8
Remaining production to limit (MMscf)	1784.2	31205.8	27499.1	25330.9
STS-Welse 786 (LaSalle)				
Minimum rate q_t (Mscf/D)	25	25	50	75
Initial rate, q_i (Mscf/D)	1588	2172	2172	2172
Di (1/days)	0.00173	0.0024	0.0024	0.0024
Time for min. rate, t (days)	2399.6	35783.3	17683.3	11650
Remaining production to limit (MMscf)	903.4	4040.3	3413.1	3046.1
STS 1 (LaSalle)				
Minimum rate q_t (Mscf/D)	25	25	50	75
Initial rate, q_i (Mscf/D)	1166.2	1411.3	1411.3	1411.3
Di (1/days)	0.0013	0.00208	0.00208	0.00208
Time for min. rate, t (days)	2955.8	26660.9	13090.1	8566.4
Remaining production to limit (MMscf)	877.8	2736.8	2266.5	1991.4
STS 3 (LaSalle)				
Minimum rate q_t (Mscf/D)	25	25	50	75
Initial rate, q_i (Mscf/D)	1923.5	2559.1	2559.1	2559.1
Di (1/days)	0.00159	0.0017	0.0017	0.0017
Time for min. rate, t (days)	2731.4	59626.8	29519.2	19483.4
Remaining production to limit (MMscf)	1194.0	6967.7	5924.2	5313.8

Table 4.20 -Continued.

	Exponential Decline	Harmonic Decline	Harmonic Decline	Harmonic Decline
Caroline Pielop (LaSalle)				
Minimum rate q_t (Mscf/D)	25	25	50	75
Initial rate, q_i (Mscf/D)	2282.6	2883.7	2883.7	2883.7
Di (1/days)	0.00167	0.00147	0.00147	0.00147
Time for min. rate, t (days)	2703.1	77789.6	38554.6	25476.3
Remaining production to limit (MMscf)	1351.8	9314.3	7954.5	7159.1
Golla 7 (LaSalle)				
Minimum rate q_t (Mscf/D)	25	25	50	75
Initial rate, q_i (Mscf/D)	2812.8	3792.1	3792.1	3792.1
Di (1/days)	0.00217	0.00168	0.00168	0.00168
Time for min. rate, t (days)	2176.5	89693.1	44548.9	29500.8
Remaining production to limit (MMscf)	1284.7	11335.2	9770.6	8855.4
Lasca ButlerSearcy Trust (Live Oak)				
Minimum rate q_t (Mscf/D)	25	25	50	75
Initial rate, q_i (Mscf/D)	1088.7	1556.5	1556.5	1556.5
Di (1/days)	0.00211	0.00413	0.00413	0.00413
Time for min. rate, t (days)	1788.5	14833.1	7295.4	4782.9
Remaining production to limit (MMscf)	504.1	1557.0	1295.7	1142.9
Sinor Ranch (Live Oak)				
Minimum rate q_t (Mscf/D)	25	25	50	75
Initial rate, q_i (Mscf/D)	1300	1824.7	1824.7	1824.7
Di (1/days)	0.00248	0.00454	0.00454	0.00454
Time for min. rate, t (days)	1593.2	15856.3	7818.0	5138.6
Remaining production to limit (MMscf)	514.1	1724.3	1445.7	1282.7
Gates 4 (Webb)				
Minimum rate q_t (Mscf/D)	25	25	50	75
Initial rate, q_i (Mscf/D)	162.5	166.3	166.3	166.3
Di (1/days)	0.00297	0.02428	0.02428	0.02428
Time for min. rate, t (days)	630.4	232.8	95.8	50.1
Remaining production to limit (MMscf)	46.3	12.9	8.2	5.4

4.7 Conclusions from Decline Curve Analysis

The production data from wells producing gas from the Eagle Ford shale in three adjacent counties were analyzed using decline curve analysis. The rate vs. time behavior of some wells shows a clear alteration in decline behavior after some production. This kind of behavior made it a challenge as to which part of data should be used in analysis. For many wells, DCA diagnostic plots showed that both exponential and harmonic behavior could be inferred. The ultimate cumulative production to a minimum economic rate and the remaining production life for each well were estimated using both models. The results varied considerably depending upon which decline model was used (exponential vs. harmonic). The results also showed that the very short production time is one of the reasons for having two different models and forecasts.

These observations clearly shows that there are uncertainties associated with using DCA as a reliable forecasting tool when applied to wells with relatively short production life. Longer production history could alleviate this uncertainty to some degree.

Based on analysis of a limited number of wells in the LaSalle county, there was no observable correlation between well performance and length of horizontal leg or number of fracture stages.

Chapter 5 Simulation Models

5.1 Introduction

In this part of the study, simulation models were used to optimize well completion and forecasting. In building simulation models, Eagle Ford shale reservoir properties were used as much as possible. The effects of different parameters were analyzed, including: matrix permeability; presence and properties of natural fractures; and hydraulic fracture spacing, half-lengths and conductivities.

Generic single-well simulation models were run with several objectives, including:

(1) To understand and quantify the dynamics of fluid flow and well performance in shale gas reservoirs

(2) To search for an optimized completion technique;

(3) To identify the optimum well spacing in different media (i.e. matrix permeability) and

(4) Generate a long production history. This allowed comparison of the observed decline curve analysis results to the simulated results and observe how accurately DCA can forecast the rest of history generated by simulation.

5.2 Simulation model building

The Resolve and CMG simulators were used independently for the simulation models. Resolve was used for shales with and without natural fractures while CMG was used only for shales with natural fractures.

The Resolve simulator employs the finite element method (FEM) and uses a tetrahedral mesh with denser meshes near the wellbore for more accurate results. The simulation models were built for different mediums which can broadly be classified into mediums with and without natural fractures. Desorption parameters obtained from previous studies (Freeman et al. 2009, Gao et al. 1994) on the Eagle Ford were used and their values are given in the relevant tables for different mediums refer to tables. The effect of desorption was observed from simulation run with different desorption parameters i.e. different Langmuir volumes and pressures (Table 5.1). Fracture closure parameters from previous study on the Eagle Ford were used (Orangi et al. 2011). The fracture closure with depletion was implemented with fracture permeability multiplier as shown in Figure 5.1. The size of model, depth, initial pressure, thickness, horizontal leg and all other relevant parameters used in these simulation models are given in Tables 5.1-5.3.

The CMG simulator makes use of finite difference method and was only applied for models with natural fractures. The CMG handles natural fractures differently from the Resovle simulator, it uses dual porosity model proposed by Warren and Root (1963). In CMG, the matrixes are surrounded by the natural fractures and evenly spaced. Different porosity values are assigned to the matrix and natural fractures. The fracture closure with depletion was implemented with fracture permeability multiplier as shown in Figure 5.1. Fracture closure parameters from previous study on the Eagle Ford were used (Orangi et al. 2011).

Comparison of results from the CMG and Resolve should show how the natural fracture distribution and character affects production. The same parameters were used to build simulation models for both simulators in order to obtain a good comparison of results. The only difference in models from the two simulators is the different ways they handle or represent natural fractures.

Table 5.1: Model parameters for medium without natural fractures (Resolve)

Model Parameters (Resolve)	
Area (ft2)	3500 X 1500 and 3500 X 3000
Thickness (ft)	150
Depth (ft)	8000
Horizontal leg (ft)	3000
Fracture stages	7 – 18
Hydraulic fracture spacing (ft)	400, 200, 100
Hydraulic fracture half-length (ft)	150, 300
Medium 1 permeability (nd)	1500
Medium 2 permeability (nd)	15000
Fluid	Dry gas
Fracture half-length (ft)	150-300
Fracture permeability, Khf1 (md)	1660000
Fracture permeability, Khf2 (md)	16600
Fracture width, Kw1 (inch)	0.039
Fracture width, Kw2 (inch)	0.0039
Langmuir volume, (scf/ton)	150, 200
Langmuir pressure, (psi)	1000, 1750
Porosity (fraction)	0.05
IGIP (MMscf)	10,090

IGIP: Initial Gas in Place

Table 5.2: Model parameters for medium with natural fractures (Resolve)

Model Parameters (Resolve)	
Area (ft2)	3500 X 1500
Thickness, layer 1(top) (ft)	1
Thickness, layer 2(middle) (ft)	150
Thickness, layer 3(bottom) (ft)	1
Depth (ft)	8000
Horizontal leg (ft)	3000
Fracture stages	7 – 18
Hydraulic fracture spacing (ft)	400, 200, 100
Hydraulic fracture half-length (ft)	150, 300
Medium 1 permeability (nd)	10
Medium 2 permeability (nd)	1
Fracture permeability, Khf1 (md)	1660000
Fracture permeability, Khf2 (md)	16600
Natural fracture permeability Knf1 (md)	1
Natural fracture permeability Knf2 (md)	0.1
Matrix porosity (fraction)	0.07
Fracture porosity (fraction)	0.03
IGIP in Fracture (MMscf)	2,430
IGIP in Matrix(MMscf)	8,460
Total IGIP (MMscf)	10,090

IGIP: Initial Gas in Place

Table 5.3: Model parameters for medium with natural fractures (CMG)

Model Parameters (CMG)	
Area (ft2)	3000 X 1500
Thickness (ft.)	50
Depth (ft.)	8000
Horizontal leg (ft.)	3000
Fracture stages	7 – 26
Hydraulic fracture spacing (ft.)	400, 200, 100
Hydraulic fracture half-length (ft.)	150, 300
Medium 1 (nd)	1000
Medium 2 (nd)	100
Fracture permeability, Khf1 (md)	1660000
Fracture permeability, Khf2 (md)	16600
Natural fracture permeability Knf1 (md)	1
Natural fracture permeability Knf2 (md)	0.1
Matrix porosity (fraction)	0.07
Fracture porosity (fraction)	0.03
Total IGIP (MMscf)	7,600

IGIP: Initial Gas in Place

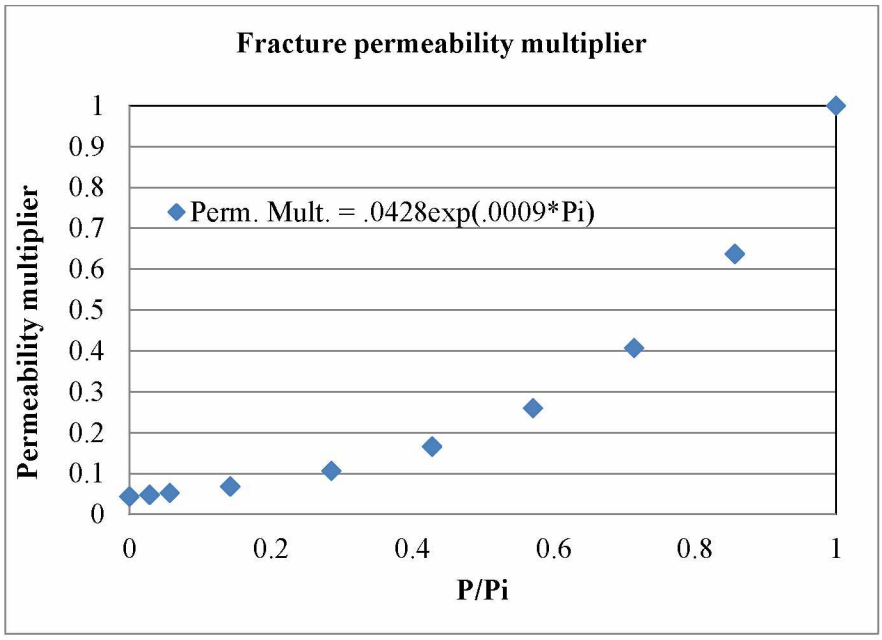

Figure 5.1: Fracture permeability multiplier (Orangi et al. 2011)

5.2.1 Media without natural fractures

Simulation models without natural fractures were built for different cases involving a number of various combinations of the medium (matrix) permeability, hydraulic fracture half-length and fracture conductivities. The various combinations involve two different values for each matrix permeability, hydraulic fracture half-length and conductivity, all of which are given in Table 5.1. The production optimization strategy for matrix without natural fracture involves evaluating three different aspects of production design: fracture spacing, well spacing and equivalent fracture configuration.

The first aspect of the production optimization design was obtaining optimum hydraulic fracture spacing. The models covered 2 mediums, 2 hydraulic fracture conductivities, 2 hydraulic fracture half-lengths, 3 different fracture spacing (see Table 5.1). The simulation was run for a different

combination of the various parameters with a total outcome of 24 different runs. The simulation results and a discussion are in section 5.2.1.1.

The next step was to optimize the well spacing for the optimum fracture spacing obtained from the previous step. For each simulation model, several horizontal observation wells were placed parallel to the producing well at different distances to observe pressure drops to abandonment pressure. The producing well's minimum bottom hole pressure was set at 100 psia and the optimum well spacing is obtained when the maximum pressure drop at the observation well is 15 psia. The choice of pressure drop should be based on field observation and experience.

The third step evaluates optimum hydraulic fracture configuration. Two hydraulic fracture half-lengths were combined with the optimum fracture spacing to obtain the optimum equivalent fracture configuration for the two different matrix permeability. The idea is to find the best fracturing design while keeping the fracturing fluid volume constant.

5.2.1.1 Results

Optimal fracture spacing

To find an optimum fracture spacing, fracture spacing of 400, 200 and 100 ft. were considered for different matrix permeability and fracture half-lengths of 150 and 300 ft. to obtain a total of 24 runs (see Table 5.4). The Resolve simulator was used for all simulation runs without natural fractures. A minimum BHP of 100 psia and minimum production rate of 50 Mscf/day were used.

The fracture spacing with the maximum ratio of cumulative gas produced to summation of all fracture lengths or "Gp/Sum(Xf)" is considered as optimum.

The cumulative produced gas depends on the matrix permeability and the equivalent fracture half-length which in turn depends on the fracture spacing for the two different fracture half-lengths considered. The fracture spacing that yield the highest value of "Gp/Sum(Xf)" is thus the optimum fracture spacing.

Results from all the simulation runs show that the fracture spacing of 400 and 200 ft. were the optimum for matrix permeability 1 and 2 (matrix 1 has the higher permeability), respectively (Figure 5.2). It can be observed from Figure 5.2 that a more permeable medium needs wider fracture spacing for optimum production performance. Matrix permeability 2 (which is less permeable than matrix permeability 1) had an optimum fracture spacing of 200 ft. while fracture spacing of 100 ft. was next in terms of production performance (Figure 5.2). One would expect a closer fracture spacing to yield the optimum for low matrix permeability; this is not the case because the hydraulic fracture permeability is also a determining factor. This shows that the optimum fracture spacing strongly depends on the type/conductivity of medium under consideration.

Table 5.4: Optimum fracture spacing for different mediums (without natural fractures), fracture spacing, half-length and conductivities.

BHP (psia)		**100**			**Initial reservoir pressure (psia)**			3500
M1(1500nd), 150 ft. half-length Khf1(1.6E6md)					**M1(1500nd), 150 ft. half-length, Khf2(1.6E4md)**			
	400	**200**	100			400	**200**	100
Gp, MMscf	98	**485**	589		Gp, MMscf	82	**432**	543
Gp/sum(Xf) Mscf/ft.	46	**115**	109		Gp/sum(Xf) Mscf/ft.	39	**102**	100
Recovery (%)	0.9	**4.8**	9.2		Recovery (%)	0.8	**4.2**	8.5
Pfinal (psia)	3462	**3292**	3256		Pfinal (psia)	3470	**3314**	3273
Producing Life, yrs	3	**15.2**	15		Producing Life, yrs	2.6	**14**	14.9
M2(15000nd), 150 ft. half-length, Kfh1(1.6E6md)					**M2(15000nd), 150 ft. half-length, Khf2(1.6E4md)**			
	400	200	100			**400**	200	100
Gp, MMscf	**2237**	2926	1722		Gp, MMscf	**1871**	2670	1582
Gp/sum(Xf) Mscf/ft.	**1065**	696	318		Gp/sum(Xf) Mscf/ft.	**890**	635	292
Recovery (%)	**22.1**	28.9	27		Recovery (%)	**18.5**	26.4	24.9
Pfinal (psia)	**2533**	2256	2770		Pfinal (psia)	**2683**	2360	2829
Producing Life, yrs	**66.8**	66.3	32.6		Producing Life, yrs	**61**	66.6	33.4
M1(1500nd), 300 ft. half-length, Khf1(1.6E6md)					**M1(1500nd), 300 ft. half-length, Khf2(1.6E4md)**			
	400	200	100			**400**	200	100
Gp, MMscf	**420**	1624	1411		Gp, MMscf	**327**	1452	1297
Gp/sum(Xf) Mscf/ft.	**100**	193	130		Gp/sum(Xf) Mscf/ft.	**77**	172	120
Recovery (%)	**4.1**	16	22.2		Recovery (%)	**3.2**	14.3	20.4
Pfinal (psia)	**3320**	2814	2919		Pfinal (psia)	**3360**	2882	2964
Producing Life, yrs	**12.8**	44.4	27.8		Producing Life, yrs	**10.7**	42.8	28.6

Table 5.4-Continued.

M2(15000nd), 300 ft. half-length, Khf1(1.6E6md)					M2(15000nd), 300 ft. half-length, Khf2(1.6E4md)			
	400	200	100			**400**	200	100
Gp, MMscf	**3737**	4432	2864		Gp, MMscf	**3067**	3936	2577
Gp/sum(Xf) Mscf/ft.	**889**	52	265		Gp/sum(Xf) Mscf/ft.	**730**	468	238
Recovery (%)	**37**	43.8	45.1		Recovery (%)	**30.3**	38.9	40.6
Pfinal (psia)	**1930**	1649	2295		Pfinal (psia)	**2194**	1853	2417
Producing Life, yrs	**84**	72.2	41.5		Producing Life, yrs	**81**	77.8	45.7

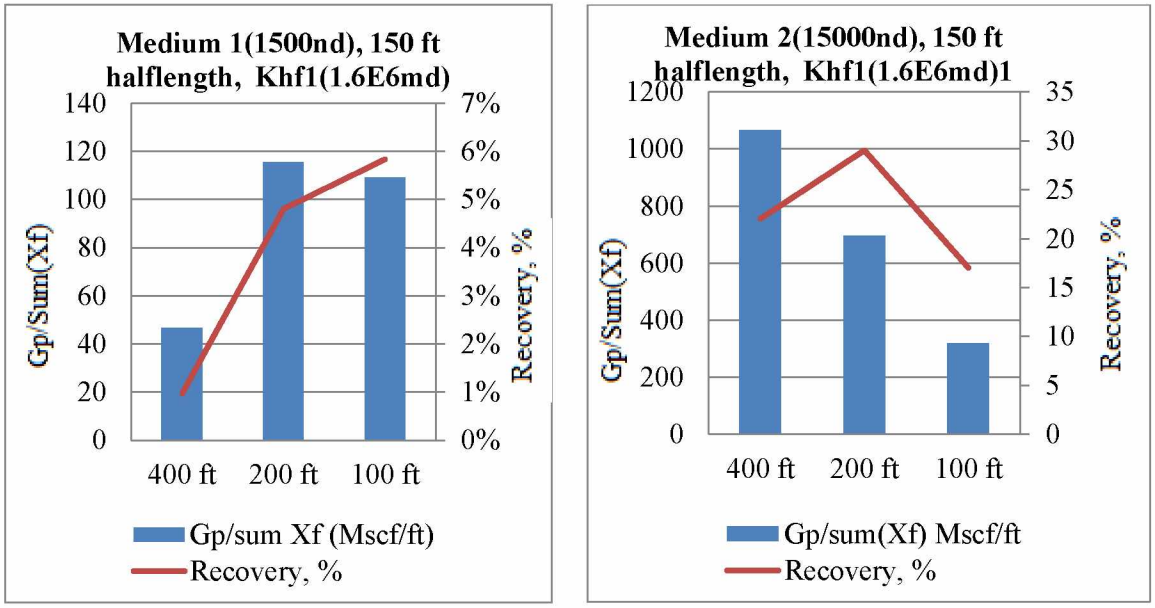

(a) **(b)**

Figure 5.2: Optimum fracture spacing for different mediums, fracture half-lengths and conductivities.

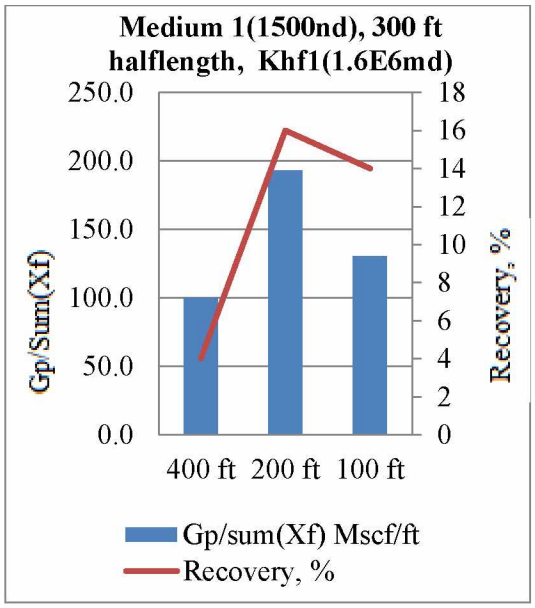

(c)

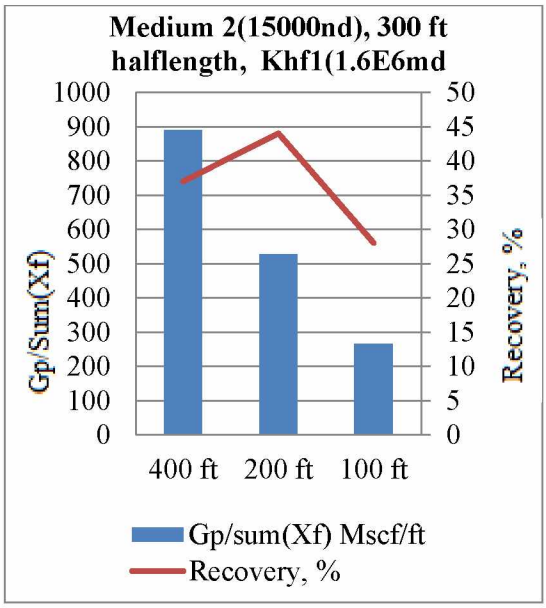

(d)

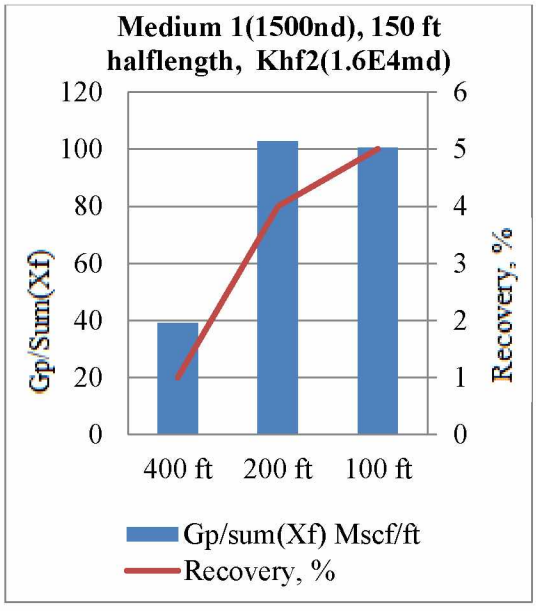

(e)

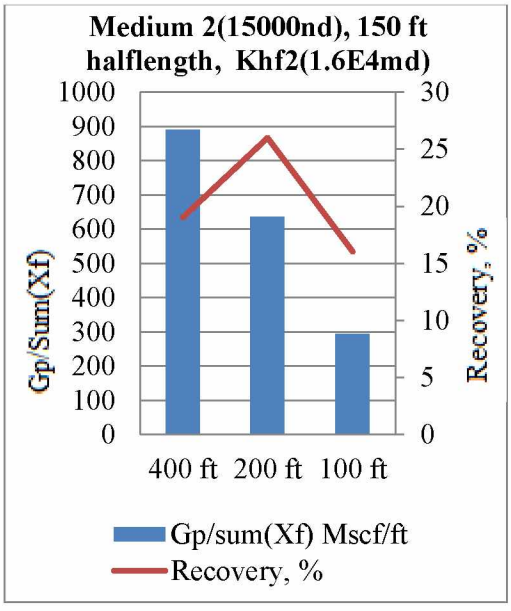

(f)

Figure 5.2-Continued.

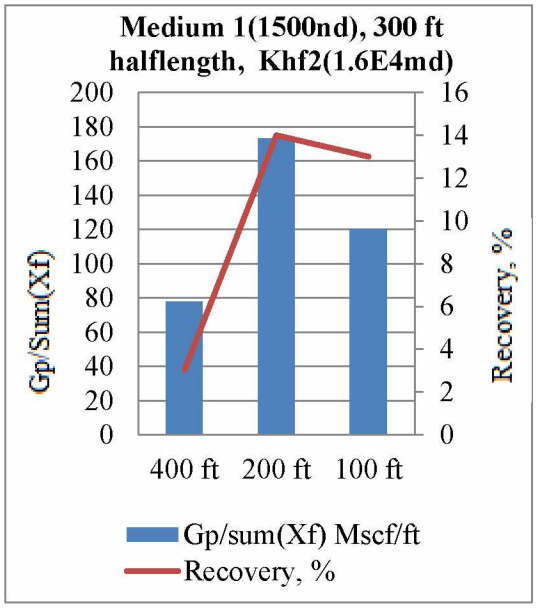

(g)

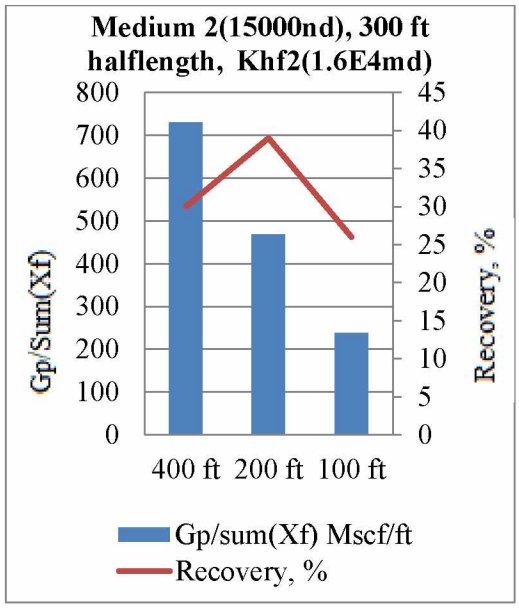

(h)

Figure 5.2-Continued.

Optimum well spacing

An optimized well spacing brings a volume of reservoir in pressure communication with the well that can be drained while it does not interfere with the drainage radii of neighboring wells. This allows development of the reservoir with the minimum number of wells as possible, which improves the economics by avoiding drilling unnecessary or more than enough wells. The challenge is still there because the reservoir quality may and will change from one location to another; however the optimization approach still works if the reservoir is well characterized in the simulation model.

Figure 5.3 shows the pressure profile for observation wells placed at different distances from the production well (for matrix without natural fractures and Xf indicating the hydraulic fracture half-

length); these observation wells were placed at some distance from the production well in order to observe pressure drop and thus determine the optimum well spacing. Table 5.5 summarizes the results of the optimum well spacing for all cases of optimum fracture spacing from the previous simulation runs.

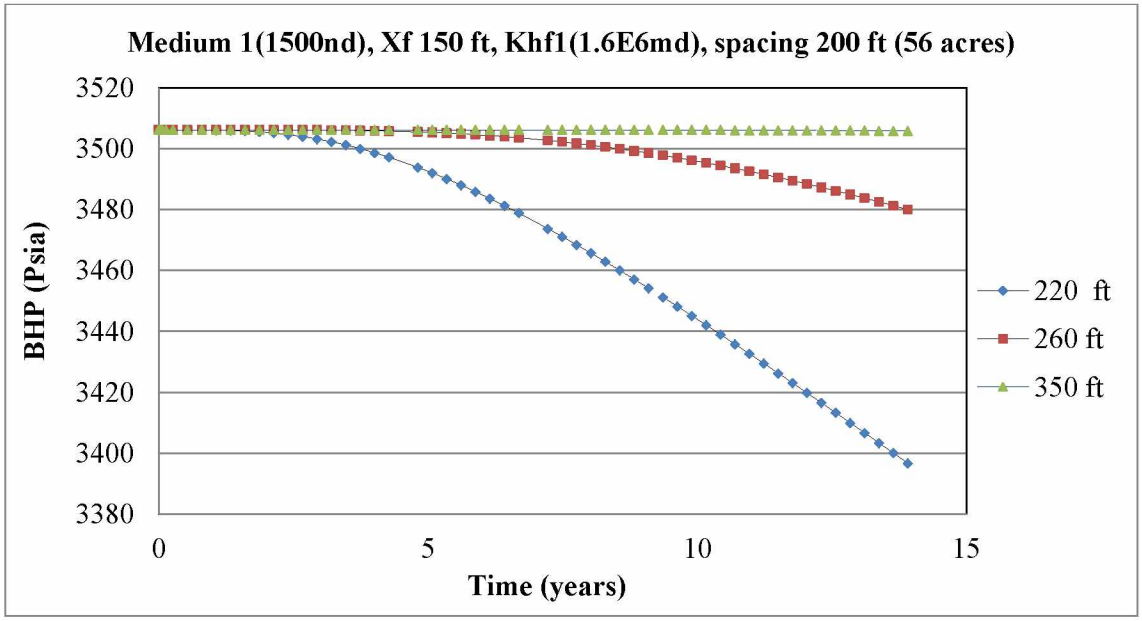

Figure 5.3: Pressure profile from observation wells at some distance from producing well.

Table 5.5: Optimum well spacing for media without natural fractures

BHP (psia)	100				
				Opt. sp. x2 (ft.)	Gp (MMscf)
M1(1500nd), Xf 150 ft., Khf1(1.6E6md), Spacing 200 ft				600	485
M1(1500nd), Xf 150 ft., Khf2(1.6E4md), Spacing 200 ft				520	427
M1(1500nd), Xf 300 ft., Khf1(1.6E6md), Spacing 200 ft				1200	1624
M1(1500nd), Xf 300 ft., Khf2(1.6E4md), Spacing 200 ft				1200	1452
M2(15000nd), Xf 300 ft., Khf1(1.6E6md), Spacing 400 ft				3000	3855
M2(15000nd), Xf 150 ft., Khf1(1.6E6md), Spacing 400 ft				2700	2168
M2(15000nd), Xf 150 ft., Kfh2(1.6E4md), Spacing 400 ft				2400	1775
M2(15000nd), Xf 300 ft., Khf2(1.6E4md), Spacing 400 ft				2900	3485

An equivalent fracture half-length of 4200 ft. was considered or assumed to obtain an optimum fracture configuration for different matrix permeability and fracture conductivities. The optimum hydraulic fracture spacing of 200 and 400 ft. obtained from the previous section were used; it resulted in 7 and 14 hydraulic fractures with fracture spacing of 400 and 200 ft. respectively. The 300 and 150 ft. fracture half-lengths were assigned to the fracture spacing of 400 and 200 ft. respectively for the horizontal leg of 1000 ft. To obtain an equivalent fracture half-length of 4200ft, two different fracture configurations were considered;

(1) 7 fractures with fracture spacing of 400 ft. and half-length of 300 ft. and

(2) 14 fractures with fracture spacing of 200 ft. and half-length of 150 ft.

Results from the simulation runs show that the 7 hydraulic fractures (300 ft. half-length) with spacing of 400 ft. gave the optimum recovery for the media with higher permeability while the 14 hydraulic fractures (150 ft. half-length) with fracture spacing of 200 ft. gave the optimum recovery for the media with lower permeability (Figure 5.4).

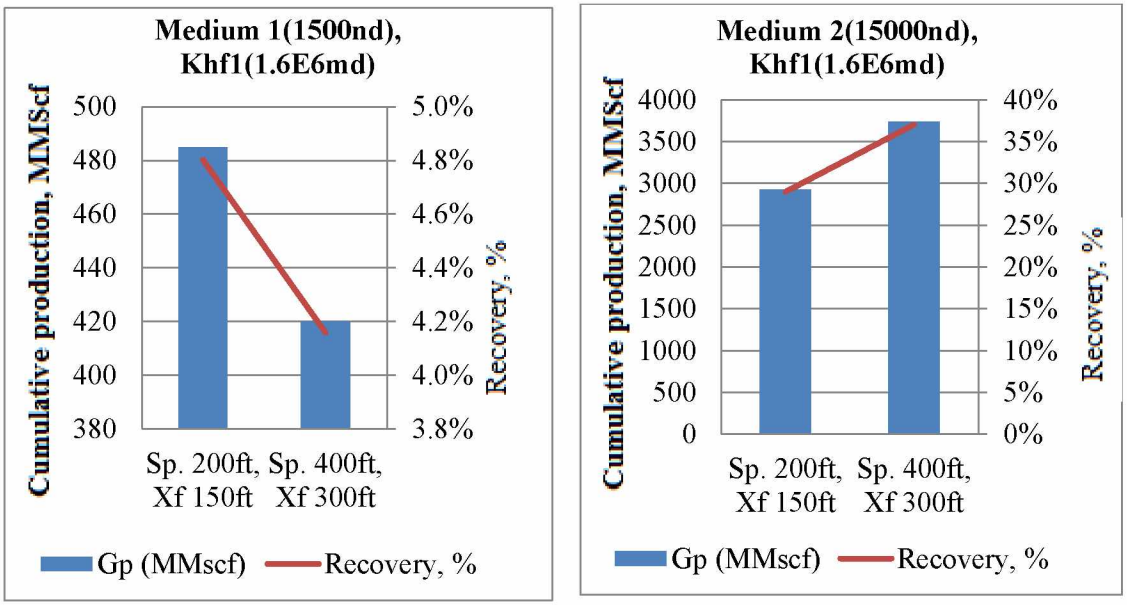

(a) **(b)**

Figure 5.4: Optimum equivalent fracture configuration for mediums without natural fractures

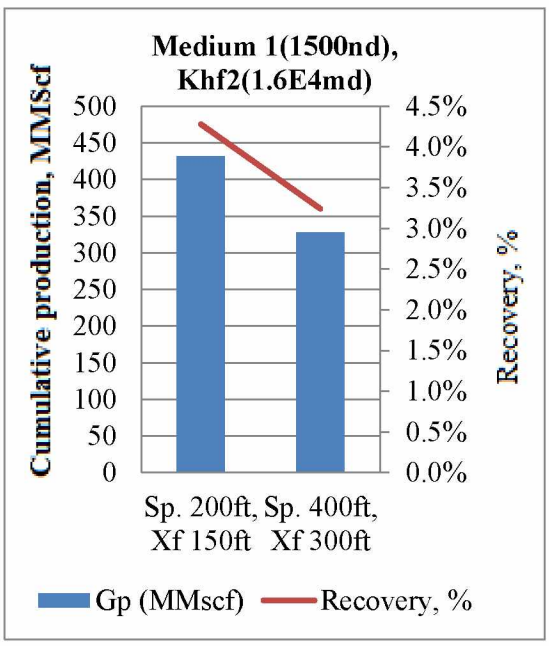

(c)

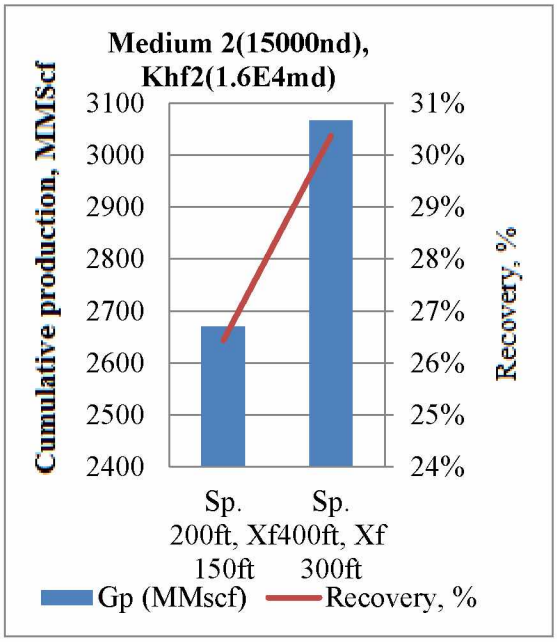

(d)

Figure 5.4-Continued.

Impact of desorption

Results from simulation runs with different desorption parameters and also without desorption show that desorption contributes considerable to the cumulative production for the range of adsorption parameters and minimum bottom hole pressure used in this study. The simulation was run to a bottom-hole pressure of 100 psia with two different extremes of Langmuir pressures of 1750 (higher Langmuir pressure) and 1000 (lower Langmuir pressure) psia (Table 5.1), and also without Langmuir parameters (no gas desorption). The more permeable medium (medium 2), fracture half-length of 300 ft. and fracture spacing of 400 ft. (the optimum spacing obtained from previous runs) were used in these simulation runs. The optimum fracture spacing was used because it gave higher recoveries and thus gave a clearer picture of the effects of desorption.

Results from these simulation runs (Figure 5.5) show up to more than 20% increase in cumulative production from desorbed gas for the Langmuir values used in this study.

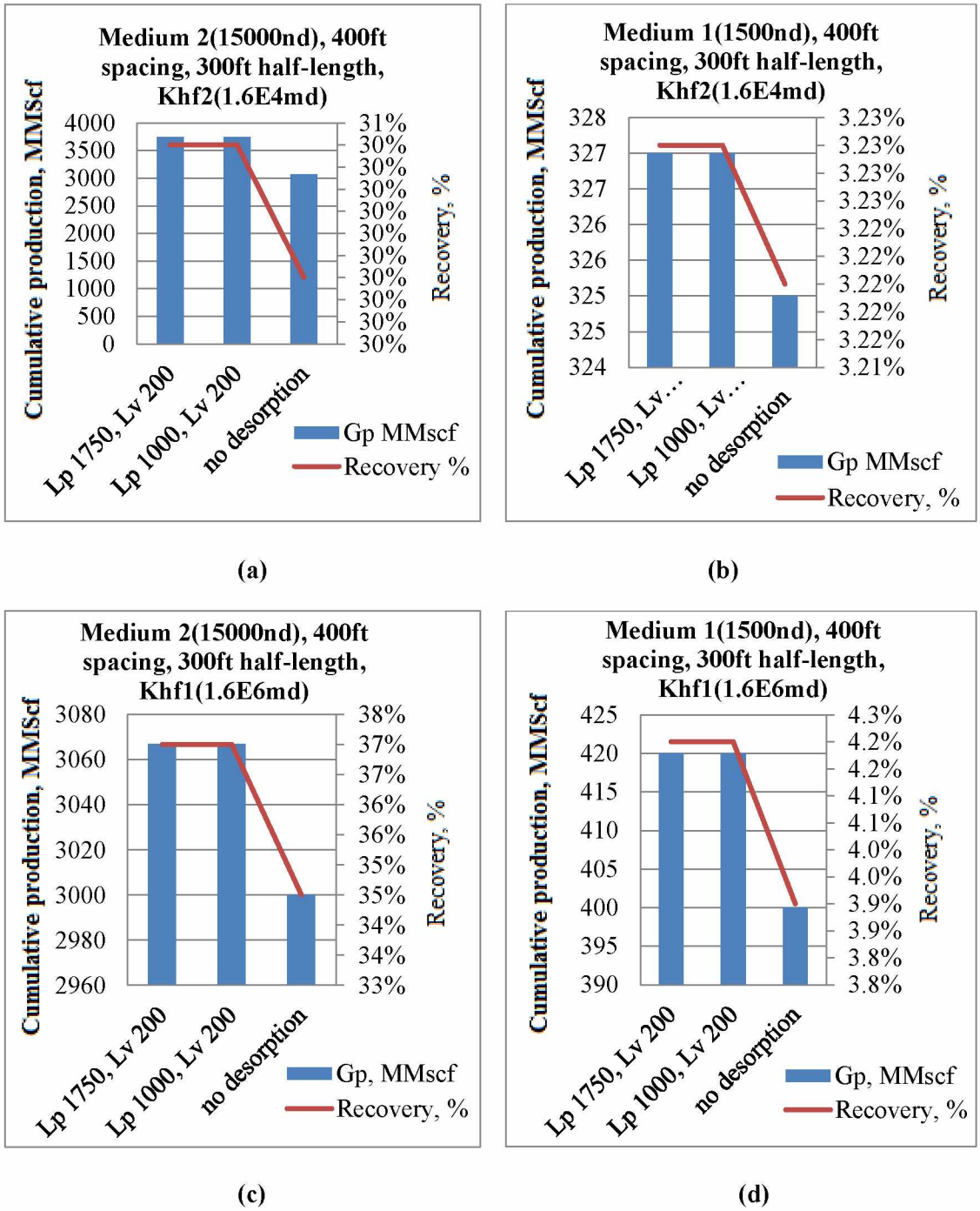

Figure 5.5: Recovery with different Langmuir parameters, and without desorption.

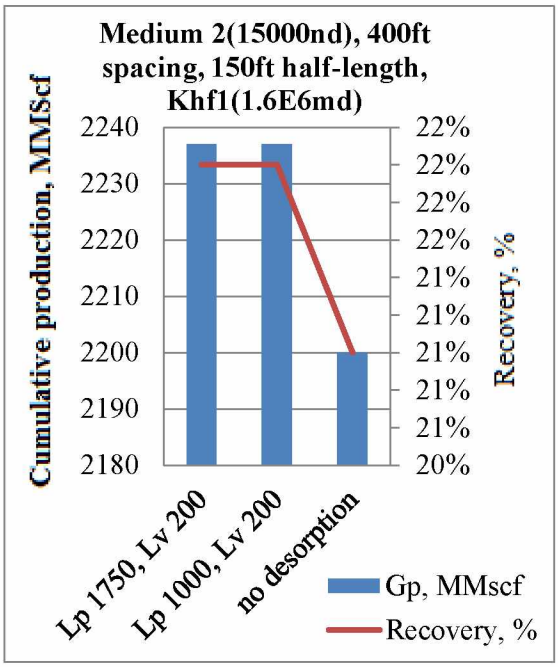

(e)

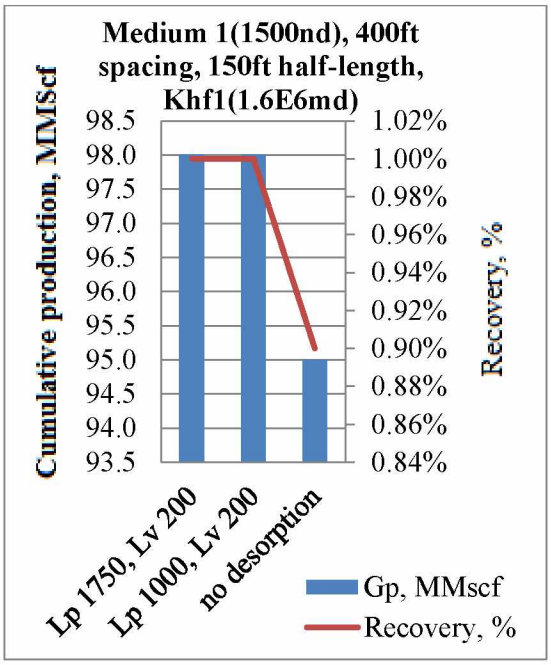

(f)

Figure 5.5-Continued.

5.2.2 Media with natural fractures (Resolve)

Simulation models with natural fractures were built and run for different cases which include a combination of natural fracture permeability, matrix permeability, hydraulic fracture half-length and conductivity. The natural fractures were represented by thin streaks of low porosity/high permeability horizontal layers above and beneath the reservoir model (Figure 5.6). Two different matrix and natural fracture permeability were used. The natural fractures were represented by thin permeable layers below and above the model. All other model parameters are the same as those given in Table 5.2.

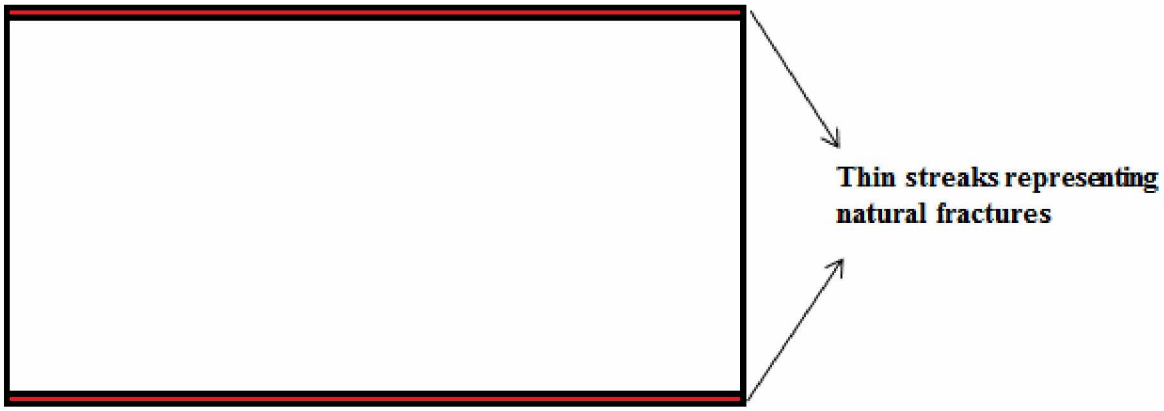

Figure 5.6: Thin streaks of more permeable layers above and beneath model representing natural fractures for Resolve

The same optimization strategy used for media without natural fractures was also applied to models with natural fractures. The three optimization stages included: 1. determining the optimum hydraulic fracture spacing; 2. determining the optimum well spacing using the results of step 1; and 3. Determining the optimum equivalent hydraulic fracture configuration representing a specified fracture fluid volume. 'Optimum configuration' is a combination of the hydraulic fracture half-length and spacing, while the 'optimum fracture spacing' involves the distance between the hydraulic fractures. The optimum fracture spacing from three different fracture spacing (100 ft., 200 ft. and 300 ft.) was first obtained. Then, the optimum well spacing was obtained using observation wells placed at various distance from the producing well.

The optimum equivalent hydraulic fracture configuration was simulated for a given equivalent hydraulic fracture half-length and for different media, natural fracture permeability, hydraulic

fracture half-lengths and conductivities. The optimum hydraulic fracture spacing of 200 and 400 ft. obtained from previous runs were used. Seven and fourteen hydraulic fractures with half-lengths of 300 ft. (spacing of 400 ft.) and 150 ft. (spacing of 200 ft.) respectively were used to obtain an equivalent or total fracture half-length of 4200ft. The minimum BHP of 100 psia and minimum production rate of 50 Mscf/day were used. These values are typically used at the Eagle Ford for optimum economic production.

5.2.2.1 Results

Simulation results for medium with natural fractures using Resolve show that the hydraulic fracture spacing of 400 ft. is the optimum for all the different combinations of reservoir and fracture parameters (Table 5.6). This suggests that the presence of natural fractures enhances communication between the matrix and fractures and has a pronounced influence on fluid flow despite of low matrix permeability.

Results for the equivalent hydraulic fracture configuration show no definite pattern in terms of optimization for different combinations of reservoir and fracture parameters (Table 5.7) i.e. one would expect the higher matrix permeability (medium 1) to give optimum recovery with the larger hydraulic fracture spacing configuration (300 ft. half-length and spacing of 400 ft.) and vice versa. The equivalent hydraulic fracture configuration varies with matrix and fracture parameters which makes the use of simulation models built from real and accurate reservoir data indispensable for obtaining the optimum equivalent fracture configuration.

Table 5.6: Optimum fracture spacing for media with natural fractures (Resolve)

RESOLVE					RESOLVE			
Medium 1(10nd), 300ft half-length, Khf1(1.6E6md),Knf1(1md)					**Medium 2(1nd), 300ft half-length, Khf1(1.6E6md), Knf1(1md)**			
	400	200	100			**400**	200	100
Gp (MMscf)	**6678**	7159	6502		Gp (MMscf)	**6541**	7120	6466
Gp/sum(Xf) Mscf/ft.	**1589.9**	852.3	602		Gp/sum(Xf) Mscf/ft.	**1557.5**	847.6	598.7
Rec. (%)	**65.8**	70.6	64.1		Rec. (%)	**64.5**	70.2	63.7
Pfinal (psia)	**794.8**	599	859.9		Pfinal (psia)	**851.9**	614	873.5
Producing Life, yrs	**52.4**	43.8	54.3		Producing Life, yrs	**50.5**	43.6	54.1
Medium 1(10nd), 300ft half-length, Khf1(1.6E6md),Knf2(0.1md)					**Medium 2(1nd), 300ft half-length, Khf1(1.6E6md), Knf2(0.1md)**			
	400	200	100			**400**	200	100
Gp (MMscf)	**4510**	5248	4085		Gp (MMscf)	**4337**	5207	4055
Gp/sum(Xf) Mscf/ft.	**1073.9**	624.8	378.2		Gp/sum(Xf) Mscf/ft.	**1032.5**	619.9	375.5
Rec. (%)	**44.5**	51.7	40.3		Rec. (%)	**42.8**	51.3	40
Pfinal (psia)	**1636**	1346	1791		Pfinal (psia)	**1706**	1361	1803
Producing Life, yrs	**75.4**	66.1	59.6		Producing Life, yrs	**72.5**	66.1	59.6
Medium 1(10nd), 300ft half-length, Khf2(1.6E4md),Knf1(1md)					**Medium 2(1nd), 300ft half-length, Khf2(1.6E4md), Knf1(1md)**			
	400	200	100			**400**	200	100
Gp (MMscf)	**5685**	6421	5974		Gp (MMscf)	**5535**	6389	5947
Gp/sum(Xf) Mscf/ft.	**1353.5**	764.4	553.2		Gp/sum(Xf) Mscf/ft.	**1317.7**	760.6	550.6
Rec. (%)	**56**	63.3	58.9		Rec. (%)	**54.6**	63	58.6
Pfinal (psia)	**1196**	909	1079		Pfinal (psia)	**1257**	920.6	1090
Producing Life, yrs	**73.5**	64.2	67.9		Producing Life, yrs	**71.4**	64.2	67.9

Table 5.6-Continued.

Medium 1(10nd), 300ft half-length, Khf2(1.6E4md),Knf2(0.1md)					**Medium 2(1nd), 300ft half-length, Khf2(1.6E4md), Knf2(0.1md)**			
	400	200	100			**400**	200	100
Gp (MMscf)	**4115**	4931	3872		Gp (MMscf)	**3952**	4895	3844
Gp/sum(Xf) Mscf/ft.	**979.7**	587	358.5		Gp/sum(Xf) Mscf/ft.	**941**	582.7	355.9
Rec. (%)	**40.6**	48.6	38.2		Rec. (%)	**39**	48.3	37.9
Pfinal (psia)	**1788**	1476	1882		Pfinal (psia)	**1854**	1490	1892
Producing Life, yrs	**79.1**	73.5	64.7		Producing Life, yrs	**76.5**	73.5	64.7

Table 5.7: Equivalent fracture configuration for mediums with natural fractures (Resolve). Optimum recovery shown in red.

RESOLVE				RESOLVE		
Medium 1(10nd), Khf1(1.6E6md), Knf1(1md)				**Medium 2(1nd), Khf1(1.6E6md), Knf1(1md)**		
	Sp. 200ft, Xf 150ft	**Sp. 400ft, Xf 300ft**			Sp. 200ft, Xf 150ft	**Sp. 400ft, Xf 300ft**
Gp (MMscf)	6598	**6677**		Gp (MMscf)	5210	**6541**
Rec. (%)	65	**65.8**		Rec. (%)	51.4	**64.5**
Pfinal (psia)	877.4	**794.5**		Pfinal (psia)	1364	**851.9**
Producing Life, yrs	55.6	**52.4**		Producing Life, yrs	55.9	**50.5**
Medium 1(10nd), Khf1(1.6E6md), Knf2(0.1md)				**Medium 2(1nd), Khf1(1.6E6md), Knf2(0.1md)**		
	Sp. 200ft, Xf 150ft	**Sp. 400ft, Xf 300ft**			**Sp. 200ft, Xf 150ft**	Sp. 400ft, Xf 300ft
Gp (MMscf)	4152	**4510**		Gp (MMscf)	**5209**	4336
Rec. (%)	40.9	**44.5**		Rec. (%)	**51.4**	42.7
Pfinal (psia)	1770.3	**1635.6**		Pfinal (psia)	**1364.8**	1705.6
Producing Life, yrs	75.7	**75.4**		Producing Life, yrs	**62.8**	72.5
Medium 1(10nd), Khf2(1.6E4md), Knf1(1md)				**Medium 2(1nd), Khf2(1.6E4md), Knf1(1md)**		
	Sp. 200ft, Xf 150ft	Sp. 400ft, Xf 300ft			**Sp. 200ft, Xf 150ft**	Sp. 400ft, Xf 300ft
Gp (MMscf)	**6112**	5684		Gp (MMscf)	**5997**	5534
Rec. (%)	**60.3**	56		Rec. (%)	**59.1**	54.6
Pfinal (psia)	**1029.1**	1196		Pfinal (psia)	**1075.2**	1257.4
Producing Life, yrs	**68.2**	73.5		Producing Life, yrs	**67.2**	71.4

Table 5.7-Continued

Medium 1(10nd), Khf2(1.6E4md), Knf2(0.1md)				**Medium 2(1nd), Khf2(1.6E4md), Knf2(0.1md)**		
	Sp. 200ft, Xf 150ft	**Sp. 400ft, Xf 300ft**			Sp. 200ft, Xf 150ft	**Sp. 400ft, Xf 300ft**
Gp (MMscf)	4011	**4114**		Gp (MMscf)	3878	**3952**
Rec. (%)	39.5	**40.6**		Rec. (%)	38.2	**39**
Pfinal (psia)	1825.6	**1787.9**		Pfinal (psia)	1875.9	**1853.7**
Producing Life, yrs	77.6	**79.1**		Producing Life, yrs	75.9	**76.5**

Figure 5.7 summarizes how the optimum equivalent fracture configuration varies in medium 1 (higher matrix permeability) and different fracture parameters. For higher hydraulic fracture conductivity (Khf2), the seven 300 ft. fracture half-length (with 400 ft. fracture spacing) configuration gave the optimum recovery for the two different natural fractures permeability (Figure 5.7 a and b). On the other hand, the lower hydraulic fracture conductivity gave two different optimum equivalent fracture configurations for the two different values of natural fracture permeability. The seven 300 ft. fracture half-length (with 400 ft. fracture spacing) configuration was the optimum for lower natural fracture value of 0.1 md while the fourteen 150 ft. fracture half-length (with 200 ft. fracture spacing) configuration yielded the optimum recovery for the higher natural fracture value of 1 md (Figure 5.7 c and d).

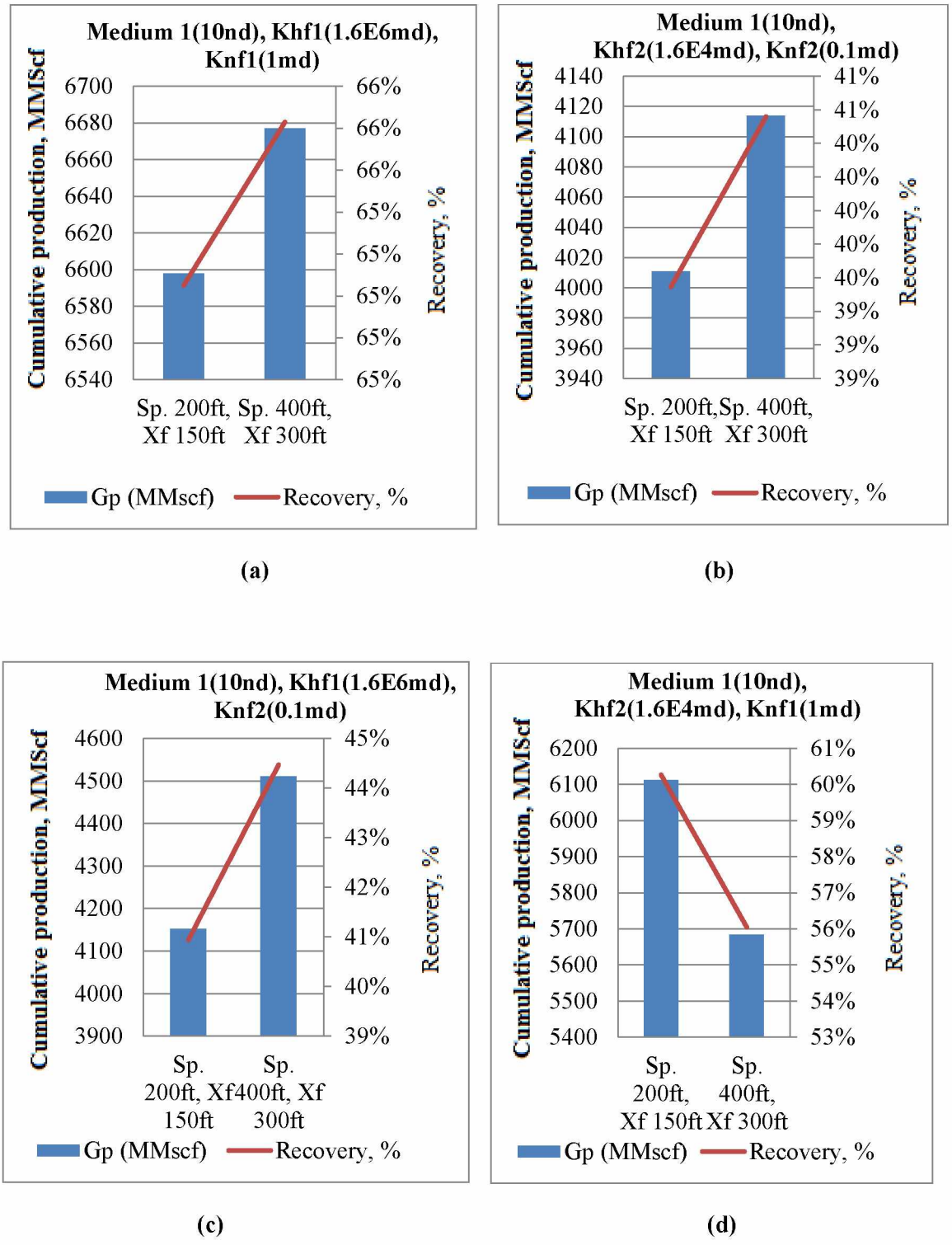

Figure 5.7: Optimum equivalent fracture configuration for medium 1 with natural fractures (Resolve).

Results for medium 2 (lower permeability) and all the various equivalent fracture configurations are given in Figure 5.8. For medium 2 with higher hydraulic fracture permeability, the fracture configuration with fracture half-length of 300 ft. (and fracture spacing of 400 ft.) gave the optimum recovery for the higher natural fracture permeability while the fracture configuration with 150 ft. fracture half-length (and fracture spacing of 200 ft.) gave the optimum for the case with lower natural fracture permeability (Figure 5.8 a and b). On the other hand, for medium 2 with lower hydraulic fracture permeability, the fracture configuration with 150 ft. fracture half-length (and fracture spacing of 200 ft.) gave the optimum recovery for higher natural fracture permeability while the fracture configuration with fracture half-length of 300 ft. (and fracture spacing of 400 ft.) gave the optimum recovery for the lower natural fracture permeability (Figure 5.8 c and d).

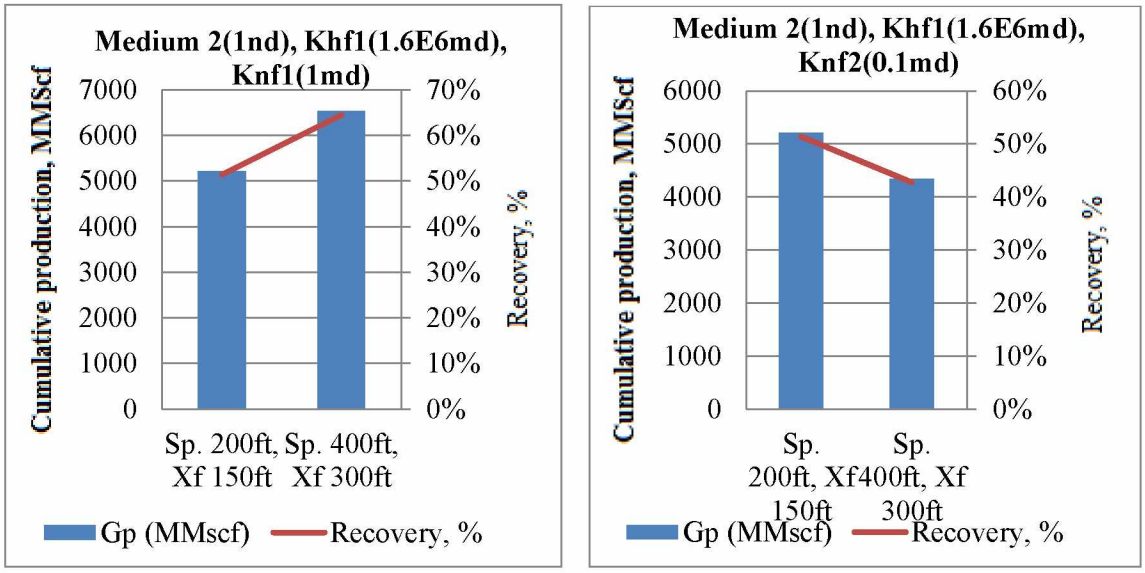

(a) **(b)**

Figure 5.8: Optimum equivalent fracture configuration for medium 2 with natural fractures (Resolve).

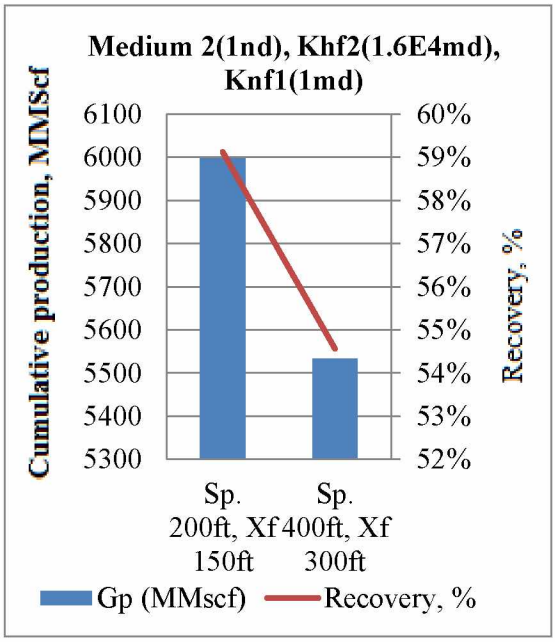

(c)

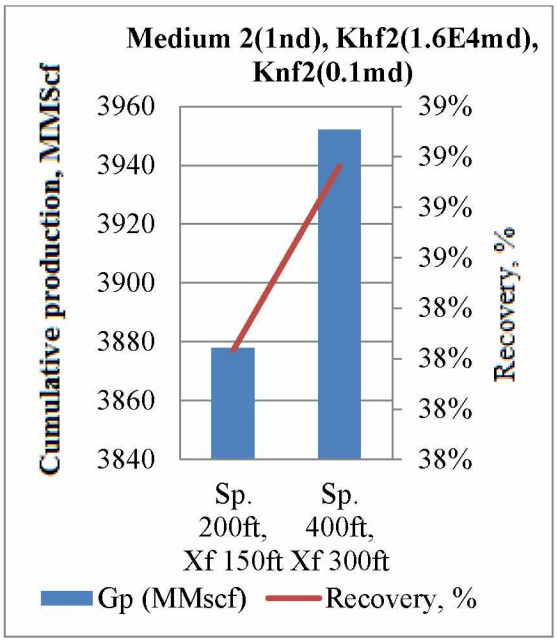

(d)

Figure 5.8-Continued.

5.2.3 Media with natural fractures (CMG)

The CMG was used to more effectively model mediums with natural fractures. Resolve represented the natural fractures by a more permeable layer above and below the model while CMG represents it more effectively with a dual porosity model (Figure 5.9). The dual porosity model having equal fracture and matrix spacing was used to model the mediums with natural fractures (Figure 5.9). CMG simulation models with natural fractures were built and run for different cases which include a combination of natural fracture permeability, medium permeability, hydraulic fracture half-length and conductivity. Two different matrix and natural fracture permeabilities were used (Table 5.3); all other model parameters for medium with natural fractures are the same as those given in Table 5.3.

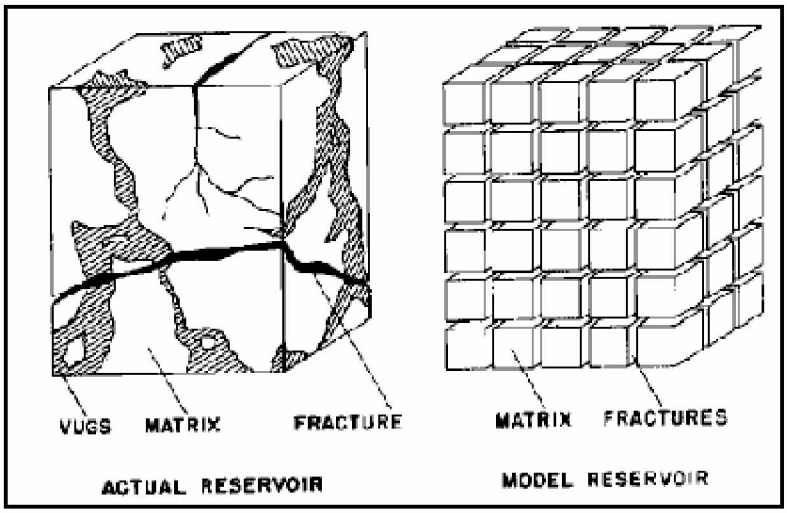

Figure 5.9: Dual porosity model (Warren and Root, 1963)

A similar optimization strategy to that used for the simulation models using Resolve was applied here. The three optimization stages included: 1. first obtaining the optimum fracture spacing; 2. obtaining the optimum well spacing; and 3. obtaining the equivalent hydraulic fracture configuration which represents a specified fracture fluid volume. The optimum hydraulic fracture spacing from three different hydraulic fracture spacing (100 ft., 200 ft. and 300 ft.) was obtained. Observation wells placed at various distance from the producing well were used to obtain the optimum well spacing.

An equivalent fracture half-length of 4200ft. was assumed, which may represent limited or fixed proppant volume. The optimum equivalent fracture configuration was simulated for this equivalent fracture half-length and for different mediums, natural fracture permeability, hydraulic fracture half-lengths and conductivities. The optimum fracture spacing of 200 and 400 ft. were used. There are two possible configurations or ways of representing this equivalent fracture half-length of 4200 ft. (given the restriction of only 2 hydraulic fracture half-length of 150 and 300

ft.): Seven and fourteen hydraulic fractures with half-lengths of 300 ft. (spacing of 400 ft.) and 150 ft. (spacing of 200 ft.) respectively.

5.2.3.1 Results

Results from simulation runs (built on data from Table 5.3) for mediums with natural fractures using CMG shows that the fracture spacing of 400 ft. is the optimum for all the different combinations of reservoir and fracture parameters (Table 5.8) i.e. 400 f.t fracture spacing gave the optimum value of the ratio of cumulative production to sum of equivalent hydraulic fracture half-length (Gp/sum(Xf)). The minimum BHP of 100 psia and minimum production rate of 50 Mscf/day were used, hydraulic fracture closure with depletion was also implemented with hydraulic fracture permeability multipliers. This suggests that the presence of natural fractures enhances communication between the matrix and natural fractures and thus increasing recovery for the larger hydraulic fracture spacing. It should be mentioned that the range of medium permeability used for cases built using CMG is two order of magnitude higher than the cases built using Resolve (Tables 5.2 and 5.3). Undoubtedly, this high medium permeability along with the way CMG represents natural fractures resulted in much higher final recoveries.

Table 5.8: Optimum fracture spacing for mediums with natural fractures (CMG). Optimum hydraulic fracture spacing shown in bold.

Medium 1(1000nd), 150 ft half-length, Khf1(1.6E6md), Knf1(1md)					**Medium 2(100nd), 150 ft half-length, Khf1(1.6E6md), Knf1**			
	400	200	100			**400**	200	100
Gp, MMscf	**7358**	7404	7409		Gp, MMscf	**7360**	7414	7423
Gp/sum(Xf) Mscf/ft	**3503**	1763	949		Gp/sum(Xf)Mscf/ft	**3505**	1765	951
Recovery (%)	**96.8**	97.4	97.5		Recovery (%)	**96.9**	97.6	97.7
Pfinal (psia)	**348.2**	286.2	274.5		Pfinal (psia)	**344.9**	281.1	269.4
Producing Life, yrs	**14**	11.5	11		Producing Life, yrs	**13**	11	11
Medium 1(1000nd), 150 ft half-length, Khf1(1.6E6md), Knf2(0.1md)					**Medium 2(100nd), 150 ft half-length, Khf1(1.6E6md), Knf2(0.1md)**			
	400	200	100			**400**	200	100
Gp, MMscf	**6933**	7087	7111		Gp, MMscf	**6935**	7395	6495
Gp/sum(Xf) Mscf/ft	**3301**	1687	911		Gp/sum(Xf)Mscf/ft	**3302**	1760	832
Recovery (%)	**91.2**	93.3	93.6		Recovery (%)	**91.3**	97.3	85.5
Pfinal (psia)	**751.7**	627.1	601.0		Pfinal (psia)	**749.6**	292.1	595.6
Producing Life, yrs	**37**	27	27		Producing Life, yrs	**42**	33	25
Medium 1(1000nd), 150 ft half-length, Khf2(1.6E4md), Knf1(1md)					**Medium 2(100nd), 150 ft half-length, Khf2(1.6E4md), Knf1(1md)**			
	400	200	100			**400**	200	100
Gp, MMscf	**7354**	7407	7419		Gp, MMscf	**6935**	7414	7412
Gp/sum(Xf) Mscf/ft	**3502**	1763	951		Gp/sum(Xf)Mscf/ft	**3302**	1765	950
Recovery (%)	**96.8**	97.5	97.6		Recovery (%)	**91.3**	97.6	97.5
Pfinal (psia)	**354.3**	288.8	274.9		Pfinal (psia)	**749.6**	281.1	270.9
Producing Life, yrs	**27**	11	11		Producing Life, yrs	**33**	11	11
Medium 1(1000nd), 150 ft half-length, Khf2(1.6E4md), Knf2(0.1md)					**Medium 2(100nd), 150 ft half-length, Khf2(1.6E4md), Knf2(0.1md)**			
	400	200	100			**400**	200	100
Gp, MMscf	**6932**	7087	7112		Gp, MMscf	**6935**	7087	7115
Gp/sum(Xf) Mscf/ft	**3301**	1687	911		Gp/sum(Xf)Mscf/ft	**3302**	1687	912
Recovery (%)	**91.2**	93.3	93.6		Recovery (%)	**91.3**	93.3	93.6
Pfinal (psia)	**751.7**	627.1	600.9		Pfinal (psia)	**749.6**	620.1	598.0
Producing Life, yrs	**37**	27	27			**44**	27	27

Table 5.8-Continued.

Medium 1(1000nd), 300 ft. half-length, Khf1(1.6E6md), Knf1(1md)					**Medium 2(100nd), 300 ft. half-length, Khf1(1.6E6md), Knf1(1md)**			
	400	200	100			**400**	200	100
Gp, MMscf	**7352**	7408	7416		Gp, MMscf	**6937**	7413	7399
Gp/sum(Xf)Mscf/ft	**1750**	882	475		Gp/sum(Xf)Mscf/ft	**1651**	882	474
Recovery (%)	**96.8**	97.5	97.6		Recovery (%)	**91.3**	97.6	97.4
Pfinal (psia)	**351.5**	287.4	277.4		Pfinal (psia)	**748.7**	281.6	276.6
Producing Life, yrs	**13**	11	11		Producing Life, yrs	**13**	11	11
Medium 1(1000nd), 300 ft. half-length, Khf1(1.6E6md), Knf2(0.1md)					**Medium 2(100nd), 300 ft. half-length, Khf1(1.6E6md), Knf2(0.1md)**			
	400	200	100			**400**	200	100
Gp, MMscf	**6934**	7132	7109		Gp, MMscf	**6937**	7090	7112
Gp/sum(Lf) Mscf/ft	**1651**	849	455		Gp/sum(Xf)Mscf/ft	**1651**	844	455
Recovery (%)	**91.3**	93.9	93.6		Recovery (%)	**91.3**	93.3	93.6
Pfinal (psia)	**750.8**	573.0	603.2		Pfinal (psia)	**748.7**	624.5	600.1
Producing Life, yrs	**35**	27	27		Producing Life, yrs	**35**	27	27
Medium 1(1000nd), 300 ft. half-length, Khf2(1.6E4md), Knf1(1md)					**Medium 2(100nd), 300 ft. half-length, Khf2(1.6E4md), Knf1(1md)**			
	400	200	100			**400**	200	100
Gp, MMscf	**7355**	7395	7392		Gp, MMscf	**7360**	7400	7422
Gp/sum(Lf) Mscf/ft	**1751**	880	473		Gp/sum(Xf)Mscf/ft	**1752**	881	475
Recovery (%)	**96.8**	97.3	97.3		Recovery (%)	**96.9**	97.4	97.7
Pfinal (psia)	**354.0**	292.1	284.7		Pfinal (psia)	**348.7**	286.7	270.2
Producing Life, yrs	**27**	11	11		Producing Life, yrs	**27**	11	11
Medium 1(1000nd), 300 ft. half-length, Khf2(1.6E4md), Knf2(0.1md)					**Medium 2(100nd), 300 ft. half-length, Khf2(1.6E4md), Knf2(0.1md)**			
	400	200	100			**400**	200	100
Gp, MMscf	**6923**	7087	7109		Gp, MMscf	**6927**	7090	7112
Gp/sum(Lf) Mscf/ft	**1648**	843	455		Gp/sum(Xf)Mscf/ft	**1649**	844	455
Recovery (%)	**91.1**	93.3	93.6		Recovery (%)	**91.2**	93.3	93.6
Pfinal (psia)	**751.8**	626.6	603.2		Pfinal (psia)	**750.8**	624.5	600.1
Producing Life, yrs	**36**	27	27		Producing Life, yrs	**36**	27	27

Results for the optimum equivalent fracture (induced fracture) configuration shows that the 200 ft. fracture spacing configuration is the optimum (highlighted in red in Table 5.9) for all combination of the various mediums and fracture parameters. This result shows that the fracture configuration with more hydraulic fractures along the horizontal leg gave the optimum recovery and can be accounted for by the uniform distribution of the natural fractures.

A large pressure drop was observed at the boundary of the model for all cases with natural fractures due to the presence of natural fractures. Consequently, so the observation wells did not give a minimum pressure drop needed to determine optimum well spacing.

Table 5.9: Optimum equivalent fracture configuration for mediums with natural fractures (CMG)). Optimum configuration shown in bold.

Medium 1(1000nd), Khf2(1.6E4md), Knf2(0.1md)				**Medium 2(100nd), Khf2(1.6E4md), Knf2(0.1md)**		
	Sp. 400ft, Xf 300ft	**Sp. 200ft, Xf 150ft**			Sp. 400ft, Xf 300ft	**Sp. 200ft, Xf 150ft**
Gp, MMscf	6923.9	**7087.2**		Gp, MMscf	6927.8	**7087**
Recovery (%)	91.1	**93.3**		Recovery (%)	91.2	**93.3**
Pfinal (psia)	751.8	**627.1**		Pfinal (psia)	750.8	**620.1**
Producing Life, yrs	36	**27**		Producing Life, yrs	36	**27**

Table 5.9-Continued.

Medium 1(1000nd), Khf1(1.6E6md), Knf1(1md)				**Medium 2(100nd), Khf1(1.6E6md), Knf1(1md)**		
	Sp. 400ft, Xf 300ft	**Sp. 200ft, Xf 150ft**			Sp. 400ft, Xf 300ft	**Sp. 200ft, Xf 150ft**
Gp, MMscf	7352.4	**7404.8**		Gp, MMscf	6937	**7414**
Recovery (%)	96.8	**97.4**		Recovery (%)	91.3	**97.6**
Pfinal (psia)	351.5	**286.2**		Pfinal (psia)	748.7	**281.1**
Producing Life, yrs	13	**11.5**		Producing Life, yrs	13	**11**
Medium 1(1000nd), Khf1(1.6E6md), Knf2(0.1md)				**Medium 2(100nd), Khf1(1.6E6md), Knf2(0.1md)**		
	Sp. 400ft, Xf 300ft	**Sp. 200ft, Xf 150ft**			Sp. 400ft, Xf 300ft	**Sp. 200ft, Xf 150ft**
Gp, MMscf	6934.1	**7087.2**		Gp, MMscf	6937	**7395.6**
Recovery (%)	91.3	**93.3**		Recovery (%)	91.3	**97.3**
Pfinal (psia)	750.8	**627.1**		Pfinal (psia)	748.7	**292.1**
Producing Life, yrs	35	**27**		Producing Life, yrs	35	**33**
Medium 1(1000nd), Khf2(1.6E4md), Knf1(1md)				**Medium 2(100nd), Khf2(1.6E4md), Knf1(1md)**		
	Sp. 400ft, Xf 300ft	**Sp. 200ft, Xf 150ft**			Sp. 400ft, Xf 300ft	**Sp. 200ft, Xf 150ft**
Gp, MMscf	7355.1	**7407.2**		Gp, MMscf	7360.3	**7414**
Recovery (%)	96.8	**97.5**		Recovery (%)	96.9	**97.6**
Pfinal (psia)	354	**288.8**		Pfinal (psia)	348.7	**281.1**
Producing Life, yrs	27	**11**		Producing Life, yrs	27	**11**

5.2.3.2 Comparison of results from CMG and Resolve

Tables 5.10 and 5.11 gives input data for both simulators. All parameters were the same except for porosities to account for the same gas in place (in both matrix and fracture) for both simulators. Comparison of results from both simulators shows an extended production period for Resolve when compared to the CMG (Figure 5.10). Figure 5.10 show that there was an early decline for Resolve while the CMG start declining at a later time. This behavior could be attributed to the different ways both simulators handles the natural fractures. CMG represents the natural fractures more effectively using the dual porosity model, so there is more communication between the natural fractures. There was thus an increased effective permeability in the CMG simulation which led to a later decline and a shorter production period.

Recovery factors for cases run using CMG are within 10% than those run using Resolve. Unlike cases reported in the previous sections, here all input properties are essentially the same for both simulators with exception of porosities to have the same amount of gas in matrix and fractures for both simulators.

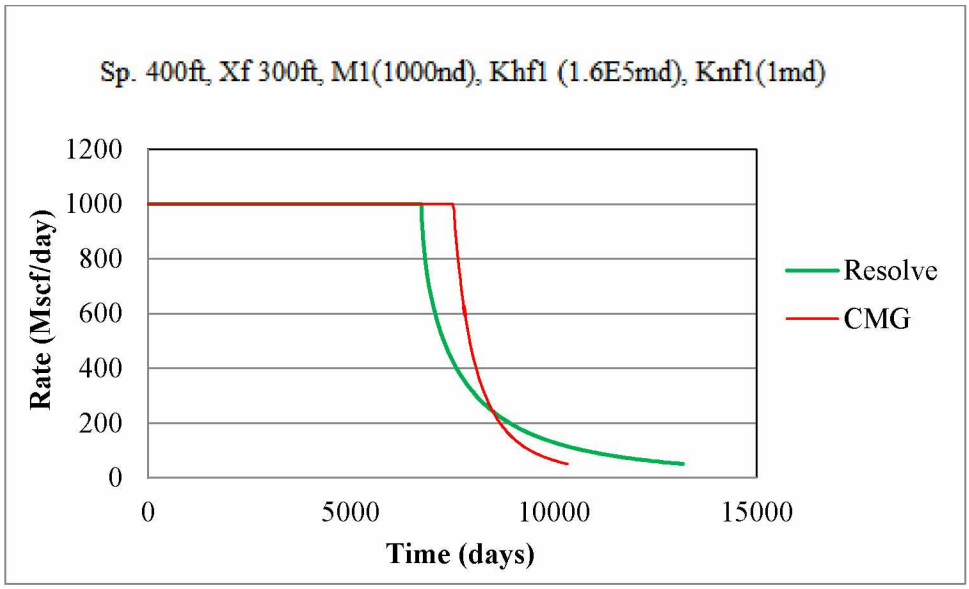

(a)

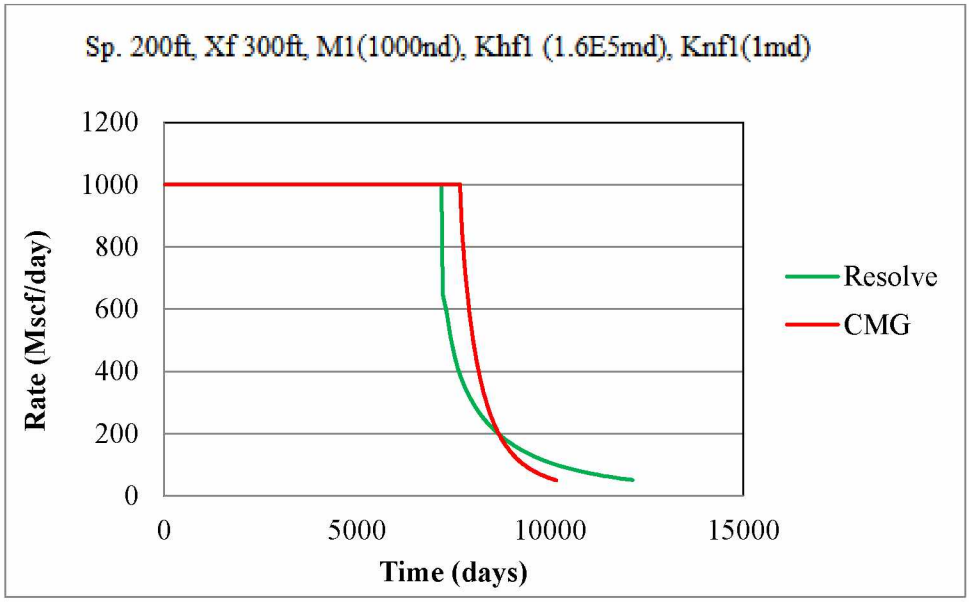

(b)

Figure 5.10: Comparison of production results for different reservoir and completion parameters for models built with the Resolve and CMG.

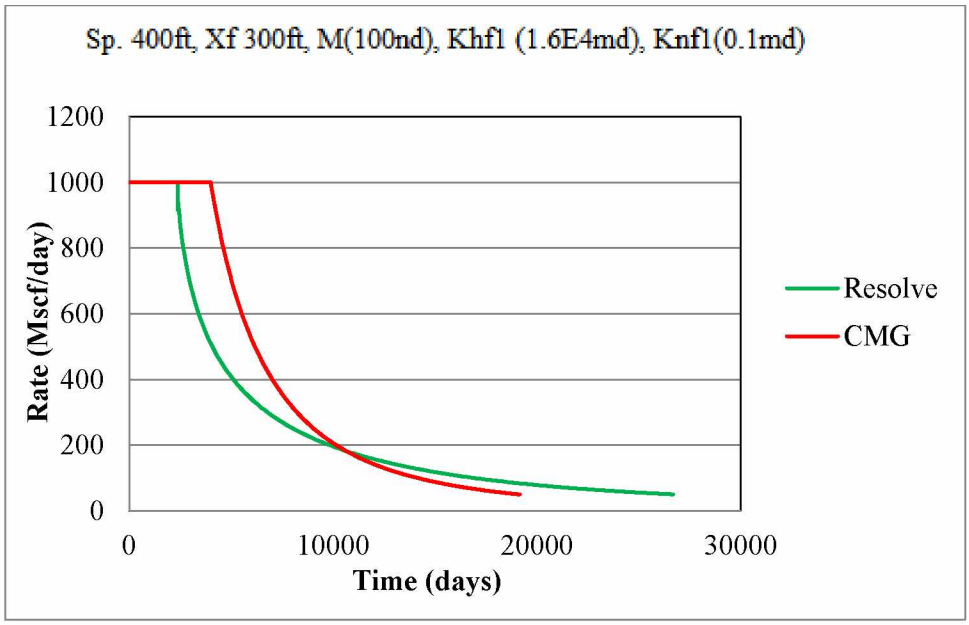

(c)

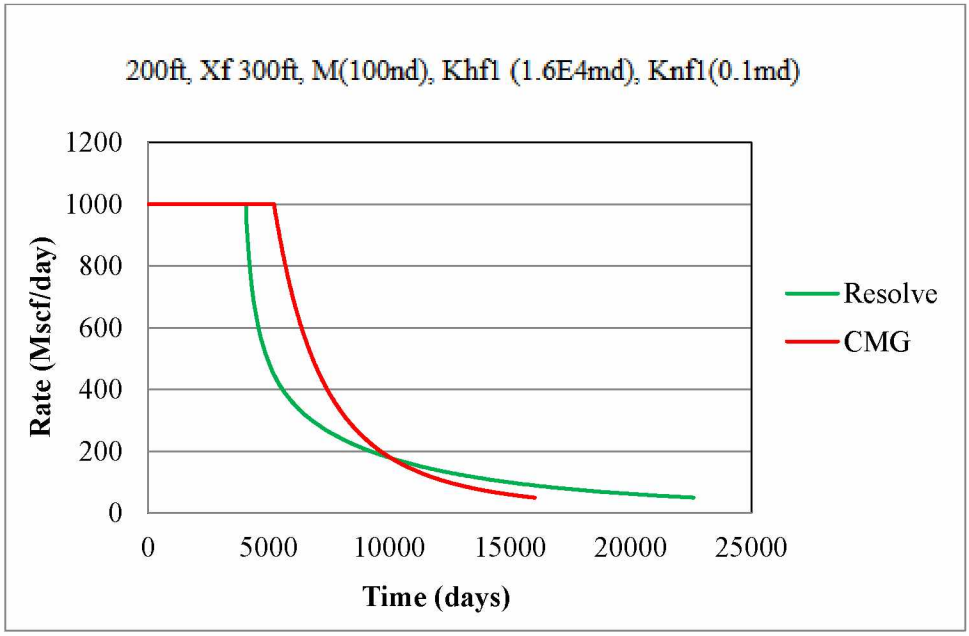

(d)

Figure 5.10-Continued.

Another observation from these results is the very high recovery obtained using CGM simulator, compared to cases run by Resolve. Ignoring the difference in thicknesses and other parameters (Tables 5.6 and 5.8), above 90% recovery were obtained from most of the CMG simulation runs. These very high recoveries are as a result of higher natural fracture densities when compared to recovery results from the Resolve. This suggest that how natural fractures are represented in the mathematical formulation on which a simulator has been built strongly affect the results.

When simulation runs with fracture closure were compared with results from that without fracture closure (Figures 5.11and 5.12), there was no significant change in recovery for the CMG simulations and only a slight increase for the Resolve simulations (less than 1%). The effects of the stress sensitive rock properties that lead to fracture closure with depletion may however lead to significant errors in reality. The errors are more intense when there is production to very low bottom hole pressures.

Which simulator is more representative in a real case scenario? CMG gives a better representation of well fractured formations with good or uniform distribution of the natural fractures. On the other hand, Resolve will more effectively model formations with little or no natural fractures. This is due to the ways both simulators represents or models natural fractures.

Which simulator to use may therefore depend upon what real data are available to incorporate into the model or suggest a model based on the natural fracture density. Ideally, geologic and/or geophysical data, such as core, field or microseismic observations are available to build the model. A complexly fractured reservoir might be better modeled by CMG, while a non-fractured or minimally fractured reservoir could be modeled using Resolve. An alternative could be matching production history with simulation models before forecasting however, history matching is not unique.

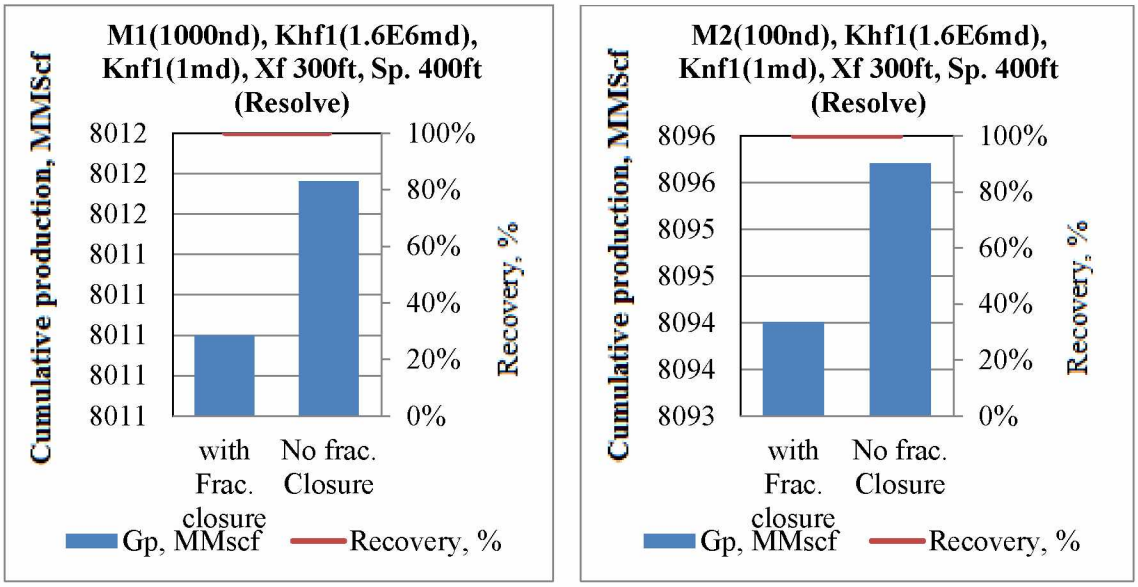

(a) (b)

Figure 5.11: Comparison of simulation results with and without fracture closure (Resolve)

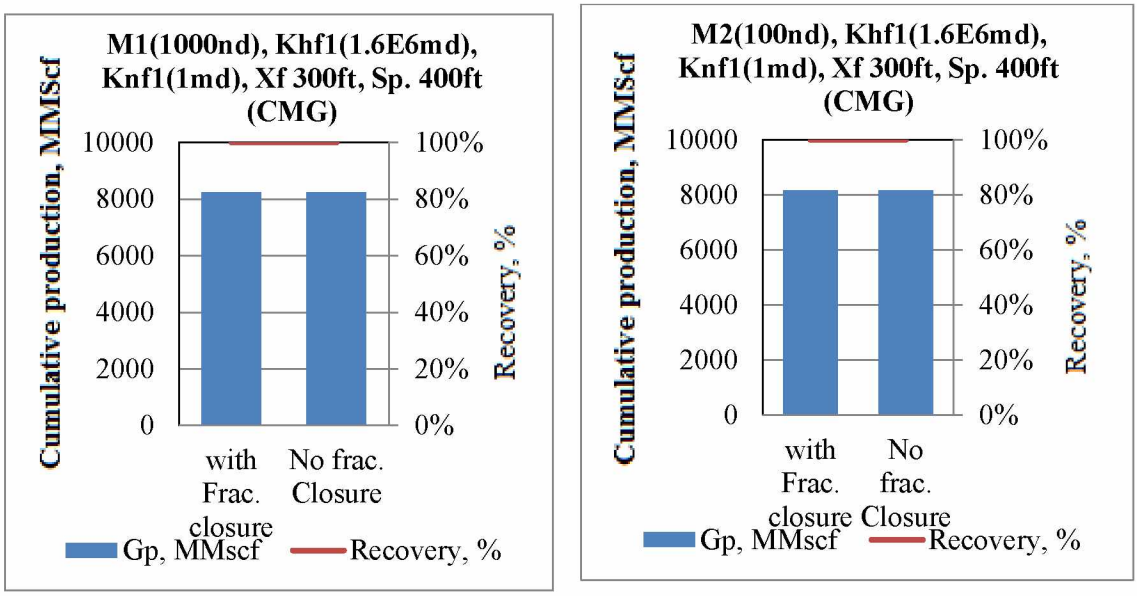

(a) (b)

Figure 5.12: Comparison of simulation results with and without fracture closure (CMG)

5.3 Decline Curve Analysis for simulation models

Decline Curve Analysis (DCA) was used to evaluate production data generated from simulation models; eight different cases were analyzed each for both the Resolve and the CMG simulators. The simulated production profiles of the wells were used to investigate how effectively the decline curve can be used to make a future production forecast. Starting from beginning of the rate versus cumulative decline and making use of the appropriate decline model, different portions (one-quarter, one-half and three quarters) of the data were fitted for decline curve analysis. Then the cumulative production values to abandonment from the decline curve analysis were compared to those from simulation.

Simulation models were built for mediums with natural fractures using both Resolve and CMG; all model properties were the same for the two simulators except for porosity values in order to obtain the same initial gas in place (both in fractures and matrix) and to see how close the predictions from these two models will be. The models parameters for the two simulators used for this analysis are given in Tables 5.10 and 5.11.

Starting from beginning of the rate versus cumulative decline, different portions (one-quarter, one-half and three quarters) of the data were fitted for decline curve analysis. Then the cumulative production values to abandonment from decline curve analysis were compared to those from simulation. The harmonic and exponential decline curve models were used to see which model best fit the generated results.

Table 5.10: Model parameters for DCA simulation model (CMG)

Area (ft2)	3500 X 1500
Thickness, layer 2(middle), ft.	150
Depth (ft.)	8000
Horizontal leg (ft.)	3000
Fracture stages	7 - 25
Hydraulic fracture spacing (ft.)	400, 200, 100
Hydraulic fracture half-length (ft.)	150, 300
Medium 1 (nd)	1000
Medium 2 (nd)	100
Hyd. Frac. Perm. Khf1 (md)	1660000
Hyd. Frac. Perm. Khf2 (md)	16600
Natural frac. Perm. Knf1 (md)	1
Natural frac. Perm. Knf2 (md)	0.1
Matrix porosity	0.0501
Fracture porosity	8.8e-5
IGIP (MMScf)	8463

IGIP: Initial Gas in Place.

Table 5.11: Model parameters for DCA simulation model (Resolve)

Area (ft2)	3500 X 1500
Thickness, layer 1(top), ft.	1
Thickness, layer 2(middle), ft.	150
Thickness, layer 3(bottom), ft.	1
Depth (ft.)	8000
Horizontal leg (ft.)	3000
Fracture stages	7 - 25
Hydraulic fracture spacing (ft.)	400, 200, 100
Hydraulic fracture half-length (ft.)	150, 300
Medium 1 (nd)	1000
Medium 2 (nd)	100
Hyd. Frac. Perm. Khf1 (md)	1660000
Hyd. Frac. Perm. Khf2 (md)	16600
Natural frac. Perm. Knf1 (md)	1
Natural frac. Perm. Knf2 (md)	0.1
Matrix porosity	0.07
Fracture porosity	0.03
IGIP (MMScf)	8463

IGIP: Initial Gas in Place.

5.3.1 Results

Results of production forecasts using different parts of the simulated decline curve are shown in Tables 5.12-5.14). The results show that the accuracy of forecast increases when longer portion of simulated production profile were used (Figures 5.13 and 5.14) for Resolve. The decline curve analysis of all the cases analyzed shows that the production forecast for one-quarter, one-half and three-quarter periods are approximately 66%, 78% and 84% respectively of the simulation values (Figures 5.15-5.20). This means that the decline curve analysis significantly under predicted the simulation values of cumulative gas produced, especially for short time periods.

The error range of final cumulative production varied from 4 to 35% (Figures 5.15-5.20) for the cases investigated here. The error was calculated by comparing the forecasted cumulative production to the actual (Figures 5.15-5.20). The error seems to be lower for cases with high medium (matrix permeability) and hydraulic fracture permeability and longer fracture half length (Figure 5.15a).

Table 5.12: Production forecast for different portions of the decline curve for mediums without natural fracture

1/4 Period				
Medium	M2(15000nd), Khf1(1.6E6md),	M2(15000nd),Khf 2(1.6E4md),	M2(15000nd),Khf 1(1.6E6md),	M2(15000nd) ,Khf2(1.6E4m d),
	Sp. 400ft, Xf 300ft	Sp. 400ft, Xf 300ft	Sp. 400ft, Xf 150ft	Sp. 400ft, Xf 150ft
Minimum rate q_t (Mscf/D)	49.95	49.95	49.95	49.95
Initial rate, q_i (Mscf/D)	305	263.549	191.89	184.07
Di (1/days)	-5.90E-07	-7.70E-07	-9.30E-07	-1.16E-06
Remaining production to limit (MMscf)	3.07E+06	2.16E+06	1.45E+06	1.12E+06
Sim. Actual Q (MMscf)	3490000	2710000	2240000	1720000
Abs(QDCA /Qsim -1)	0.121	0.203	0.353	0.345
1/2 Period				
Medium	M2(15000nd),Kh f1(1.6E6md),	M2(15000nd),Khf 2(1.6E4md),	M2(15000nd),Kh f1(1.6E6md),	M2(15000nd) ,Khf2(1.6E4m d),
	Sp. 400ft, Xf 300ft	Sp. 400ft, Xf 300ft	Sp. 400ft, Xf 150ft	Sp. 400ft, Xf 150ft
Minimum rate q_t (Mscf/D)	49.95	49.95	49.95	49.95
Initial rate, q_i (Mscf/D)	294.8	228.39	178.04	167.33
Di (1/days)	5.50E-07	6.3E-07	7.90E-07	8.8E-07
Remaining production to limit (MMscf)	3230000	2410000	1610000	1370000
Sim. Actual Q (MMscf)	3490000	2710000	2240000	1720000
Abs(QDCA /Qsim -1)	0.075	0.109	0.281	0.199

Table 5.12-Continued.

3/4 Period				
Medium	M2(15000nd), Khf1(1.6E6md),	M2(15000nd) ,Khf2(1.6E4md),	M2(15000nd), Khf1(1.6E6md) ,	M2(15000nd),Khf2(1.6E4md),
	Sp. 400ft, Xf 300ft	Sp. 400ft, Xf 300ft	Sp. 400ft, Xf 150ft	Sp. 400ft, Xf 150ft
Minimum rate q_t (Mscf/D)	49.95	49.95	49.95	49.95
Initial rate, q_i (Mscf/D)	286.47	236.67	169.073	159.939
Di (1/days)	-5.20E-07	-6.10E-07	-7.00E-07	-7.50E-07
Remaining production to limit (MMscf)	3.36E+06	2.55E+06	1.74E+06	1.55E+06
Sim. Actual Q (MMscf)	3490000	2710000	2240000	1720000
Abs(QDCA /Qsim -1)	0.038	0.059	0.222	0.096
1/4 Period				
Medium	M1(1500nd), Khf1(1.6E6md),	M1(1500nd), Khf2(1.6E4md),	M1(1500nd),Khf1(1.6E6md),	M1(1500nd),Khf2(1.6E4md),
	Sp. 200ft, Xf 300ft	Sp. 200ft, Xf 300ft	Sp. 200ft, Xf 150ft	Sp. 200ft, Xf 150ft
Minimum rate q_t (Mscf/D)	49.95	49.95	49.95	49.95
Initial rate, q_i (Mscf/D)	128.157	177.73	128.157	107.02
Di (1/days))	4.47E-06	0.00000152	4.47E-06	0.00000401
Remaining production to limit (MMscf)	211000	835000	211000	190000
Sim. Actual Q (MMscf)	341000	1190000	341000	287000
Abs(QDCA /Qsim -1)	0.382	0.302	0.382	0.338

Table 5.12-Continued.

1/2 Period				
Medium	M1(1500nd), Khf1(1.6E6md),	M1(1500nd),Khf2(1.6E4md),	M1(1500nd), Khf1(1.6E6md),	M1(1500nd),Khf2(1.6E4md),
	Sp. 200ft, Xf 300ft	Sp. 200ft, Xf 300ft	Sp. 200ft, Xf 150ft	Sp. 200ft, Xf 150ft
Minimum rate q_t (Mscf/D)	49.95	49.95	49.95	49.95
Initial rate, q_i (Mscf/D)	120.3	163.45	120.3	102.89
Di (1/days)	0.00000345	0.00000116	0.00000345	0.00000327
Remaining production to limit (MMscf)	255000	1020000	255000	221000
Sim. Actual Q (MMscf)	341000	1190000	341000	287000
Abs(QDCA /Qsim -1)	0.253	0.146	0.253	0.23

3/4 Period				
Medium	M1(1500nd),Khf1(1.6E6md),	M1(1500nd),Khf2(1.6E4md),	M1(1500nd),Khf1(1.6E6md),	M1(1500nd),Khf2(1.6E4md),
	Sp. 200ft, Xf 300ft	Sp. 200ft, Xf 300ft	Sp. 200ft, Xf 150ft	Sp. 200ft, Xf 150ft
Minimum rate q_t (Mscf/D)	49.95	49.95	49.95	49.95
Initial rate, q_i (Mscf/D)	113.81	160.2755	113.81	99.158
Di (1/days))	0.00000286	0.00000105	0.00000286	0.0000028
Remaining production to limit (MMscf)	288000	1110000	288000	245000
Sim. Actual Q (MMscf)	341000	1190000	341000	287000
Abs(QDCA/Q sim -1)	0.156	0.072	0.156	0.147

Table 5.13 : Production forecast for different portions of the decline curve for mediums with natural fracture (Resolve).

1/4 Period				
Medium	M 1(1000nd), Khf1(1.6E6md), Knf1(1md), Xf 150, Sp.200	M 1(1000nd), Khf1(1.6E6md), Knf1(1md), Xf 300, Sp.400	M 2(100nd), Khf1(1.6E6md), Knf1(1md), Xf 150, Sp.200	M 2(100nd), Khf1(1.6E6md), Knf1(1md), Xf 300, Sp.400
Minimum rate q_t (Mscf/D)	49.95	49.95	49.95	49.95
Initial rate, q_i (Mscf/D)	507.8	389.7	432.6	571.94
Di (1/days)	0.000232	0.000219	0.000203	0.000275
Remaining Time to limit (days)	9.99E+03	9.38E+03	1.06E+04	8.87E+03
Sim. Actual Time (days)	1.77E+05	1.58E+04	2.08E+04	1.63E+04
Abs(TDCA/T sim -1)	0.437	0.407	0.49	0.455
1/2 Period				
Medium	M 1(1000nd), Khf1(1.6E6md), Knf1(1md), Xf 150, Sp.200	M 1(1000nd), Khf1(1.6E6md), Knf1(1md), Xf 300, Sp.400	M 2(100nd), Khf1(1.6E6md), Knf1(1md), Xf 150, Sp.200	M 2(100nd), Khf1(1.6E6md), Knf1(1md), Xf 300, Sp.400
Minimum rate q_t (Mscf/D)	49.95	49.95	49.95	49.95
Initial rate, q_i (Mscf/D)	449.08	355.47	373.735	495.91
Di (1/days))	0.000176	0.000172	0.000145	0.000208
Remaining Time to limit (days)	1.24E+04	1.14E+04	1.39E+04	1.10E+04
Sim. Actual Time (days)	1.77E+05	1.58E+04	2.08E+04	1.63E+04
Abs(TDCA/T sim -1)	0.297	0.278	0.334	0.323

Table 5.13-Continued.

3/4 Period				
Medium	M 1(1000nd), Khf1(1.6E6md), Knf1(1md), Xf 150, Sp.200	M 1(1000nd), Khf1(1.6E6md), Knf1(1md), Xf 300, Sp.400	M 2(100nd), Khf1(1.6E6md), Knf1(1md), Xf 150, Sp.200	M 2(100nd), Khf1(1.6E6md), Knf1(1md), Xf 300, Sp.400
Minimum rate q_t (Mscf/D)	49.95	49.95	49.95	49.95
Initial rate, q_i (Mscf/D)	400.27	324.47	328.22	437
Di (1/days)	0.000145	0.000144	0.000114	0.000166
Remaining Time to limit (days)	14300	1.29+04	16400	13000
Sim. Actual Time (days)	177000	15800	20800	16300
Abs(TDCA/Tsim -1)	0.19	0.179	0.212	0.198

Table 5.14 : Production forecast for different portions of the decline curve for mediums with natural fracture (CMG).

1/4 Period				
Medium	M 1(1000nd), Khf1(1.6E6md), Knf1(1md), Xf 300, Sp.400	M 1(1000nd), Khf2(1.6E4md), Knf1(1md), Xf 300, Sp.400	M 2(100nd), Khf1(1.6E6md), Knf1(1md), Xf 150, Sp.200	M 2(100nd), Khf1, Knf1(1md), Xf 300, Sp.400
Minimum rate q_t (Mscf/D)	50	50	50	50
Initial rate, q_i (Mscf/D)	500.6	364.8	438.81	473.9
Di (1/days)	1.20E-03	1.10E-03	1.53E-03	1.63E-03
Remaining Time to limit (days)	1.92E+03	1.81E+03	1.42E+03	1.38E+03
Sim. Actual Time (days)	2.82+03	2.67E+03	2.16E+03	2.19E+03
Abs(TDCA/Tsim -1)	0.32	0.32	0.35	0.37
1/2 Period				
Medium	M 1(1000nd), Khf1(1.6E6md), Knf1(1md), Xf 300, Sp.400	M 1(1000nd), Khf2(1.6E4md), Knf1(1md), Xf 300, Sp.400	M 2(100nd), Khf1(1.6E6md), Knf1(1md), Xf 150, Sp.200	M 2(100nd), Khf1(1.6E6md), Knf1(1md), Xf 300, Sp.400
Minimum rate q_t (Mscf/D)	50	50	50	50
Initial rate, q_i (Mscf/D)	460.1	344.74	409.1	436.07
Di (1/days)	1.04E-03	9.31E-04	1.29E-03	1.33E-03
Remaining Time to limit (days)	2.14E+03	2.07E+03	1.63E+03	1.63E+03
Sim. Actual Time (days)	2.82+03	2.67E+03	2.16E+03	2.19E+03
Abs(TDCA/Tsim -1)	0.24	0.23	0.24	0.26

Table 5.14-Continued.

3/4 Period				
Medium	M 1(1000nd), Khf1(1.6E6md), Knf1(1md), Xf 300, Sp.400	M 1(1000nd), Khf2(1.6E4md), Knf1(1md), Xf 300, Sp.400	M 2(100nd), Khf1(1.6E6md), Knf1(1md), Xf 150, Sp.200	M 2(100nd), Khf1(1.6E6md), Knf1(1md), Xf 300, Sp.400
Minimum rate q_t (Mscf/D)	50	50	50	50
Initial rate, q_i (Mscf/D)	420	322.5	378.84	397.53
Di (1/days)	0.000889	0.000814	0.00112	0.00113
Remaining Time to limit (days)	2390	2290	1810	1830
Sim. Actual Time (days)	2.82+03	2670	2160	2190
Abs(TDCA/Tsim -1)	0.15	0.15	0.17	0.16

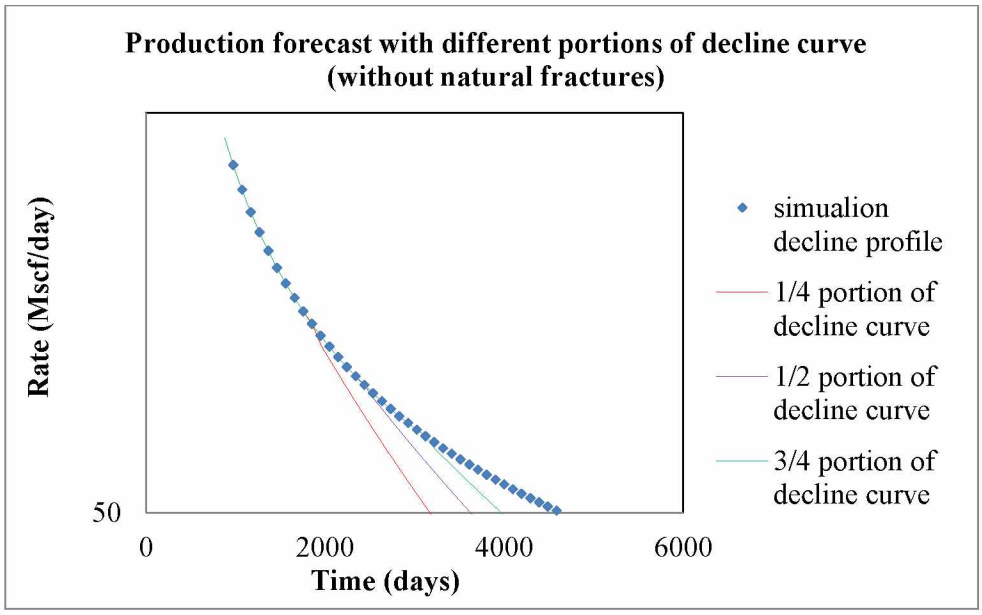

Figure 5.13: Simulation production profile and forecast from DCA using different portions of curve for medium without natural fractures(Resolve).

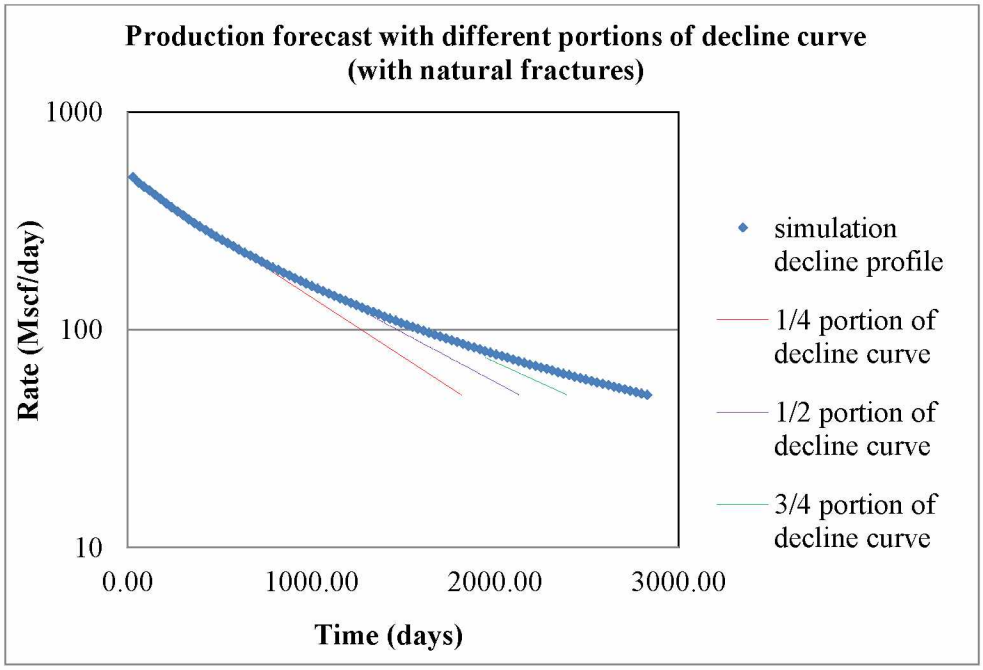

Figure 5.14: Simulation production profile and forecast from DCA using different portions of curve for medium with natural fractures(Resolve)

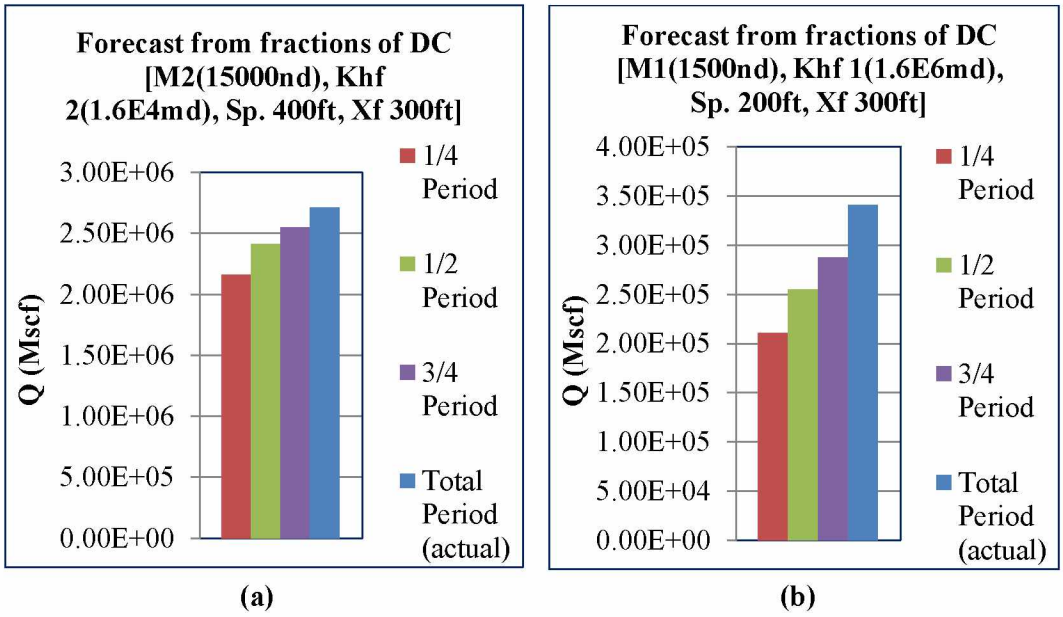

Figure 5.15: Comparison of cumulative produced gas from DCA forecasts with simulation when different portions of decline history are used (Mediums without natural fractures).

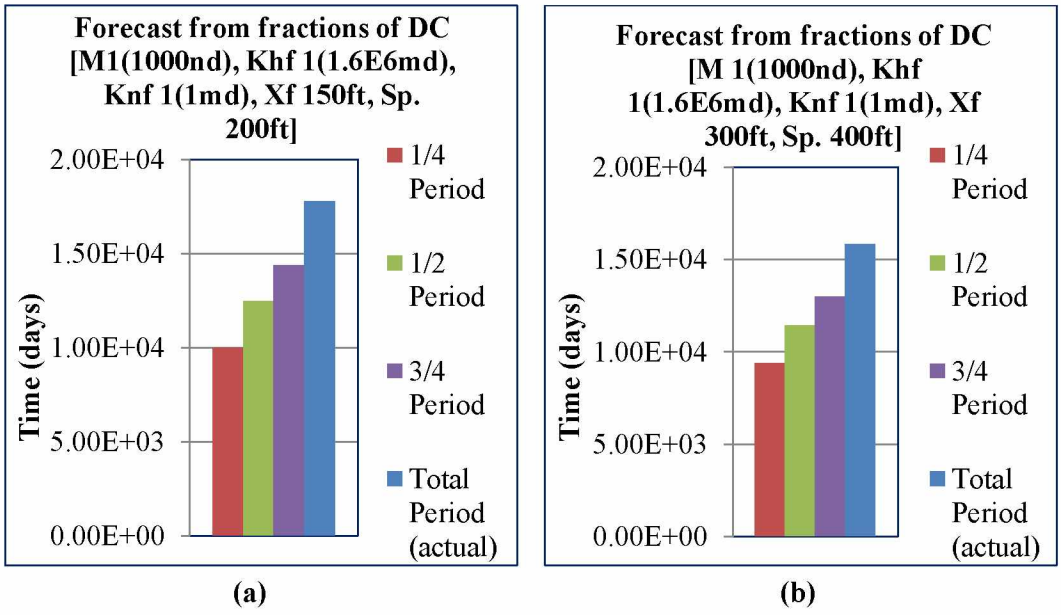

Figure 5.16: Comparison of cumulative produced gas from DCA forecasts with simulation when different portions of decline history are used (Mediums with natural fractures for Resolve)

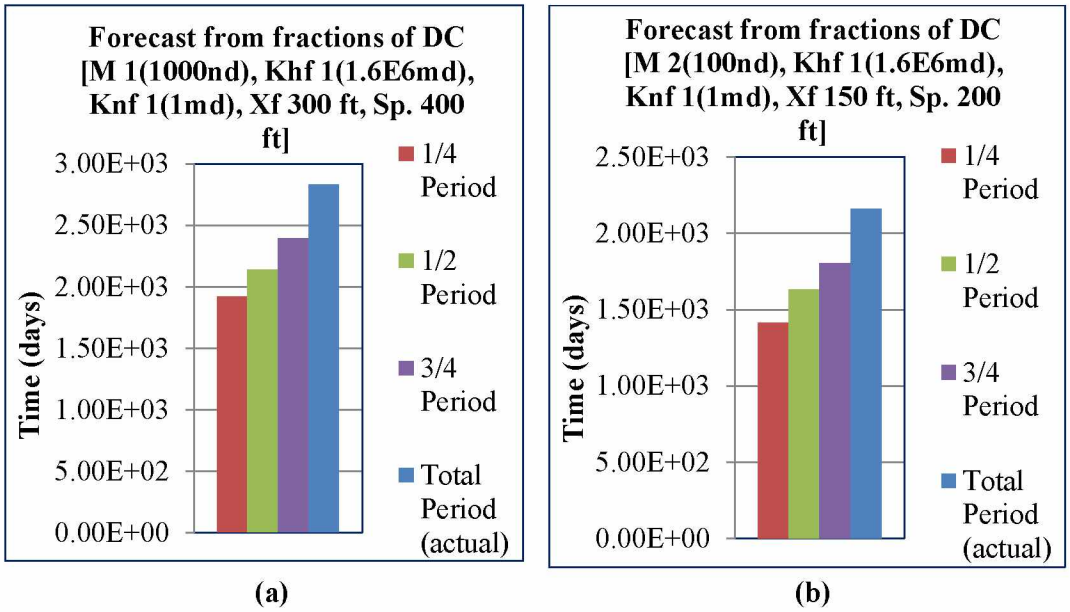

Figure 5.17: Comparison of cumulative produced gas from DCA forecasts with simulation when different portions of decline history are used (Mediums with natural fractures for CMG)

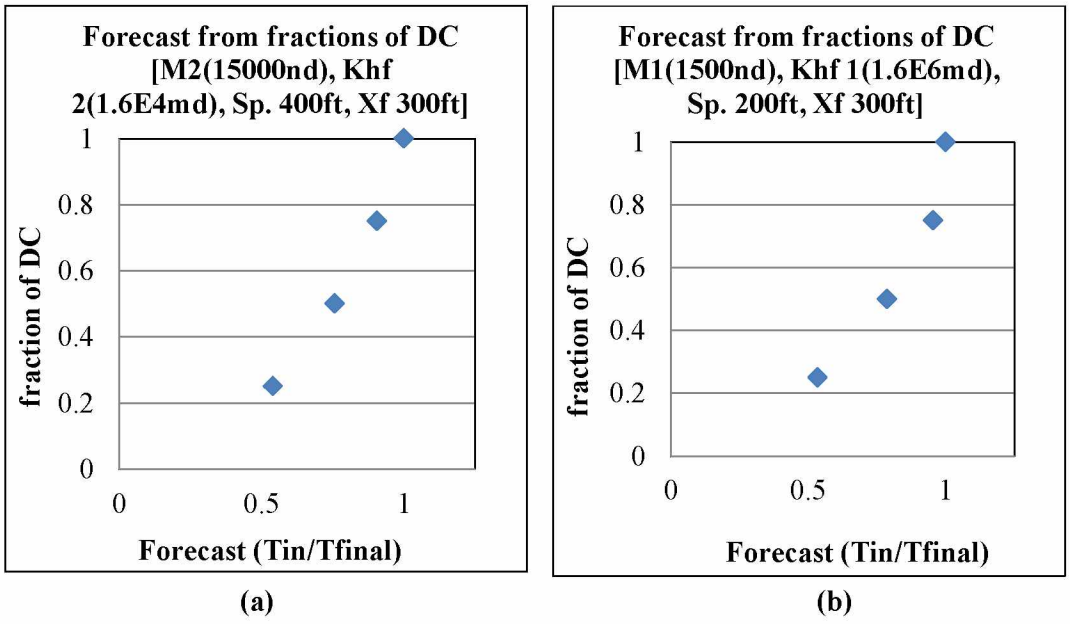

Figure 5.18: Comparison of DCA with simulation when different portion of simulated history is used by DCA (Mediums without natural fractures).

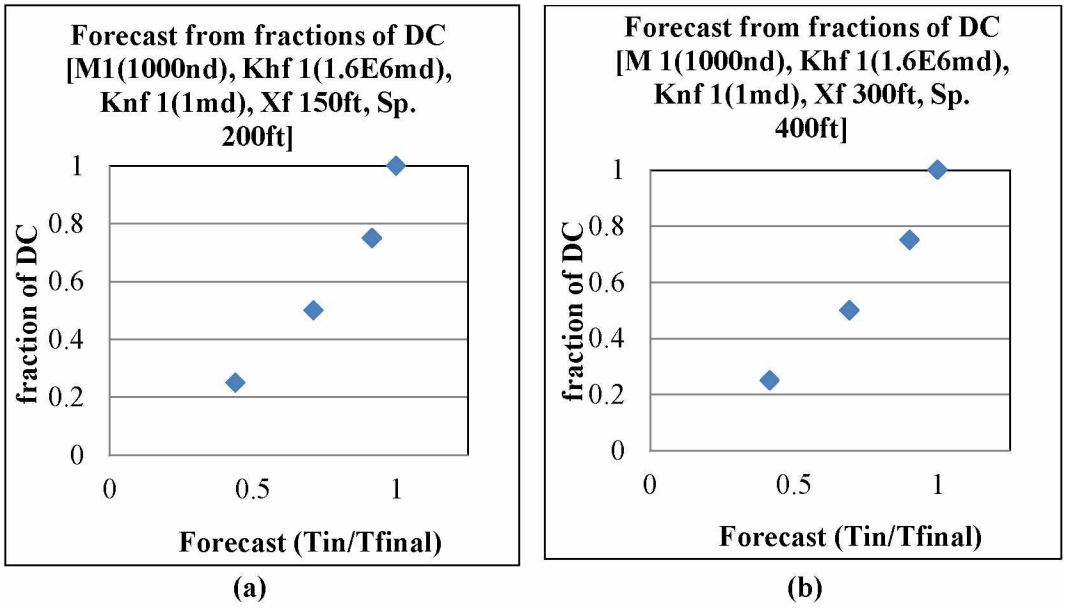

Figure 5.19: Comparison of DCA with simulation when different portion of simulated history is used by DCA (Mediums with natural fractures for Resolve).

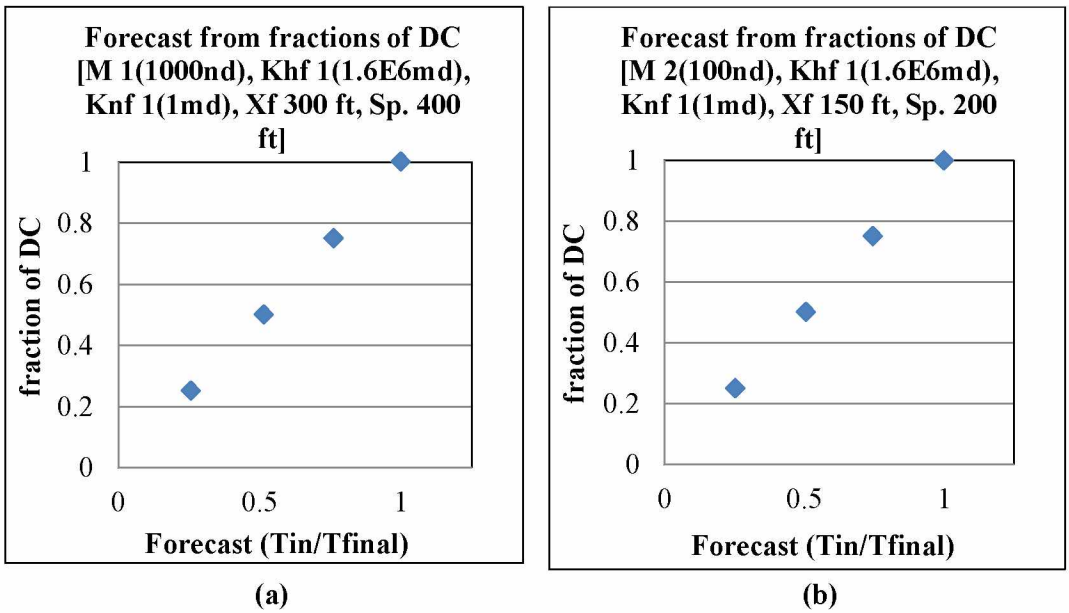

Figure 5.20: Comparison of DCA with simulation when different portion of simulated history is used by DCA (Mediums with natural fractures for CMG).

Comparison of simulation runs using the CMG and Resolve models show that there is an extended period of time to reach the production limit for the Resolve (e.g. Figure 5.21; additional rate versus time plots for different reservoir and completion parameters are provided in Appendix I).

One possible explanation for this phenomenon is the lower frequency of natural fracture occurrences in the Resolve model when compared with models built with the CMG (dual porosity model). This could make a difference because the higher frequency of natural fracture occurrence in CMG resulted in increased effective model permeability. Another explanation could be that these two simulators use the same data differently. Reduction in fracture conductivity will reduce the production rate and can equally prolong the production life. CMG has more effective model permeability than Resolve due to the way it models the natural fractures.

For media with natural fractures, the DCA also tends to under predict the simulated result when only a fraction of the decline curve was used for the analysis for models built with both the Resolve and CMG simulators for mediums with natural fractures (e.g. Figures 5.13, 5.14 and Appendix II). This observation showed that the DCA does not give a good or reliable forecast with very short production history. Forecasts from DCA are always improved with more production data (longer production history).

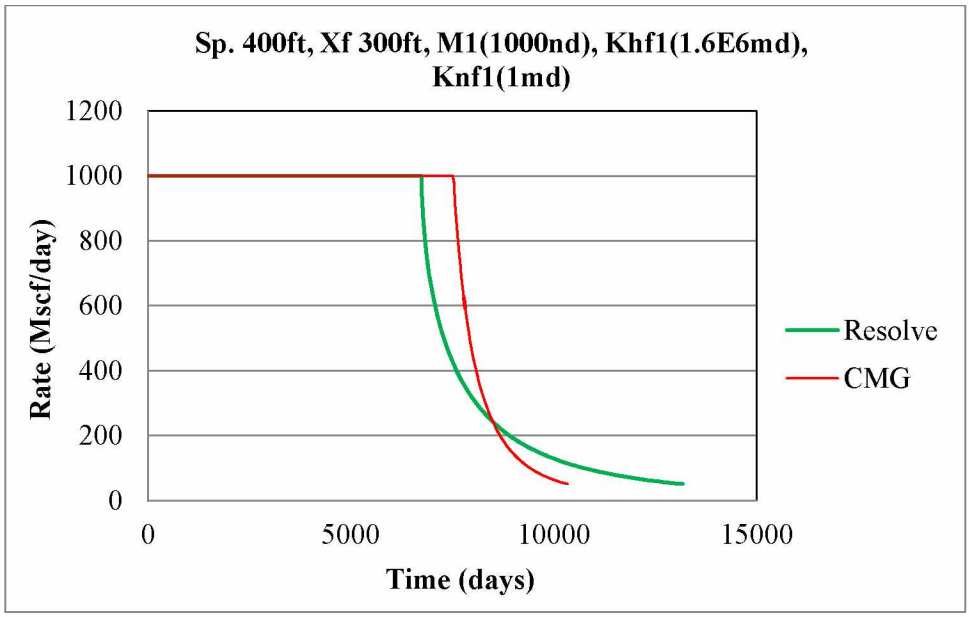

Figure 5.21: Comparison of production results for different reservoir and completion parameters for models built with the Resolve and CMG.

Chapter 6 Conclusions and Recommendations

6.1 Conclusions

The following conclusions may be deduced from this study:

1. Due to the complex interplay between different elements, including reservoir character, fractures and well bore, results from the decline curve analysis applied to wells with short production history could be unrealistic.
2. The hydraulic fracture spacing may be optimized to increase recovery by considering various factors such as the medium permeability, density and permeability of natural fractures, if present, and hydraulic fracture half-length. The latter strongly depends on in-situ stress and mechanical properties of the rock. If the presence/influence of natural fractures is negligible, higher medium permeability allows for wider fracture spacing, if reachable. The mediums with permeability of 15000 nd gave an optimum hydraulic fracture spacing of 400 ft. while those with 1500 nd gave an optimum of 200 ft.
3. The optimum well spacing optimizes production from shale gas reservoirs. Simulation models with observation wells can be used to obtain the optimum well spacing. Mediums with higher permeability can be exploited by drilling less wells and wider well spacing. In reservoirs without natural fractures, more permeable mediums (15000 nd) yielded an optimum well spacing of up to 3000 ft. while the less permeable mediums gave minimum optimum well spacing of 520 ft.
4. The desorbed gas showed to contribute to up to an extra 20% in the cumulative produced gas for the cases we investigated in this study.

5. There was a discrepancy in forecasts between the CMG and Resolve models built using the same input parameters, probably due to how the two simulators handled natural fractures. The CMG tends to give a higher forecast due to the uniform distribution of natural fractures.
6. The production forecasts from DCA for the updated production data (an extended 9 months period) gave an increase in forecasted rates of up to 43%. This is an indication of how unreliable the decline curve could be for wells with short production histories.
7. The use of simulation models in combination with the DCA helps to give a better production forecast as the decline curve analysis alone tends to under-predict future production. The optimization scheme proposed in this study relies heavily on simulation. The input data are extremely important for reliable predictions.

6.2 Recommendations

1. Simulation models built for this study made use of limited publicly available reservoir properties from the Eagle Ford shale. Since the accuracy of simulation output depends on that of the input data, it is strongly recommended to use accurate and complete data as much as possible. Predictions from a model tuned by matching past history are more reliable.
2. Type and properties of hydraulic fractures are controlled by rock mechanical properties and in-situ stress conditions. The use of hydraulic fracturing software to complement the optimization process would enhance results and also broaden the scope of study to optimize the hydraulic fracturing design.
3. Production from shale wells commences after completing hydraulic fracturing job when the formation in the vicinity of induced fracture face are partially filled with filtrate from

fracturing fluids. Presence of such fluid will block the gas passage while its displacement depends on a lot of parameters and could take a long time. We have not considered this in our study. It is recommended to include fracturing data in the simulation.

4. The optimization strategy in this study was based on cumulative production, for simplicity purpose. Economic analysis of generated simulation results would be a better approach or an alternative.
5. It is recommended that to obtain better results, the Resolve should be used to model formations with little or no natural fractures while the CMG would give better results for well fractured formations when only these two simulators are available.

Nomenclature

Fw1 = Fracture width 1

Fw2 = Fracture width 2

Khf1 = Hydraulic fracture permeability 1

Khf2 =Hydraulic fracture permeability 2

Knf1 =Natural fracture permeability 1

Knf2 =Natural fracture permeability 2

Lp =Langmuir pressure

Lv =Langmuir volume

Pf =Final pressure

M1 =Medium 1

M2 =Medium 1

Xf =Fracture half-length

Λ =Interporosity coefficient

Q =cumulative production

Tp =Total production time

References

Anderson, D.M., Nobakht, M., Moghadam, S. and Mattar, L. 2010. Analysis of Production Data From Fractured Shale Gas Wells. Paper SPE 131787 presented at the SPE Unconventional Gas Conference, Pittsburgh, Pennsylvania, USA, 23-25 February 2010. http://dx.doi.org/10.2118/131787-ms

Arps, J.J. 1945. Analysis of Decline Curves. Trans. A.I.M.E **160** 228-247.

Bai, M. 2011. Improved Understanding of Fracturing Tight-Shale Gas Formations. Paper SPE 140968 presented at the SPE Production and Operations Symposium, Oklahoma City, Oklahoma, USA, 27-29 March 2011. http://dx.doi.org/10.2118/140968-ms

Bello, R.O. and Wattenbarger, R.A. 2010. Multi-stage Hydraulically Fractured Horizontal Shale Gas Well Rate Transient Analysis. Paper SPE 126754 presented at the North Africa Technical Conference and Exhibition, Cairo, Egypt, 14-17 February 2010. http://dx.doi.org/10.2118/126754-ms

Bennett, C.O., Camacho-V., R.G., Reynolds, A.C. and Raghavan, R. 1985. Approximate Solutions for Fractured Wells Producing Layered Reservoirs. **25** (5): 729-742. SPE-11599. http://dx.doi.org/10.2118/11599-pa

Brown, M.L., Ozkan, E., Raghavan, R.S. and Kazemi, H. 2009. Practical Solutions for Pressure Transient Responses of Fractured Horizontal Wells in Unconventional Reservoirs. Paper SPE 125043 presented at the SPE Annual Technical Conference and Exhibition, New Orleans, Louisiana, 4-7 October 2009. http://dx.doi.org/10.2118/125043-ms

Bumb, A.C. and McKee, C.R. 1988. Gas-Well Testing in the Presence of Desorption for Coalbed Methane and Devonian Shale. SPE Formation Evaluation **3** (1): 179-185. 15227. http://dx.doi.org/10.2118/15227-pa

Carlson, E.S. and Mercer, J.C. 1991. Devonian Shale Gas Production: Mechanisms and Simple Models. SPE Journal of Petroleum Technology (4): 476-482. 00019311. http://dx.doi.org/10.2118/19311-pa

Chen, H.-C., Chen, M. and Davis, D.A. 1997. Numerical Simulation of Transient Flows Induced By a Berthing Ship. International Journal of Offshore and Polar Engineering **7** (4): ISOPE-97-07-4-277.

Cheng, Y. 2010. Impact of Water Dynamics in Fractures on the Performance of Hydraulically Fractured Wells in Gas Shale Reservoirs. Paper SPE 127863 presented at the SPE International Symposium and Exhibiton on Formation Damage Control, Lafayette, Louisiana, USA, 10-12 February 2010. http://dx.doi.org/10.2118/127863-ms

Crafton, J.W. 2010. Flowback Performance in Intensely Naturally Fractured Shale Gas Reservoirs. Paper SPE 131785-MS presented at the SPE Unconventional Gas Conference, Pittsburgh, Pennsylvania, USA, 23-25 February 2010. http://dx.doi.org/10.2118/131785-ms

Deswaan O. A. 1976. Analytic Solutions for Determining Naturally Fractured Reservoir Properties by Well Testing. **16** (3): 117-122. 5346. http://dx.doi.org/10.2118/5346-pa

Du, C., Zhang, X., Zhan, L., Gu, H., Hay, B., Tushingham, K. and Ma, Y.Z. 2010. Modeling Hydraulic Fracturing Induced Fracture Networks in Shale Gas Reservoirs as a Dual Porosity System. Paper SPE 132180 presented at the International Oil and Gas Conference and Exhibition in China, Beijing, China, 8-10 June 2010. http://dx.doi.org/10.2118/132180-ms

EIA. 2010. Blog, http://eaglefordshaleblog.com/ (accessed 23 March 2012).

EIA. 2011. Review of Emerging Resources: U.S. Shale Gas and Shale Oil Plays. Independent Statistics and Analysis

EIA, I. 2009. Review of Emerging Resources: U.S. Shale Gas and Shale Oil Plays. Independent Statistics and Analysis

El-Banbi, A., H. and Wattenbarger, R.A. 1998. Analysis of Linear Flow in Gas Well Production. Paper SPE 00039972 presented at the SPE Gas Technology Symposium, Calgary, Alberta, Canada, 01/01/1998. http://dx.doi.org/10.2118/39972-ms

Fan, L., Luo, F., Lindsay, G.J., Thompson, J.W. and Robinson, J.R. 2011. The Bottom-Line of Horizontal Well Production Decline in the Barnett Shale. Paper SPE 141263 presented at the SPE Production and Operations Symposium, Oklahoma City, Oklahoma, USA, 27-29 March 2011. http://dx.doi.org/10.2118/141263-ms

Frantz, J.H., Sawyer, W.K., MacDonald, R.J., Williamson, J.R., Johnston, D. and Waters, G. 2005. Evaluating Barnett Shale Production Performance Using an Integrated Approach. Paper SPE 96917 presented at the SPE Annual Technical Conference and Exhibition, Dallas, Texas, 9-12 October 2005. http://dx.doi.org/10.2118/96917-ms

Freeman, C.M., Moridis, G.J., Ilk, D. and Blasingame, T.A. 2009. A Numerical Study of Performance for Tight Gas and Shale Gas Reservoir Systems. Paper SPE 124961 presented at the SPE Annual Technical Conference and Exhibition, New Orleans, Louisiana, 4-7 October 2009. http://dx.doi.org/10.2118/124961-ms

Gale, J.E. 1982. The Effects Of Fracture Type (Induced Versus Natural) On The Stress-Fracture Closure-Fracture Permeability Relationships. Paper SPE 82-290 presented at the The 23rd U.S Symposium on Rock Mechanics (USRMS), Berkeley, California, 25-27 August, 1982

Gao, C., Lee, W.J., Spivey, J.P. and Semmelbeck, M.E. 1994. Modeling Multilayer Gas Reservoirs Including Sorption Effects. Paper SPE 29173 presented at the SPE Eastern Regional Meeting, Charleston, West Virginia, 8-10 November 1994. http://dx.doi.org/10.2118/29173-ms

Geology.com. 2010. Eagle Ford Shale - Oil and Natural Gas, http://geology.com/articles/eagle-ford/ (accessed 28 March 2012).

Hill, D.G., Nelson, C.R. 2000. Gas Productive Fractured Shales—An Overview and Update. Gas tips **7** (2):

Liu, J., Liu, J., Liu, K., Elsworth, D. and Wang, J. 2009. Hydromechanics of a Virtual Rock Core. Paper SPE ARMA-09-035 presented at the 28 June-1 July 2009.

Martin, R., Baihly, J.D., Malpani, R., Lindsay, G.J. and Atwood, W.K. 2011. Understanding Production from Eagle Ford-Austin Chalk System. Paper SPE SPE-145117-MS presented at the SPE Annual Technical Conference and Exhibition, Denver, Colorado, USA, 30 October-2 November 2011. http://dx.doi.org/10.2118/145117-ms

Medeiros, F., Kurtoglu, B., Ozkan, E. and Kazemi, H. 2010. Analysis of Production Data From Hydraulically Fractured Horizontal Wells in Shale Reservoirs. SPE Reservoir Evaluation & Engineering **13** (3): 559-568. 110848-PA. http://dx.doi.org/10.2118/110848-pa

Medeiros, F., Ozkan, E. and Kazemi, H. 2007. Productivity and Drainage Area of Fractured Horizontal Wells in Tight Gas Reservoirs. Paper SPE 108110 presented at the Rocky Mountain Oil & Gas Technology Symposium, Denver, Colorado, U.S.A., 16-18 April 2007. http://dx.doi.org/10.2118/108110-ms

Moridis, G.J., Blasingame, T.A. and Freeman, C.M. 2010. Analysis of Mechanisms of Flow in Fractured Tight-Gas and Shale-Gas Reservoirs. Paper SPE 139250 presented at the SPE Latin American and Caribbean Petroleum Engineering Conference, Lima, Peru, 1-3 December 2010. http://dx.doi.org/10.2118/139250-ms

Orangi, A., Nagarajan, N.R., Honarpour, M.M. and Rosenzweig, J.J. 2011. Unconventional Shale Oil and Gas-Condensate Reservoir Production, Impact of Rock, Fluid, and Hydraulic Fractures. Paper SPE SPE-140536-MS presented at the SPE Hydraulic Fracturing Technology Conference, The Woodlands, Texas, USA, 01/01/2011. http://dx.doi.org/10.2118/140536-ms

Ozkan, E., Brown, M.L., Raghavan, R. and Kazemi, H. 2011. Comparison of Fractured-Horizontal-Well Performance in Tight Sand and Shale Reservoirs. SPE Reservoir Evaluation & Engineering **14** (2): 248-259. 121290-PA. http://dx.doi.org/10.2118/121290-pa

Page, J.C. and Miskimins, J.L. 2009. A Comparison of Hydraulic and Propellant Fracture Propagation in a Shale Gas Reservoir. (5): 26-30. PETSOC-09-05-26. http://dx.doi.org/10.2118/09-05-26

Raghavan, R.S., Chen, C.-C. and Agarwal, B. 1997. An Analysis of Horizontal Wells Intercepted by Multiple Fractures. SPE Journal **02** (03): 235-245. 27652. http://dx.doi.org/10.2118/27652-pa

RRC. 2011. http://www.rrc.state.tx.us/data/online (accessed 23 September 2011).

Samandarli, O., Ahmadi, H.A.A. and Wattenbarger, R.A. 2011. A Semi-Analytic Method for History Matching Fractured Shale Gas Reservoirs. Paper SPE 144583 presented at the SPE Western North American Region Meeting, Anchorage, Alaska, USA, 7-11 May 2011. http://dx.doi.org/10.2118/144583-ms

Serra, K., Reynolds, A.C. and Raghavan, R. 1983. New Pressure Transient Analysis Methods for Naturally Fractured Reservoirs(includes associated papers 12940 and 13014). SPE Journal of Petroleum Technology (12): 2271-2283. 00010780. http://dx.doi.org/10.2118/10780-pa

Sondhi, N. 2011. Petrophysical Characterization of Eagle Ford Shale. MS thesis, University of Oklahoma, Norman, Oklahoma (May 2011)

Warren, J.E., Root, P.J. 1963. The Behavior of Naturally Fractured Reservoirs. Paper presented at SPE Conference, Los Angeles, USA, May 1963.

Yost II, A.B. 1994. Analysis of Production Response to CO2/Sand Fracturing: A Case Study. Paper SPE 29191 presented at the SPE Eastern Regional Meeting, Charleston, West Virginia, 8-10 November 1994. http://dx.doi.org/10.2118/29191-ms

Zhang, X., Du, C., Deimbacher, F., Crick, M. and Harikesavanallur, A. 2009. Sensitivity Studies of Horizontal Wells with Hydraulic Fractures in Shale Gas Reservoirs. Paper SPE 13338 presented at the International Petroleum Technology Conference, Doha, Qatar, 7-9 December 2009. http://dx.doi.org/10.2523/13338-ms

Zuber, M.D., Lee, W.J. and Gatens III, J.M. 1987. Effect of Stimulation on the Performance of Devonian Shale Gas Wells. SPE Production Engineering **02** (04): 250-256. 14508. http://dx.doi.org/10.2118/14508-pa

Appendix I

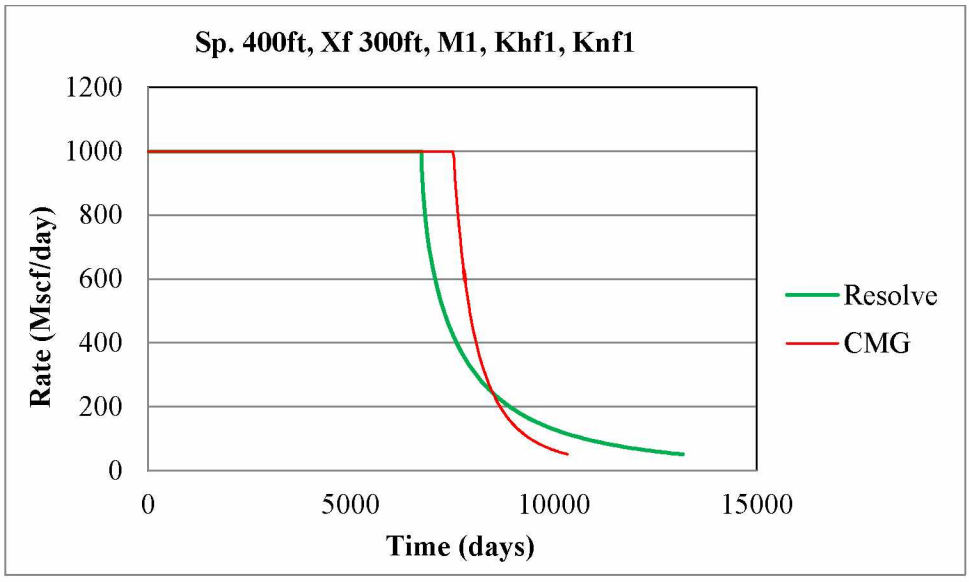

(a)

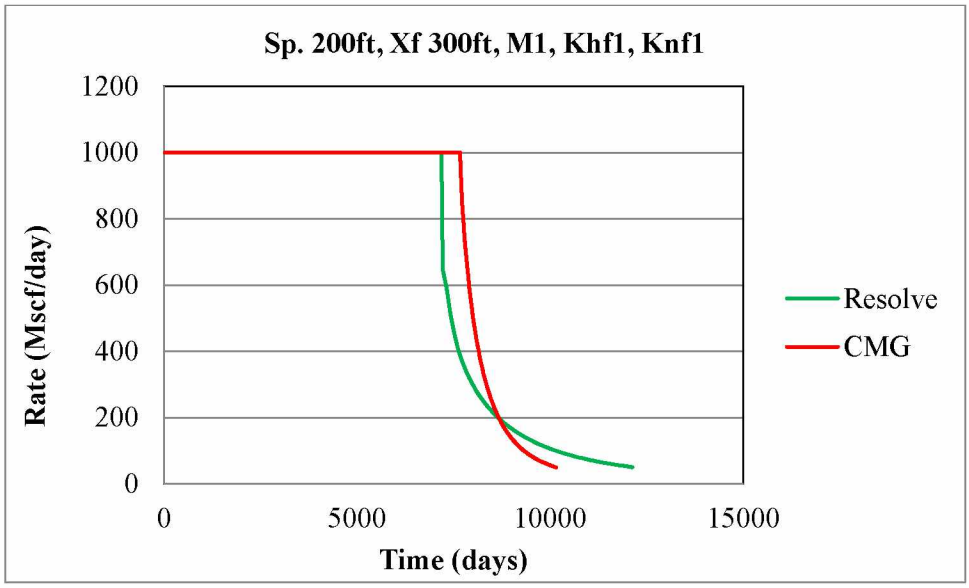

(b)

Figure I- 1: Comparison of production results for different reservoir and completion parameters for models built with the Resolve and CMG.

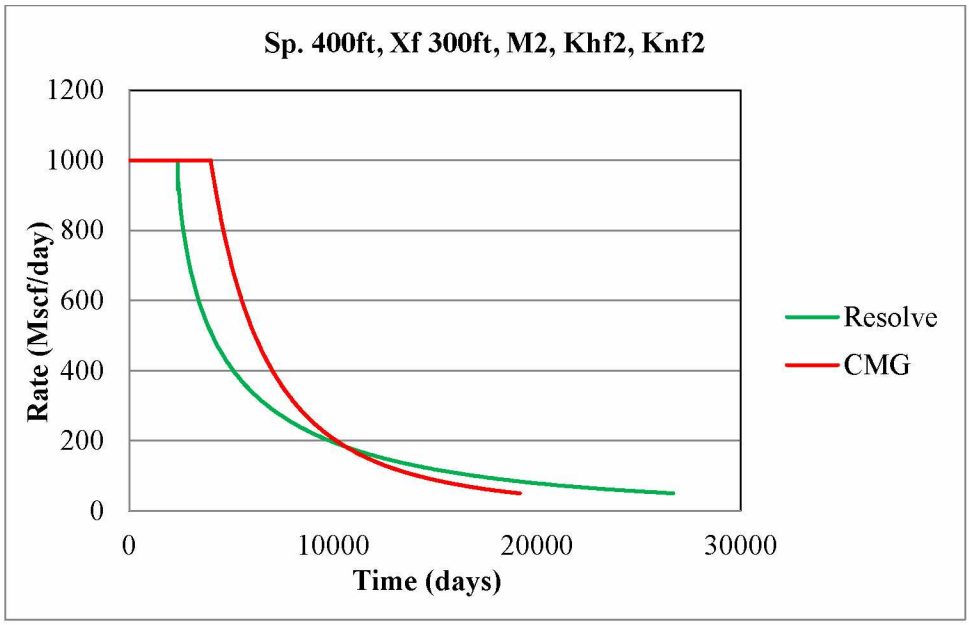

(c)

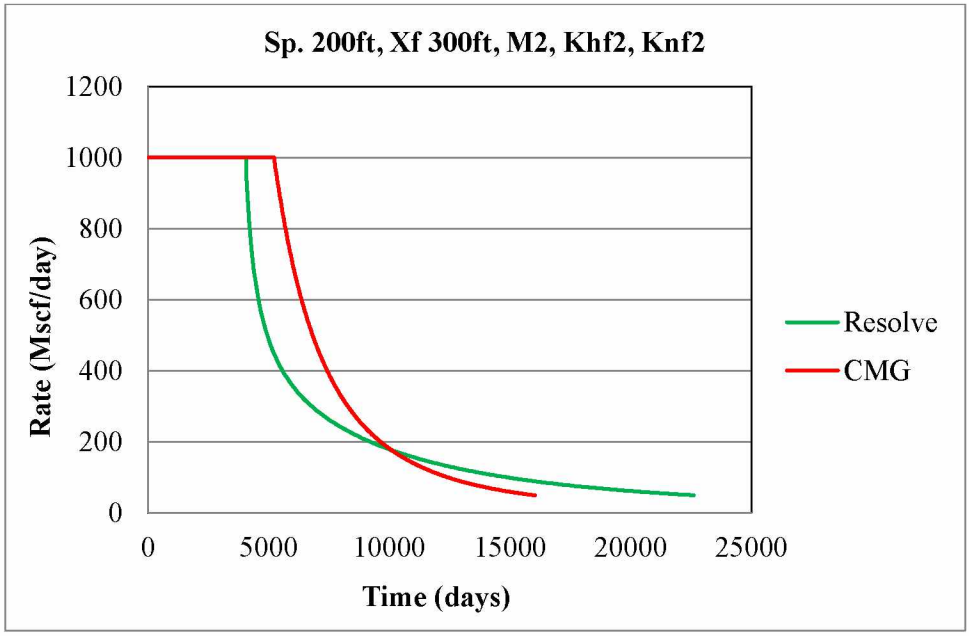

(d)

Figure I-1 Continued.

Appendix II

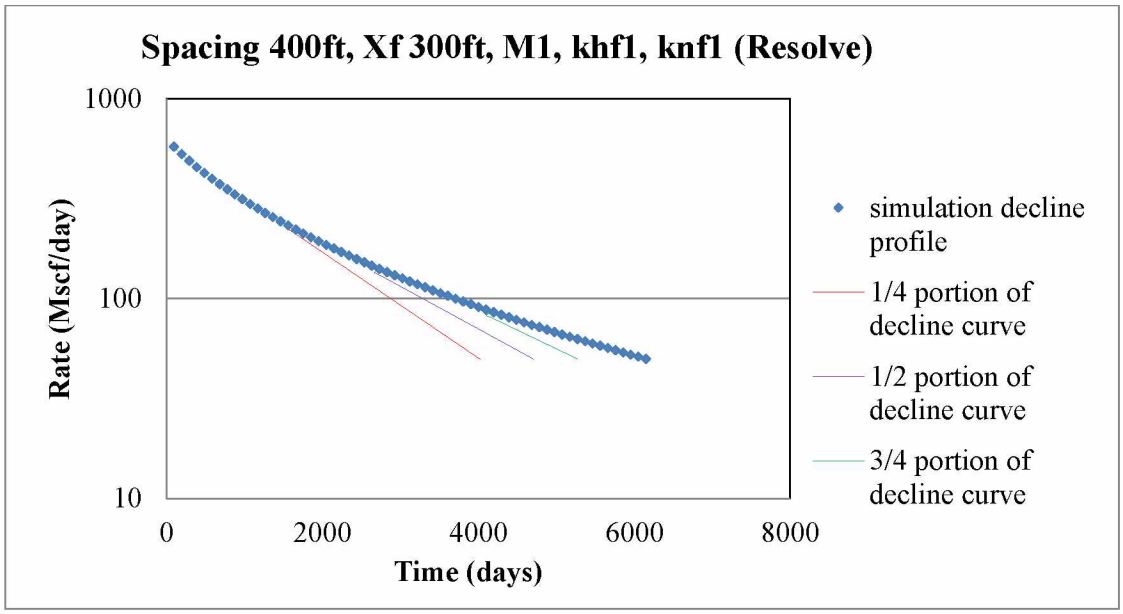

(a)

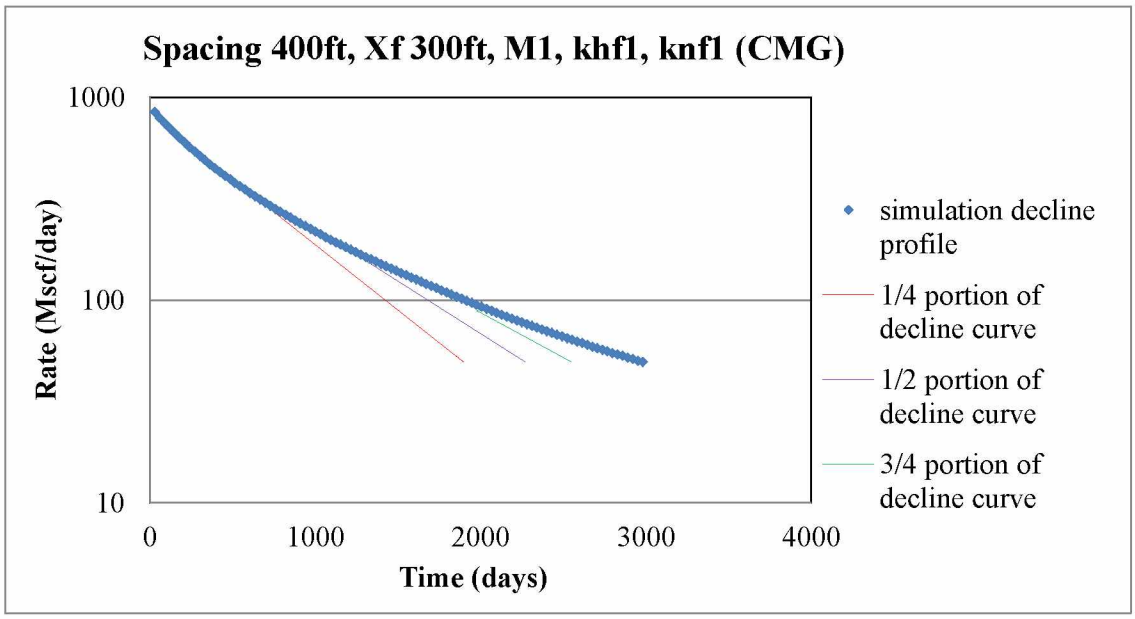

(b)

Figure II- 1: DCA using different fractions of decline curve for simulated results for both the Resolve and CMG (mediums with natural fractures)

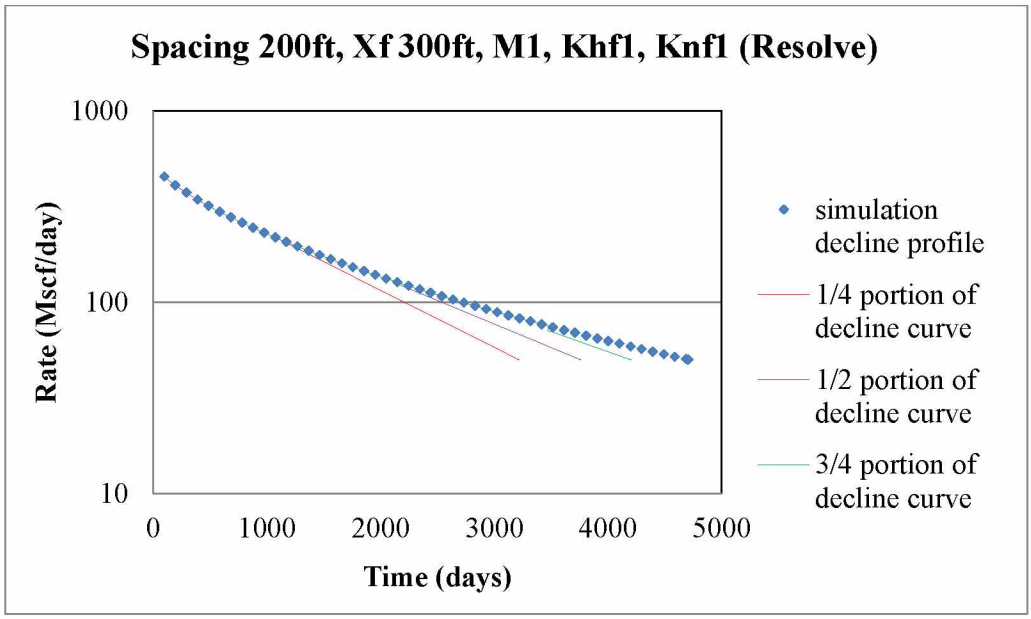

(c)

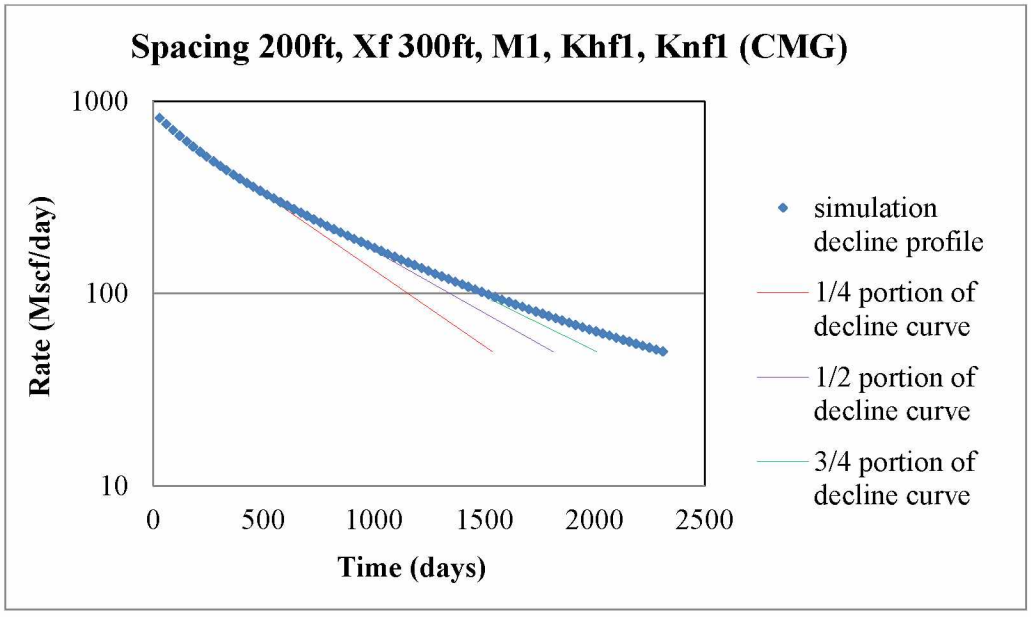

(d)

Figure II-1 Continued.

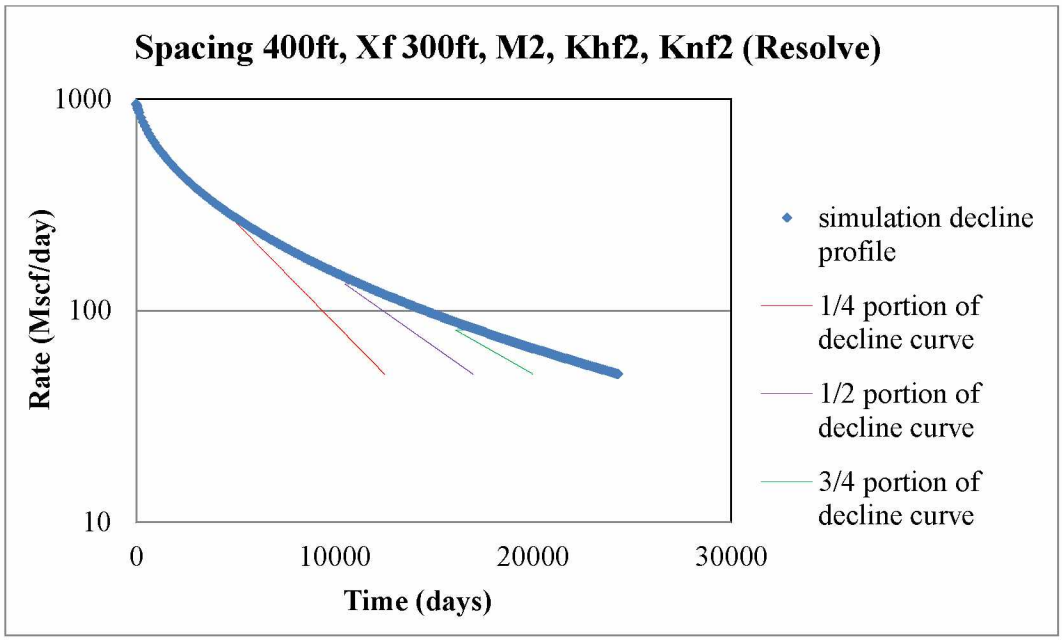

(e)

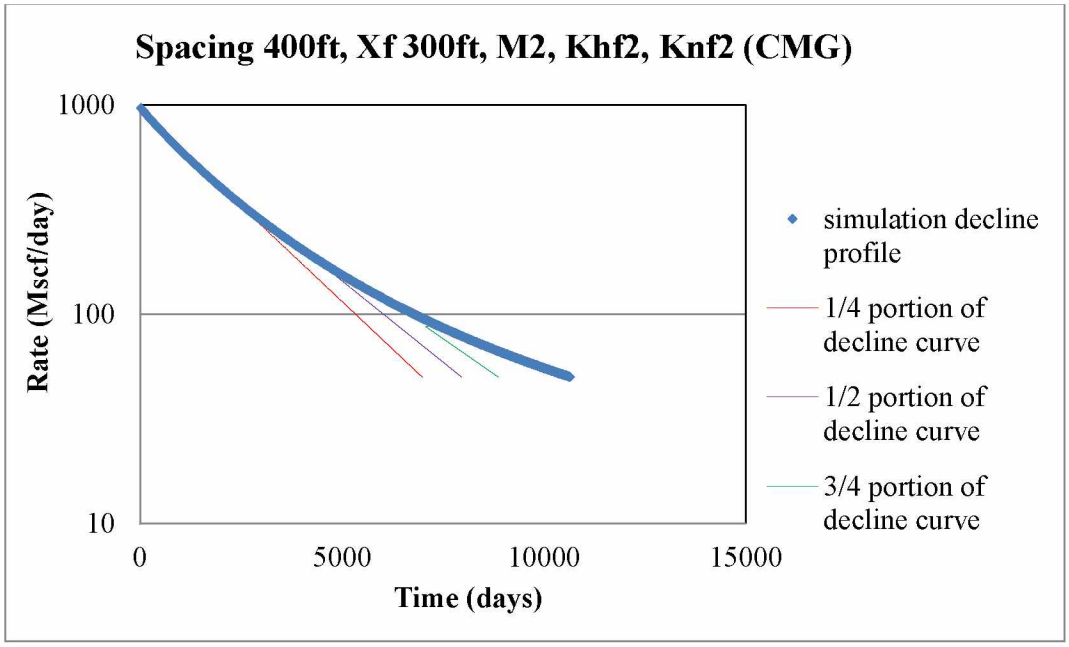

(f)

Figure II-1 Continued.

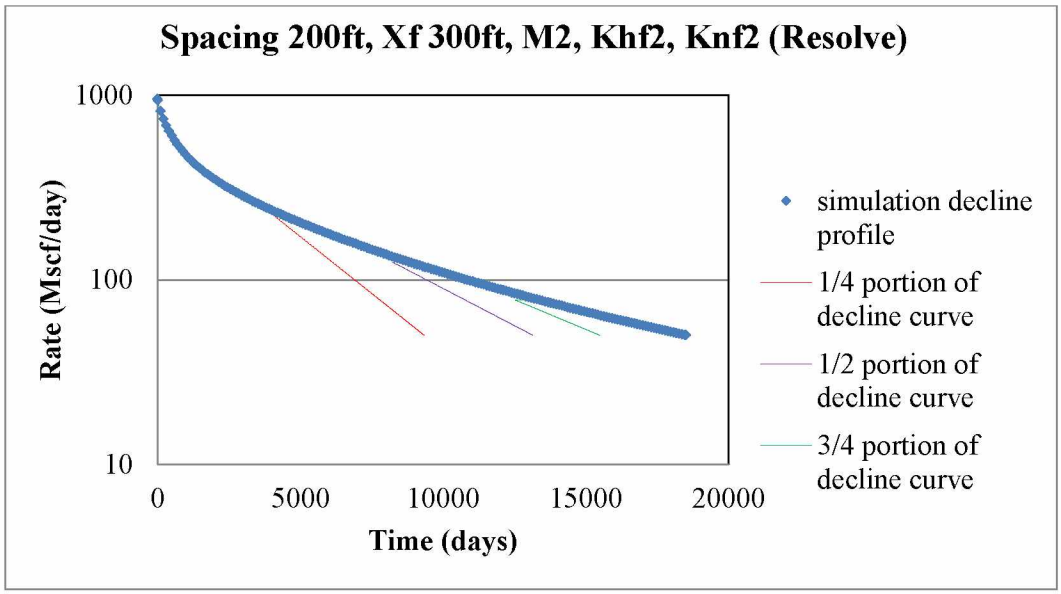

(g)

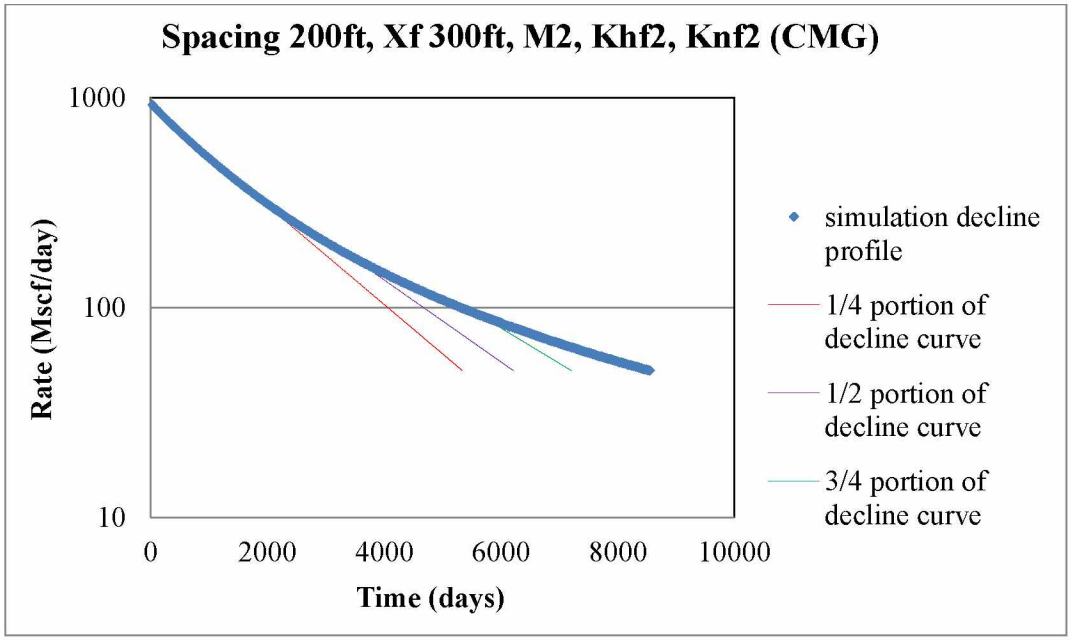

(i)

Figure II-1 Continued.

Appendix III

Table III- 1: Production history for well #1: Evans H unit, LaSalle County

Evans H	#253413						
Horizontal leg (ft)	3692						
Fracture stages	12						
Month	Well days Online	Producing	Gas	Gp	qg	q/qi	Average rate,
		times (days)	(MCF)	(MMscf)	(Mscf/D)		Q/t (MMscf/D)
9-Aug	20	20	40351	40	2018	1	2
9-Sep	30	50	57121	97	1904	0.94	1.9
9-Oct	31	81	41646	139	1343	0.67	1.7
9-Nov	30	111	32424	172	1081	0.54	1.5
9-Dec	31	142	28884	200	932	0.46	1.4
10-Jan	31	173	22190	223	716	0.36	1.3
10-Feb	29	202	19874	242	685	0.34	1.2
10-Mar	31	233	20649	263	666	0.33	1.1
10-Apr	30	263	20575	284	686	0.34	1.1
10-May	31	294	18666	302	602	0.29	1
10-Jun	30	324	12553	315	418	0.21	1
10-Jul	31	355	12912	328	417	0.21	0.9
10-Aug	31	386	10543	338	340	0.17	0.9
10-Sep	30	416	9745	348	325	0.16	0.8
10-Oct	31	447	9601	358	310	0.15	0.8
10-Nov	30	477	8288	366	276	0.14	0.8
10-Dec	31	508	8194	374	264	0.13	0.7
11-Jan	31	539	7974	382	257	0.13	0.7
11-Feb	29	568	7286	389	251	0.13	0.7
11-Mar	31	599	8033	398	259	0.13	0.7
11-Apr	30	629	7888	405	263	0.13	0.6

Table III- 2: Production history for well #1: Hawkville unit, LaSalle County.

Hawkville (Eagle Ford)	#244785						
Horizontal leg (ft)	2990						
Fracture stages	10						
Month	Well days Online	Producing	Gas	Gp	qg	q/qi	Average rate,
		times (days)	(MCF)	(MMscf)	(Mscf/D)		Q/t (MMscf/D)
8-Oct	18	18	93230	93230	5179	1	5179.4
8-Nov	30	48	95043	93325	3168	0.6	1944.3
8-Dec	31	79	78022	93403	2517	0.5	1182.3
9-Jan	31	110	71566	93475	2309	0.4	849.8
9-Feb	29	139	55836	93531	1925	0.4	672.9
9-Mar	31	170	39400	93570	1271	0.2	550.4
April-09	30	200	11695	93582	390	0.1	467.9
May-09	31	231	0	93582	0	0	405.1
9-Jun	30	261	29729	93611	991	0.2	358.7
9-Jul	31	292	64980	93676	2096	0.4	320.8
9-Aug	31	323	39897	93716	1287	0.2	290.1
9-Sep	30	353	51868	93768	1729	0.3	265.6
9-Oct	31	384	59967	93828	1934	0.4	244.3
9-Nov	30	414	49500	93878	1650	0.3	226.8
9-Dec	31	445	46525	93924	1501	0.3	211.1
10-Jan	31	476	44084	93968	1422	0.3	197.4
10-Feb	29	505	40527	94009	1398	0.3	186.2
10-Mar	31	536	44138	94053	1424	0.3	175.5
10-Apr	30	566	38249	94091	1275	0.2	166.2
10-May	31	597	36343	94127	1172	0.2	157.7
10-Jun	30	627	34565	94162	1152	0.2	150.2
10-Jul	31	658	34263	94196	1105	0.2	143.2
10-Aug	31	689	32585	94229	1051	0.2	136.8
10-Sep	30	719	42218	94271	1407	0.3	131.1
10-Oct	31	750	33703	94305	1087	0.2	125.7
10-Nov	30	780	32003	94337	1067	0.2	120.9

Table III-2: Production history for well #1: Hawkville unit, LaSalle County - Continued

Hawkville (Eagle Ford)	#244785						
Horizontal leg (ft)	2990						
Fracture stages	10						
Month	Well days Online	Producing	Gas	Gp	qg	q/qi	Average rate,
		times (days)	(MCF)	(MMscf)	(Mscf/D)		Q/t (MMscf/D)
10-Dec	31	811	31490	94368	1016	0.2	116.4
11-Jan	31	842	32064	94400	1034	0.2	112.1
11-Feb	29	871	27231	94428	939	0.2	108.4
11-Mar	31	902	30923	94458	998	0.2	104.7
11-Apr	30	932	29101	94488	970	0.2	101.4

Table III- 3: Production history for well #1: Brown Trust unit 1, LaSalle County.

Brown Trusts	#255434						
Horizontal leg (ft)	3417						
Fracture stages	8						
Month	Well days Online	Producing	Gas	Gp	qg	q/qi	Average rate,
		times (days)	(MCF)	(MMscf)	(Mscf/D)		Q/t (MMscf/D)
9-Mar	4	4	10356	10	2589	1	2.6
9-Apr	30	34	121723	132	4057	1.57	3.9
9-May	31	65	116485	249	3758	1.45	3.8
9-Jun						0	
9-Jul	31	96	149237	398	4814	1.86	4.1
9-Aug	31	127	94358	492	3044	1.18	3.9
9-Sep	30	157	108428	601	3614	1.4	3.8
9-Oct	31	188	96182	697	3103	1.2	3.7
9-Nov	30	218	72620	769	2421	0.94	3.5
9-Dec	31	249	73213	843	2362	0.91	3.4
10-Jan	31	280	69755	912	2250	0.87	3.3
10-Feb	29	309	76139	988	2625	1.01	3.2
10-Mar	31	340	72933	1061	2353	0.91	3.1
10-Apr	30	370	62238	1124	2075	0.8	3.0
10-May	31	401	57550	1181	1856	0.72	2.9
10-Jun	30	431	53929	1235	1798	0.69	2.9
10-Jul	31	462	53290	1288	1719	0.66	2.8
10-Aug	31	493	50559	1339	1631	0.63	2.7
10-Sep	30	523	47610	1387	1587	0.61	2.7
10-Oct	31	554	49807	1436	1607	0.62	2.6
10-Nov	30	584	41051	1477	1368	0.53	2.5
10-Dec	31	615	43739	1521	1411	0.55	2.5
11-Jan	31	646	47099	1568	1519	0.59	2.4
11-Feb	29	675	39245	1608	1353	0.52	2.4
11-Mar	31	706	40171	1648	1296	0.5	2.3
11-Apr	30	736	37764	1685	1259	0.49	2.3

Table III- 4: Production history for well #1: South Texas Syndicate unit, LaSalle County

South Texas Syndicate	#254365						
Horizontal leg (ft)	3284						
Fracture stages							
Month	Well days Online	Producing	Gas	Gp	qg	q/qi	Average rate,
		times (days)	(MCF)	(MMscf)	(Mscf/D)		Q/t (MMscf/D)
9-Jul	6	6	13910	14	2318	1	2.3
9-Aug	31	37	123258	137	3976	1.72	3.7
9-Sep	30	67	97369	235	3246	1.4	3.5
9-Oct	31	98	60955	295	1966	0.85	3.0
9-Nov	30	128	45003	340	1500	0.65	2.7
9-Dec	31	159	54147	395	1747	0.75	2.5
10-Jan	31	190	42510	437	1371	0.59	2.3
10-Feb	29	219	32090	469	1107	0.48	2.1
10-Mar	31	250	38416	508	1239	0.54	2.0
10-Apr	30	280	27800	535	927	0.4	1.9
10-May	31	311	30847	566	995	0.43	1.8
10-Jun	30	341	26592	593	886	0.38	1.7
10-Jul	31	372	25629	619	827	0.36	1.7
10-Aug	31	403	32217	651	1039	0.45	1.6
10-Sep	30	433	21563	672	719	0.31	1.6
10-Oct	31	464	32138	704	1037	0.45	1.5
10-Nov	30	494	27409	732	914	0.39	1.5
10-Dec	31	525	28241	760	911	0.39	1.4
11-Jan	31	556	26686	787	861	0.37	1.4
11-Feb	29	585	16827	804	580	0.25	1.4
11-Mar	31	616	12643	816	408	0.18	1.3
11-Apr	30	646	101	816	3	0	1.3

Table III- 5: Production history for well #1: Brown Trust unit 2, LaSalle County.

Brown Trusts	#257681						
Horizontal leg (ft)	5193						
Fracture stages							
Month	Well days Online	Producing	Gas	Gp	qg	q/qi	Average rate,
		times (days)	(MCF)	(MMscf)	(Mscf/D)		Q/t (MMscf/D)
10-May	13	13	51680	52	3975	1	4.0
10-Jun	30	43	105885	158	3530	0.89	3.7
10-Jul	31	74	91586	249	2954	0.74	3.4
10-Aug	31	105	77486	327	2500	0.63	3.1
10-Sep	30	135	70831	397	2361	0.59	2.9
10-Oct	31	166	64970	462	2096	0.53	2.8
10-Nov	30	196	50365	513	1679	0.42	2.6
10-Dec	31	227	40076	553	1293	0.33	2.4
11-Jan	31	258	42620	595	1375	0.35	2.3
11-Feb	29	287	52217	648	1801	0.45	2.3
11-Mar	31	318	50590	698	1632	0.41	2.2
11-Apr	30	348	44644	743	1488	0.37	2.1

Table III- 6: Production history for well #1: South Texas Syndicate unit 2, LaSalle County.

South Texas Syndicate	#255011						
Horizontal leg (ft)	4802						
Fracture stages							
Month	Well days Online	Producing	Gas	Gp	qg	q/qi	Average rate,
		times (days)	(MCF)	(MMscf)	(Mscf/D)		Q/t (MMscf/D)
9-Oct	3	3	18117	18	6039	1	6.0
9-Nov	30	33	192615	211	6421	1.06	6.4
9-Dec	31	64	180661	391	5828	0.97	6.1
10-Jan	31	95	178934	570	5772	0.96	6.0
10-Feb	29	124	132859	703	4581	0.76	5.7
10-Mar	31	155	157252	860	5073	0.84	5.6
10-Apr	30	185	112339	973	3745	0.62	5.3
10-May	31	216	145243	1118	4685	0.78	5.2
10-Jun	30	246	125952	1244	4198	0.7	5.1
10-Jul	31	277	121848	1366	3931	0.65	4.9
10-Aug	31	308	111817	1478	3607	0.6	4.8
10-Sep	30	338	100209	1578	3340	0.55	4.7
10-Oct	31	369	96561	1674	3115	0.52	4.5
10-Nov	30	399	86977	1761	2899	0.48	4.4
10-Dec	31	430	84262	1846	2718	0.45	4.3
11-Jan	31	461	87163	1933	2812	0.47	4.2

Table III- 7: Production history for well #1: J.C.Martin 1850 unit, LaSalle County.

J.C Martin 1850	#251771						
Horizontal leg (ft)	4577						
Fracture stages	18						
Month	Well days Online	Producing	Gas	Gp	qg	q/qi	Average rate,
		times (days)	(MCF)	(MMscf)	(Mscf/D)		Q/t (MMscf/D)
9-Jul	15	15	124856	125	8324	1	8.3
9-Aug	31	46	218290	343	7042	0.85	7.5
9-Sep	30	76	144830	488	4828	0.58	6.4
9-Oct	31	107	111249	599	3589	0.43	5.6
9-Nov	30	137	38324	638	1277	0.15	4.7
9-Dec	31	168	80629	718	2601	0.31	4.3
10-Jan	31	199	72683	791	2345	0.28	4.0
10-Feb	29	228	62821	854	2166	0.26	3.7
10-Mar	31	259	62996	917	2032	0.24	3.5
10-Apr	30	289	56792	973	1893	0.23	3.4
10-May	31	320	55108	1029	1778	0.21	3.2
10-Jun	30	350	40381	1069	1346	0.16	3.1
10-Jul	31	381	40403	1109	1303	0.16	2.9
10-Aug	31	412	43465	1153	1402	0.17	2.8
10-Sep	30	442	40353	1193	1345	0.16	2.7
10-Oct	31	473	32135	1225	1037	0.13	2.6
10-Nov	30	503	32820	1258	1094	0.13	2.5
10-Dec	31	534	33095	1291	1068	0.13	2.4
11-Jan	31	565	30212	1321	975	0.12	2.3
11-Feb						0	
11-Mar	31	596	23761	1345	766	0.09	2.3
11-Apr	30	626	22936	1368	765	0.09	2.2

Table III- 8: Production history for well #1: STS-Welse unit, LaSalle County.

STS-Welse 786	#254484						
Horizontal leg (ft)	4295						
Fracture stages	15						
Month	Well days Online	Producing	Gas	Gp	qg	q/qi	Average rate,
		times (days)	(MCF)	(MMscf)	(Mscf/D)		Q/t (MMscf/D)
9-Oct	6	6	17711	18	2952	1	3.0
9-Nov						0	
9-Dec	31	37	69713	87	2249	0.76	2.4
10-Jan	31	68	48242	136	1556	0.53	2.0
10-Feb	29	97	39205	175	1352	0.46	1.8
10-Mar	31	128	39572	214	1277	0.43	1.7
10-Apr	30	158	34057	249	1135	0.39	1.6
10-May	31	189	32031	281	1033	0.35	1.5
10-Jun	30	219	28991	310	966	0.33	1.4
10-Jul	31	250	27592	337	890	0.3	1.3
10-Aug	31	281	25656	363	828	0.28	1.3
10-Sep	30	311	23309	386	777	0.26	1.2
10-Oct	31	342	21577	408	696	0.24	1.2
10-Nov	30	372	21654	429	722	0.25	1.2
10-Dec	31	403	24844	454	801	0.27	1.1
11-Jan	31	434	18659	473	602	0.2	1.1
11-Feb	29	463	16464	489	568	0.19	1.1
11-Mar	31	494	18233	508	588	0.2	1.0
11-Apr	30	524	16668	524	556	0.19	1.0

Table III- 9: Production history for well #1: STS unit 1, LaSalle County.

STS 1	#254322						
Horizontal leg (ft)	4145						
Fracture stages	15						
Month	Well days Online	Producing	Gas	Gp	qg	q/qi	Average rate,
		times (days)	(MCF)	(MMscf)	(Mscf/D)		Q/t (MMscf/D)
9-Oct	30	30	152380	152	5079	1	5.1
9-Nov	30	60	98297	251	3277	0.65	4.2
9-Dec	31	91	71218	322	2297	0.45	3.5
10-Jan	31	122	56599	378	1826	0.36	3.1
10-Feb	29	151	46099	425	1590	0.31	2.8
10-Mar	31	182	44228	469	1427	0.28	2.6
10-Apr	30	212	36570	505	1219	0.24	2.4
10-May	31	243	32315	538	1042	0.21	2.2
10-Jun	30	273	29524	567	984	0.19	2.1
10-Jul	31	304	27102	594	874	0.17	2.0
10-Aug	31	335	25720	620	830	0.16	1.9
10-Sep	30	365	24296	644	810	0.16	1.8
10-Oct	31	396	21488	666	693	0.14	1.7
10-Nov	30	426	19409	685	647	0.13	1.6
10-Dec	31	457	20337	706	656	0.13	1.5
11-Jan	31	488	19498	725	629	0.12	1.5
11-Feb	29	517	19416	744	670	0.13	1.4
11-Mar	31	548	16335	761	527	0.1	1.4
11-Apr	30	578	16989	777	566	0.11	1.3

Table III- 10: Production history for well #1: STS unit 1, LaSalle County.

STS 2	#251818						
Horizontal leg (ft)	4256						
Fracture stages	15						
Month	Well days Online	Producing	Gas	Gp	Qg	q/qi	Average rate,
		times (days)	(MCF)	(MMscf)	(Mscf/D)		Q/t (MMscf/D)
9-Sep	15	15	85185	85	5679	1	5.7
9-Oct	31	46	96663	182	3118	0.55	4.0
9-Nov	30	76	53243	235	1775	0.31	3.1
9-Dec	31	107	55058	290	1776	0.31	2.7
10-Jan	31	138	51311	341	1655	0.29	2.5
10-Feb	29	167	40345	382	1391	0.25	2.3
10-Mar	31	198	39946	422	1289	0.23	2.1
10-Apr	30	228	32046	454	1068	0.19	2.0
10-May	31	259	29197	483	942	0.17	1.9
10-Jun	30	289	25938	509	865	0.15	1.8
10-Jul	31	320	23790	533	767	0.14	1.7
10-Aug	31	351	22664	555	731	0.13	1.6
10-Sep	30	381	33076	588	1103	0.19	1.5
10-Oct	31	412	31003	619	1000	0.18	1.5
10-Nov	30	442	24643	644	821	0.15	1.5
10-Dec	31	473	14638	659	472	0.08	1.4
11-Jan	31	504	28617	687	923	0.16	1.4
11-Feb	29	533	20748	708	715	0.13	1.3
11-Mar	31	564	22095	730	713	0.13	1.3
11-Apr	30	594	19591	750	653	0.12	1.3

Table III- 11: Production history for well #1: STS unit 3, LaSalle County

STS 3	#254479						
Horizontal leg (ft)	4523						
Fracture stages	15						
Month	Well days Online	Producing	Gas	Gp	qg	q/qi	Average rate,
		times (days)	(MCF)	(MMscf)	(Mscf/D)		Q/t (MMscf/D)
9-Oct	18	18	135696	136	7539	1	7.5
9-Nov	30	48	172075	308	5736	0.76	6.4
9-Dec	31	79	118598	426	3826	0.51	5.4
10-Jan	31	110	76817	503	2478	0.33	4.6
10-Feb	29	139	67292	570	2320	0.31	4.1
10-Mar	31	170	64372	635	2077	0.28	3.7
10-Apr	30	200	53478	688	1783	0.24	3.4
10-May	31	231	47605	736	1536	0.2	3.2
10-Jun	30	261	38332	774	1278	0.17	3.0
10-Jul	31	292	40680	815	1312	0.17	2.8
10-Aug	31	323	37950	853	1224	0.16	2.6
10-Sep	30	353	35398	888	1180	0.16	2.5
10-Oct	31	384	32642	921	1053	0.14	2.4
10-Nov	30	414	29948	951	998	0.13	2.3
10-Dec	31	445	26140	977	843	0.11	2.2
11-Jan	31	476	29218	1006	943	0.13	2.1
11-Feb	29	505	23576	1030	813	0.11	2.0
11-Mar	31	536	21960	1052	708	0.09	2.0
11-Apr	30	566	22145	1074	738	0.1	1.9

Table III- 12: Production history for well #1: Caroline Pielop unit, LaSalle County.

Caroline Pielop	#254449						
Horizontal leg (ft)	3896						
Fracture stages	12						
Month	Well days Online	Producing	Gas	Gp	Qg	q/qi	Average rate,
		times (days)	(MCF)	(MMscf)	(Mscf/D)		Q/t (MMscf/D)
10-Jan	18	18	85021	850	4723	1	47.2
10-Feb	29	47	105270	955	3630	0.77	20.3
10-Mar	31	78	83510	1039	2694	0.57	13.3
10-Apr	30	108	67875	1107	2263	0.48	10.2
10-May	31	139	67930	1175	2191	0.46	8.5
10-Jun	30	169	57501	1232	1917	0.41	7.3
10-Jul	31	200	61116	1293	1971	0.42	6.5
10-Aug	31	231	51462	1345	1660	0.35	5.8
10-Sep	30	261	46074	1391	1536	0.33	5.3
10-Oct	31	292	44835	1436	1446	0.31	4.9
10-Nov	30	322	39807	1476	1327	0.28	4.6
10-Dec	31	353	38985	1515	1258	0.27	4.3
11-Jan	31	384	34767	1549	1122	0.24	4.0
11-Feb	29	413	30310	1580	1045	0.22	3.8
11-Mar	31	444	20591	1600	664	0.14	3.6
11-Apr	30	474	32732	1633	1091	0.23	3.4

Table III- 13: Production history for well #1: Golla 7 unit, LaSalle County.

Golla 7	#255730						
Horizontal leg (ft)	3682						
Fracture stages	13						
Month	Well days Online	Producing	Gas	Gp	qg	q/qi	Average rate,
		times (days)	(MCF)	(MMscf)	(Mscf/D)		Q/t (MMscf/D)
9-Dec	30	30	17842	18	595	1	0.6
10-Jan	31	61	184624	202	5956	10	3.3
10-Feb	29	90	131132	334	4522	7.6	3.7
10-Mar	31	121	113112	447	3649	6.14	3.7
10-Apr	30	151	91061	538	3035	5.1	3.6
10-May	31	182	87717	625	2830	4.76	3.4
10-Jun	30	212	78029	704	2601	4.37	3.3
10-Jul	31	243	66583	770	2148	3.61	3.2
10-Aug	31	274	65282	835	2106	3.54	3.0
10-Sep	30	304	53968	889	1799	3.03	2.9
10-Oct	31	335	51770	941	1670	2.81	2.8
10-Nov	30	365	46394	988	1546	2.6	2.7
10-Dec	31	396	44667	1032	1441	2.42	2.6
11-Jan	31	427	43545	1076	1405	2.36	2.5
11-Feb	29	456	38673	1114	1334	2.24	2.4
11-Mar	31	487	38615	1153	1246	2.09	2.4
11-Apr	30	517	36310	1189	1210	2.04	2.3

Table III- 14: Production history for well #1: Eskew West Unit, Live Oak County

Eskew West Unit	#254315						
Horizontal leg (ft)							
Fracture stages							
Month	Well days Online	Producing	Gas	Gp	qg	q/qi	Average rate,
		times (days)	(MCF)	(MMscf)	(Mscf/D)		Q/t (MMscf/D)
9-Jul	19	19	8998	9	474	1	0.5
9-Aug	31	50	79388	88	2561	5.41	1.8
9-Sep	31	81	55944	144	1805	3.81	1.8
9-Oct	30	111	29226	174	974	2.06	1.6
9-Nov	31	142	29084	203	938	1.98	1.4
9-Dec	30	172	28782	231	959	2.03	1.3
10-Jan	31	203	21504	253	694	1.47	1.2
10-Feb	31	234	22606	276	729	1.54	1.2
10-Mar	29	263	19401	295	669	1.41	1.1
10-Apr	31	294	18575	314	599	1.27	1.1
10-May	30	324	16100	330	537	1.13	1.0
10-Jun	31	355	14908	345	481	1.02	1.0
10-Jul	31	386	13370	358	431	0.91	0.9
10-Aug	31	417	10607	368	342	0.72	0.9
10-Sep	30	447	9096	378	303	0.64	0.8
10-Oct	31	478	8861	386	286	0.6	0.8
10-Nov	30	508	10038	396	335	0.71	0.8
10-Dec	31	539	10317	407	333	0.7	0.8
11-Jan	31	570	9917	417	320	0.68	0.7
11-Feb	29	599	7458	424	257	0.54	0.7
11-Mar	31	630	7195	431	232	0.49	0.7
11-Apr	30	660	4922	436	164	0.35	0.7

Table III- 15: Production history for well #1: Lasca ButlerSearcy Trust unit, Live Oak County.

Lasca B Trust	# 254301						
Horizontal leg (ft)	4758						
Fracture stages							
Month	Well days Online	Producing	Gas	Gp	qg	q/qi	Average rate,
		times (days)	(MCF)	(MMscf)	(Mscf/D)		Q/t (MMscf/D)
9-May	31	31	66279	66	2138	1	2.1
9-Jun	30	61	30747	97	1025	0.48	1.6
9-Jul	31	92	24685	122	796	0.37	1.3
9-Aug	31	123	22345	144	721	0.34	1.2
9-Sep	30	153	25765	170	859	0.4	1.1
9-Oct	31	184	21821	192	704	0.33	1.0
9-Nov	30	214	18771	210	626	0.29	1.0
9-Dec	31	245	17619	228	568	0.27	0.9
10-Jan	31	276	16038	244	517	0.24	0.9
10-Feb	29	305	14560	259	502	0.24	0.8
10-Mar	31	336	13701	272	442	0.21	0.8
10-Apr	30	366	11808	284	394	0.18	0.8
10-May						0	
10-Jun	30	396	13316	297	444	0.21	0.8
10-Jul	31	427	13535	311	437	0.2	0.7
10-Aug	31	458	11667	323	376	0.18	0.7
10-Sep	30	488	11441	334	381	0.18	0.7
10-Oct	31	519	11146	345	360	0.17	0.7
10-Nov	30	549	10961	356	365	0.17	0.6
10-Dec	31	580	10208	366	329	0.15	0.6
11-Jan	31	611	10353	377	334	0.16	0.6
11-Feb	29	640	7691	384	265	0.12	0.6
11-Mar	31	671	10034	394	324	0.15	0.6
11-Apr	30	701	9190	404	306	0.14	0.6

Table III- 16: Production history for well #1: Kunde Unit 1, Live Oak County.

Kunde Unit 1	#249741						
Horizontal leg (ft)							
Fracture stages							
Month	Well days Online	Producing	Gas	Gp	qg	q/qi	Average rate,
		times (days)	(MCF)	(MMscf)	(Mscf/D)		Q/t (MMscf/D)
8-Apr	13	13	7955	8	612	1	0.6
8-May	31	44	18614	27	600	0.98	0.6
8-Jun	30	74	55565	82	1852	3.03	1.1
8-Jul	31	105	1331	83	43	0.07	0.8
8-Aug	31	136	0	83	0	0	0.6
8-Sep	30	166	29047	113	968	1.58	0.7
8-Oct	31	197	30178	143	973	1.59	0.7
8-Nov	30	227	15565	158	519	0.85	0.7
8-Dec	31	258	11642	170	376	0.61	0.7
9-Jan	31	289	10401	180	336	0.55	0.6
9-Feb	29	318	28405	209	979	1.6	0.7
9-Mar	31	349	24461	233	789	1.29	0.7
9-Apr	30	379	21714	255	724	1.18	0.7
9-May	31	410	21783	277	703	1.15	0.7
9-Jun	30	440	17074	294	569	0.93	0.7
9-Jul	31	471	13491	307	435	0.71	0.7
9-Aug	31	502	22133	329	714	1.17	0.7
9-Sep	30	532	17427	347	581	0.95	0.7
9-Oct	31	563	15537	362	501	0.82	0.6
9-Nov	30	593	14278	377	476	0.78	0.6
9-Dec	31	624	13501	390	436	0.71	0.6
10-Jan	31	655	13647	404	440	0.72	0.6
10-Feb	29	684	11742	415	405	0.66	0.6
10-Mar	31	715	12001	427	387	0.63	0.6
10-Apr	30	745	10766	438	359	0.59	0.6
10-May	31	776	10062	448	325	0.53	0.6

Table III-16: Production history for well #1: Kunde Unit 1, Live Oak County - Continued

Kunde Unit 1	#249741						
Horizontal leg (ft)							
Fracture stages							
Month	Well days Online	Producing	Gas	Gp	qg	q/qi	Average rate,
		times (days)	(MCF)	(MMscf)	(Mscf/D)		Q/t (MMscf/D)
10-Jun	30	806	11501	460	383	0.63	0.6
10-Jul	31	837	12240	472	395	0.65	0.6
10-Aug	31	868	11207	483	362	0.59	0.6
10-Sep	30	898	10438	494	348	0.57	0.6
10-Oct	31	929	10377	504	335	0.55	0.5
10-Nov	30	959	10526	515	351	0.57	0.5
10-Dec	31	990	3627	518	117	0.19	0.5
11-Jan	31	1021	359	519	12	0.02	0.5
11-Feb	29	1050	5694	524	196	0.32	0.5
11-Mar	31	1081	4486	529	145	0.24	0.5
11-Apr	30	1111	6529	535	218	0.36	0.5

Table III- 17: Production history for well #1: Sinor Ranch Unit 1, Live Oak County.

Sinor Ranch	#254906						
Horizontal leg (ft)	2553						
Fracture stages							
Month	Well days Online	Producing	Gas	Gp	qg	q/qi	Average rate,
		times (days)	(MCF)	(MMscf)	(Mscf/D)		Q/t (MMscf/D)
9-Oct	14	14	71279	71	5091	1	5.1
9-Nov	30	44	120529	192	4018	0.79	4.4
9-Dec	31	75	74768	267	2412	0.47	3.6
10-Jan	31	106	54659	321	1763	0.35	3.0
10-Feb	29	135	37442	359	1291	0.25	2.7
10-Mar	31	166	36551	395	1179	0.23	2.4
10-Apr	30	196	34182	429	1139	0.22	2.2
10-May	31	227	30117	460	972	0.19	2.0
10-Jun	30	257	25259	485	842	0.17	1.9
10-Jul	31	288	24830	510	801	0.16	1.8
10-Aug	31	319	22425	532	723	0.14	1.7
10-Sep	30	349	20169	552	672	0.13	1.6
10-Oct	31	380	19054	571	615	0.12	1.5
10-Nov	30	410	17353	589	578	0.11	1.4
10-Dec	31	441	16823	605	543	0.11	1.4
11-Jan	31	472	15570	621	502	0.1	1.3
11-Feb	29	501	13673	635	471	0.09	1.3
11-Mar	31	532	13819	649	446	0.09	1.2
11-Apr	30	562	13327	662	444	0.09	1.2

Table III- 18: Production history for well #1: Kunde unit 2, Live Oak County.

Kunde unit 2	#225297						
Horizontal leg (ft)							
Fracture stages							
Month	Well days Online	Producing	Gas	Gp	qg	q/qi	Average rate,
		times (days)	(MCF)	(MMscf)	(Mscf/D)		Q/t (MMscf/D)
6-Aug	25	25	26	0	1		
6-Sep	30	55	15529	16	518	1	0.3
6-Oct	31	86	17532	33	566	1.09	0.4
6-Nov	30	116	5795	39	193	0.37	0.3
6-Dec	31	147	16309	55	526	1.02	0.4
7-Jan	31	178	13862	69	447	0.86	0.4
7-Feb	29	207	13635	83	470	0.91	0.4
7-Mar	31	238	12334	95	398	0.77	0.4
7-Apr	30	268	11711	107	390	0.75	0.4
7-May	31	299	12172	119	393	0.76	0.4
7-Jun	30	329	12209	131	407	0.79	0.4
7-Jul	31	360	11395	143	368	0.71	0.4
7-Aug	31	391	9828	152	317	0.61	0.4
7-Sep	30	421	0	152	0	0	0.4
7-Oct	31	452	2335	155	75	0.15	0.3
7-Nov	30	482	0	155	0	0	0.3
7-Dec	31	513	3453	158	111	0.22	0.3
8-Jan	31	544	10881	169	351	0.68	0.3
8-Feb	29	573	8325	177	287	0.56	0.3
8-Mar	31	604	6290	184	203	0.39	0.3
8-Apr	30	634	8002	192	267	0.52	0.3
8-May	31	665	7214	199	233	0.45	0.3
8-Jun	30	695	3793	203	126	0.24	0.3
8-Jul	31	726	4921	208	159	0.31	0.3
8-Aug	31	757	5836	213	188	0.36	0.3
8-Sep	30	787	6192	220	206	0.4	0.3
8-Oct	31	818	6423	226	207	0.4	0.3

Table III- 18: Production history for well #1: Kunde unit 2, Live Oak County - Continued

8-Nov	30	848	5694	232	190	0.37	0.3
8-Dec	31	879	5232	237	169	0.33	0.3
9-Jan	31	910	5675	243	183	0.35	0.3
9-Feb	29	939	4681	247	161	0.31	0.3
9-Mar	31	970	5059	252	163	0.32	0.3
9-Apr	30	1000	3841	256	128	0.25	0.3
9-May	31	1031	3060	259	99	0.19	0.3
9-Jun	30	1061	1354	261	45	0.09	0.2
9-Jul	31	1092	3432	264	111	0.21	0.2
9-Aug	31	1123	4278	268	138	0.27	0.2
9-Sep	30	1153	4766	273	159	0.31	0.2
9-Oct	31	1184	3815	277	123	0.24	0.2
9-Nov	30	1214	3162	280	105	0.2	0.2
9-Dec	31	1245	4396	284	142	0.27	0.2
10-Jan	31	1276	3660	288	118	0.23	0.2
10-Feb	29	1305	4177	292	144	0.28	0.2
10-Mar	31	1336	4393	297	142	0.27	0.2
10-Apr	30	1366	2942	300	98	0.19	0.2
10-May	31	1397	0	300	0	0	0.2
10-Jun	30	1427	1301	301	43	0.08	0.2
10-Jul	31	1458	3647	305	118	0.23	0.2
10-Aug	31	1489	3039	308	98	0.19	0.2
10-Sep	30	1519	2222	310	74	0.14	0.2
10-Oct	31	1550	3901	314	126	0.24	0.2
10-Nov	30	1580	1944	316	65	0.13	0.2
10-Dec	31	1611	2110	318	68	0.13	0.2
11-Jan	31	1642	279	318	9	0.02	0.2
11-Feb	29	1671	0	318	0	0	0.2
11-Mar	31	1702	1976	320	64	0.12	0.2
11-Apr	30	1732	1545	322	52	0.1	0.2

Table III- 19: Production history for well #1: Marlene Olson unit 2, Live Oak County.

Marlene Olson	#251511						
Horizontal leg (ft)							
Fracture stages							
Month	Well days Online	Producing	Gas	Gp	qg	q/qi	Average rate,
		times (days)	(MCF)	(MMscf)	(Mscf/D)		Q/t (MMscf/D)
9-Feb	29	29	2761	3	95	1	0.1
9-Mar	31	60	3401	6	110	1.15	0.1
9-Apr	30	90	1397	8	47	0.49	0.1
9-May	31	121	2458	10	79	0.83	0.1
9-Jun	30	151	1949	12	65	0.68	0.1
9-Jul	31	182	2176	14	70	0.74	0.1
9-Aug	31	213	2030	16	65	0.69	0.1
9-Sep	30	243	10	16	0	0	0.1
9-Oct	31	274	1572	18	51	0.53	0.1
9-Nov	30	304	1023	19	34	0.36	0.1
9-Dec	31	335	967	20	31	0.33	0.1
10-Jan	31	366	1824	22	59	0.62	0.1
10-Feb	29	395	2294	24	79	0.83	0.1
10-Mar	31	426	2014	26	65	0.68	0.1
10-Apr	30	456	1288	27	43	0.45	0.1
10-May	31	487	1415	29	46	0.48	0.1
10-Jun	30	517	1161	30	39	0.41	0.1
10-Jul	31	548	1471	31	47	0.5	0.1
10-Aug	31	579	814	32	26	0.28	0.1
10-Sep	30	609	1355	33	45	0.47	0.1
10-Oct	31	640	1126	35	36	0.38	0.1
10-Nov	30	670	1175	36	39	0.41	0.1
10-Dec	31	701	1063	37	34	0.36	0.1
11-Jan	31	732	1071	38	35	0.36	0.1
11-Feb	29	761	873	39	30	0.32	0.1
11-Mar	31	792	1148	40	37	0.39	0.1
11-Apr	30	822	643	40	21	0.23	0.0

Table III- 20: Production history for well #1: Gates unit 1, Webb County.

Gates unit 1	#258655						
Horizontal leg (ft)							
Fracture stages							
Month	Well days Online	Producing	Gas	Gp	qg	q/qi	Average rate,
		times (days)	(MCF)	(MMscf)	(Mscf/D)		Q/t (MMscf/D)
10-May	26	26	6287	6	242	1	0.2
10-Jun	30	56	9157	15	305	1.26	0.3
10-Jul	31	87	8178	24	264	1.09	0.3
10-Aug	31	118	2262	26	73	0.3	0.2
10-Sep	30	148	4425	30	148	0.61	0.2
10-Oct	31	179	8467	39	273	1.13	0.2
10-Nov	30	209	7944	47	265	1.1	0.2
10-Dec	31	240	8034	55	259	1.07	0.2
11-Jan	31	271	7815	63	252	1.04	0.2
11-Feb	29	300	4869	67	168	0.69	0.2

Table III- 21: Production history for well #1: Gates unit 2, Webb County.

Gates unit 2	#258921						
Horizontal leg (ft)							
Fracture stages							
Month	Well days Online	Producing	Gas	Gp	qg	q/qi	Average rate,
		times (days)	(MCF)	(MMscf)	(Mscf/D)		Q/t (MMscf/D)
10-Oct	29	29	4600	5	159	1	0.2
10-Nov	30	59	4733	9	158	1	0.2
10-Dec	31	90	4539	14	146	0.92	0.2
11-Jan	31	121	4316	18	139	0.88	0.2
11-Feb	29	150	2554	21	88	0.56	0.1
11-Mar	31	181	2910	24	94	0.59	0.1
11-Apr	30	211	3815	27	127	0.8	0.1
11-May	31	242	3376	31	109	0.69	0.1
11-Jun	30	272	2206	33	74	0.46	0.1

Table III- 22: Production history for well #1: Gates unit 3, Webb County.

Gates unit 3	#258925						
Horizontal leg (ft)							
Fracture stages							
Month	Well days Online	Producing	Gas	Gp	qg	q/qi	Average rate,
		times (days)	(MCF)	(MMscf)	(Mscf/D)		Q/t (MMscf/D)
10-Oct	31	31	2938	3	95	1	0.1
10-Nov	30	61	2889	6	96	1.02	0.1
10-Dec	31	92	4643	10	150	1.58	0.1
11-Jan	31	123	5658	16	183	1.93	0.1
11-Feb	29	152	2006	18	69	0.73	0.1
11-Mar	31	183	4121	22	133	1.4	0.1
11-Apr	30	213	2821	25	94	0.99	0.1
11-May	31	244	1716	27	55	0.58	0.1
11-Jun	30	274	5329	32	178	1.87	0.1

Table III- 23: Production history for well #1: Gates unit 4, Webb County.

Gates unit 4	#258924						
Horizontal leg (ft)	4324						
Fracture stages							
Month	Well days Online	Producing	Gas	Gp	qg	q/qi	Average rate,
		times (days)	(MCF)	(MMscf)	(Mscf/D)		Q/t (MMscf/D)
10-Oct	31	31	5642	6	182	1	0.2
10-Nov	30	61	5642	11	188	1.03	0.2
10-Dec	31	92	6193	17	200	1.1	0.2
11-Jan	31	123	6387	24	206	1.13	0.2
11-Feb	29	152	4209	28	145	0.8	0.2
11-Mar	31	183	4291	32	138	0.76	0.2
11-Apr	30	213	4003	36	133	0.73	0.2
11-May	31	244	3242	40	105	0.58	0.2
11-Jun	30	274	3187	43	106	0.58	0.2

Table III- 24: Production history for well #1: Gates unit 5, Webb County.

Gates unit 5	#258923						
Horizontal leg (ft)	4053						
Fracture stages							
Month	Well days Online	Producing	Gas	Gp	qg	q/qi	Average rate,
		times (days)	(MCF)	(MMscf)	(Mscf/D)		Q/t (MMscf/D)
10-Oct	31	31	4418	4	143	1	0.1
10-Nov						0	
10-Dec	31	62	3997	8	129	0.91	0.1
11-Jan	31	93	4293	13	138	0.97	0.1
11-Feb	29	122	2990	16	103	0.72	0.1
11-Mar	31	153	4171	20	135	0.94	0.1
11-Apr	30	183	2755	23	92	0.64	0.1
11-May	31	214	3181	26	103	0.72	0.1
11-Jun	30	244	2312	28	77	0.54	0.1